

**PRODUCTION OF POLYOL CARBONATES AND  
THEIR INTERCALATION INTO SMECTITE CLAYS**

**Uzma Shaheen**

Doctor of Philosophy

2014



# PRODUCTION OF POLYOL CARBONATES AND THEIR INTERCALATION INTO SMECTITE CLAYS

**Uzma Shaheen**

A thesis submitted to the Faculty of Science  
Monash University, in fulfilment of the  
requirements for the degree of  
**DOCTOR OF PHILOSOPHY**

School of Chemistry  
Monash University  
Clayton, Australia

2014

## **Copyright Notices**

### **Notice 1**

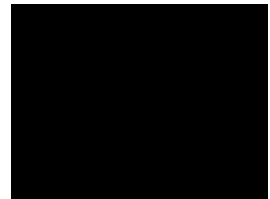
Under the Copyright Act 1968, this thesis must be used only under the normal conditions of scholarly fair dealing. In particular no results or conclusions should be extracted from it, nor should it be copied or closely paraphrased in whole or in part without the written consent of the author. Proper written acknowledgement should be made for any assistance obtained from this thesis.

### **Notice 2**

I certify that I have made all reasonable efforts to secure copyright permissions for third-party content included in this thesis and have not knowingly added copyright content to my work without the owner's permission.

## STATEMENT

*To best of the author's knowledge and belief, this thesis contains no material which has been accepted for the award of any other degree or diploma in any university and contains no material previously published or written by another person except where due reference is made.*



Uzma Shaheen  
School of Chemistry  
Monash University



# Table of Contents

Abstract	i
Acknowledgements .....	iii
List of Figures .....	v
List of Schemes .....	x
List of Tables .....	xii
Abbreviations.....	xiv
Publications and Presentations .....	xvii
<b>Chapter 1</b> Introduction.....	1
1.1 Background .....	1
1.2 Research Hypothesis.....	4
1.3 Organic Carbonates – Properties and Reactions .....	6
1.3.1 Cyclic organic carbonates .....	8
1.3.2 Polymerization of cyclic carbonates .....	10
1.4 Clay mineral.....	16
1.4.1 Intercalation of organic molecules.....	19
1.4.2 Polymer intercalated clay complexes: nanocomposites .....	22
1.5 Research Approach .....	27
1.6 Hypothesis and objectives .....	28
1.7 Thesis overview.....	29
1.8 References.....	31
<b>Chapter 2</b> Production of glycerol carbonate and other cyclic carbonates .....	44
2.1 Introduction .....	44
2.2 Objectives.....	47
2.3 Results and discussion.....	48
2.3.1 Synthesis of glycerol carbonate.....	48
2.3.2 Synthesis of cyclic carbonates from other 1,2-diols.....	63
2.4 Conclusion.....	78
2.5 References.....	78
<b>Chapter 3</b> Interaction of glycerol carbonate and other cyclic carbonates with Na-smectite .....	82
3.1 Introduction .....	82

3.2	Objective.....	83
3.3	Results and discussion .....	84
3.3.1	Interaction of glycerol carbonate with Na-smectite.....	84
3.3.2	Preparation of cyclic carbonates intercalated Na-smectites complexes.....	108
3.4	Conclusions.....	123
3.5	References .....	124
	<b>Chapter 4</b> Derivatization of glycerol carbonate and polymerization of cyclic carbonates .....	130
4.1	Introduction.....	130
4.2	Objective.....	131
4.3	Results and discussion .....	132
4.3.1	Functionalization of glycerol carbonate .....	132
4.3.2	Intercalation of ester and bromo functional cyclic carbonates.....	136
4.3.3	Reactions of cyclic carbonates .....	138
4.3.3.2.1	O-alkylation of glycerol carbonate with allyl bromide and 4-bromomethyl-1,3-dioxolan-2-one.....	140
4.3.3.2.2	O-Alkylation of glycerol.....	142
4.3.4	Polymerization of monomers containing pendant cyclic carbonate .....	148
4.4	Conclusion .....	155
4.5	References .....	156
	<b>Chapter 5</b> Preparation of polymer Na-smectite nanocomposites containing pendant cyclic carbonate .....	159
5.1	Introduction.....	159
5.2	Objectives .....	161
5.3	Results and discussion .....	162
5.3.1	Formation of polymers/Na-smectite nanocomposites by solution intercalation and clay <i>in-situ</i> polymerization .....	162
5.3.2	Isolation of polymers formed by <i>in-situ</i> polymerization.....	175
5.3.3	Treatment of polymer nanocomposites with sodium chloride .....	181
5.3.4	Thermal properties of intercalated polymer/Na-smectite nanocomposites .....	182
5.4	Conclusions.....	191
5.5	References .....	192
	<b>Chapter 6</b> Experimental.....	194
6.1	Materials and methods.....	194

6.2	Experimental for Chapter 2- Production of glycerol carbonate and other cyclic carbonates.....	200
6.3	Experimental for Chapter 3- Interaction of glycerol carbonate and other cyclic carbonates with Na-smectite.....	212
6.4	Experimental for Chapter 4- Derivatization of glycerol carbonate and polymerization of cyclic carbonates.....	217
6.5	Experimental for Chapter 5- Preparation of polymer/Na-smectite nanocomposites .....	235
6.6	References.....	237
	<b>Chapter 7</b> Concluding Remarks.....	240
7.1	Major Outcomes .....	240
7.2	Research Directions.....	244
7.3	References.....	245
	Appendix 1- Crystal structure and data for tetrahydrofuro[3,4-d][1,3]dioxol-2-one (8A).....	246
	Appendix 2- TGA curves.....	251



## Abstract

In hyper-saline conditions, clays in geosynthetic clay liners contract and fail to form a hydraulic barrier due to removal of water from the interlayer spaces of smectite, which is the swelling mineral component of bentonites used in geosynthetic clay liners.

Five-membered cyclic carbonates such as propylene carbonate have been reported to form stable intercalated complexes with hydrated Na-smectite, which maintain swollen states at <1M saline solutions. It is unknown whether propylene carbonate can retain the interlayer water within the smectite upon exposure to more saline solutions (>1M). Glycerol carbonate was selected as an alternative candidate as it possesses a hydroxyl functionality which may assist in retention of interlayer water and which also can be synthesized from inexpensive reactants. A green, solvent free approach was developed for scalable production of glycerol carbonate from glycerol and urea. Glycerol carbonate was obtained in 83% yield under optimal conditions of glycerolysis of urea using a novel zinc monoglycerolate (ZMG) catalyst. The isocyanate ligand coordinated to the metal glycerolate was believed to be the key intermediate in the catalytic cycle (Turney et al., 2013). This methodology was extended to the synthesis of other cyclic carbonates starting from urea and various 1,2-diols employing the ZMG catalyst. Transesterification using dimethyl carbonate (an expensive reagent) was shown to be an alternative way to synthesize cyclic carbonates. Comparative yields for the products via two methods were obtained.

The intercalation of glycerol carbonate into the interlayer galleries of sodium smectite was studied. The main driving force for intercalation of these molecules was considered to be the solvation of interlayer sodium cations. FTIR showed the presence of interlayer

water in Na-smectite. Model FTIR studies based on varying amounts of water and sodium chloride in glycerol carbonate showed that water, as well as sodium cations, were interacting with glycerol carbonate. Long-term stability studies of glycerol carbonate in saline solution (1M) indicated it to be stable. Intercalated complexes of other cyclic carbonates with Na-smectite were prepared and characterized.

Long term exposure of cyclic carbonates may result in the leaching out of cyclic carbonates from the clay. This can be addressed by modifying cyclic carbonates into polymers with a pendant cyclic carbonate. The hydroxyl functionality of glycerol carbonate was used to prepare various cyclic carbonate derivatives (esters, tosyl and bromo) that would potentially be useful in preparation of intercalated complexes. O-alkylation of hydroxyl containing cyclic carbonate resulted in precursor monomers. Ring opening polymerization of an epoxy cyclic carbonate resulted in selective opening of the epoxide ring to yield a polyether with retention of the cyclic carbonate. Photopolymerization of a styrene monomer with a pendant cyclic carbonate group yielded polystyrene with pendant cyclic carbonates. Polyether nanocomposites prepared via solution intercalation and *in-situ* ring opening polymerization resulted in intercalated and intercalated-disordered nanocomposites, respectively. Partially intercalated-disordered polystyrene cyclic carbonate nanocomposites were obtained via *in-situ* polymerization and solution intercalation approaches as determined on the basis of XRD. The *in-situ* formed polymer was separated from the clay and was similar to pure polymer synthesized independently. NaCl (3M) treatment with polyether nanocomposites revealed it to be stable when compared with epoxy monomer intercalated.

# Acknowledgements

I would like to extend my deepest gratitude to my supervisors, Tony Patti, Terry Turney and Will Gates, for their significant input, guidance and support during my PhD. It has been always a great pleasure to me to have them as my supervisors, for training me and for their valuable discussions and suggestions in every step of my research.

I am very grateful to Dr. Kei Saito for his invaluable help and for allowing me to learn from his vast experience in polymer science and for taking time to read chapter 4 of this thesis.

I would like to thank my advisors, Prof. Alan Chaffee and Dr. Toby Bell, for their constant support and advice that helped set the direction of my research.

I deeply appreciate Dr. Sanjitha Kulasegaram for her time to continue the laboratory work in my absence regarding mechanistic studies of glycerol carbonate.

I acknowledge Faculty of Science Dean's International Postgraduate Research Scholarship and School of Chemistry Stipend Scholarship, Monash University for providing me a chance to pursue my studies, providing me resources and funding for this research. I gratefully acknowledge MIGR for a travel grant to attend the 6<sup>th</sup> International Conference on Green and Sustainable Chemistry (GSC-6) held in UK in June 2013.

Many thanks to Craig Forsyth, Roderick Mackie, Finlay Shanks, Sally Duck and Peter Nicholas for providing instrumental support and Dr. Priscilla Johnston for running CHN analyses.

I truly enjoyed the valuable discussions and chit chat with Andras Fehervari, Dr. Gagan Kaur, Dr. Sepa Nanayakkara, Duy Pham, Chadin Kulsing, Yada Nossol, Leesun Kim, Dr. Shahid Kazi, Dr. Brenda Leung and Mr. Pas Florio.

I would like to thank my family members, Mian Adeel Fareed, Faisal Mehmood, Misbah Shaheen, Adnan Yousaf and Aliza Ahmad for their support, encouragement and for providing interests outside of my studies. Finally, I'd like to thank my father Ghulam Fareed and especially my mother Khadija Fareed, who has done more than anyone could over the course of my PhD.

# List of Figures

Figure 1.1: A sample of geosynthetic clay liner (GCL). The sample is about 10 mm thick, including about 5 mm of bentonite between two sheets of geotextiles. ....	2
Figure 1.2: Conceptualization of the interaction between exchange cations, cationic water and cyclic carbonate within the interlayer space of smectite.....	4
Figure 1.3: Schematic model of interactions of sodium bentonite (clay) and cyclic carbonate intercalated sodium bentonite complex with water at low and high salinity.....	6
Figure 1.4: Ring opening polymerization of six membered cyclic carbonates. ....	11
Figure 1.5: Ring opening polymerization of five-membered cyclic carbonates.....	12
Figure 1.6: Anionic ring opening polymerization of methyl 4,6- <i>O</i> -benzylidene-2,3- <i>O</i> -carbonyl- $\alpha$ -D-glucopyranoside. ....	12
Figure 1.7: Structures of a) the <i>cis</i> - b) <i>trans</i> -cyclohexane-1,2-diyl carbonates and c) 4-((oxiran-2-ylmethoxy)methyl)-1,3-dioxolan-2-one. ....	13
Figure 1.8: Cyclic carbonate monomers useful in radical polymerization. ....	14
Figure 1.9: Styrene monomers with five-membered cyclic carbonate functionality.....	15
Figure 1.10: Structure of montmorillonite. ....	17
Figure 1.11: Type of composites arising from interaction of clay and polymers.....	23
Figure 2.1: Synthesis of glycerol carbonate from carbon monoxide. ....	44
Figure 2.2: Reaction of glycidol with carbon dioxide to produce glycerol carbonate.....	45
Figure 2.3: Synthesis of glycerol carbonate from carbon dioxide employing a transition metal catalyst. ....	45
Figure 2.4: Formation of glycerol carbonate from transesterification using dimethyl carbonate. ... .....	46
Figure 2.5: Synthesis of glycerol carbonate from supercritical carbon dioxide employing zeolite. .....	46
Figure 2.6: Reaction of glycerol and urea to obtain glycerol carbonate. ....	47
Figure 2.7: Structure of glycerol urethane. ....	49
Figure 2.8: Side products formed in the reaction of glycerol with urea. ....	50
Figure 2.9: Trend of glycerol conversion with temperature. ....	53

Figure 2.10: Percent selectivity patterns of products as a function of temperature. ....	53
Figure 2.11: Effect of time on glycerol conversion in the catalysed and uncatalysed processes.....	54
Figure 2.12: Effect of time on the yield of glycerol carbonate in the catalysed and uncatalysed reactions.....	56
Figure 2.13: Steps for the reaction of glycerol with urea. ....	59
Figure 2.14: FTIR spectra for the reaction of ZnO with glycerol and urea.....	61
Figure 2.15: a) IR spectrum; b) XRD spectrum of recovered solid (from reaction of glycerol and urea employing ZnO catalyst).....	62
Figure 2.16: General mechanism for the cyclization of various 1,2-diols catalyzed by ZMG. ....	64
Figure 2.17: Formation of different products from <i>trans</i> -1,2-cyclohexanediol. ....	72
Figure 2.18: Formation of hexahydrobenzo[d][1,3]dioxol-2-one (6A) from <i>cis</i> -1,2-cyclohexanediol.....	73
Figure 2.19: A single crystal structure of 8A as determined from X-ray diffraction. (Molecular diagram with non-hydrogen atoms represented by 50% thermal ellipsoids and hydrogen atoms as spheres of arbitrary size). ....	75
Figure 2.20: 3-D representation of formation of product 8A and 8B. ....	77
Figure 3.1: XRD traces of a) Na-smectite, and varying amounts of glycerol carbonate/Na-smectite as b) 20 wt% c) 30 wt% d) 40 wt% e) 50 wt% f) 60 wt% g) 70 wt% h) 80 wt% and i) 90 wt% of glycerol carbonate in Na-smectite.....	86
Figure 3.2: Change in gallery height and FWHM values of Na-smectite by varying the amount of glycerol carbonate (For 20-40 wt%, two reflections were present and gallery height calculated for each reflection). ....	88
Figure 3.3: Possible occupancy models for the swollen states on the basis of the relative size of the GC molecule and the measured <i>d</i> (001) reflection: a) Na-smectite b) 30 wt% glycerol carbonate, c) 50 wt%, d) 90 wt% of glycerol carbonate. ....	90
Figure 3.4: FTIR spectra of a) glycerol carbonate intercalated sodium smectite b) glycerol carbonate, and c) Na-smectite.....	91
Figure 3.5: Figure showing comparison of FTIR spectra of a) subtracted glycerol carbonate (glycerol carbonate intercalated sodium smectite-Na-smectite), and b) glycerol carbonate. ....	92
Figure 3.6: XRD spectra of Na-smectite along with 1A/Na-smectite complex. ....	95
Figure 3.7: A representative figure suggesting possible arrangement of glycerol carbonate molecules within interlayer gallery of Na-smectite along with the molecular length of	

glycerol carbonate, where a = Na-smectite without any glycerol carbonate, b and c = arrangement of 2.5 molecules of glycerol carbonate per unit cell of smectite. ....	98
Figure 3.8: FTIR spectra of a) Na-smectite b) oven dried glycerol carbonate/Na-smectite and c) oven dried glycerol carbonate. ....	99
Figure 3.9: Structure of glycerol carbonate. ....	100
Figure 3.10: Stacked FTIR spectra of glycerol carbonate with varying the percentage of water. ....	101
Figure 3.11: Effect of concentration of water on hydroxyl and carbonyl stretch of glycerol carbonate. Error bars for the FTIR are in the range of $\pm 2 \text{ cm}^{-1}$ after triplicate measurements. ....	102
Figure 3.12: Plot of concentration of sodium chloride versus wavenumbers of $\nu(\text{O-H})_{\text{str}}$ and $\nu(\text{C=O})_{\text{str}}$ of glycerol carbonate. Error bars for the FTIR are in the range of $\pm 2 \text{ cm}^{-1}$ after triplicate measurements. ....	103
Figure 3.13: Influence of concentration of water on O-H and C=O stretching of glycerol carbonate (with 10,000 ppm sodium chloride). Error bars for the FTIR are in the range of $\pm 2 \text{ cm}^{-1}$ after triplicate measurements. ....	105
Figure 3.14: Structure of 4-(2-ethyl)-1,3-dioxolan-2-one (2A). ....	108
Figure 3.15: XRD diffraction patterns of various amounts (10-90 wt%) of 2A in 2A/Na-smectite complexes, where a) 10 wt% b) 20 wt% c) 30 wt% d) 40 wt% e) 50 wt% f) 60 wt% g) 70 wt% h) 80 wt% and i) 90 wt% of 2A in Na-smectite. ....	109
Figure 3.16: Structure of 4-(4-butyl)-1,3-dioxolan-2-one (3A). ....	110
Figure 3.17: XRD spectra of various amounts of 3A in 3A/Na-smectite, where, a) 20 wt% b) 30 wt% c) 40 wt% d) 50 wt% e) 60 wt% f) 70 wt% and g) 80 wt%. ....	111
Figure 3.18: Change in gallery height of Na-smectite by varying amounts of 2A & 3A (For some amounts of cyclic carbonates, two reflections were present and gallery heights calculated for each reflection). ....	113
Figure 3.19: Structure of various cyclic carbonates, 2A) 4-(2-hydroxyethyl)-1,3-dioxolan-2-one, 2C) methyl (2-(2-oxo-1,3-dioxolan-4-yl)ethyl) carbonate, 3A) 4-(4-hydroxybutyl)-1,3-dioxolan-2-one, 3C) methyl (4-(2-oxo-1,3-dioxolan-4-yl)butyl) carbonate, 4A) 4-((benzyloxy)methyl)-1,3-dioxolan-2-one, 5A) 4,4'-(oxybis(methylene))bis(1,3-dioxolan-2-one), 6A) hexahydrobenzo[d][1,3]dioxol-2-one and 8A) tetrahydrofuro[3,4-d][1,3]dioxol-2-one. ....	115
Figure 3.20: XRD spectra of various cyclic carbonates intercalated Na-smectite complexes, a) Na-smectite, b) PC/Na-smectite, c) 2C/Na-smectite, d) 3C/Na-smectite, e) 4A/Na-smectite, f) 5A/Na-smectite, g) 6A/Na-smectite, and h) 8A/Na-smectite. ....	115
Figure 3.21: FTIR spectra of 4-((benzyloxy)methyl)-1,3-dioxolan-2-one (4A) intercalated sodium smectite, sodium smectite and 4A. ....	117

Figure 3.22: Structure of methyl (4-(2-oxo-1,3-dioxolan-4-yl)butyl) carbonate (3C). .....	117
Figure 3.23: Various derivatives of glycerol carbonate. ....	119
Figure 3.24: Gallery height relationship between hydroxyl, linear, alkyl and alkoxy cyclic carbonates. ....	120
Figure 3.25: Cyclic carbonate with additional linear carbonate, methyl (4-(2-oxo-1,3-dioxolan-4-yl)ethyl) carbonate (2C). ....	120
Figure 4.1: Functionalization of glycerol carbonate to synthesize cyclic carbonate precursors. ....	130
Figure 4.2: XRD traces of, a) Na-smectite, b) 12A/Na-Smectite, c) 9A/Na-smectite, d) ethanol/Na-smectite, and e) 10A/Na-smectite. ....	137
Figure 4.3: Mechanism for O-alkylation of glycerol carbonate with 4-vinylbenzyl bromide. ....	146
Figure 4.4: Hydrolysis of 4-vinylbenzyl acetate. ....	147
Figure 4.5: Structure of 4-((oxiran-2-ylmethoxy)methyl)-1,3-dioxolan-2-one (OMD). ....	148
Figure 4.6: Assignment of signals in <sup>1</sup> H-NMR spectra of a) monomer, BMD and b) polymer, PBMD. ....	153
Figure 4.7: <sup>1</sup> H-NMR spectra of a) BBD (monomer), and b) PBBD (polymer). ....	155
Figure 5.1: Approaches used for synthesis of polymer-smectite nanocomposites. ....	161
Figure 5.2: XRD patterns of the nanocomposites with different POMD amounts obtained via solution intercalation (in acetone) and <i>in-situ</i> polymerization a) POMD (50 wt%)/Na-smectite after solution intercalation, b) POMD (20 wt%)/Na-smectite after solution intercalation, c) POMD (10 wt%)/Na-smectite after solution intercalation, d) POMD-1/Na smectite after <i>in-situ</i> polymerization, e) OMD (50 wt%)/Na-smectite, and f) Na-smectite. ....	163
Figure 5.3: Comparison of FTIR spectra between 1400 and 600 cm <sup>-1</sup> of a) POMD-1/Na-smectite nanocomposites obtained via <i>in-situ</i> polymerization, b) POMD (50 wt%)/Na-smectite prepared by solution intercalation, c) OMD/Na-smectite, and d) Na-smectite. ....	166
Figure 5.4: FTIR spectra of a) POMD-1 obtained after subtracting FTIR of Na-smectite from POMD-1/Na-smectite, b) POMD obtained from ring opening polymerization, and c) OMD (monomer). ....	168
Figure 5.5: XRD patterns of a) PBMD-1/Na-smectite prepared by <i>in-situ</i> method, b) BMD/Na-smectite, c) PBMD (50 wt%)/Na-smectite, d) PBMD (20 wt%)/Na-smectite obtained via solution, e) PBMD (10 wt%)/Na-smectite, and f) pure Na-smectite. ....	169

Figure 5.6: a) Plot of $d(001)$ spacing versus Na-smectite, PBMD-1/Na-smectite obtained via <i>in-situ</i> polymerization along with monomer, BMD/Na-smectite, b) Plot of $d$ -spacing of nanocomposites with varying (wt%) amount of PBMD in Na-smectite obtained via solution intercalation. ....	170
Figure 5.7: Stacked FTIR spectra of a) PBMD-1/Na-smectite, b) PBMD (50 wt%)/Na-smectite obtained via solution and <i>in-situ</i> polymerization, c) BMD/Na-smectite, and d) Na-smectite. ....	171
Figure 5.8: Comparison of FTIR spectra of a) PBMD-1 obtained from subtraction of Na-smectite from PBMD-1/Na-smectite, and b) pure PBMD. ....	172
Figure 5.9: Plot of $d(001)$ as well as full width at half maximum (FWHM) versus amount of addition of PBBD to Na-smectite. ....	173
Figure 5.10: Stacked XRD patterns of a) POMD-A, b) POMD-1/Na-smectite prepared by <i>in-situ</i> method, and c) Na-smectite. ....	177
Figure 5.11: XRD traces of a) Na-smectite, b) PBMD/Na-smectite, and c) PBMD-A obtained after washing with acetonitrile. ....	178
Figure 5.12: FTIR spectra of a) POMD, neat polymer, and b) POMD-B (extracted polymer). ....	179
Figure 5.13: Comparison of $^1\text{H-NMR}$ spectra in $\text{CDCl}_3$ of a) OMD, monomer, b) Neat polyether (POMD), and c) extracted polymer, POMD-B. ....	180
Figure 5.14: XRD diffraction patterns of a) POMD/Na-smectite, b) POMD/Na-smectite after treatment with 3M NaCl, c) OMD/Na-smectite (XRD trace was run at a different parameters), and d) OMD/Na-smectite after treatment with 3M sodium chloride. ....	181
Figure 5.15: Glass transition temperature of a) neat polystyrene with pendant cyclic carbonate, PBBD and b) PBBD (50 wt%)/Na-smectite nanocomposite. ....	183
Figure 5.16: Glass transitions temperature of the a) neat polyether POMD, b) POMD/Na-smectite obtained via solution intercalation, and c) POMD-1/Na-smectite prepared by <i>in-situ</i> method. The arrows indicate the glass transition temperatures. ....	184
Figure 5.17: TGA curve of Na-smectite showing weight losses. ....	186
Figure 5.18: A comparison of thermogravimetric analysis (TGA) of the a) Na-smectite, b) POMD (10 wt%)/Na-smectite, c) POMD (20 wt%)/Na-smectite, d) POMD-1/Na-smectite prepared by <i>in-situ</i> method, e) POMD (50 wt%)/Na-smectite, and f) neat polyether, POMD (b,d & e prepared by solution intercalation approach, see Appendix 2 for derivative curve). ....	187
Figure 5.19: Thermogravimetric analysis (TGA) curves of the a) POMD-B, b) POMD-1/Na-smectite prepared by <i>in-situ</i> polymerization, c) POMD (neat polymer), d) POMD-A (acetone extracted polymer). ....	190

## List of Schemes

Scheme 2.1: Synthetic scheme for the preparation of glycerol carbonate using ZMG as a catalyst. ....	50
Scheme 2.2: General reaction for the synthesis of cyclic carbonates (1A-8A). ....	63
Scheme 2.3: Reaction of 1,2,4-butanetriol with urea and dimethyl carbonate. ....	65
Scheme 2.4: Reaction of 1,2,6-hexanetriol with urea or dimethyl carbonate. ....	66
Scheme 2.5: Reaction of 1,2,6-hexanetriol with urea or dimethyl carbonate. ....	67
Scheme 2.6: Reactions of diglycerol – Formation of cyclic carbonate derivatives. ....	68
Scheme 2.7: Products obtained in the reaction of <i>meso</i> -erythritol with urea. ....	74
Scheme 2.8: Formation of product 8A and 8B from <i>meso</i> -erythritol. Reaction intermediate, 2,3,4-trihydroxybutyl carbamate preferentially cyclizes to form 8B and not 8C with an equivalent of urea with the elimination of ammonia and carbon dioxide. Once 8B formed, it reacts with another equivalent of urea to yield 8A. ....	76
Scheme 4.1: Synthesis of ester derivatives of glycerol carbonate. ....	132
Scheme 4.2: Synthesis of tosylated glycerol carbonate. ....	133
Scheme 4.3: Conventional and microwave method to synthesize 4-bromomethyl-1,3-dioxolan-2-one (12A). ....	133
Scheme 4.4: Reaction showing different products obtained from the reaction of glycerol carbonate with phosphorus tribromide. ....	134
Scheme 4.5: Synthesis of 4-((allyloxy)methyl)-1,3-dioxolan-2-one (16A). ....	141
Scheme 4.6: Oxidation of double bond in 4-((allyloxy)methyl)-1,3-dioxolan-2-one. ....	141
Scheme 4.7: Attempted synthesis of dimer of glycerol carbonate. ....	141
Scheme 4.8: O-alkylation of glycerol with 4-vinylbenzyl chloride and bromide. ....	142
Scheme 4.9: Synthesis of 4-vinylbenzyl bromide from 4-vinylbenzyl chloride. ....	143
Scheme 4.10: Synthesis of alkyl-aryl ether containing cyclic carbonate (BMD) from glycerol carbonate. ....	144
Scheme 4.11: O-alkylation to form alkyl-aryl ether containing cyclic carbonate. ....	147
Scheme 4.12: Ring opening polymerization of 4-((oxiran-2-ylmethoxy)methyl)-1,3-dioxolan-2-one (OMD) to yield various polyethers at different conditions. ....	149

Scheme 4.13: Radical photopolymerization of styrene monomers retaining pendant five-membered cyclic carbonate moiety. ....	151
--	-----

# List of Tables

Table 1.1: Some examples of organic carbonates .....	7
Table 2.1: Glycerol carbonate production from various catalysts .....	49
Table 2.2: Effect of temperature on glycerol conversion and glycerol carbonate selectivity .....	51
Table 2.3: Uncatalysed and catalysed reactions .....	55
Table 2.4: Molar ratio change (of urea) on glycerol conversion and glycerol carbonate selectivity .....	57
Table 2.5: Re-cycling of ZMG and yield of glycerol carbonate .....	58
Table 2.6: Glycerol conversion and glycerol carbonate selectivity when using ZnO .....	60
Table 2.7: Conversion of 1,2,4-butanetriol and selectivity as determined by GLC .....	65
Table 2.8: Selectivity of side products in the reaction of 1,2,6-hexanetriol .....	66
Table 2.9: Comparison of reactions of 1-(benzyloxy)ethane-1,2-diol (4) .....	68
Table 2.10: Effect of urea and DMC molar ratio on selectivity of 4,4'-(oxybis(methylene))bis(1,3-dioxolan-2-one) (5A) .....	69
Table 2.11: Products obtained from reaction of <i>cis</i> -1,2-cyclohexanediol with urea .....	70
Table 2.12: Selectivity of products from the reaction of <i>trans</i> -1,2-cyclohexanediol with urea ....	71
Table 2.13: Selectivity of 8A and 8B upon change in amount of urea .....	74
Table 3.1: Full width at half maximum (FWHM) values and <i>d</i> (001) spacing for 1A intercalated Na-smectite complexes .....	87
Table 3.2: Percent weight loss in glycerol carbonate and its intercalated complexes and resulting <i>d</i> -spacing of intercalated complex .....	94
Table 3.3: Information about Na-smectite (Trugel) and number of glycerol carbonate molecules per unit cell of Na-smectite. Data on Trugel chemistry and crystallography provided by Dr. W.P. Gates (Monash University) .....	97
Table 3.4: Stability data (IR and <sup>13</sup> C-NMR) of glycerol carbonate at different pH values .....	107
Table 3.5: Full width at half maximum (FWHM) values for 2A and 3A intercalated Na-smectite complexes .....	112
Table 3.6: Infrared absorption peaks for sodium smectite complexes with compounds 2A-3A .....	114

Table 3.7: FTIR frequencies of main functional groups in cyclic carbonate upon smectite complex formation .....	118
Table 3.8: <i>d</i> (001) spacing of cyclic carbonates/Na-smectite, molecular length of respective cyclic carbonates with number of molecules calculated per unit cell for each system .....	122
Table 4.1: Comparison between conventional and microwave assisted synthesis of 4-bromomethyl-1,3-dioxolan-2-one (12A).....	135
Table 4.2: Major FTIR absorption frequencies of intercalated cyclic carbonate complexes .....	138
Table 4.3: Reactions of tosylated glycerol carbonate with different nucleophiles.....	139
Table 4.4: Conversion and selectivity of different products obtained by reaction of glycerol with 4-vinylbenzyl derivatives.....	143
Table 4.5: Conversion and selectivity of products using 4-vinylbenzyl derivatives .....	145
Table 4.6: Table showing selectivity and yields of the monomeric products via O-alkylation ....	148
Table 4.7: Ring opening polymerization of 4-((oxiran-2-ylmethoxy)methyl)-1,3-dioxolan-2-one (OMD).....	150
Table 4.8: Effect of time on conversion of BMD and yield of PBMD.....	152
Table 4.9: Yield and molecular weight of polymers with a pendant cyclic carbonate obtained via radical photopolymerization of pendant cyclic carbonate monomers with styrene functionality .....	154
Table 5.1: XRD characterization of polymer nanocomposites containing cyclic carbonate obtained via <i>in-situ</i> polymerizations and solution intercalation method.....	165
Table 5.2: Infrared frequencies of the main characteristic absorbance bands of pure PBBD and PBBD/Na-smectite obtained via solution intercalation .....	174
Table 5.3: Types of nanocomposites obtained via <i>in-situ</i> method and solution intercalation approach .....	175
Table 5.4: Characterization of extracted polymers from <i>in-situ</i> polymerized sample.....	176
Table 5.5: Glass transition temperature of pure polymers along with their nanocomposites....	185
Table 5.6: Information of thermal degradation of Na-smectite, neat polymers and nanocomposites obtained by thermogravimetric analysis.....	189

## Abbreviations

AIBN	=	Azoisobutyronitrile
ATRP	=	Atom Transfer Radical Polymerization
<i>n</i> Bu <sub>4</sub> NI	=	Tetrabutyl nitrogen iodide
BBD	=	4-(4-((4-Vinylbenzyl)oxy)butyl)-1,3-dioxolan-2-one
BED	=	4-(4-((4-Vinylbenzyl)oxy)ethyl)-1,3-dioxolan-2-one
BMD	=	4-(4-((4-Vinylbenzyl)oxy)methyl)-1,3-dioxolan-2-one
BPD-1	=	3-((4-Vinylbenzyl)oxy)propane-1,2-diol
BPD-2	=	3-((4-Vinylbenzyl)oxy)propane-1,3-diol
BPO	=	Benzoyl peroxide
CEC	=	Cation Exchange Capacity
CC	=	Cyclic carbonate
Conv.	=	Conversion
CaCl <sub>2</sub>	=	Calcium chloride
DCM	=	Dichloromethane
DMC	=	Dimethyl carbonate
DMF	=	Dimethyl formamide
DMSO	=	Dimethyl sulfoxide
DSC	=	Differential Scanning Calorimetry
EA	=	Ethyl acetate
EC	=	Ethylene carbonate
EI	=	Electron Impact

ESI-MS	=	Electrospray Ionization Mass Spectrometry
FID	=	Flame Ionization Detector
FTIR	=	Fourier Transform Infrared Spectroscopy
FWHM	=	Full width at half maximum intensity
GAMESS	=	General Atomic and Molecular Electronic Structure System
GC	=	Glycerol carbonate
GLC	=	Gas Chromatography
GC-MS	=	Gas Chromatography-Mass Spectrometry
GCL	=	Geosynthetic Clay Liner
GPC	=	Gel Permeation Chromatography
HPLC	=	High Performance Liquid Chromatography
HDTMA	=	Hexadecyltrimethylammonium
IR	=	Infrared
KBr	=	Potassium bromide
MCPBA	=	meta-Chloroperoxy benzoic acid
MW	=	Microwave
OMD	=	4-((Oxiran-2-ylmethoxy)methyl)-1,3-dioxolan-2-one
Na-smectite	=	Sodium smectite
NaCl	=	Sodium chloride
NaI	=	Sodium iodide
NaHCO <sub>3</sub>	=	Sodium bicarbonate
NMR	=	Nuclear Magnetic Resonance
Ni[P(OC <sub>2</sub> H <sub>5</sub> ) <sub>3</sub> ] <sub>4</sub>	=	Tetrakis(triethyl phosphite)nickel (0)

PBr <sub>3</sub>	=	Phosphorous tribromide
NaH	=	Sodium hydride
PBBD	=	Poly[4-(((4-vinylbenzyl)oxy)butyl)-1,3-dioxolan-2-one]
PBMD	=	Poly[4-(((4-vinylbenzyl)oxy)methyl)-1,3-dioxolan-2-one]
POMD	=	Poly[oxy(ethane-1-(((methyloxy)methyl)oxirane)-1,2-diyl)]
K <sub>2</sub> CO <sub>3</sub>	=	Potassium carbonate
Ph <sub>3</sub> P	=	Triphenyl phosphine
PC	=	Propylene carbonate
POE	=	Poly(ethylene oxide)
POED	=	Poly[oxy(ethane-1,2-diyl)]
PVA	=	Poly(vinyl alcohol)
ROP	=	Ring Opening Polymerization
AgNO <sub>3</sub>	=	Silver nitrate
(LC/MS) (TOF)	=	Time of Flight Liquid Chromatography Mass Spectrometry
TMS	=	Tetramethyl silane
<i>p</i> -TSOH	=	para-Toluenesulfonic acid
TGA	=	Thermogravimetric Analysis
TLC	=	Thin Layer Chromatography
ZnO	=	Zinc oxide
ZMG	=	Zinc monoglycerolate
ZnSO <sub>4</sub>	=	Zinc sulfate
XRD	=	X-ray Diffraction

# Publications and Presentations

## *Journal papers (attached to back of the thesis)*

- Turney, T.W., Patti, A., Gates, W.P., **Shaheen U.** and Kulasegaram, S., “Formation of glycerol carbonate from glycerol and urea catalyzed by metal monoglycerolates”, *Green Chem.*, 2013, 15, 1925-1931.
- Kulasegaram, S., **Shaheen U.** Turney, T.W., Gates, W.P. and Patti, A.F., “Zinc monoglycerolate as a catalyst for the conversion of 1,3- and higher diols to diurethanes”, *Green Chem.*, (submitted, July 2014).

## *Referred Conference Proceedings*

- **Shaheen, U.**, Kulasegaram, S., Gates, W.P., Turney, T.W., Patti, A. and Daoud, W., “Modification of clay liners to improve barrier capabilities for hyper-saline leachates”, *Proceedings of the Australian Regolith and Clays Conference*, Mildura, Victoria Australia 7-10 February 2012. Pp 41-42.
- **Shaheen, U.**, Fehervari, A., Kulasegaram, S., Gates, W.P., Turney, T.W., Patti, A., and Bouazza, A., “Saline stable glycerol carbonate-bentonite complexes”, *XV International Clay Conference*, Rio de Janeiro, Brazil. 7-11 July 2013.

## *Oral Presentations*

- **Shaheen, U.**, Kulasegaram, S., Turney, T.W., Patti, A. and Gates, W.P., “Mechanism of metal glycerolate-catalysed synthesis of glycerol carbonate from glycerol and urea”, *RACI Annual postgraduate symposium on Inorganic Chemistry*, RMIT University, Melbourne, Australia. 29<sup>th</sup> November 2013.

## **Poster Presentations**

- **Shaheen, U.**, Turney, T.W., Patti, A., Gates, W.P. and Daoud, W., “Modification of clay liners to improve barrier capabilities for hyper-saline leachates”, *3<sup>rd</sup> Asia-Oceania conference on Green & Sustainable Chemistry (AOC-3)*, Melbourne, Australia, 4-7 December 2011.
- **Shaheen, U.**, Kulasegaram S., Gates, W.P., Turney T.W., Patti A., Daoud W. “Modification of clay liners to improve barrier capabilities for hyper-saline leachates. Australian Regolith and Clays Conference, Mildura 7-10 February 2012. [http://www.smectech.com.au/ACMS/ACMS\\_Conferences/ACMS22/Proceedings/PDF/S1P\\_6%20ACMS22%20Shaheen%20et%20al.pdf](http://www.smectech.com.au/ACMS/ACMS_Conferences/ACMS22/Proceedings/PDF/S1P_6%20ACMS22%20Shaheen%20et%20al.pdf).
- **Shaheen, U.**, Fehervari A, Kulasegaram, S., Gates, W.P., Turney T.W., and Patti A. Saline-stable glycerol carbonate – bentonite complexes. 15<sup>th</sup> International Clay Conference, Rio de Janeiro, Brazil, 7-11 July 2013.
- **Shaheen, U.**, Fehervari, A., Kulasegaram, S., Turney, T.W., Patti, A., and Gates, W.P., “Zinc monoglycerolate (ZMG)-catalysed solvent free synthesis of cyclic carbonates from 1,2-polyols for application in the osmotic protection of clays”, *6<sup>th</sup> International Conference on Green and Sustainable Chemistry (GSC-6)*, The Nottingham University, Nottingham, United Kingdom. 4-7 August 2013.

# Chapter 1 Introduction

## 1.1 Background

Geosynthetic clay liners (GCLs) are widely employed as components of barriers in hydraulic containments such as landfills, surface impoundments, dams and ponds (Gates et al., 2009) but are now increasingly being considered for use in a large range of mining industry applications (Hornsey et al., 2010, Bouazza and Gates, 2014) due to their low hydraulic conductivity. The GCL design consists of a layer of bentonite contained between two layers of geotextile. These layers are held together by either needle punching or stitching (Figure 1.1). For GCLs manufactured in Australia, the bonding is further enhanced by heating the needle-punched fibres from the non-woven cover geotextile to the underside of the woven carrier geotextile. GCLs provide a low permeability that slows the rate of leachate seepage from impoundments thereby providing environmental protection from the leachates. The lower the hydraulic conductivity, generally, the more effective the GCL will be in retaining the waste or seepage within the surface impoundments.



**Figure 1.1:** A sample of geosynthetic clay liner (GCL). The sample is about 10 mm thick, including about 5 mm of bentonite between two sheets of geotextiles.

The mining industry, for example, potash and phosphate mining (Higgins et al., 2001) routinely results in production of hyper-saline leachates in huge quantities. These wastes may be stored in surface impoundments or “settlement impoundments”, where the aqueous phase evaporates resulting in leachates having extreme ionic strengths ( $>1-2M$ ). For lining applications, bentonite with high smectite content is desired. Smectites are swelling clay minerals and montmorillonite is the most common species. It is well known that bentonites containing sodium smectite can swell and form an effective seal to most leachates. Smectites undergo significant increases in hydraulic conductivity when exposed to high salinity leachates (Bouazza and Gates, 2014).

While GCLs provide suitable protection against transport of low salinity waters (Jo et al., 2005), when GCLs are employed as hydraulic barrier materials to high saline leachates at waste facilities, the barrier performance may be insufficient. This loss of protection capability can be attributed to a decrease in the swelling of bentonite against high ionic

strength leachates, thereby, enabling these leachates to potentially contaminate underlying sediments and groundwater. The hydraulic conductivity value of GCL generally increases with an increase in the soluble salt levels of the leachate (Xue et al., 2012).

Various types of modified bentonite based materials have been developed with improved chemical and functional capabilities (Gates, 2004, Gates et al., 2004, Onikata et al., 1999a, Yang and Lo, 2004) which may be used in GCLs. Literature evidence (Onikata et al., 1996) is available which suggests that propylene carbonate-montmorillonite intercalated complexes have potential for use in high saline waste storage facilities. Thus, the interaction between propylene carbonate and montmorillonite has been studied to understand the mechanism of osmotic swelling of montmorillonite (Onikata et al., 1999a). Propylene carbonate has been found to form complexes with montmorillonite effectively maintaining swelling of montmorillonite in brine solutions as well as fresh water (Kondo, 1996).

The environmental application of propylene carbonate/bentonite complexes in coastal brine areas as impermeable soil material has been reported (Onikata et al., 1996). Recently, Onikata et al. have shown that sodium bentonite when modified with propylene carbonate exhibits swelling characteristics in 1M NaCl comparable to unmodified Na-bentonite in distilled water (Onikata et al., 2000, Onikata., 2002, Katsumi et al., 2008b). Studies have indicated that this behaviour is retained for concentrations up to 1M NaCl (Onikata et al., 2000, Katsumi et al., 2008a) and 0.5M CaCl<sub>2</sub> (Katsumi et al., 2001), but it is still unknown whether it will be retained against hyper-saline waters (>1M). These compounds have been investigated for the application as barrier materials at waste containment facilities.

## 1.2 Research Hypothesis

Cyclic carbonates, such as propylene carbonate (PC) have the potential to form stable intercalated complexes with bentonite. These intercalates can maintain crystalline swollen states at elevated ionic strengths even up to 1M NaCl and 0.5M CaCl<sub>2</sub>. PC possesses a unique ability which enables bentonite to resist changes in interlayer water brought about by salts in bulk solution. This fact can be attributed to its high dielectric permittivity and dipolar properties (Onikata et al., 1999a). Cyclic carbonate can efficiently penetrate into the interlayer galleries of clay minerals and can then form hydrogen bonds with the outermost layer of water surrounding the interlayer cations in bentonite (Figure 1.2). These bonds are able to resist the osmotic potential exerted by high ionic strength leachates and thus, enable the complex to retain a larger interlayer spacing compared to smectites without the cyclic carbonate.

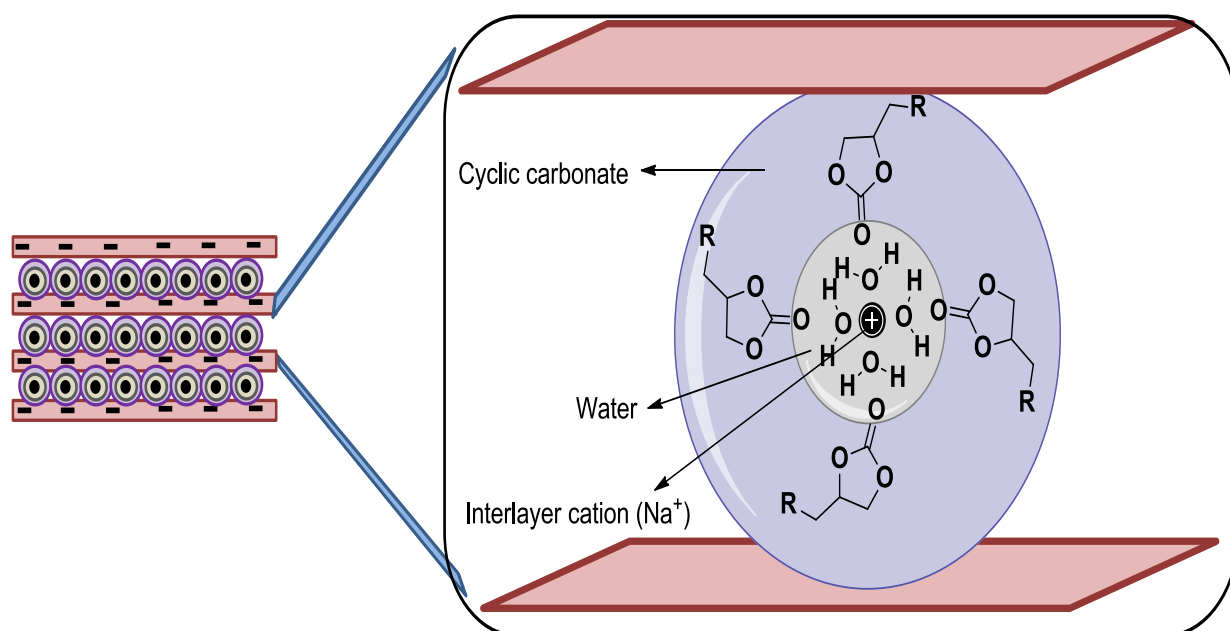


**Figure 1.2:** Conceptualization of the interaction between exchange cations, cationic water and cyclic carbonate within the interlayer space of smectite.

Under low salinity conditions, bentonite takes up and holds water strongly resulting in expansion (swelling) of the clay thus acting as a barrier for the movement of water molecules. High ionic strength ( $>1M$ ) conditions exert an osmotic potential which forces water out of the interlayer space of the clay mineral. The bentonite thus experiences shrinkage due to a decrease in volume under hyper-saline conditions as the smectite interlayer water is removed (Figure 1.3, upper half). This problem may be mitigated, at least partially, by reacting a cyclic carbonate with bentonite; the organic carbonate intercalates the smectite, forms strong bonds directly with the interlayer cation and maintains a greater crystalline volume and swollen state, thereby potentially providing a more effective hydraulic barrier to higher salinity leachates (Figure 1.3, lower half).

Glycerol carbonate (GC) is a novel candidate for this purpose and can be obtained in bulk from cheap raw materials such as glycerol and urea. Glycerol carbonate exhibits a high dielectric constant and a high boiling point (Chernyak, 2006). The free hydroxyl can be modified or replaced to give other reactive functionalities or may be useful in retention of water.

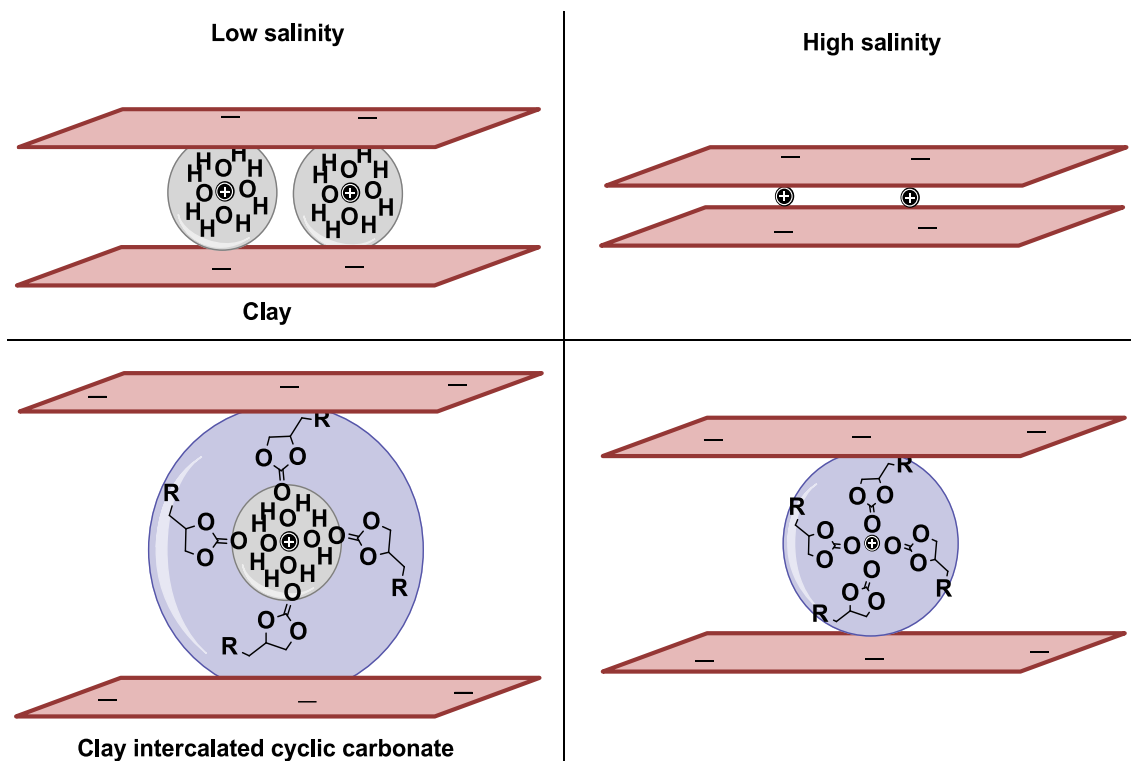


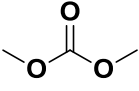
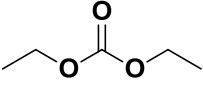
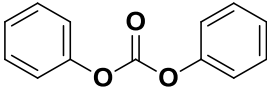
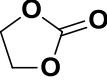
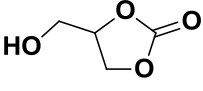
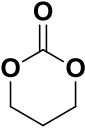
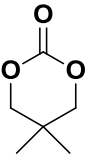
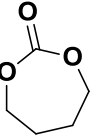
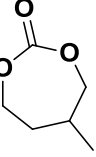
**Figure 1.3:** Schematic model of interactions of sodium bentonite (clay) and cyclic carbonate intercalated sodium bentonite complex with water at low and high salinity.

Therefore, a key hypothesis to be tested here is that bentonite modified with glycerol carbonate may maintain a greater crystalline volume and retain sorbed water at elevated bulk water salinity levels compared to non-modified Na-bentonite.

### 1.3 Organic Carbonates - Properties and Reactions

Organic carbonates are diesters of carbonic acid. In contrast to carbonic acid, the esters are stable and can be used as intermediates for synthesis or as polar, aprotic solvents for industrial applications. Organic carbonates can be divided into cyclic and non-cyclic carbonates (Table 1.1).

**Table 1.1:** Some examples of organic carbonates

Organic carbonates		Name	Structure	Reference
Class	Subclass			
Non-cyclic/linear carbonates	-	Dimethyl carbonate		(An et al., 2012)
		Diethyl carbonate		(Du et al., 2012)
		Diphenyl carbonate		(Fan et al., 2011)
Cyclic carbonates	Five-membered	Ethylene carbonate		(Tian et al., 2012)
		Glycerol carbonate	 (1)	(Rokicki et al., 2005)
	Six-membered	Trimethylene carbonate		(Pyo and Hatti-Kaul, 2012)
		5,5-Dimethyl-1,3-dioxan-2-one		(Pearson et al., 2011)
	Seven-membered	1,3-Dioxepan-2-one		(Giannocco et al., 2006)
5-Methyl-1,3-dioxepan-2-one			(Brignou et al., 2010)	

### 1.3.1 Cyclic organic carbonates

Cyclic organic carbonates are industrially and synthetically important chemicals having unique properties such as high polarity and a propensity for coordinating with metal cations (Chernyak, 2006). These carbonates have been used for optical, magnetic and electronic applications (Yang and Lo, 2004).

Propylene carbonate (PC) has been used as a carrier solvent for topically applied medicines and cosmetics (Yang and Lo, 2004) while ethylene carbonate (EC) is a widely employed solvent or plasticizer for polymer-supported electrolytes. In addition, PC and EC are employed as electrolytes in lithium ion batteries (Yang and Lo, 2004). Cyclic carbonates are employed as intermediates for organic and polymeric synthesis and ingredients for pharmaceutical and fine chemicals in biomedical applications. Borner et al. (2009) have shown that cyclic carbonates can be used as solvents for rhodium-catalyzed, asymmetric hydrogenations and palladium-catalyzed, asymmetric allylic substitution reactions (Schäffner et al., 2008, Schäffner et al., 2009). The cyclic carbonate, 2-oxo-1,3-dioxolan-4-yl-(methyl-2-bromo-2-methylpropanoate), has been used as a functionalized initiator for atom transfer radical polymerization (ATRP) reactions (Palaskar et al., 2010).

Five-membered cyclic organic carbonates are very useful as polar aprotic (propensity to donate or share electrons) solvents. In addition to high solvency, they possess low flammability, high boiling and flash points, low odour levels, low vapour pressure (Verevkin et al., 2008) and low toxicities (Beyer et al., 1987). These properties make these cyclic carbonates environmentally sustainable replacements for polar aprotic solvents like dimethyl formamide (DMF) and dimethyl sulfoxide (DMSO) (Clegg et al.,

2010). Glycerol carbonate is particularly significant due to the ease of its synthesis in bulk from inexpensive raw materials such as glycerol and urea. In addition, the free hydroxyl can be modified to give other reactive functionalities.

Many derivatives of cyclic carbonates have been synthesized that contain additional functionality or reactive groups in addition to the cyclic carbonate ring. These functionalities such as hydroxyl, vinyl moieties, esters and ethers enable the properties of the molecule to be modified.

Glycerol carbonate (GC), in particular, is a versatile organic carbonate with a free hydroxyl group. Glycerol carbonate exhibits a high dielectric constant and a high boiling point (Chernyak, 2006). These properties make it an attractive candidate as a high temperature solvent. It can be used as a polar high boiling point solvent or as an intermediate in organic synthesis (glycerol carbonate ester) (Mouloungui and Pelet, 2001). It can also be used to prepare monoglycerides (Ghandi et al., 2007) and glycidol (Roberts et al., 1995). Glycerol carbonate has been used as a protecting group in carbohydrate chemistry (Desai et al., 1995), as an additive in lithium ion battery technology (Chen et al., 2003) and as a component in membranes for gas separation (Kovvali and Sirkar, 2002). It finds use in cosmetics as an emulsifier (Kahre et al., 1999) and for the production of surfactants (Mouloungui and Pelet, 2001).

In relation to this study, glycerol carbonate, for example, may provide greater resistance and performance to hyper-saline waters than even PC, when intercalated into bentonite. In addition, epoxy or styrene functionalized cyclic carbonates could be useful in the preparation of functional polymers containing a pendant cyclic carbonate.

### **1.3.2 Polymerization of cyclic carbonates**

Long term exposure of cyclic carbonate intercalated montmorillonite nanocomposites to hyper-saline leachates may result in leaching of the cyclic carbonates from the bentonite and/or these compounds may not be chemically stable, one strategy available which can be adopted to prevent the leaching of cyclic carbonates from bentonite, may be:

- Modification of cyclic carbonates into sheet or chain like functional polymers containing cyclic carbonate as a pendant group with enhanced long term stability, performance and chemical resistance. It is well known that polymers interact strongly with clay minerals (Alexandre and Dubois, 2000) when compared with small molecules.

In addition to stability, resulting carbonate-bentonite nano-complexes may have important features, such as enhanced barrier properties, affording increased potential for their use as hydraulic barriers to hyper-saline leachates.

Properties of polymers may be controlled through a combination of monomer composition, polymerization methods and post-polymer treatment. This gives polymer chemistry flexibility and versatility that enables the synthesis of a wide range of materials with different properties. The use of monomers of desired functionality is required, alternatively, monomers, which allow introduction of these functionalities through post-polymerization functionalization may be used.

#### **1.3.2.1 Ring opening polymerization of cyclic carbonates**

Cyclic carbonates can undergo ring opening polymerization to yield aliphatic polycarbonates. Polycarbonates are amorphous polymers with excellent material properties. They incorporate many desirable attributes of metals, glasses and synthetics

such as transparency, rigidity, high impact resistance and heat-deflection temperature (up to 148 °C) (Fried, 2003). These are also expected to find use in biomedical applications due to their low toxicity (Mindemark et al., 2012). Polycarbonates are currently being synthesized industrially through the phosgene process; an interfacial polymerization of phosgene and bisphenol A, using methylene chloride and water as the solvents (Kohno and Sakakura, 2009).

Six-membered cyclic carbonates are the most widely studied class of cyclic carbonate monomers because of their stability and ease of synthesis as well as suitability for ring opening polymerization (Rokicki, 2000).

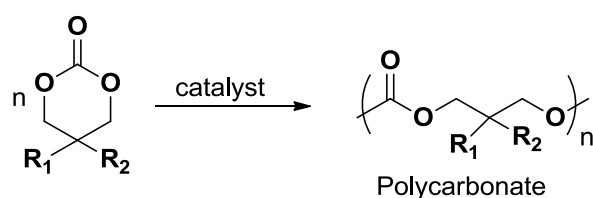


**Figure 1.4:** Ring opening polymerization of six membered cyclic carbonates.

Five-membered cyclic carbonates undergo ring opening polymerization, but with difficulty due to the higher stability of the monomer. However, ring opening polymerization of five-membered cyclic carbonates has been reported to proceed in the presence of catalysts, such as metal alkoxides (Vogdanis et al., 1990) and metal acetylacetonates, as well as metal alkyls (Soga et al., 1977). It was observed that for ethylene carbonate, no polymer was formed below 100 °C and for propylene carbonate, the polymerization did not take place significantly even at 140 °C over a few days (Soga et al., 1977, Vogdanis et al., 1990). The polymerization was always accompanied by partial decarboxylation, which exceeds more than 50 mol% and is independent of the polymerization conditions. Thus, the ring opening polymerization of 5-membered ring

alkylene carbonates fails to produce thermodynamically stable poly(alkylene carbonate)s but leads to poly(alkylene ether carbonate)s with contents of carbonate units lower than 50 mol% (Figure 1.5).

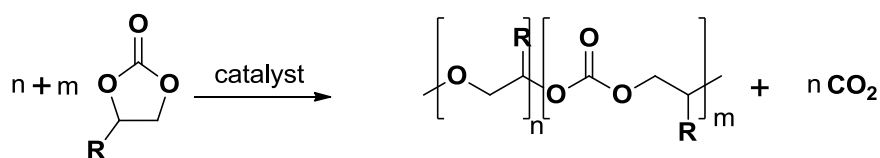


**Figure 1.5:** Ring opening polymerization of five-membered cyclic carbonates.

However, in contrast to the typical behavior of five-membered cyclic carbonates, anionic ring opening polymerization of methyl 4,6-*O*-benzylidene-2,3-*O*-carbonyl- $\alpha$ -D-glucopyranoside produced polycarbonate without any elimination of carbon dioxide at relatively low temperature (below 60 °C) (Figure 1.6) (Haba et al., 2005, Azechi et al., 2013).

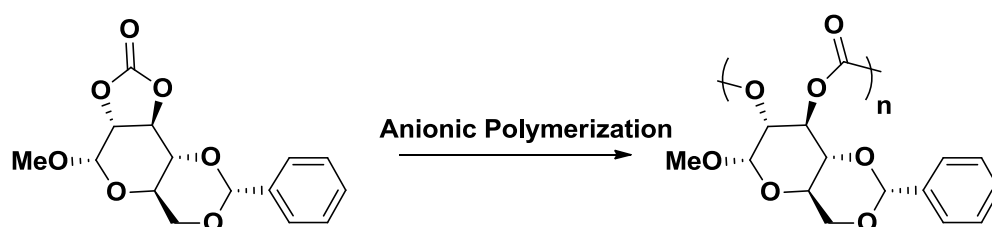


**Figure 1.6:** Anionic ring opening polymerization of methyl 4,6-*O*-benzylidene-2,3-*O*-carbonyl- $\alpha$ -D-glucopyranoside.

The unusual reactivity of the methyl 4,6-*O*-benzylidene-2,3-*O*-carbonyl- $\alpha$ ,D-glucopyranoside was revealed by performing anionic polymerization (initiated by *t*-BuOK) of five-membered cyclic carbonates fused to a cyclohexane ring, that is, the *trans*- and *cis*-cyclohexane-1,2-diyl carbonates (*trans*- and *cis*-, respectively) (Figure 1.7). Only, the *trans*- form has been found to yield polymer without elimination of carbon dioxide,

whereas, the *cis*- form has not been successfully polymerized to date (Tezuka et al., 2013). This suggests the unreactivity of the *cis*- form of the five-membered cyclic carbonate ring upon anionic polymerization conditions.

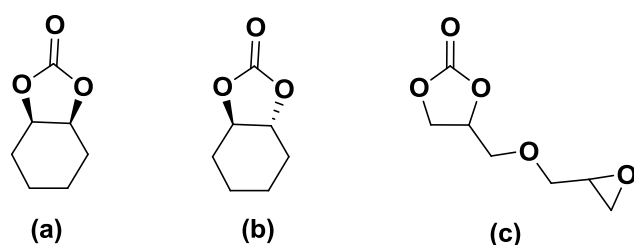


**Figure 1.7:** Structures of a) the *cis*- b) *trans*-cyclohexane-1,2-diyl carbonates and c) 4-((oxiran-2-ylmethoxy)methyl)-1,3-dioxolan-2-one.

Others have shown that the ring opening polymerization of five-membered cyclic carbonates requires a significantly higher temperature (Soga et al., 1977, Vogdanis et al., 1990) and the *cis*- cyclic carbonate functional group will be retained by employing anionic ring opening polymerization (Tezuka et al., 2013). 4-((Oxiran-2-ylmethoxy)methyl)-1,3-dioxolan-2-one (c) (Figure 1.7) could be synthesized from allyloxy glycerol carbonate (h) (Figure 1.8) and anionic ring opening conditions will possibly result in retention of five-membered cyclic carbonate and selective ring opening of epoxide moiety producing a polyether with a pendant five-membered cyclic carbonate group.

### 1.3.2.2 Polymerization with retention of five-membered cyclic carbonate moiety

One of the most common and versatile methods for preparing polymers that contain a cyclic carbonate as a pendant group is via free radical polymerization of an unsaturated monomer containing the cyclic carbonate functionality (Ochiai et al., 2005).

#### 1.3.2.2.1 Radical polymerization of unsaturated monomers with cyclic carbonate moiety

Five-membered cyclic carbonates are the most widely studied class for radical homopolymerization retaining the cyclic carbonate moiety (Clements, 2003, Rokicki and Lewandowski, 1987, Rokicki and Wojciechowski, 1990). Several cyclic carbonate containing polymers have been prepared from corresponding cyclic carbonate monomers (Figure 1.8) including vinylene carbonate (d), vinyl ethylene carbonate (e), methacrylate (f), acrylate (g), and allyloxy glycerol carbonate (h). These polymers have shown promise in a number of different applications such as thermosetting coatings (Rokicki and Wojciechowski, 1990, Rokicki and Lewandowski, 1987) and immobilization of enzymes (Chen et al., 1993).

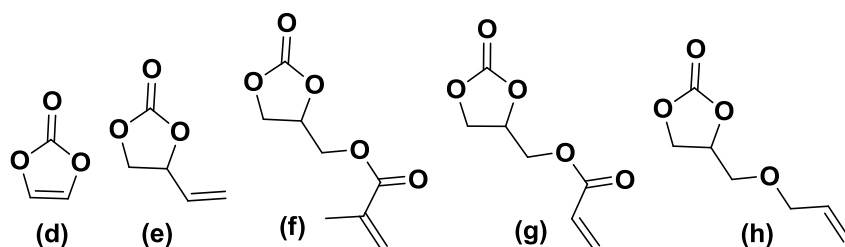


**Figure 1.8:** Cyclic carbonate monomers useful in radical polymerization.

Radical polymerization of vinylene carbonate (d) has been found to occur in the presence of dimethyl sulfoxide producing a low polymer yield (62%) (Huang et al., 1990). Vinyl ethylene carbonate (e) polymerizes using benzoyl peroxide (BPO) or azoisobutyronitrile (AIBN) with a low conversion (43%). Higher molecular weight polymer is difficult to achieve due to the degradative chain reaction that occurs during the polymerization process (Asahara et al., 1973). Methacrylate (f) and acrylate (g) derivatives are very prone to polymerization during purification steps even in the presence of inhibitor and result in formation of polymers with limited solubility in dipolar aprotic solvents (Clements, 2003). Insoluble and cross-linked polymers have been obtained by homopolymerization of methacrylate- (Fang, 1961) and acrylate- (Brosse et al., 1990) bearing cyclic carbonate, while soluble homopolymers have been reported by using well-purified monomers. 4-(((4-Vinylbenzyl)oxy)methyl)-1,3-dioxolan-2-one (i) can be readily polymerized to a polymer having a 5-membered carbonate structure in every repeating unit. Radical homopolymerization of (j) has been reported to occur in the presence of solvents, such as dimethyl formamide (DMF) and methyl ethyl ketone thereby, producing low yield of polymers (46% and 62%) (Miyata et al., 2012). Radical polymerization is the most convenient way to yield a polymer with retention of the cyclic carbonate.

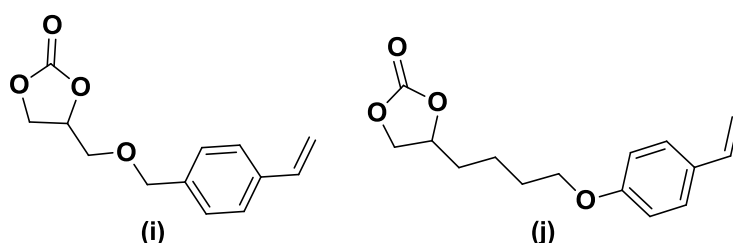


**Figure 1.9:** Styrene monomers with five-membered cyclic carbonate functionality.

In this study, 4-(((4-vinylbenzyl)oxy)methyl)-1,3-dioxolan-2-one (i) and 4-(((4-vinylbenzyl)oxy)butyl)-1,3-dioxolan-2-one (j) with a styrene functionality and a pendant five-membered cyclic carbonate (Figure 1.9) were prepared. Radical polymerizations for cyclic carbonate containing monomers discussed so far require a solvent such as dimethyl sulfoxide (DMSO) or DMF to proceed and have a further drawback of low polymer yield due to low monomer conversion. There is no literature available on radical photopolymerization of cyclic carbonate monomers such as 4-(((4-vinylbenzyl)oxy)methyl)-1,3-dioxolan-2-one (i) and 4-(((4-vinylbenzyl)oxy)butyl)-1,3-dioxolan-2-one (j). Radical photopolymerization of these monomers could be attempted with the aim of forming a polystyrene backbone with a pendant five-membered cyclic carbonate moiety.

#### **1.4 Clay mineral**

To understand the complex morphologies that occur in the cyclic carbonate/smectite nanocomposites, it is important to review the structural details of layered silicates and their properties. The term smectite encompasses a diverse group of clay minerals. Clay minerals are hydrous aluminium silicates and may be defined broadly as those minerals which dominantly make up the colloidal fraction of sediments and sedimentary rocks (Velde, 1992).

Bentonite is a soft volcanic rock initially deposited as ash in water (Clem and Doehler, 1963). Smectite is the main crystalline component of bentonite. In addition to smectite, bentonite contains variable portions of other minerals, usually quartz, feldspar, volcanic glass, gypsum, or pyrite (Clem and Doehler, 1963). Montmorillonite is a member of the

smectite group (Balogh and Laszlo, 1993, Adams, 1987) and belongs to the general family of 2:1 layered silicates (or 2:1 phyllosilicates).

The crystal lattice of montmorillonite consists in part of a layer formed from two tetrahedral sheets of silica on either side of an octahedral sheet of aluminium or magnesium (Figure 1.10) (Velde, 1992). Stacking of adjacent layers leads to a regular van der Waals gap between each layer, forming an interlayer space or gallery space. Thus a unit cell of montmorillonite (or any smectite) includes both the crystal lattice and the interlayer space (Velde, 1992). Due to isomorphous substitution within the crystal lattice (for example,  $\text{Al}^{3+}$  replaced by  $\text{Mg}^{2+}$  or  $\text{Fe}^{2+}$ ) a negative charge imbalance is created and is expressed at the layer surface (Theng, 2012). These charges are counterbalanced by alkali or alkaline earth cations situated inside the interlayer space (interlayer). In montmorillonite, sodium ions can be exchanged by any other soluble metal ion.

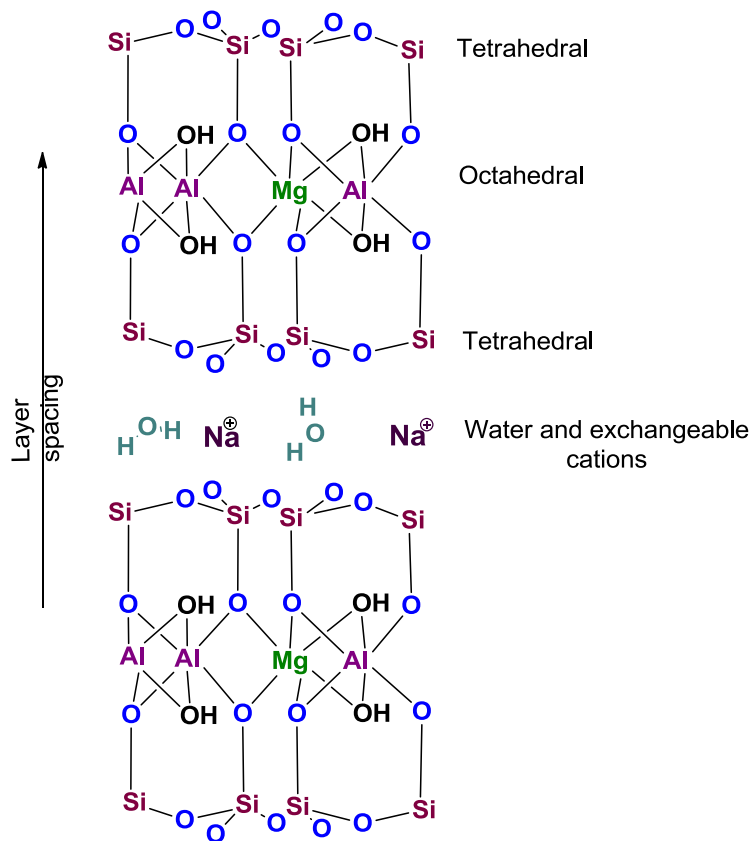


Figure 1.10: Structure of montmorillonite (Theng, 2012).

The cation exchange capacity of montmorillonite is an important factor for its popularity for use in catalysis (Nagendrappa, 2002), enabling high levels of exchange with reactive cations and to remove toxins or impurities from liquids. Exchangeable cations frequently present in unmodified montmorillonite include  $\text{Na}^+$ ,  $\text{K}^+$  and  $\text{Ca}^{2+}$  (Brigatti et al., 2013).

Montmorillonite has a characteristic high swelling capacity and adsorbs water whenever it is available. Montmorillonite hydration can occur (i) in the interlayer, (ii) as unlimited adsorption of water on internal and external surfaces, and (iii) as capillary condensation of free water in micropores. The main elements of interlayer hydration are (i) hydration of interlayer cations, (ii) interaction of clay mineral surfaces with water molecules and interlayer cations, and (iii) water activity in the clay mineral–water system (Güven, 1992). The swelling of montmorillonite is affected by the nature of the exchangeable cation in the interlayer space, the layer charge, and the Brownian swelling that occurs between two different smectite particles (Ferrage et al., 2005, Ferrage et al., 2007, Ferrage et al., 2010).

Two types of hydration complexes in the interlayer space can form: inner sphere and outer sphere. In the first case, the cation is directly connected to the clay mineral surface on one side and to a number of water molecules on the other side, whereas in outer-sphere complexes the interlayer cation is completely surrounded by water molecules and interacts with the clay mineral surface through water (Ferrage et al., 2005).

The hydration of cations present in montmorillonite imparts a hydrophilic nature to the clay surface. The sodium ions can take up water which creates interlayer spacing. Sodium bentonite is capable of swelling by up to 8 to 15 times its dry weight (Clem and Doehler, 1963).

### **1.4.1 Intercalation of organic molecules**

Intercalation of ethylene glycol (1,2-ethanediol) and glycerol (1,2,3-propanetriol) in expanding 2:1 clay minerals has been widely used for the routine identification of montmorillonite and vermiculite (Bergaya et al., 2006). Intercalation is the process of inserting organic or inorganic molecules into the interlayer of the clay mineral structure. It is well known that smectites, e.g., sodium montmorillonite and calcium montmorillonite, can be treated with organic molecules, in which the organic molecules are intercalated between adjacent, planar silicate layers, thereby substantially increasing the interlayer (interlaminar) spacing between the adjacent silicate layers (Theng, 1974, Lagaly et al., 2013). Montmorillonite-organic intercalation compounds have been widely investigated and the mechanisms of clay-organic interactions have been reported (Theng, 1974).

Inorganic exchangeable cations of clay can be replaced by organic cations through exchange reactions. In most cases, the organic bases are aliphatic or aromatic amines (Lagaly, 1986, Weiss, 1963a) and nitrogen containing heterocycles or macrocycles (Lailach and Brindley, 1969). The bonding mechanism between the organic cation and charged clay layer is primarily electrostatic but van der Waal's attraction forces between organic species and the silicate surface, as well as between adjacent organic species themselves add to adsorption forces. Intercalation of neutral organic molecules into smectites was first studied to aid the routine identification of montmorillonite by MacEwan (Brindley et al., 1946, MacEwan, 1948, MacEwan, 1944) and Bradley (1945). Neutral molecules penetrate into the interlayer space of smectites by adsorption. Adsorption of neutral molecules by smectites is driven by various chemical interactions such as hydrogen bonding, ion-dipole interaction, co-ordination bonds, acid-base

reaction, charge transfer and Van der Waal's forces (Breen, 2002, Dultz, 2002, Lagaly, 1984, Lagaly and Koester, 1993, Theng, 1974, Weiss, 1963b). Exchange of interlayer cations, adsorption of polar molecules through ion-dipole interactions, hydrogen bonding, and protonation are all suggested intercalation mechanisms. Exchangeable cations (via co-ordination complexes) and surface oxygen (H-bonding with O-H and NH<sub>2</sub> containing compounds) of tetrahedral sheets are the possible adsorption sites in smectites (Sandi, 2005).

Interlayer water also affects the adsorption of organics by either facilitating or inhibiting their penetration. Organic molecules may displace or compete with water for the co-ordination sites around the exchangeable cation and result in one of the following phenomena:

- 1) Organic molecules replace interlayer water and co-ordinate directly with the exchangeable cation. Polar molecules such as alcohols, amines, amides, ketones, nitriles, crown ethers and urea have been reported to form intercalation complexes with smectites (Rausell-Colom and Serratosa, 1987, Theng, 1974, Dultz, 2002).
- 2) Organic molecules can occupy a site in the second hydration sphere around the cation via bridging water molecules. This type of bridging has also been observed for pyridine (Farmer and Mortland, 1966) and benzonitrile sorbed onto montmorillonite (Serratosa, 1968).
- 3) Adsorption may occur by protonation of organic bases when adsorbed as neutral molecules into smectite. The available proton sources in Na-montmorillonite are interlayer water molecules or short-chain alkylammonium saturated clays. The most common mechanism is transfer of protons from interlayer water to

adsorbed organic molecules. Adsorption of aliphatic amines in montmorillonite undergoes this mechanism (Calvet and Et, 1964).

In the specific case of cyclic carbonates, phenomena 1 and 2 above are both important. Unmodified clays are compatible (Diakoumakos and Kotzev, 2013) with cyclic carbonates, because unmodified montmorillonite layers are generally hydrophilic. The water miscible cyclic carbonates are able to penetrate the interlayer of the clay (Onikata et al., 1999a, Diakoumakos and Kotzev, 2013). Cyclic carbonate, such as propylene carbonate (PC) has been intercalated successfully within montmorillonite layers as studied by Onikata et al. (1999b) and Katsumi et al.(2008b). According to Onikata et al., the carbonyl group coordinating to the interlayer cations via water molecules resulted in a shift of the  $\nu(\text{C=O})_{\text{str}}$  stretching band by  $<20 \text{ cm}^{-1}$  (Figure 1.2). However, the band showed a much greater red-shift of  $>30 \text{ cm}^{-1}$  if the  $\nu(\text{C=O})_{\text{str}}$  group coordinated directly to the interlayer cations (Onikata et al., 1999a, Onikata et al., 2000). The relatively small shifts of the  $\nu(\text{C=O})_{\text{str}}$  were observed by (Onikata et al., 1999a) for the PC-montmorillonite complexes with different interlayer cations suggesting that the propylene carbonate molecules are bound to the interlayer cations through bridging water molecules. The water molecules are so strongly bound to the interlayer cations in the complexes that heating at  $105 \text{ }^\circ\text{C}$  cannot remove all the water molecules (Onikata et al., 1999a).

Propylene carbonate/bentonite has been found to maintain a low hydraulic conductivity value up to a molar concentration of 1M NaCl. However, when the molar concentration of the NaCl solution is  $>1\text{M}$ , the hydraulic conductivity is nearly identical to that of bentonite (Katsumi et al., 2008a). Propylene carbonate (PC) can easily form a hydration shell by forming intermolecular hydrogen bonds between the outer limits of the

hydration shells of the exchange cations. PC thereby can expand the space between adjacent clay layers. Propylene carbonate/bentonite activates the osmotic swelling of bentonite in fresh water as well as electrolytic chemical solutions (1M NaCl), whereas the unmodified sodium bentonite cannot sufficiently swell in these latter solutions.

Failure of PC/bentonite upon exposure to hyper-saline solutions (>1M) can be addressed by using glycerol carbonate/bentonite as an alternative. Glycerol carbonate can be obtained in bulk from cheap raw materials such as glycerol and urea, exhibits a high dielectric constant and a higher boiling point than PC (Chernyak, 2006). The free hydroxyl group in glycerol carbonate may assist in maintaining swollen states (may be useful in retention of water) in high saline conditions and may be modified to give other reactive functionalities.

#### **1.4.2 Polymer intercalated clay complexes: nanocomposites**

The interaction of clay minerals with organic macromolecules has received considerable attention because of the use of clays and polymers in many industrial applications and in soil conditioning (Theng, 1982). The addition of clay (bentonite) particles to a polymer strengthens the material and can also improve fire retardant and gas barrier properties (Okada and Usuki, 2006, Rao and Pochan, 2007).

As a result of the nanometer-sized dispersion of layered silicate within a polymer matrix, plastics made up of polymer layered silicate nanocomposites usually exhibit improved mechanical properties, thermal stability and gas barrier properties compared to the original polymers alone (Darlington et al., 2004). At high clay to polymer ratios, geotextiles containing polyacrylamide and/or a polyacrylic acid have been patented to

provide a hydraulic barrier with excellent low hydraulic conductivity (Darlington et al., 2004).

Generally, the amount of polymer dispersion in the clay mineral component determines the structure of the nanocomposites. Two main types of polymer–clay morphologies can be obtained depending upon the interaction between the clay and the polymer matrix: intercalated and exfoliated (Alexandre and Dubois, 2000). The intercalated structure is obtained from the penetration of polymer chains into the galleries of clay, ideally resulting in alternate layers of polymer and inorganic layers (Figure 1.11). An exfoliated structure results when the individual silicate layers are completely separated from the bulk mineral phase and are thus dispersed randomly within the polymer matrix.

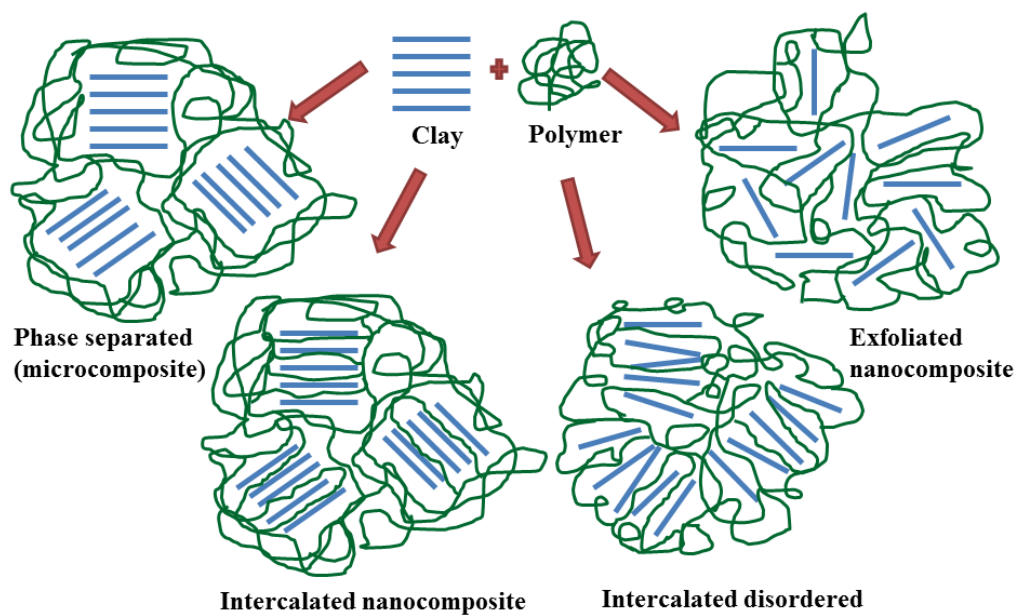


**Figure 1.11:** Type of composites arising from interaction of clay and polymers (Alexandre and Dubois, 2000).

Moreover, intermediate structures in which silicates are partially exfoliated can be obtained (Alexandre and Dubois, 2000). In contrast, when the polymer and silicate are

immiscible, the layers do not separate and the components exist as phase-separated physical mixtures.

Direct intercalation is a common method to intercalate neutral and polar polymers such as poly(vinyl alcohol) (PVA) (Greenland, 1963, Ogata et al., 1997) and poly(ethylene oxide) (PEO) (Ruiz-Hitzky and Aranda, 1990). The main driving force for intercalation of these compounds is ion-dipole interactions between the interlayer cation and a polar unit such as oxygen present in the polymer. The presence of interlayer water may result in other types of mechanisms for polymer-clay interaction, such as hydrogen bonding and water bridging. Similarly, the oxygen atoms of the clay silicate surface may form H-bonds with hydrogens of polymer aliphatic chains. Intercalation of polyoxyethylenes into smectite has been achieved by direct adsorption. Using this method, intercalation only occurs for certain polymer/solvent pairs, such as polymers with little or no polarity into layered structures.

Ruiz-Hitzky et al. (1978) have investigated the intercalation of macrocyclic polyethers into smectites for their application as solid electrolytes and ion selective membranes (Aranda et al., 1994, Ruiz-Hitzky and Casal, 1978, Ruiz-Hitzky et al., 2001). Aranda et al. (1994) and Ruiz-Hitzky et al. (1978, 2001) have shown that the polyether can be potentially intercalated into unmodified sodium smectite. Use of various polar solvents (water, methanol and mixtures (1:1) of water/methanol and methanol/acetonitrile) has caused swelling of sodium montmorillonite provoking cracking of the films.

Polyvinyl alcohols have been intercalated into a variety of montmorillonites in their sodium, calcium and cesium forms (Greenland, 1963). Adsorption of polyvinyl alcohols occurred primarily on the external surfaces of clay crystallites (Greenland, 1963). Hydrogen bonding was involved between hydroxyls of the polymer and oxygen of

montmorillonite surface for the attachment. More recently, Strawhecker and Manias (2000) used a solution intercalation method in an attempt to produce PVA/montmorillonite nanocomposites films. Elevated temperature was needed to dissolve the polymer in the solvent and a 20 wt% clay containing nanocomposite formed, revealed the co-existence of silicate layers in the intercalated and exfoliated states.

Formation of polymer intercalated compounds by *in-situ* polymerization of various monomers, such as vinyl acetate and acrylonitrile, was first studied by Blumstein (1961) employing benzoyl peroxide as a catalyst. Long reaction times were needed to produce moderate yield of polymeric product at 100 °C. This method involves intercalation of the precursor monomer followed by polymerization in the interlayer region of clay. In general, monomers showing affinity to be adsorbed by smectite can undergo *in-situ* polymerization.

The preparation of polymer-clay nanocomposites with polymers of low polarity, such as polystyrene, requires either the modification of interlayer space of the clay or addition of functional groups to the polymer to facilitate intercalation.

- Organophilic clays are examples of modified clays formed by exchanging quaternary ammonium compounds onto silicate layers, changing the generally hydrophilic layer silicate surface into a generally hydrophobic one, which is then compatible with conventional polymers (Wang et al., 2003). Polystyrene-organoclay nanocomposites can be obtained by reacting vinylbenzyltrimethylammonium clay with styrene monomer (Moet and Akelah, 1993) by an *in-situ* approach. Although the polystyrene was well intercalated, one drawback in this procedure was that the macromolecule

produced was not pure polystyrene, but rather a copolymer between styrene and vinylbenzyltrimethylammonium cations.

- Another approach used polystyrene with grafted functionalities that interacted either with the surface of clay mineral or with the exchangeable ions. Polystyrene containing a crown ether group (i.e., poly(4'-vinylbenzo-15-crown-5)) was intercalated on muscovite mica (Herzog et al., 1994). The crown ether coordinates to the external surface of the mica and hence, the polymer was attached to the surface. No adsorption of low molecular weight crown ether was found.

Sodium montmorillonite has been intercalated with carboxylate salts to prepare carboxylate clays (Rousseaux et al., 2010). These carboxylate clays have been used to synthesize polypropylene-graft-maleic anhydride/clay nanocomposites. Intercalated and exfoliated polypropylene carbonate/montmorillonite complexes have been prepared and their thermal decomposition temperature, storage modulus and Young's modulus of nanocomposites were improved compared to those of polypropylene carbonate (Rousseaux et al., 2010). Polypropylene carbonate smectite nanocomposites have been prepared to improve thermal and mechanical properties of polypropylene carbonate (Zhang et al., 2008).

A very low clay mineral filler content (5 wt% or less) has been used to prepare various polymer-clay nanocomposites mentioned above which resulted in complex mixtures and morphologies of nanocomposites.

## 1.5 Research Approach

Propylene carbonate/sodium smectite is the only studied candidate, prior to this work, shown to improve barrier properties of GCLs. Currently, there is no literature available for polymeric nanocomposites containing polymers bearing a pendant five-membered cyclic carbonate moiety. The research reported herein will utilize the cyclic carbonate based monomers for the modification of smectite interactions with high salinity water. Increased smectite interactions would be achieved by using polymers with pendant cyclic carbonate functionality and subsequently, significant enhancement in nanocomposite properties may be possible. Unmodified smectite will be compatible for preparation of polyether nanocomposites and polystyrene containing pendant functionality such as five-membered cyclic carbonate nanocomposites (cyclic carbonate grafted functionality to ensure affinity between polymer and smectite).

Two potential approaches that could be used for the preparation of polymeric clay nanocomposites have been identified as:

- Direct intercalation of the polymer with five-membered cyclic carbonate functionality by adsorption from solution.
- *In-situ* intercalative polymerization in the interlayer spaces, which requires previous intercalation of monomer precursors containing five-membered cyclic carbonate moiety into sodium smectite and a second activation step to induce polymerization.

Thus, intercalation of five-membered cyclic carbonate containing polymers such as polyether and polystyrene has potential to provide an efficient way to improve the properties of polymers (thermal and mechanical properties) as well as properties of

polymer-clay nanocomposites useful as barriers with low hydraulic conductivity to saline leachates.

## 1.6 Hypothesis and objectives

The hypothesis tested was that glycerol carbonate and its derivatives can be intercalated into sodium smectite and form stable intercalates. Furthermore, a selection of polymers containing the five-membered cyclic carbonate ring can be more effective intercalates. These carbonate-bentonite complexes are expected to resist osmotic dehydration of the reactive montmorillonite, due to their ability to maintain a crystalline swollen state in hyper-saline solutions. This hypothesis was addressed through the following research objectives:

- To develop a green method for producing glycerol carbonate starting from inexpensive raw materials such as glycerol and urea. To apply the new methodology for the synthesis of glycerol carbonate to other polyols to obtain respective cyclic carbonates employing zinc monoglycerolate as a catalyst in conjunction with a transesterification approach.
- To examine the interaction and behavior of glycerol carbonate smectite intercalates and to carry out stability studies of glycerol carbonate at standard temperature and pressure in laboratory conditions. To prepare intercalated complexes of other cyclic carbonates with Na-smectite.
- To convert glycerol carbonate into a variety of derivatives with additional functionality in order to generate cyclic carbonate derivatives for intercalation and/or polymerization by nucleophilic substitution reactions of selected cyclic

carbonates. To synthesize homopolymers containing cyclic carbonate moieties by ring opening and radical photopolymerization in laboratory conditions.

- To synthesize polymer clay intercalates by solution intercalation and to examine the *in-situ* polymerization of cyclic organic carbonate monomers within the bentonite interlayers to yield novel task-specific intercalates and to evaluate their properties.

It should be recognized that while this study focuses on the application of cyclic carbonate/bentonite complexes for use as hydraulic barriers to hyper-saline leachates, the nanocomposites have many unique characteristics which may prove to have use in other applications, from fields as diverse as plastic reinforcement to flame retardants. It is hoped that this research will form the basis of further exploratory applications of this novel class of organo-clay nanocomposites.

## 1.7 Thesis overview

The thesis has been divided into 7 chapters, **Chapter 1** introduces the scope of research and describes previous research related to the propylene carbonate intercalated complexes and polymerization of pendant cyclic carbonate precursors along with polypropylene carbonate nanocomposites based on smectite clays.

**Chapter 2** describes the synthesis of glycerol carbonate using different methods such as transesterification and glycerolysis of urea using different catalysts. A green synthesis method employing zinc monoglycerolate (ZMG) as a catalyst was developed for synthesis of glycerol carbonate from glycerol and urea. This chapter also describes the synthesis of various polyol carbonates starting from various polyols employing the ZMG approach introduced earlier in chapter 2. Glycerol carbonate and cyclic carbonates

synthesized in this chapter was used for the intercalation into Na-smectite which will be described in chapter 3.

**Chapter 3** focuses on the intercalation of glycerol carbonate in sodium smectite. This chapter describes the effect of glycerol carbonate concentration on gallery height of Na-smectite. Subsequently, the interaction of glycerol carbonate with Na-smectite was studied by detailed FTIR spectroscopy investigations. In addition, this chapter also describes preparation of cyclic carbonate intercalated complexes with Na-smectite. The effect of molecular length of various cyclic carbonates on gallery height of Na-smectite was also evaluated.

**Chapter 4** focuses on derivatization of glycerol carbonate. Various derivatives of glycerol carbonate such as ester, tosyl and bromo were prepared for intercalation into Na-smectite. O-alkylation of glycerol carbonate and relevant cyclic carbonates were performed to obtain monomeric precursors. This chapter also describes the polymerization of pendant five membered cyclic carbonate containing monomers. We focus on the synthesis of two types of polymers, polyether and polystyrene containing a pendant cyclic carbonate obtained via ring opening polymerization of epoxide and radical photopolymerization.

In **Chapter 5**, nanocomposites of the synthesized polymers with Na-smectite were successfully prepared by *in-situ* and solution intercalation approach and characterized.

**Chapter 6** contains full experimental details concerning the chemical syntheses and analytical protocols used in the project.

The final chapter, **Chapter 7**, draws conclusions of the research and suggests potential avenues for future research on the topic of polyol carbonates and their intercalation into Na-smectite.

## 1.8 References

- ADAMS, J. M. 1987. Synthetic organic chemistry using pillard, cation-exchanged and Acid-treated Montmorillonite catalysts-a review. *Applied Clay Science*, 2, 309-342.
- ALEXANDRE, M. & DUBOIS, P. 2000. Polymer-layered silicate nanocomposites: preparation, properties and uses of a new class of materials. *Materials Science and Engineering: R: Reports*, 28, 1-63.
- AN, H., ZHAO, X., GUO, L., JIA, C., YUAN, B. & WANG, Y. 2012. Synthesis of diethyl carbonate from ethyl carbamate and ethanol over ZnO-PbO catalyst. *Appl. Catal., A*, 433-434, 229-235.
- ARANDA, P., CASAL, B., FRIPIAT, J. J. & RUIZ-HITZKY, E. 1994. Intercalation of macrocyclic compounds (crown ethers and cryptands) into 2:1 type phyllosilicates; Stability and calorimetric Study. *Langmuir*, 10, 1207-1212.
- ASAHARA, T., SENO, M. & IMAI, T. 1973. Polymerization of vinyl ethylene carbonate and polymer reaction. *Seisan-Kenkyu*, 25, 297-299.
- AZECHI, M., MATSUMOTO, K. & ENDO, T. 2013. Anionic ring-opening polymerization of a five-membered cyclic carbonate having a glucopyranoside structure. *Journal of Polymer Science Part A: Polymer Chemistry*, 51, 1651-1655.
- BALOGH, M., LASZLO, P. 1993. *Organic chemistry using clays*, Berlin, Springer-Verlag.
- BERGAYA, F., THENG, B. K. G. & LAGALY, G. 2006. *Handbook of Clay Science*, UK, Elsevier Ltd.
- BEYER, K. H. JR., BERGFELD, W. F., BERNDT, W. D., CARLTON, W.H., HOFFMAN, D. K., SCHROETER, A. L. & SHANK, R. C. 1987. Final Report on the Safety Assessment of Propylene Carbonate. *International Journal of Toxicology*, 6, 23-51.

- BLUMSTEIN, A. 1961. Polymerization in adsorbed layers I. *Bull. Soc. Chim. Fr.*, 899-905.
- BOUAZZA, A. & GATES, W. P. 2014. Overview of performance compatibility issues of GCLs with respect to leachates of extreme chemistry. *Geosynthetics International* [Online], 21.  
<http://www.icevirtuallibrary.com/content/article/10.1680/gein.14.00006>.
- BRADLEY, W. F. 1945. Molecular Associations between Montmorillonite and Some Polyfunctional Organic Liquids<sup>1</sup>. *Journal of the American Chemical Society*, 67, 975-981.
- BREEN, C. 2002. Organo-Clay Complexes and Interactions: edited by S. Yariv and H. Cross. Marcel Dekker New York, 2002, viii + 688 pages. *Clays and Clay Minerals*, 50, 533-534.
- BRIGATTI, M. F., GALÁN, E. & THENG, B. K. G. 2013. Chapter 2 - Structure and Mineralogy of Clay Minerals. In: FAÏZA, B. & GERHARD, L. (eds.) *Developments in Clay Science*. Elsevier.
- BRIGNOU, P., PRIEBE, G. M., CASAGRANDE, O., CARPENTIER, J.-F. & GUILLAUME, S. M. 2010. Polycarbonates Derived from Green Acids: Ring-Opening Polymerization of Seven-Membered Cyclic Carbonates. *Macromolecules*, 43, 8007-8017.
- BRINDLEY, G. W., ROBINSON, K. & MACEWAN, D. M. C. 1946. The clay minerals halloysite and metahalloysite. *Nature (London, U. K.)*, 157, 225-226.
- BROSSE, J.-C., COUVRET, D., CHEVALIER, S. & SENET, J.-P. 1990. Monomères acryliques à fonction carbonate cyclique, 1. Synthèse et polymérisation. *Die Makromolekulare Chemie, Rapid Communications*, 11, 123-128.
- CALVET, R. & ET, A. 1964. Constituent protons, free protons, and adsorbed water [in clay minerals]. *Bull. Groupe Fr. Argiles*, 14, 59-98.

- CHEN, C.-H., HYUNG, Y. E., VISSERS, D. R. & AMINE, K. 2003. Lithium ion battery with improved safety. *US Patent 20030157413A1*.
- CHEN, G., VAN DER DOES, L. & BANTJES, A. 1993. Investigations on vinylene carbonate. V. Immobilization of alkaline phosphatase onto LDPE films cografed with vinylene carbonate and N-vinyl-N-methylacetamide. *Journal of Applied Polymer Science*, 47, 25-36.
- CHERNYAK, Y. 2006. Dielectric Constant, Dipole Moment, and Solubility Parameters of Some Cyclic Acid Esters. *Journal of Chemical & Engineering Data*, 51, 416-418.
- CLEGG, W., HARRINGTON, R. W., NORTH, M., PIZZATO, F. & VILLUENDAS, P. 2010. Cyclic carbonates as sustainable solvents for proline-catalysed aldol reactions. *Tetrahedron: Asymmetry*, 21, 1262-1271.
- CLEM, A. G. & DOEHLER, R. W. 1963. Industrial applications of bentonite. *Clays Clay Minerals, Proc. Natl. Conf. Clays Clay Minerals*, 10, 272-283.
- CLEMENTS, J. H. 2003. Reactive Applications of Cyclic Alkylene Carbonates. *Ind. Eng. Chem. Res.*, 42, 663-674.
- DARLINGTON, J. W., DOTLICH, N. A., MATTERN, C. M., CARRIKER, R. W. & CLAREY, M. W. 2004. Hydraulic barrier and its formation. *US Patent 20040058077 A1*.
- DESAI, T., GIGG, J. & GIGG, R. 1995. Cyclic carbonates as protecting groups in cyclitol chemistry. *Carbohydr. Res.*, 277, C5-C7.
- DIAKOUMAKOS, C. D. & KOTZEV, D. L. 2013. Non-isocyanate-based polyurethane and hybrid polyurethane-epoxy nanocomposite polymer compositions. *US Patent 8450413 B2*.
- DU, J., SHI, J., LI, Z., LIU, Z., FAN, X. & TAO, C. 2012. Ionic liquid mediated CO<sub>2</sub> activation for DMC synthesis. *J. Nat. Gas Chem.*, 21, 476-479.

- DULTZ, S. 2002. *Organo-Clay Complexes and Interactions* Edited by S. Yariv and H. Cross. *J. Plant Nutr. Soil Sci.*, 165, 659.
- FAN, G.-Z., ZHAO, H.-T., DUAN, Z.-X., FANG, T., WAN, M.-H. & HE, L.-N. 2011. A novel method to synthesize diphenyl carbonate from carbon dioxide and phenol in the presence of methanol. *Catal. Sci. Technol.*, 1, 1138-1141.
- FANG, J. C. 1961. Polymerizable esters of acrylic and methacrylic acid and polymers thereof. *US Patent 2967173*.
- FARMER, V. C. & MORTLAND, M. M. 1966. An infrared study of the coordination of pyridine and water to exchangeable cations in montmorillonite and saponite. *J. Chem. Soc. A*, 344-351.
- FERRAGE, E., LANSON, B., MALIKOVA, N., PLANÇON, A., SAKHAROV, B. A. & DRITS, V. A. 2005. New Insights on the Distribution of Interlayer Water in Bi-Hydrated Smectite from X-ray Diffraction Profile Modeling of 00l Reflections. *Chemistry of Materials*, 17, 3499-3512.
- FERRAGE, E., LANSON, B., MICHOT, L. J. & ROBERT, J.-L. 2010. Hydration Properties and Interlayer Organization of Water and Ions in Synthetic Na-Smectite with Tetrahedral Layer Charge. Part 1. Results from X-ray Diffraction Profile Modeling. *The Journal of Physical Chemistry C*, 114, 4515-4526.
- FERRAGE, E., LANSON, B., SAKHAROV, B. A., GEOFFROY, N., JACQUOT, E. & DRITS, V. A. 2007. Investigation of dioctahedral smectite hydration properties by modeling of X-ray diffraction profiles: Influence of layer charge and charge location. *American Mineralogist*, 92, 1731-1743.
- FRIED, J. R. 2003. *Polymer science and technology*, New Jersey, Prentice Hall.

- GATES, W. P. 2004. Crystalline swelling of organo-modified clays in ethanol–water solutions. *Applied Clay Science*, 27, 1-12.
- GATES, W. P., BOUAZZA, A. & CHURCHMAN, G. J. 2009. Bentonite Clay Keeps Pollutants at Bay. *Elements*, 5, 105-110.
- GATES, W. P., NEFIODOVAS, A. & PETER, P. 2004. Permeability of an Organo-Modified bentonite to Ethanol-Water solutions. *Clays and Clay Minerals*, 52, 192-203.
- GHANDI, M., MOSTASHARI, A., KAREGAR, M. & BARZEGAR, M. 2007. Efficient synthesis of  $\alpha$ -monoglycerides via solventless condensation of fatty acids with glycerol carbonate. *J. Am. Oil Chem. Soc.*, 84, 681-685.
- GIANNOCCARO, P., DANIELE, C., SALVATORE, D., ERNESTO, M., EUGENIO, Q. & MICHELE, A. 2006. Interaction of PdCl<sub>2</sub>-2-( $\beta$ -diphenylphosphine)ethylpyridine Complex with Diols and CO: Synthesis of New Alkoxy carbonyl Complexes, Key Intermediates to Cyclic Carbonates. *Organometallics*, 25, 2872-2879.
- GREENLAND, D. J. 1963. Adsorption of poly(vinyl alcohols) by montmorillonite. *J. Colloid Sci.*, 18, 647-64.
- GÜVEN, N. 1992. Molecular aspects of clay-water interactions Clay-Water Interface and Its Rheological Implications, *CMS Workshop Lectures*, Güven, N., Pollastro R. M., (Eds.), 1-80.
- HABA, O., TOMIZUKA, H. & ENDO, T. 2005. Anionic Ring-Opening Polymerization of Methyl 4,6-O-Benzylidene-2,3-O- carbonyl- $\alpha$ -d-glucopyranoside: A First Example of Anionic Ring-Opening Polymerization of Five-Membered Cyclic Carbonate without Elimination of CO<sub>2</sub>. *Macromolecules*, 38, 3562-3563.
- HERZOG, E., CASERI, W. & SUTER, U. W. 1994. Adsorption of polymers with crown ether substituents on muscovite mica. *Colloid Polym. Sci.*, 272, 986-90.

- HIGGINS, J., ALOISI, J., WANDA, H. & ZHAO, W. 2001. *Environmental aspects of phosphate and potash mining*, Paris, France, UNEP and IFA.
- HORNSEY, W. P., SCHEIRS, J., GATES, W. P. & BOUAZZA, A. 2010. The impact of mining solutions/liquors on geosynthetics. *Geotextiles and Geomembranes*, 28, 191-198.
- HUANG, J., CHEN, G., TIJSMAN, E., VAN DER DOES, L. & BANTJES, A. 1990. Investigations on vinylene carbonate. I. Preparation and properties of poly(vinylene carbonate). *Chin. J. Polym. Sci.*, 8, 197-203.
- JO, H. Y., BENSON, C. H., SHACKELFORD, C. D., LEE, J.-M. & EDIL, T. B. 2005. Long-Term Hydraulic Conductivity of a Geosynthetic Clay Liner Permeated with Inorganic Salt Solutions. *Journal of Geotechnical and Geoenvironmental Engineering*, 131, 405-417.
- KAHRE, J., LOEHL, T., TESMANN, H. & HENSEN, H. 1999. Glycerin carbonate as emulsifier in cosmetic preparations. *DE Patent 19756454C1*.
- KATSUMI, T., ISHIMORI, H. & FUKAGAWA, R. 2008. Evaluating methods to modify the chemical resistance of geosynthetic clay liners. *Proceedings of the 4th Asian Regional Conference on Geosynthetics*, 17-20 June, Shanghai, China. 526-531.
- KATSUMI, T., ISHIMORI, H., ONIKATA, M. & FUKAGAWA, R. 2008b. Long-term barrier performance of modified bentonite materials against sodium and calcium permeant solutions. *Geotextiles and Geomembranes*, 26, 14-30.
- KATSUMI, T., ONIKATA, M., HASEGAWA, S., LIN, L.-C., KUNDO, M. & KAMON, M. 2001. Chemical Compatibility of Modified Bentonite Permeated with Inorganic Chemical solutions. In: YONG, R. N. & THOMAS, H. R. (eds.) *Geoenvironmental Engineering: Geoenvironmental Impact management*. London: Thomas Telford Ltd.

- KOHNO, K. & SAKAKURA, T. 2009. Catalytic Transformation of Carbon Dioxide to Organic Carbonates. *Journal of Synthetic Organic Chemistry, Japan*, 67, 921-933.
- KONDO, M. 1996. Method of activation of clay and activated clay. *US Patent 5573583*.
- KOVVALI, A. S. & SIRKAR, K. K. 2002. Carbon Dioxide Separation with Novel Solvents as Liquid Membranes. *Ind. Eng. Chem. Res.*, 41, 2287-2295.
- LAGALY, G. 1984. Clay-organic interactions. *Philos. Trans. R. Soc. London, Ser. A*, 311, 315-332.
- LAGALY, G. 1986. Interaction of alkylamines with different types of layered compounds. *Solid State Ionics*, 22, 43-51.
- LAGALY, G. & KOESTER, H. M. 1993. Clays and clay minerals. *Steinkopff*, 1-32.
- LAGALY, G., OGAWA, M. & DEKANY, I. 2013. Clay mineral-organic interactions. *Dev. Clay Sci.*, 5, 435-505.
- LAILACH, G. E. & BRINDLEY, G. W. 1969. Clay-organic studies. XV. Specific co-absorption of purines and pyrimidines by montmorillonite. *Clays Clay Miner.*, 17, 95-100.
- MACEWAN, D. M. C. 1944. Identification of the montmorillonite group of minerals by x-rays. *Nature (London, U. K.)*, 154, 577-578.
- MACEWAN, D. M. C. 1948. Complexes of clays with organic compounds. I. Complex formation between montmorillonite and halloysite and certain organic liquids. *Trans. Faraday Soc.*, 44, 349-367.
- MINDEMARK, J., TABATA, Y. & BOWDEN, T. 2012. Low Charge Density Cationic Polymers for Gene Delivery: Exploring the Influence of Structural Elements on in vitro Transfection. *Macromolecular Bioscience*, 12, 840-848.

- MIYATA, T., MATSUMOTO, K., ENDO, T., YONEMORI, S. & WATANABE, S. 2012. Synthesis and radical polymerization of styrene-based monomer having a five-membered cyclic carbonate structure. *J. Polym. Sci., Part A: Polym. Chem.*, 50, 3046-3051.
- MOET, A. S. & AKELAH, A. 1993. Polymer-clay nanocomposites: polystyrene grafted onto montmorillonite interlayers. *Mater. Lett.*, 18, 97-102.
- MOULOINGUI, Z. & PELET, S. 2001. Study of the acyl transfer reaction: Structure and properties of glycerol carbonate esters. *European Journal of Lipid Science and Technology*, 103, 216-222.
- NAGENDRAPPA, G. 2002. Organic synthesis using clay catalysts: Clays for "green chemistry". *Resonance*, 7, 64-77.
- OCHIAI, B., MATSUKI, M., NAGAI, D., MIYAGAWA, T. & ENDO, T. 2005. Radical polymerization behavior of a vinyl monomer bearing five-membered cyclic carbonate structure and reactions of the obtained polymers with amines. *Journal of Polymer Science Part A: Polymer Chemistry*, 43, 584-592.
- OGATA, N., KAWAKAGE, S. & OGIHARA, T. 1997. Poly(vinyl alcohol)-clay and poly(ethylene oxide)-clay blends prepared using water as solvent. *J. Appl. Polym. Sci.*, 66, 573-581.
- OKADA, A. & USUKI, A. 2006. Twenty years of polymer-clay nanocomposites. *Macromolecular materials and engineering*, 291, 1449-1476.
- ONIKATA, M., KONDO, M. & KAMON, M. 1996. Development and characterization of a multiswellable bentonite. *Environmental Geotechnics. Proc. 2nd Congress Environmental Geotechnics*, 587-590.

- ONIKATA, M., KONDO, M., HAYASHI, N. & YAMANAKA, S. 1999a. Complex Formation of Cation-Exchanged Montmorillonites with Propylene Carbonate: Osmotic Swelling in Aqueous Electrolyte Solutions. *Clays and Clay Minerals*, 47, 672-677.
- ONIKATA, M., KONDO, M. & YAMANAKA, S. 1999b. Swelling of Formamide-Montmorillonite Complexes in Polar Liquids. *Clays and Clay Minerals*, 47, 678-681.
- ONIKATA, M., FUJITA, K., KONDO, M. & YAMANAKA, S. 2000. Complex formation of homoionic montmorillonites with propylene carbonate and osmotic swelling in aqueous electrolyte solutions. *Mol. Cryst. Liq. Cryst. Sci. Technol., Sect. A*, 341, 345-350.
- ONIKATA, M. 2002. General Review (Japanese), Swelling properties of layered clay mineral montmorillonite and interaction with organic compounds. *Hyomen*, 40, 203-214.
- PALASKAR, D. V., SANE, P. S. & WADGAONKAR, P. P. 2010. A new ATRP initiator for synthesis of cyclic carbonate-terminated poly(methyl methacrylate). *Reactive and Functional Polymers*, 70, 931-937.
- PEARSON, D. M., CONLEY, N. R. & WAYMOUTH, R. M. 2011. Palladium-catalyzed carbonylation of diols to cyclic carbonates. *Adv. Synth. Catal.*, 353, 3007-3013.
- PYO, S.-H. & HATTI-KAUL, R. 2012. Selective, Green Synthesis of Six-Membered Cyclic Carbonates by Lipase-Catalyzed Chemospecific Transesterification of Diols with Dimethyl Carbonate. *Adv. Synth. Catal.*, 354, 797-802.
- RAO, Y. & POCHAN, J. M. 2007. Mechanics of polymer-clay nanocomposites. *Macromolecules*, 40, 290-296.

- RAUSSELL-COLOM, J. A. & SERRATOSA, J. M. 1987. Reactions of clays with organic substances. *Mineral. Soc. Monogr.*, 6, 371-422.
- ROBERTS, G., MINIHAN, A. R., LAAN, J. A. M. & ESHUIS, J. J. W. 1995. Glycerol oligomerization and catalyst. *WO Patent 9521210A1*.
- ROKICKI, G. 2000. Aliphatic cyclic carbonates and spiroorthocarbonates as monomers. *Progress in Polymer Science*, 25, 259-342.
- ROKICKI, G. & LEWANDOWSKI, M. 1987. Epoxy resins modified by carbon dioxide. *Die Angewandte Makromolekulare Chemie*, 148, 53-66.
- ROKICKI, G., RAKOCZY, P., PARZUCHOWSKI, P. & SOBIECKI, M. 2005. Hyperbranched aliphatic polyethers obtained from environmentally benign monomer: glycerol carbonate. *Green Chemistry*, 7, 529-539.
- ROKICKI, G. & WOJCIECHOWSKI, C. 1990. Epoxy resin modified by aliphatic cyclic carbonates. *Journal of Applied Polymer Science*, 41, 647-659.
- ROUSSEAU, D. D. J., SCLAVONS, M., GODARD, P. & MARCHAND-BRYNAERT, J. 2010. Carboxylate clays: A model study for polypropylene/clay nanocomposites. *Polymer Degradation and Stability*, 95, 1194-1204.
- RUIZ-HITZKY, E. & CASAL, B. 1978. Crown ether intercalations with phyllosilicates. *Nature*, 276, 596-597.
- RUIZ-HITZKY, E. & ARANDA, P. 1990. Polymer-salt intercalation complexes in layer silicates. *Adv. Mater. (Weinheim, Fed. Repub. Ger.)*, 2, 545-547.
- RUIZ-HITZKY, E., CASAL, B., ARANDA, P. & GALVAN, J. C. 2001. Inorganic-organic nanocomposite materials based on macrocyclic compounds. *Reviews in Inorganic Chemistry*, 21, 125-159.

- SANDI, G. 2005. S. M. AUERBACH, K. A. CARRADO, P. K. DUTTA (EDs.), Handbook of Layered Materials, Marcel Dekker, New York, NY, 2004, 650 pp. *Microporous Mesoporous Mater.*, 81, 375-376.
- SCHÄFFNER, B., ANDRUSHKO, V., BAYARDON, J., HOLZ, J. & BÖRNER, A. 2009. Organic carbonates as alternative solvents for asymmetric hydrogenation. *Chirality*, 21, 857-861.
- SCHÄFFNER, B., HOLZ, J., VEREVKIN, S. P. & BÖRNER, A. 2008. Organic Carbonates as Alternative Solvents for Palladium-Catalyzed Substitution Reactions. *ChemSusChem*, 1, 249-253.
- SERRATOSA, J. M. 1968. Infrared study of benzonitrile (C<sub>6</sub>H<sub>5</sub>CN)-montmorillonite complexes. *Amer. Mineral.*, 53, 1244-51.
- SOGA, K., TAZUKE, Y., HOSODA, S. & IKEDA, S. 1977. Polymerization of propylene carbonate. *Journal of Polymer Science: Polymer Chemistry Edition*, 15, 219-229.
- STRAWHECKER, K. E. & MANIAS, E. 2000. Structure and Properties of Poly(vinyl alcohol)/Na<sup>+</sup> Montmorillonite Nanocomposites. *Chem. Mater.*, 12, 2943-2949.
- TEZUKA, K., KOMATSU, K. & HABA, O. 2013. The anionic ring-opening polymerization of five-membered cyclic carbonates fused to the cyclohexane ring. *Polym. J. (Tokyo, Jpn.)*, 45, 1183-1187.
- THENG, B. K. G. 1974. *The Chemistry of Clay-Organic Reactions*, Halsted.
- THENG, B. K. G. 1982. Clay-Polymer Interactions: Summary and Perspectives. *Clays and Clay Minerals*, 30, 1-10.
- THENG, B. K. G. 2012. Chapter 1 - The Clay Minerals. *In: THENG, B. K. G. (ed.) Developments in Clay Science*. Elsevier.

- TIAN, D., LIU, B., GAN, Q., LI, H. & DARENSBOURG, D. J. 2012. Formation of Cyclic Carbonates from Carbon Dioxide and Epoxides Coupling Reactions Efficiently Catalyzed by Robust, Recyclable One-Component Aluminum-Salen Complexes. *ACS Catal.*, 2, 2029-2035.
- VELDE, B. 1992. *Introduction to clay minerals: chemistry, origin, uses and environmental significance*, London, Chapman & Hall.
- VEREVKIN, S. P., TOKTONOV, A. V., CHERNYAK, Y., SCHÄFFNER, B. & BÖRNER, A. 2008. Vapour pressure and enthalpy of vaporization of cyclic alkylene carbonates. *Fluid Phase Equilibria*, 268, 1-6.
- VOGDANIS, L., MARTENS, B., UCHTMANN, H., HENSEL, F. & HEITZ, W. 1990. Synthetic and thermodynamic investigations in the polymerization of ethylene carbonate. *Die Makromolekulare Chemie*, 191, 465-472.
- WANG, S., HU, Y., ZHONGKAI, Q., WANG, Z., CHEN, Z. & FAN, W. 2003. Preparation and flammability properties of polyethylene/clay nanocomposites by melt intercalation method from Na<sup>+</sup> montmorillonite. *Materials Letters*, 57, 2675-2678.
- WEISS, A. 1963a. Organic Derivatives of Mica-type Layer-Silicates. *Angewandte Chemie International Edition in English*, 2, 134-144.
- WEISS, A. 1963b. Organic derivatives of micaceous layered silicates. *Angew. Chem.*, 75, 113-22.
- XUE, Q., ZHANG, Q. & LIU, L. 2012. Impact of High Concentration Solutions on Hydraulic Properties of Geosynthetic Clay Liner Materials. *Materials*, 5, 2326-2341.
- YANG, X. & LO, I. 2004. Flow of Gasoline through Composite Liners. *Journal of Environmental Engineering*, 130, 886-890.

ZHANG, Z., LEE, J.-H., LEE, S.-H., HEO, S.-B. & PITTMAN JR, C. U. 2008. Morphology, thermal stability and rheology of poly(propylene carbonate)/organoclay nanocomposites with different pillaring agents. *Polymer*, 49, 2947-2956.

# Chapter 2      Production of glycerol carbonate and other cyclic carbonates

## 2.1 Introduction

Glycerol carbonate (4-hydroxymethyl-2-oxo-1,3-dioxolane) was selected as a promising candidate in potential GCL applications, bearing both a hydroxyl and cyclic carbonate group, where the hydroxyl group may assist in retention of interlayer water in clay barrier systems exposed to high salinity. Although a variety of methods are reported for the synthesis of glycerol carbonate, only recently has there been a drive towards greener routes (Ochoa-Gómez et al., 2012). Glycerol carbonate can be synthesized by direct carbonation of glycerol with phosgene (Strain, 1948), carbon monoxide and oxygen using copper and palladium catalysts (Sonnati et al., 2013) (Figure 2.1).

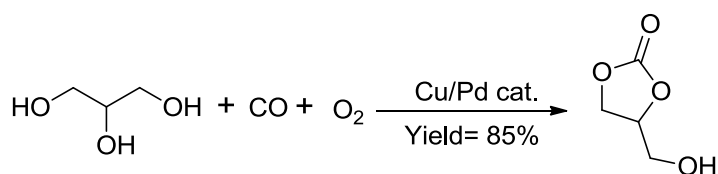


**Figure 2.1:** Synthesis of glycerol carbonate from carbon monoxide.

However, both phosgene and carbon monoxide are toxic and pose considerable environmental and human health risks. An alternative approach involves the reaction of glycidol with carbon dioxide (Figure 2.2). Many catalysts have been reported for conversion of epoxides to cyclic carbonates, such as quaternary ammonium halides, KI-18-crown-6 ether, (porphinato)aluminum alkoxide, NaI and Ph<sub>3</sub>P (Sonnati et al., 2013). For complete conversion of glycidol, an excess of carbon dioxide is needed and the reactions are often performed at high pressure.

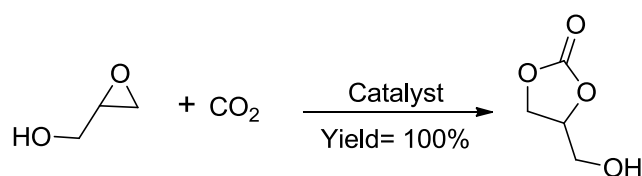


**Figure 2.2:** Reaction of glycidol with carbon dioxide to produce glycerol carbonate.

Direct carboxylation of glycerol carbonate from glycerol and carbon dioxide using transition metal alkoxides have been carried out, but the yields reported were low (Dibenedetto et al., 2006) (Figure 2.3).

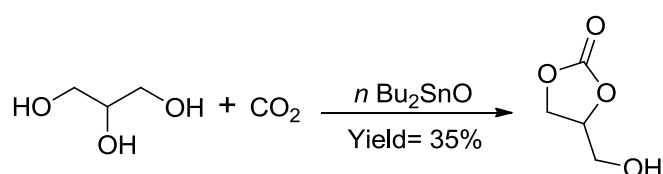


**Figure 2.3:** Synthesis of glycerol carbonate from carbon dioxide employing a transition metal catalyst.

Glycerol carbonate is obtained industrially from glycerol and dialkyl carbonates, ethylene carbonate or dimethyl carbonate, by transesterification (Mouloungui et al., 1996). Using ethylene carbonate, ethylene glycol is obtained as a by-product which makes its separation from glycerol carbonate difficult due to the high boiling points of both products. One alternative is the use of dimethyl carbonate as a carbonate source (Figure 2.4). Transcarbonations of glycerol with alkyl carbonates are reversible reactions, and therefore a high mole ratio of alkyl carbonate to glycerol is needed to shift the chemical equilibrium towards glycerol carbonate. The carbonylation agents are typically generated via catalytic oxidative carbonylation of methanol with oxygen (Tundo and Selva, 2002).

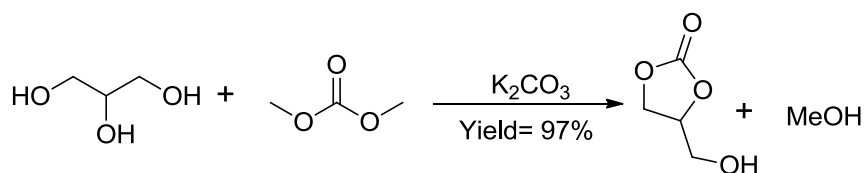


**Figure 2.4:** Formation of glycerol carbonate from transesterification using dimethyl carbonate.

Attempts have been made to produce glycerol carbonate directly from glycerol and CO<sub>2</sub> under supercritical conditions employing zeolites (Figure 2.5) (Vieville et al., 1999) or Sn catalysts (Aresta et al., 2006). Up to now this approach has been unsuccessful because yields were lower than 8%, as the original Sn catalyst was converted into an oligomer, which showed reduced catalytic activity (Aresta et al., 2006).

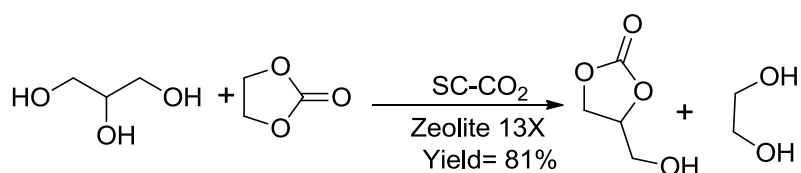


**Figure 2.5:** Synthesis of glycerol carbonate from supercritical carbon dioxide employing zeolite.

Another interesting route for producing glycerol carbonate is via the catalysed combination of glycerol and urea. The main advantage of this method is that urea is readily available and is a cheap reactant and the NH<sub>3</sub> co-product may be recycled into synthesis of further urea. A gold based catalyst supported on MgO (2.5% Au/MgO) has also been used, however this process suffered from a relatively low yield of 55% (Hammond et al., 2011). Greater yields for glycerol carbonate were observed with a palladium based catalyst supported on magnesium oxides (1.0% Pd/MgO) (Rahim et al., 2012). Park et al. (2012) have quoted a yield of 80% by using zinc chloride as a catalyst which generated zinc monoglycerolate (ZMG) and ammonium chloride *in-situ* (Figure 2.6).

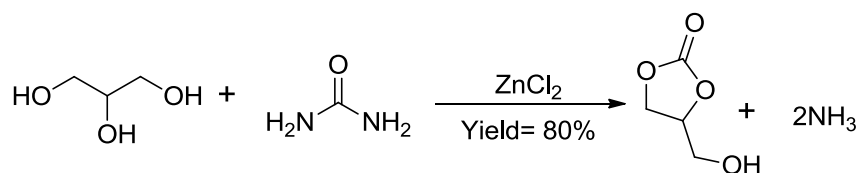


**Figure 2.6:** Reaction of glycerol and urea to obtain glycerol carbonate.

Recently, Zn containing catalysts such as acetate, chloride, bromide and smectites have been used to produce glycerol carbonate (Fujita et al., 2013).

The carbonating source used here was urea with ZMG as a precursor catalyst in the absence of further activating species, such as ammonium chloride. This same ZMG/urea approach was also applied to various 1,2-diols to synthesize a variety of cyclic carbonates and organic carbamates.

## 2.2 Objectives

The objective of this part of the project was to evaluate the synthesis of glycerol carbonate with various methods described in literature with the objective of developing a greener method capable of being scaled up for industrial production. The synthesis of glycerol carbonate (4-hydroxymethyl-1,3-dioxolan-2-one) was attempted using three reported approaches in order to develop a novel catalyst for the glycerolysis of urea.

1. Reaction of dimethyl carbonate with glycerol (Rokicki et al., 2005).
2. Reaction of urea with glycerol using zinc oxide catalyst (Climent et al., 2010).
3. Reaction of urea with glycerol catalysed by zinc sulfate (Yoo and Mouloungui, 2003).

A related objective was to extend the ZMG approach developed at Monash (Turney et al 2013) for the synthesis of glycerol carbonate to the synthesis of other cyclic carbonates starting from urea and various 1,2-diols. The results of our method could then be

compared with the established transesterification approach with dimethyl carbonate and potassium carbonate.

## 2.3 Results and discussion

### 2.3.1 Synthesis of glycerol carbonate

#### 2.3.1.1 Synthesis of glycerol carbonate via different reported routes

The reaction of dimethyl carbonate with glycerol (Rokicki et al., 2005) was carried out under mild conditions. Dimethyl carbonate was used in a molar excess (3:1) to shift the reaction equilibrium towards the product. The resulting glycerol carbonate was obtained in quantitative yield in 2.5 hours. The reaction progress was monitored by FTIR at intervals of 15 minutes, by observing the strong peak at  $1780\text{ cm}^{-1}$   $\nu(\text{C=O})_{\text{str}}$  build. On reaction completion, methanol and unreacted dimethyl carbonate were removed by distillation at  $40\text{ }^{\circ}\text{C}$  under reduced pressure.

The other reaction conditions, employing zinc oxide in the glycerolysis of urea, involved using an amount of catalyst equivalent to 5% by weight relative to glycerol. The crude mixture obtained contained glycerol carbonate, glycerol carbamate, (5-hydroxymethyl) oxazolidin-2-one and glycidol, consistent with the results reported by Climent et al. (2010).

In the third method, the reaction of glycerol and urea was carried out in the presence of hydrated zinc sulfate as a catalyst (Yoo and Mouloungui, 2003). Glycerol urethane (Figure 2.7) was produced as a side product in this reaction and was confirmed by gas chromatography.

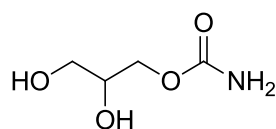


**Figure 2.7:** Structure of glycerol urethane.

On the basis of these preliminary studies, the glycerolysis of urea was studied using ZMG as a catalyst.

### 2.3.1.2 Zinc monoglycerolate (ZMG) catalysed synthesis of glycerol carbonate

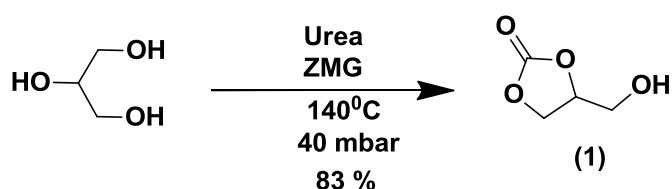
The use of zinc monoglycerolate (ZMG) as a catalyst appears to be an entirely new route for the synthesis of glycerol carbonate. In this method, ZMG itself was synthesized from zinc oxide and glycerol (Radoslovich et al., 1970). ZMG was then used in a catalytic amount with glycerol and urea in *i*-propanol as a solvent. This solvent was selected because the temperature could be raised up to 170 °C, in addition to the good miscibility of glycerol with urea and easy recovery of ZMG (Table 2.1).

**Table 2.1:** Glycerol carbonate production from various catalysts

Reference	Catalyst	Conv. (%)	Selectivity (%)	Yield <sup>a</sup> (%)
(Rokicki et al., 2005)	K <sub>2</sub> CO <sub>3</sub> <sup>b</sup>	99	97	96
(Climent et al., 2010)	ZnO <sup>c</sup>	47	79	37
(Yoo and Mouloungui, 2003)	ZnSO <sub>4</sub> <sup>c</sup>	39	93	36
-	ZMG <sup>c</sup>	36	83	30

<sup>a</sup>Yield determined by gas chromatography. <sup>b</sup>Dimethyl carbonate was used as a carbonating source. <sup>c</sup>Urea was used as a carbonating source.

The yield of glycerol carbonate from this reaction was poor (Table 2.1) and to improve the yield of glycerol carbonate, a solvent free approach was adopted and any ammonia formed was removed by reducing the pressure in the reaction, thereby shifting the reaction equilibrium in favour of the desired product. The reaction was performed at different temperatures, time and molar ratios to optimize reaction parameters. The standard conditions subsequently established for maximum conversion and selectivity are 5 wt% ZMG to glycerol, where 1.5 molar equivalents of urea is used with respect to glycerol at 140 °C and 40 mbar over 7h (Turney et al., 2013). The side products (Figure 2.8) from this reaction were identified using GC-MS.



**Scheme 2.1:** Synthetic scheme for the preparation of glycerol carbonate using ZMG as a catalyst.

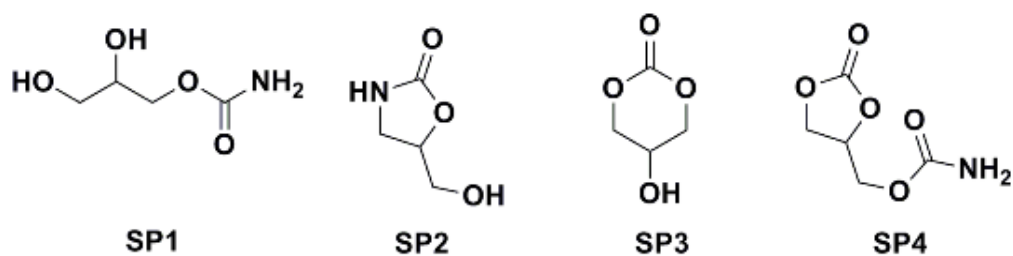


**Figure 2.8:** Side products formed in the reaction of glycerol with urea.

Conversion, selectivity and yield were calculated with respect to glycerol, using gas chromatography. The calculation of the percent glycerol conversion (X) and % yield (glycerol carbonate) was determined as follows:

$$\% \text{ Glycerol conversion} = X = [(X_2 - X_1) / X_2] \times 100$$

$$\% \text{ Spectroscopic yield (glycerol carbonate)} = Y \times X$$

Where  $X_1$  = unreacted glycerol (observed amount by GLC (gas chromatography)),  $X_2$  = initial amount of glycerol and  $Y$  = amount of glycerol carbonate formed.

**Table 2.2:** Effect of temperature on glycerol conversion and glycerol carbonate selectivity

Temp. (°C)	Conv. (%)	% Selectivity					Yield by GLC <sup>b</sup> (%)
		GC <sup>a</sup>	SP1	SP2	SP3	SP4	
100	12	48	47	3	0	2	6
110	17	46	50	4	0	0	8
120	26	72	24	2	2	0	19
130	31	74	22	2	2	0	23
140	60	90	4	1	3	2	54
150	71	92	1	1	5	1	65

Mean  $\pm$  2% (Standard deviation of each analysis), n=3. Reaction conditions: 5 wt% catalyst with respect to glycerol, time 7h, molar ratio of glycerol:urea (1:1), pressure 40 mbar. <sup>a</sup>Glycerol carbonate. <sup>b</sup>Yields of glycerol carbonate were determined by gas chromatography.

For each time interval, aliquots from the reaction were sampled three times. The standard deviation (S) of replicates (three) have been calculated using the following formula:

$$S = \frac{\sqrt{\sum(X - M)^2}}{\sqrt{n - 1}}$$

Where n = number of values in the data set, X = each value in the data and M = mean (average) value of data. The standard deviations fall in the range of  $\pm 2\%$ .

The temperature, time and molar ratio of glycerol and urea played a critical role in the catalysed reaction. Figure 2.9 reports the trend in formation of glycerol carbonate with respect to temperature; the reactions were carried out at 40 mbar pressure for 7 hours. The reaction was found to be dependent on temperature; in fact the reactivity of glycerol and urea remained rather low up to 130 °C. A sudden increase was observed between 130 and 140 °C, but the yield did not significantly rise at higher temperatures. The selectivity for glycerol carbonate increased as the temperature raised and peaks at 92%. Glycerol urethane was observed as the major intermediate which was consumed proportionately to the glycerol carbonate being formed (Figure 2.10).

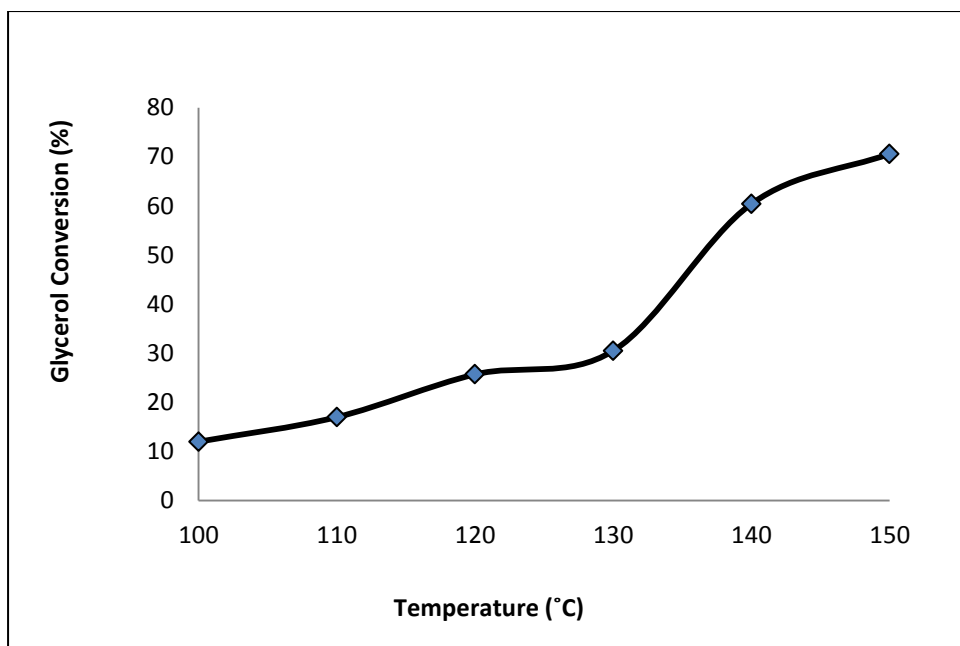


Figure 2.9: Trend of glycerol conversion with temperature.

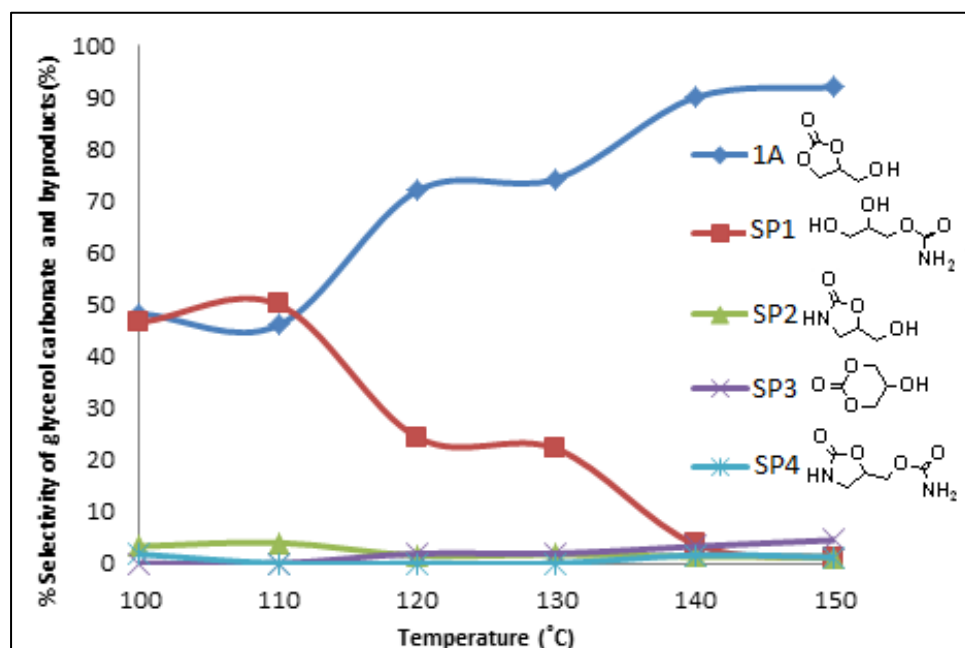
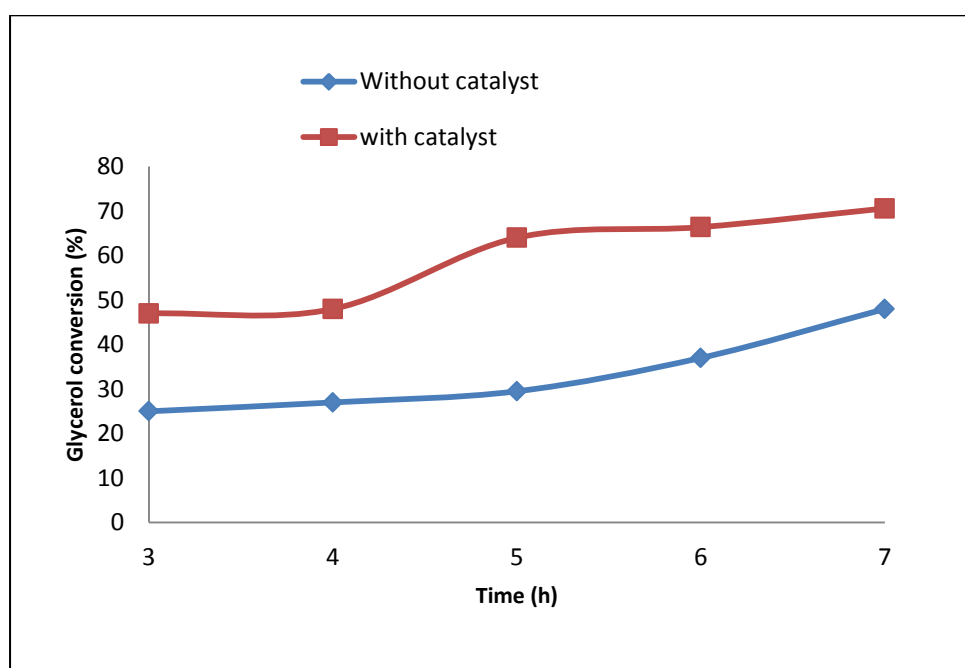


Figure 2.10: Percent selectivity patterns of products as a function of temperature.

Figure 2.11 and Figure 2.12 show the influence of time on the conversion of glycerol and amount of glycerol carbonate formed, respectively. After 3 hours of thermal reaction (i.e., without catalyst) at 150 °C, a conversion of 25% (and yield of 18%) was reached,

and remained essentially constant for 5 hours. The maximum yield obtained in the uncatalysed process after 7 hours was 29%, indicating that the formation of glycerol carbonate occurred even in the absence of catalyst, but the yield was low. Conversely, in the catalysed process a rise in glycerol conversion (64%) was observed between 4 and 5 hours (Figure 2.11). After 7 hours of reaction the glycerol conversion was 71%. After 5 hours, a maximum selectivity of 93% (Table 2.3) was obtained. The optimum yield at 7 hours was 65%. The glycerol urethane (SP1) was present in >25% selectivity in all time intervals for the uncatalysed reaction whereas in the catalysed process, the selectivity of SP1 decreased with the time which suggested enhanced conversion of glycerol as well as SP1 to glycerol carbonate.



**Figure 2.11:** Effect of time on glycerol conversion in the catalysed and uncatalysed processes.

**Table 2.3:** Uncatalysed and catalysed reactions

Catalyst amount <sup>a</sup> (%)	Time (h)	Conv. (%)	% Selectivity					Yield by GLC (%)
			GC <sup>b</sup>	SP1	SP2	SP3	SP4	
0	3	25	72	25	1	1	1	18
0	4	27	69	27	1	2	1	19
0	5	30	64	31	1	3	1	19
0	6	37	64	31	1	3	1	24
0	7	48	62	30	2	5	1	29
5	3	47	86	10	1	2	2	40
5	4	48	87	7	1	3	2	42
5	5	64	93	1	1	4	1	60
5	6	66	92	2	1	4	1	61
5	7	71	92	1	1	5	1	65

Mean  $\pm$  2% (Standard deviation of each analysis), n=3. Reaction conditions: temperature 150 °C, molar ratio of urea/glycerol (1), pressure 40 mbar, yield by gas chromatography.

<sup>a</sup>Catalyst amount with respect to weight of glycerol. <sup>b</sup>Glycerol carbonate.

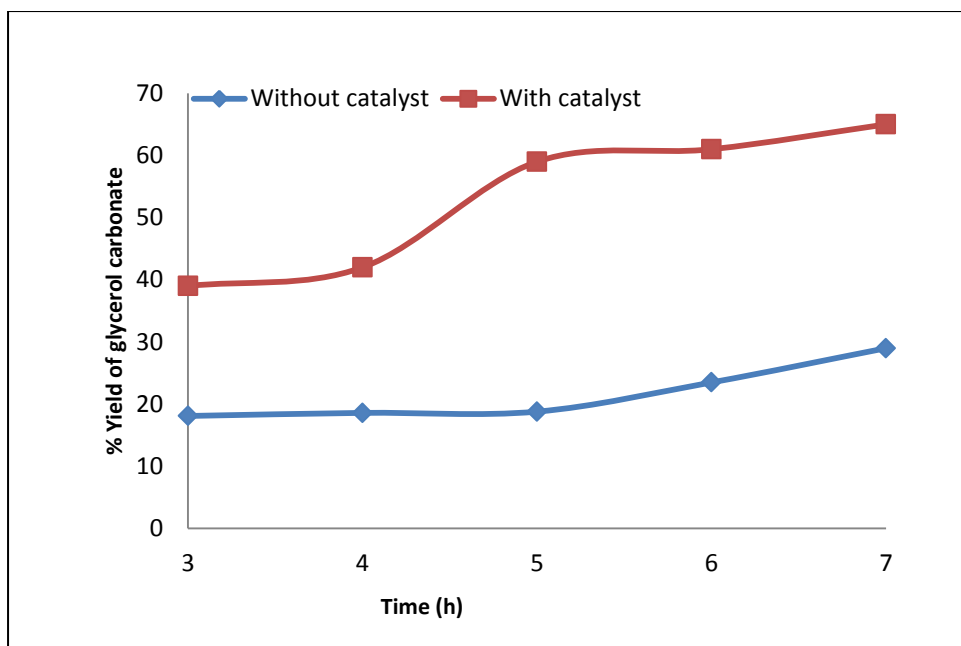


**Figure 2.12:** Effect of time on the yield of glycerol carbonate in the catalysed and uncatalysed reactions.

**Table 2.4:** Molar ratio change (of urea) on glycerol conversion and glycerol carbonate selectivity

Molar ratio gly:urea	Time (h)	Conv. (%)	% Selectivity					Yield by GLC (%)
			GC <sup>a</sup>	SP1	SP2	SP3	SP4	
1:1	3	47	86	10	0	2	2	40
	4	48	87	7	1	3	2	42
	5	64	93	1	1	3	2	60
	6	66	92	2	1	4	1	61
	7	71	92	1	1	5	1	65
1:1.5	3	67	81	12	0	2	5	54
	4	78	85	6	1	3	5	67
	5	91	78	7	1	4	10	72
	6	91	80	1	7	3	9	73
	7	91 <sup>b</sup>	82 <sup>a</sup>	1	3	3	11	75 <sup>a</sup>

Mean  $\pm$  2% (Standard deviation of each analysis), n=3. Reaction conditions: catalyst (ZMG) amount 5 wt% with respect to glycerol, temperature 150 °C and pressure 40 mbar. <sup>a</sup>Glycerol carbonate. <sup>b</sup>At 140 °C, the conversion was 98% whereas, selectivity and yield of glycerol carbonate were 85 and 83%, respectively.

Increasing the molar ratio of urea to glycerol from 1:1 to 1.5:1 had a significant effect on the conversion. After 5 hours, a maximum conversion was obtained (91%) compared to 71% conversion at 7 hours, for the 1:1 reaction (Table 2.4). However, the selectivity for glycerol carbonate dropped from 92% to 82% after 7 hours when an excess of urea was used. As a result, there was a noticeable increase in SP4 formation. But the yield of glycerol carbonate significantly increased due to increased glycerol conversion to 75%

after 7 hours at 150 °C when 1.5 equivalents of urea was used. Overall, the selectivity for glycerol carbonate decreased due to the subsequent reaction of glycerol carbonate with excess urea to form SP4.

For industrial applications, an important consideration should be catalyst recovery and reuse. In order to determine the extent of catalyst recovery and reuse, two re-cycling experiments were performed. The recovery of catalyst was 90% of the total amount used during the first cycle while 84% of ZMG was recovered in the second cycle. This loss may be attributed to mechanical loss of catalyst during experimental workup. The data (Table 2.5) suggests that ZMG retains its high activity when reused over two cycles, making it an attractive process.

**Table 2.5:** Re-cycling of ZMG and yield of glycerol carbonate

Time (h)	1 <sup>st</sup> cycle			2 <sup>nd</sup> cycle		
	Conv. (%)	% Selectivity	Yield <sup>a</sup> (%)	Conv. (%)	% Selectivity	Yield <sup>a</sup> (%)
3	42	93	39	40	93	37
4	48	90	43	45	87	39
5	51	90	46	49	92	45
6	59	93	55	55	96	53

Mean  $\pm$  2% (Standard deviation of each analysis), n=3. Reaction conditions: catalyst (ZMG) amount 5 wt% with respect to glycerol, glycerol to urea 1:1 mole equivalents, temperature 140 °C and pressure 40 mbar.

<sup>a</sup>Yield by gas chromatography.

The reaction of glycerol with urea proceeded in two steps; the first step was formation of glycerol urethane with liberation of one mole of ammonia followed by intramolecular

cyclization of glycerol urethane to produce glycerol carbonate and the removal of the second mole of ammonia.

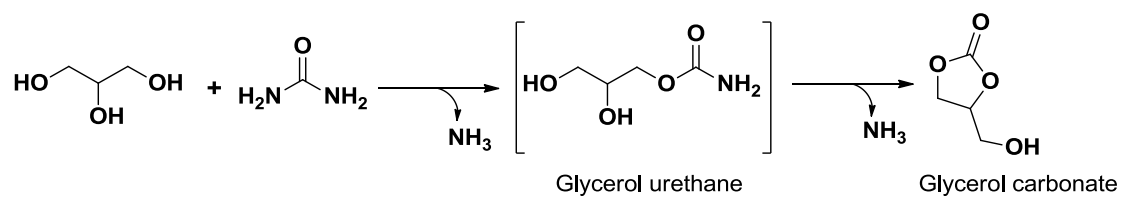


**Figure 2.13:** Steps for the reaction of glycerol with urea.

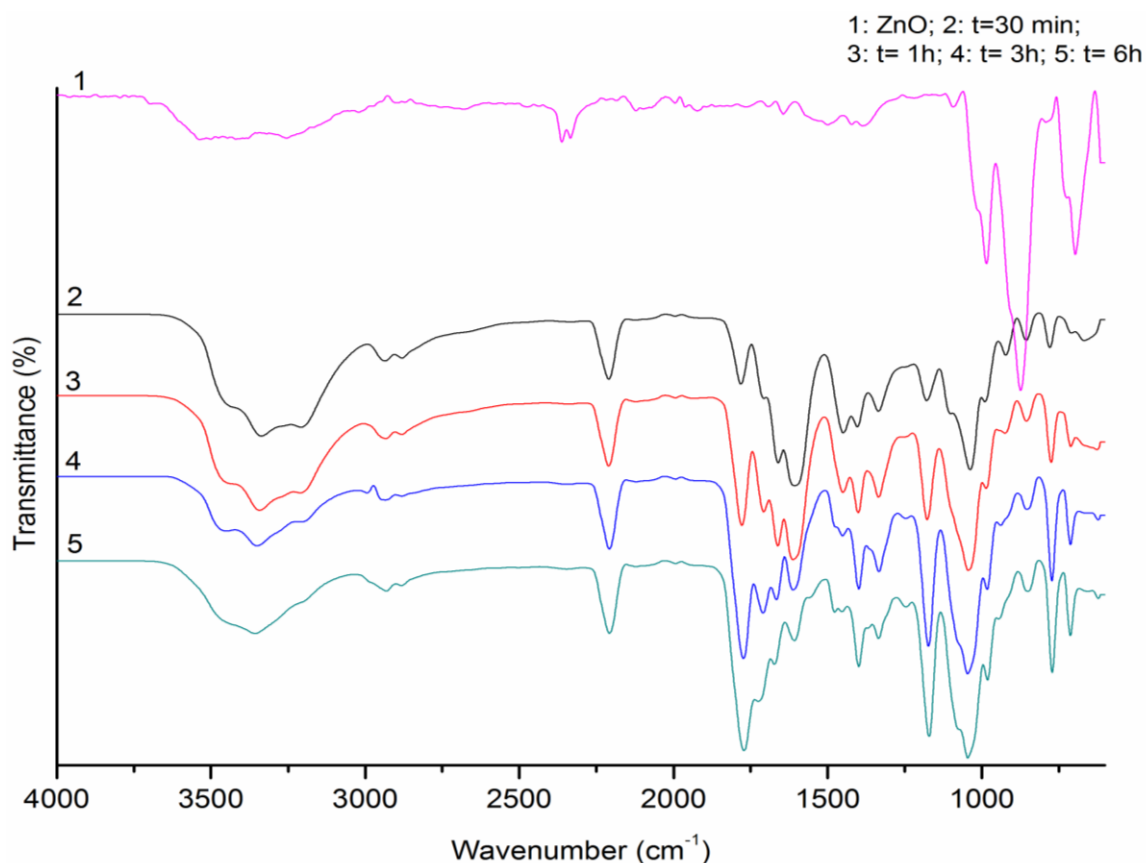
Mechanistic studies for this reaction were carried out in a separate investigation and will be discussed in Section 2.3.2. When ZMG was compared to ZnO, it was found that a homogeneous, clear reaction medium was formed. The same was also observed with the ZnO and ZMG was formed *in-situ* as an intermediate. In this case the conversion was 81% and the yield 73% after 7 hours of reaction time (Table 2.6).

**Table 2.6:** Glycerol conversion and glycerol carbonate selectivity when using ZnO

Time (h)	Conv. (%)	% Selectivity					Yield by GLC <sup>b</sup> (%)
		GC <sup>a</sup>	SP1	SP2	SP3	SP4	
0.5	26	83	14	1	1	1	22
1.5	44	92	5	1	1	1	41
2	62	92	5	0	2	1	57
3	75	94	2	1	2	1	70
4	80	94	2	2	1	0	75
5	82	93	1	3	1	2	76
6	82	92	0	3	2	3	75
7	81	91	0	6	1	2	73

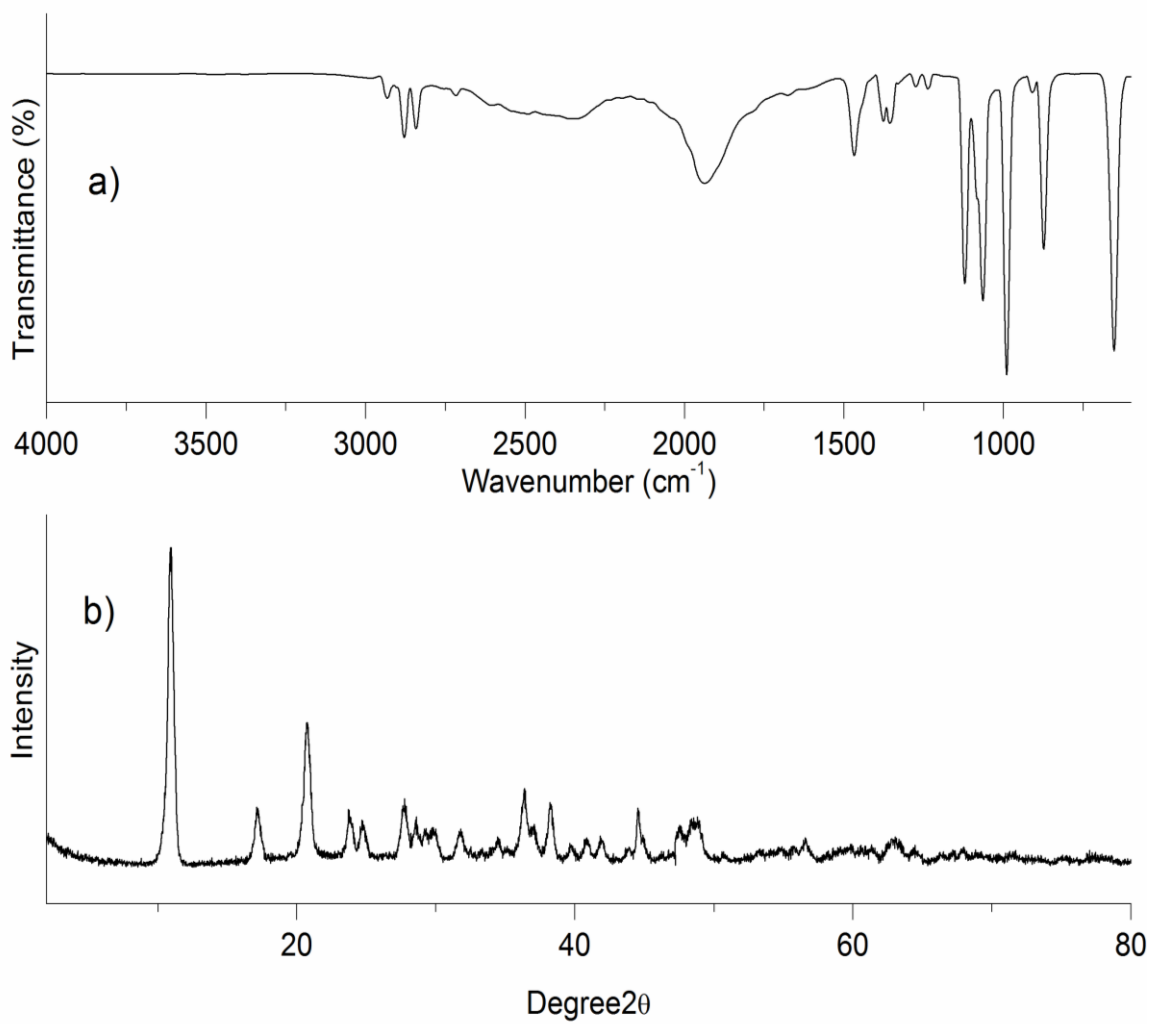
Mean  $\pm$  2% (Standard deviation of each analysis), n=3. Reaction conditions: catalyst (ZnO) amount 5 wt% with respect to glycerol, time 7h, molar ratio of glycerol:urea (1:1.5), pressure 40 mbar and temperature, 140 °C. <sup>a</sup>Glycerol carbonate. <sup>b</sup>Yields of glycerol carbonate were determined by gas chromatography.

Figure 2.14 shows the FTIR for sample aliquots taken at intervals of 30 min, 1h, 3h and 6h. The FTIR showed a strong band at 2197 cm<sup>-1</sup>, characteristic of  $\nu_{\text{asym}}(\text{NCO})_{\text{str}}$  of a coordinated isocyanate ligand.



**Figure 2.14:** FTIR spectra for the reaction of ZnO with glycerol and urea.

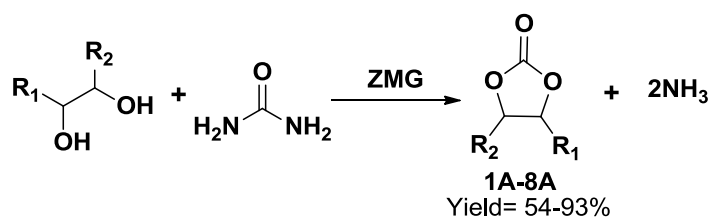
FTIR and powder-XRD were performed on the solid recovered after reaction (Figure 2.15). The XRD of the recovered solid was similar to ZMG itself (Yildirim and Durucan, 2010). On work-up with methanol, the catalytic species (ZnO) converted to ZMG, which was consistent with our previous observations with ZMG. Further details regarding the mechanism of the ZMG catalysed glycerolysis of urea can be found in the Monash University study reported by Turney, et al. (2013).



**Figure 2.15:** a) IR spectrum; b) XRD spectrum of recovered solid (from reaction of glycerol and urea employing ZnO catalyst).

### 2.3.2 Synthesis of cyclic carbonates from other 1,2-diols

The cyclization of other 1,2-diols with urea was investigated (Scheme 2.2), at the optimized condition (for glycerol carbonate) of 140 °C, 40 mbar pressure, with 5 wt% ZMG over 7 hours.



- (1)R<sub>1</sub>= CH<sub>2</sub>OH, R<sub>2</sub>= H (2)R<sub>1</sub>= (CH<sub>2</sub>)<sub>2</sub>OH, R<sub>2</sub>= H  
(3)R<sub>1</sub>= (CH<sub>2</sub>)<sub>4</sub>OH, R<sub>2</sub>= H (4)R<sub>1</sub>= CH<sub>2</sub>OCH<sub>2</sub>Ph, R<sub>2</sub>= H  
(5)R<sub>1</sub>= CH<sub>2</sub>OCH<sub>2</sub>CH(OH)CH<sub>2</sub>OH, R<sub>2</sub>= H  
(6&7)R<sub>1</sub> or R<sub>2</sub> = -(CH<sub>2</sub>)<sub>4</sub>- (8)R<sub>1</sub>= CH(OH)CH<sub>2</sub>OH, R<sub>2</sub>= H

**Scheme 2.2:** General reaction for the synthesis of cyclic carbonates (**1A-8A**).

After the reaction, ZMG was recovered by adding methanol to the homogeneous reaction mixture. The general mechanism for the cyclization of 1,2-diols is given in Figure 2.15. ZMG reacts with urea to form an intermediate diol urethane complex of zinc isocyanate (I) as evidenced by FTIR (Turney et al., 2013). This metal intermediate can then directly eliminate a proton to produce the diol urethane intermediate (II) or cyclize with the elimination of ammonia to afford cyclic carbonate and ZMG with labile amine ligands (III) as shown in (Figure 2.16).

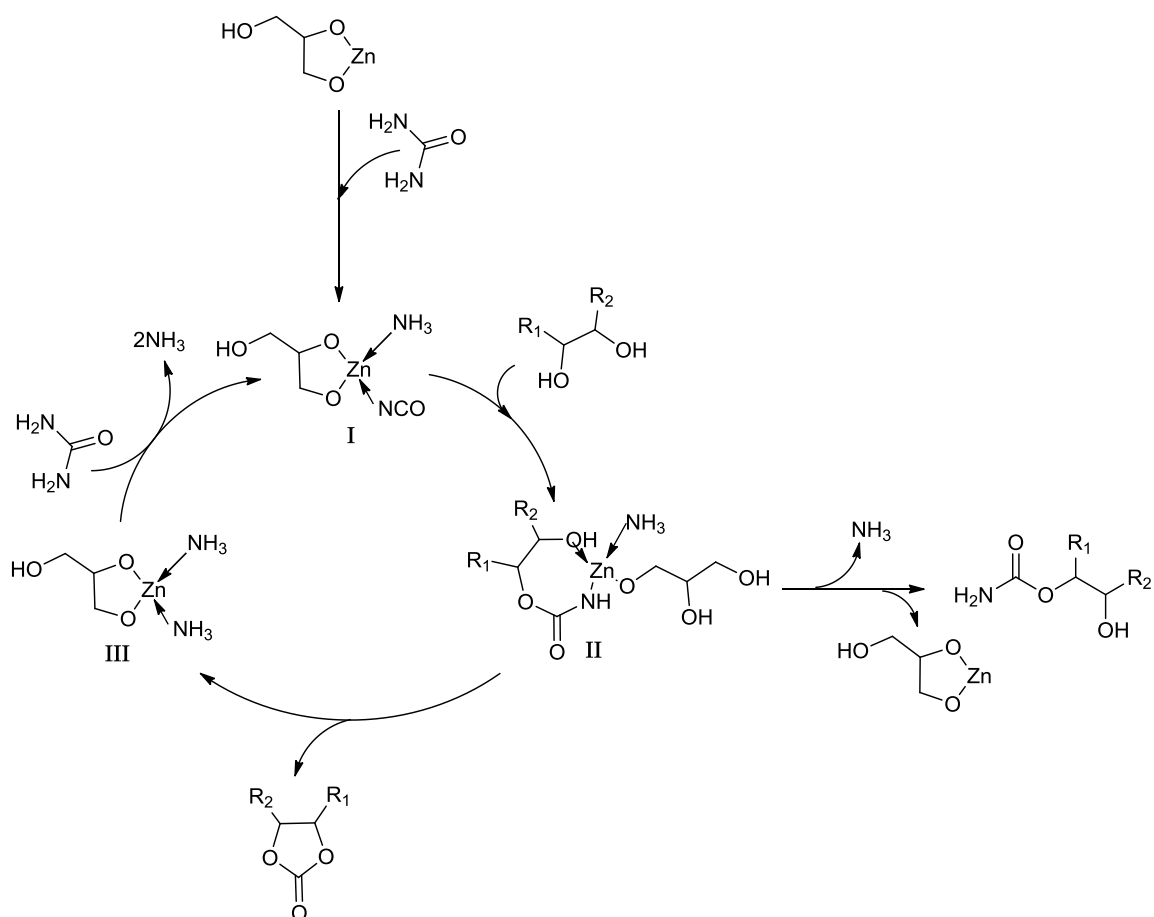
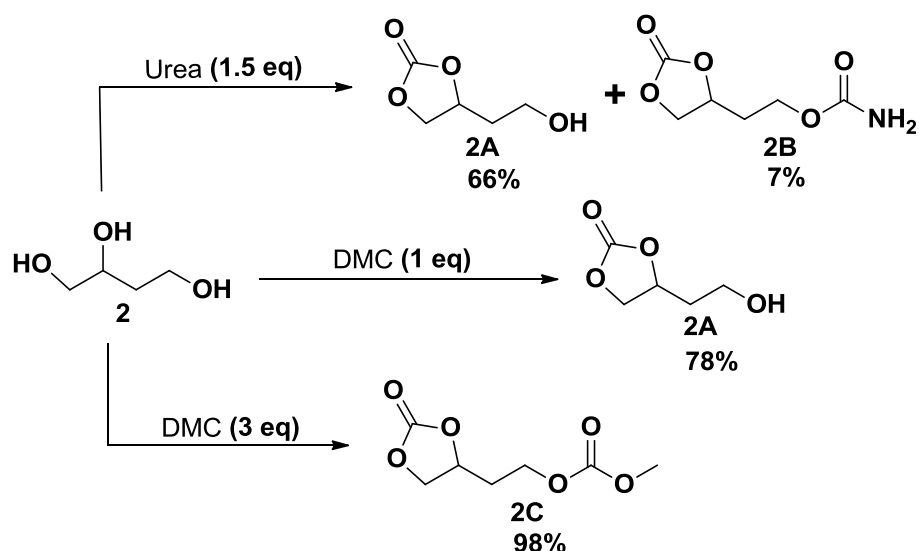


**Figure 2.16:** General mechanism for the cyclization of various 1,2-diols catalyzed by ZMG.

In reacting 1,2,4-butanetriol (**2**) with urea and a ZMG catalyst, 4-(2-hydroxyethyl)-1,3-dioxolan-2-one (**2A**) was obtained in 66% yield with a conversion of 73% (Scheme 2.3) and interestingly, 6-membered cyclic carbonate resulting from cyclization of the 1,4-hydroxyl was not formed at all.



**Scheme 2.3:** Reaction of 1,2,4-butanetriol with urea and dimethyl carbonate.

**Table 2.7:** Conversion of 1,2,4-butanetriol and selectivity as determined by GLC

Carbonating source (mole equivalent)	Conv. %	% Selectivity			Reference
		2A	2B	2C	
Urea (1.5)	73	91	9	0	-
DMC (3)	100	2	0	98	(Tomczyk et al., 2012)
DMC (1)	78	100	0	0	(Tomczyk et al., 2012)

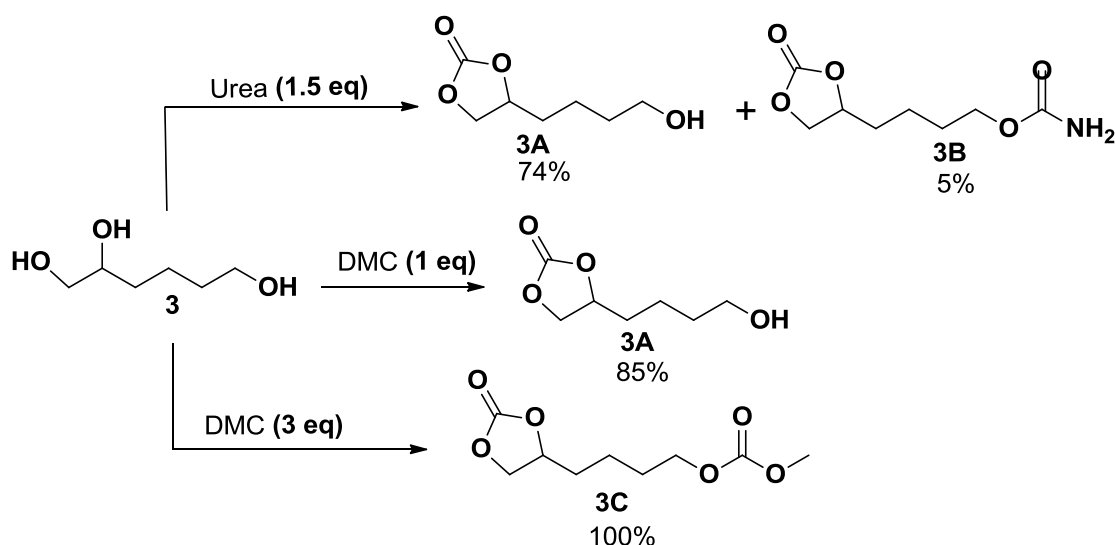
The terminal mono-urethane by-product, **2B** was formed in small amounts and identified by GC-MS. Due to the excess of urea, the free hydroxyl in **2A** further reacted to produce the urethane by-product **2B**. When 1,2,4-butanetriol was reacted with 1 equivalent of dimethyl carbonate (DMC) in the presence of a 0.03 mol (catalytic amount) of potassium carbonate, **2A** was obtained in 78% yield and 78% conversion. When 3 equivalents of dimethyl carbonate was used, **2B** was formed which reacts with another equivalent of dimethyl carbonate forming **2C** (Table 2.7) in 98% yield with a conversion

of 100%. With **2C**, the acyclic  $\nu(\text{C=O})_{\text{str}}$  by IR was observed at  $1749\text{ cm}^{-1}$  (in comparison to the cyclic  $\nu(\text{C=O})_{\text{str}}$  at  $1797\text{ cm}^{-1}$ ).  $^1\text{H-NMR}$  showed the characteristic singlet for the methyl protons (methoxy group in linear carbonate, **2C**) at 3.79 ppm. **2A** and **2C** have been synthesized using a literature method for transesterification (Tomczyk et al., 2012). When ZMG was used with 1.5 equivalents of urea, a comparable selectivity was obtained for synthesis of **2A**.

1,2,6-Hexanetriol (**3**) when reacted with urea and ZMG or dimethyl carbonate (Table 2.8) gave 4-(4-hydroxybutyl)-1,3-dioxolan-2-one (**3A**).

**Table 2.8:** Selectivity of side products in the reaction of 1,2,6-hexanetriol

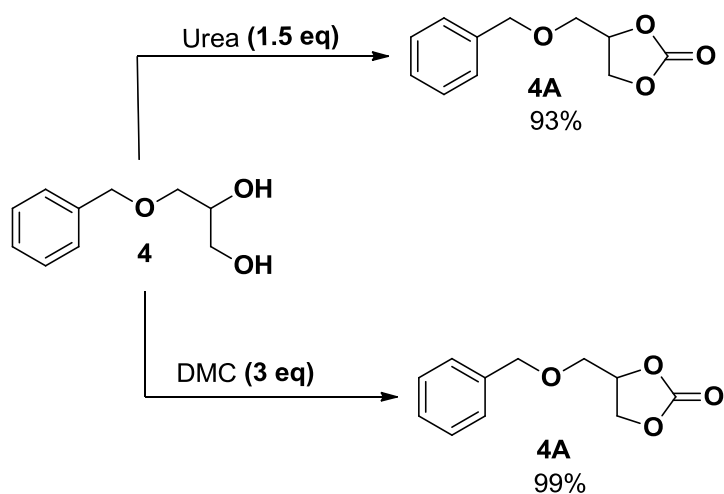
Carbonating source (mole equivalent)	Conv. %	% Selectivity			Reference
		<b>3A</b>	<b>3B</b>	<b>3C</b>	
Urea (1.5)	79	94	6	0	-
DMC (3)	100	0	0	100	(Tomczyk et al., 2012)
DMC (1)	88	96	0	4	(Tomczyk et al., 2012)



**Scheme 2.4:** Reaction of 1,2,6-hexanetriol with urea or dimethyl carbonate.

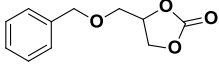
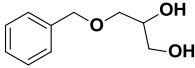
With 1.5 equivalents of urea, **3A** was obtained in 74% yield and with 1 equivalent of dimethyl carbonate, **3A** was obtained in 85% yield. In using 3 equivalents of dimethyl carbonate, **3C** was formed quantitatively (Scheme 2.4). Here too the glycerolysis of urea runs parallel to the transesterification method.

The reaction of 1-(benzyloxy)ethane-1,2-diol (**4**) with urea and ZMG under optimal conditions (Turney et al, 2013) gave 4-((benzyloxy)methyl)-1,3-dioxolan-2-one (**4A**) in 93% yield. With dimethyl carbonate, **4A** was obtained in 99% yield (Table 2.9). No side products were observed in either reaction due to the absence of an additional hydroxyl group. **4A** has been synthesized previously in 54% yield from carbon fixation of respective epoxide employing an organocatalyst and a co-catalyst, *n*Bu<sub>4</sub>NI (Whiteoak et al., 2012).

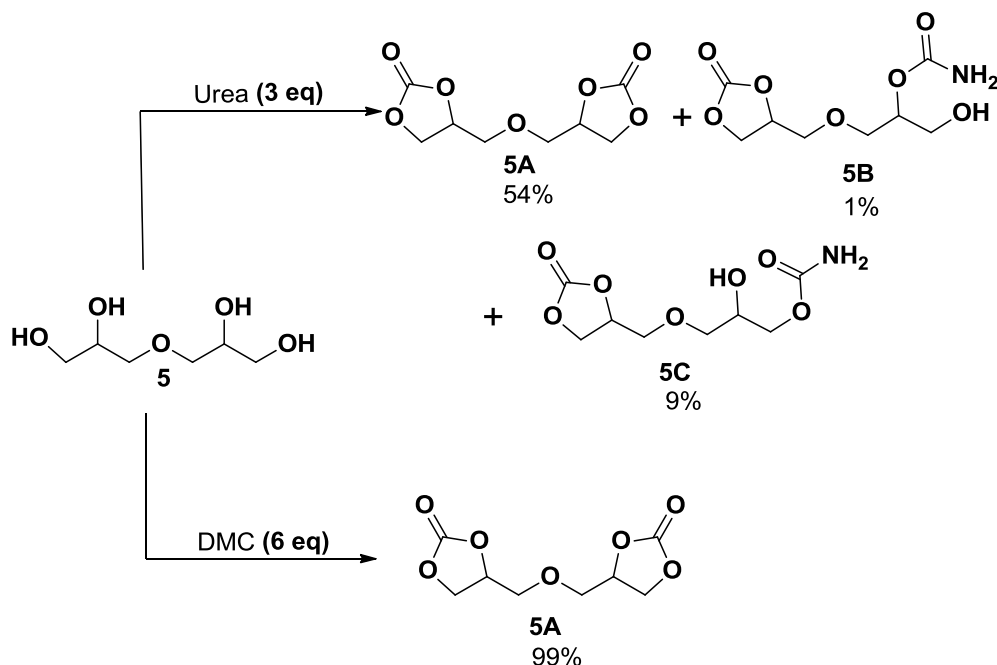


**Scheme 2.5:** Reaction of 1,2,6-hexanetriol with urea or dimethyl carbonate.

**Table 2.9:** Comparison of reactions of 1-(benzyloxy)ethane-1,2-diol (**4**)

Substrate	Carbonating source (mole equivalent)	Conv. %	% Selectivity  <b>4A</b>
	Urea (1.5)	93	100
	DMC (3)	99	100

When diglycerol (**5**) and urea/ZMG were reacted at different molar ratios (Table 2.10), it was observed that diglycerol conversion and 4,4'-(oxybis(methylene))bis(1,3-dioxolan-2-one) (**5A**) selectivity increased with increasing molar ratio of urea from 1 to 3.



**Scheme 2.6:** Reactions of diglycerol – Formation of cyclic carbonate derivatives.

**Table 2.10:** Effect of urea and DMC molar ratio on selectivity of 4,4'-(oxybis(methylene))bis(1,3-dioxolan-2-one) (**5A**)

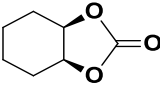
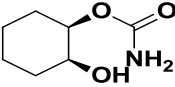
Carbonating source (mole equivalent)	Conv. %	% Selectivity	
		<b>5A</b>	<b>5B</b>
Urea (1)	32	58	42
Urea (2)	59	74	26
Urea (3)	65	83	16
DMC (1)	22	100	0
DMC (6)	99	100	0

In addition to **5A**, urethane intermediates **5B** and **5C** were also observed (Scheme 2.6). Formation of intermediate **5C** was preferred over **5B** as it is the less hindered urethane. With 6 equivalents of dimethyl carbonate, **5A** was obtained quantitatively with no evidence for the mono-cyclic product.

For compounds **4A** and **5A**, transesterification with dimethyl carbonate gave good yields with high selectivity. It is worth mentioning that product **5A** has been synthesized from the respective epoxide in the past with yield of 93% (Rokicki and Kuran, 1984). Higher yields were obtained with the transesterification approach compared with our method of urea/ZMG.

When *cis*-1,2-cyclohexanediol and *trans*-1,2-cyclohexanediol were reacted with urea/ZMG, the preferred selectivity was different in both cases.

**Table 2.11:** Products obtained from reaction of *cis*-1,2-cyclohexanediol with urea

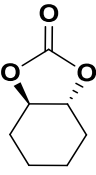
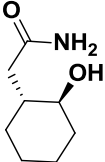
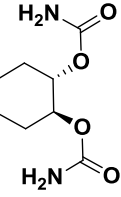
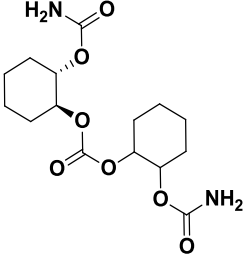
Carbonating source (mole equivalent)	Conv. %	% Selectivity	
			
Urea (1.5)	87	86	15

Gabriele et al (2011) reported the formation of **6A** from the reaction of 1,2-epoxycyclohexane with oxygen using bimetallic aluminium complexes and tetrabutylammonium bromide catalysts (Beattie et al., 2013), while **7A** was obtained in 20% yield from palladium catalyzed oxidative carbonylation of *trans*-1,2-cyclohexandiol (Gabriele et al., 2011).

The reaction of *cis*-1,2-cyclohexanediol resulted in the formation of a hexahydrobenzo[d][1,3]dioxol-2-one (**6A**) in 75% yield, along with intermediate, 2-hydroxycyclohexyl carbamate (**6B**) (Table 2.11). The sterically hindered by-products, cyclohexane-1,2-diyl dicarbamate (**6C**) and (carbonylbis(oxy))bis(cyclohexane-2,1-diyl) dicarbamate, (**6D**) were not observed with *cis*-1,2-cyclohexanediol.

In contrast, the reaction mixture from *trans*-1,2-cyclohexanediol comprised of mainly urethane intermediates, **7C** and **7D**. Cyclohexane-1,2-diyl dicarbamate (**7C**) was obtained (See general mechanism, Figure 2.15) as a major product with 67% selectivity and with 70% conversion from *trans*-1,2-cyclohexanediol (Table 2.12).

**Table 2.12:** Selectivity of products from the reaction of *trans*-1,2-cyclohexanediol with urea

Conv. %	% Selectivity			
				
	<b>7A</b>	<b>7B</b>	<b>7C</b>	<b>7D</b>
70	7	7	67	20

The difference between *cis* and *trans*-1,2-cyclohexanediol reactivity to form either cyclic carbonates or diurethanes, depends upon the conformation of 1,2-cyclohexanediol. The chair form of *trans*-1,2-cyclohexanediol can exist in two possible conformations, where the hydroxyl groups are in a diaxial and diequatorial position (Figure 2.17). The most stable conformation of *trans*-1,2-cyclohexanediol is diaxial, where the two hydroxyls are furthest apart from each other due to lone pair repulsion. In the case of the diequatorial conformation, the two hydroxyls are close to each other, contributing to lone pair repulsion, hence this conformation is not favoured. Due to the failure of flipping of the di-axial to the di-equatorial form (which is energetically least favoured), only 5% of hexahydrobenzo[d][1,3]dioxol-2-one (**7A**) is formed.

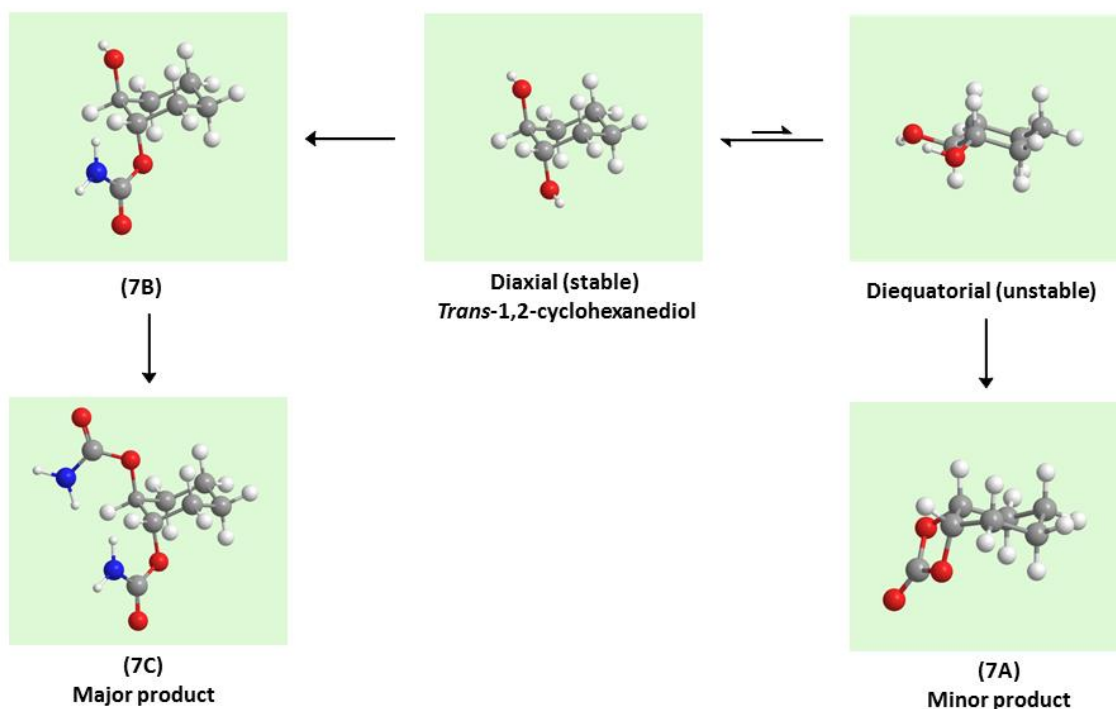


**Figure 2.17:** Formation of different products from *trans*-1,2-cyclohexanediol.

*Cis*-1,2-cyclohexanediol has a conformation of axial-equatorial and equatorial-axial hydroxyl groups. Both these conformations are energetically equivalent. Therefore, the two hydroxyls in both conformations are near enough to form a five-membered cyclic carbonate (Figure 2.18), hexahydrobenzo[d][1,3]dioxol-2-one (**6A**). It can be concluded that the two hydroxyls should be present in an axial-equatorial position which is in *cis*-geometry in order to successfully form the cyclic carbonate.

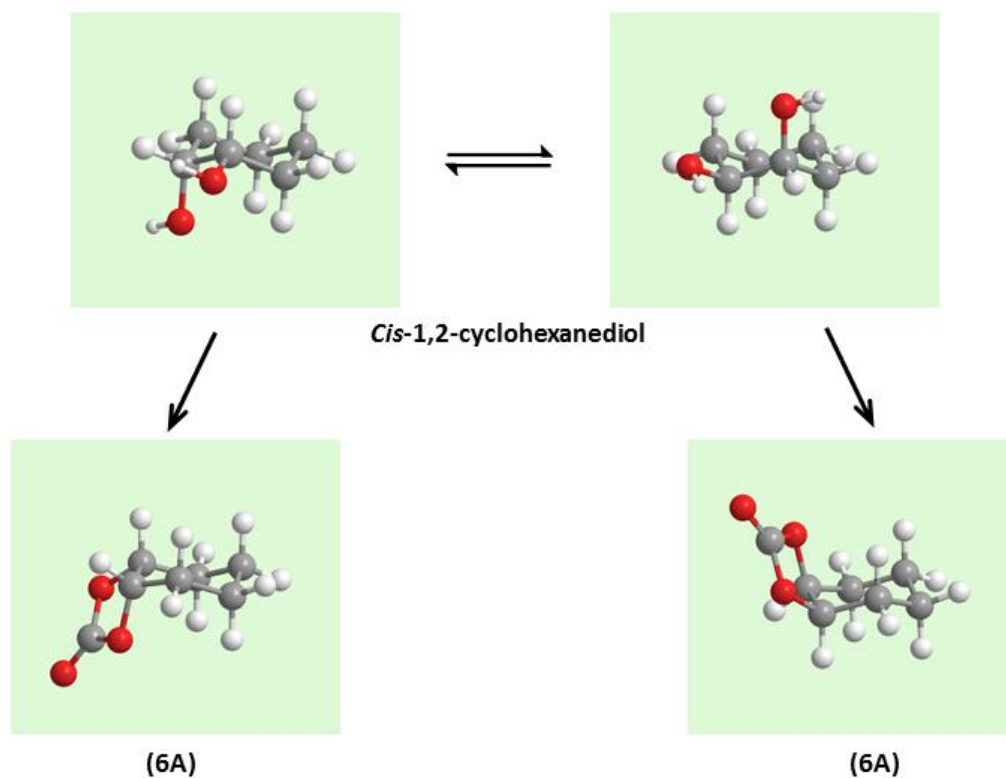
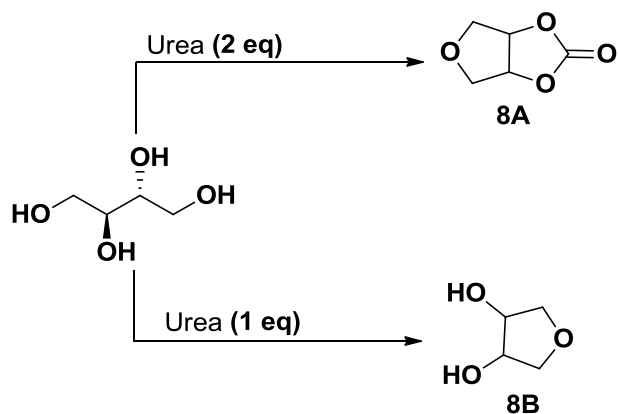


**Figure 2.18:** Formation of hexahydrobenzo[d][1,3]dioxol-2-one (**6A**) from *cis*-1,2-cyclohexanediol.

When *meso*-erythritol was reacted with an equivalent of urea employing ZMG catalyst, a mixture of two products, tetrahydrofuro[3,4-d][1,3]dioxol-2-one (**8A**) and tetrahydrofuran-3,4-diol (**8B**) were formed with 96% conversion, where the major product was (**8B**) with 86% selectivity (Scheme 2.7, Table 2.13).



**Scheme 2.7:** Products obtained in the reaction of *meso*-erythritol with urea.

**Table 2.13:** Selectivity of **8A** and **8B** upon change in amount of urea

Carbonating source (mole equivalent)	Conv. %	% Selectivity	
		<b>8A</b>	<b>8B</b>
Urea (1)	96	14	86
Urea (2)	100	98	2

When two moles of urea were used with **8**, tetrahydrofuro[3,4-d][1,3]dioxol-2-one (**8A**) was obtained as a major product with 98% selectivity and 98% yield. A single crystal x-ray diffraction analysis performed by Craig Forsyth at Monash (Figure 1, see Appendix 1) confirmed the identity to be tetrahydrofuro[3,4-d][1,3]dioxol-2-one (**8A**). **8A** and **8B** have been produced using dimethyl carbonate/ethylene carbonate to give 86% and 96% yield (Tomczyk et al., 2012) using dioxane and toluene as a solvent.

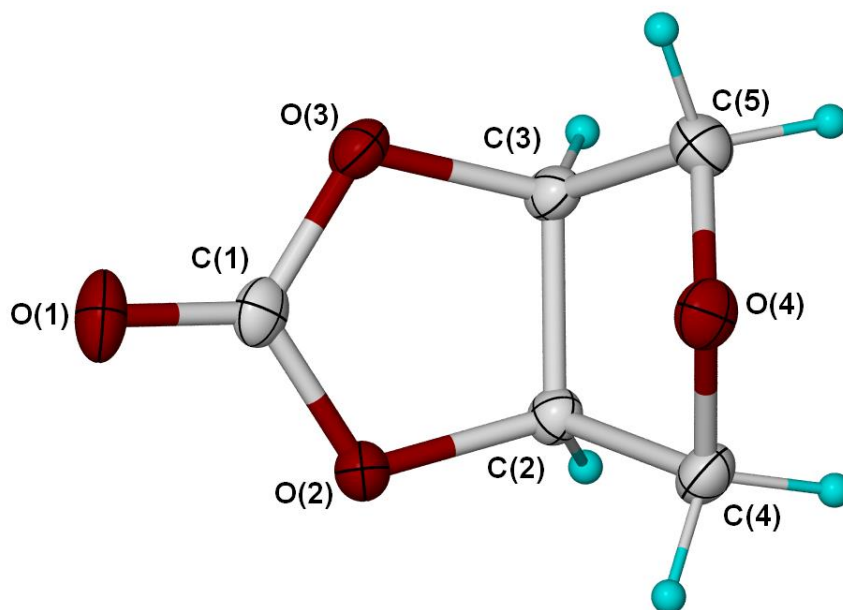
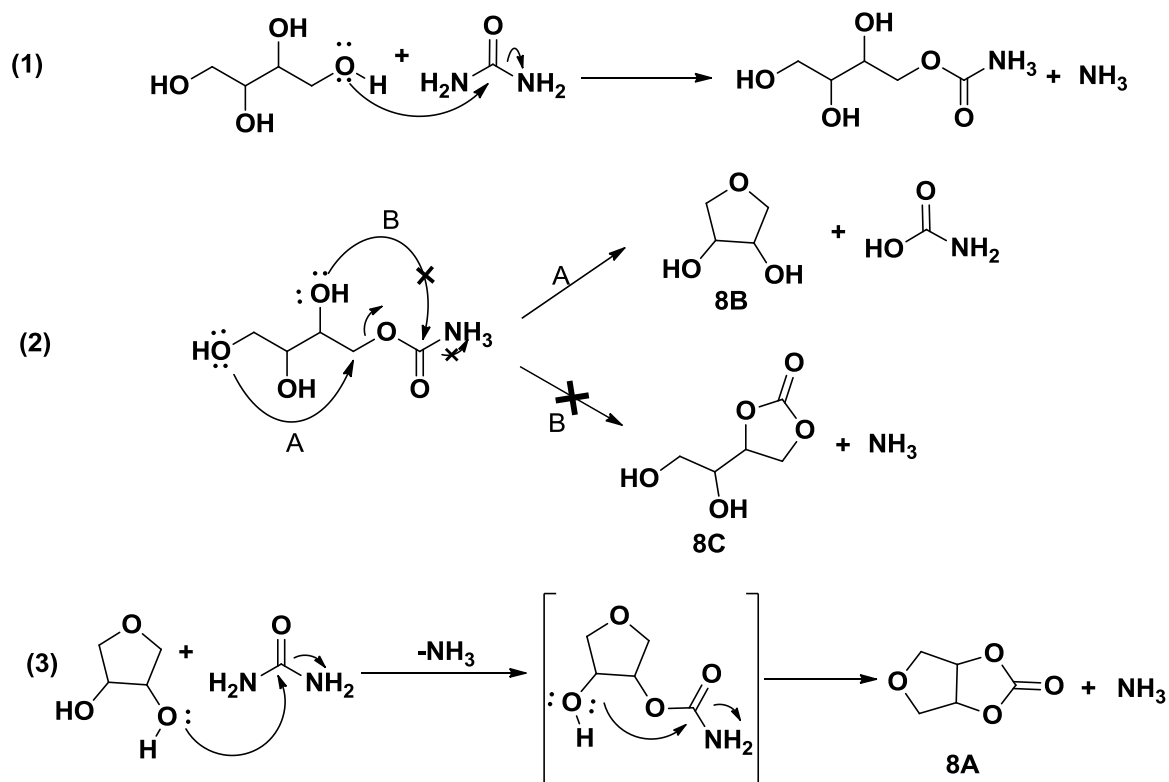


**Figure 2.19:** A single crystal structure of **8A** as determined from X-ray diffraction. (Molecular diagram with non-hydrogen atoms represented by 50% thermal ellipsoids and hydrogen atoms as spheres of arbitrary size).

It is proposed here that the formation of **8A** and **8B** proceeds as shown in Scheme 2.8; where 2,3,4-trihydroxybutyl carbamate preferentially cyclizes to form **8B** and not **8C** with an equivalent of urea. Once formed, it reacts with the excess urea as shown in step 3 to yield **8A**. Since **8A** is a significant product formed, this formation mechanism is the most probable.



**Scheme 2.8:** Formation of product **8A** and **8B** from *meso*-erythritol. Reaction intermediate, 2,3,4-trihydroxybutyl carbamate preferentially cyclizes to form **8B** and not **8C** with an equivalent of urea with the elimination of ammonia and carbon dioxide. Once **8B** formed, it reacts with another equivalent of urea to yield **8A**.

The lowest energy form of *meso*-erythritol occurs when the two terminal hydroxyl groups are in close proximity to each other rather than the 1,2-hydroxyls. So when 2,3,4-trihydroxybutyl carbamate is formed, a likely scenario is nucleophilic attack of the terminal hydroxyl on the methylene carbon adjacent to the carbamate group producing **8B** (Pathway A, Scheme 2.8). The distance between the terminal hydroxyl and the carbonyl atom on carbamate group is only 3.22 Å, compared to the distance of 4.67 Å between the second hydroxyl group and the carbonyl carbon atom on the carbamate group (Pathway B, Scheme 2.8; Figure 2.20) also explains the exclusive formation of **8B**

rather than **8C**. Our results using the ZMG catalyst are similar to the results obtained by Tomczyk (2012).

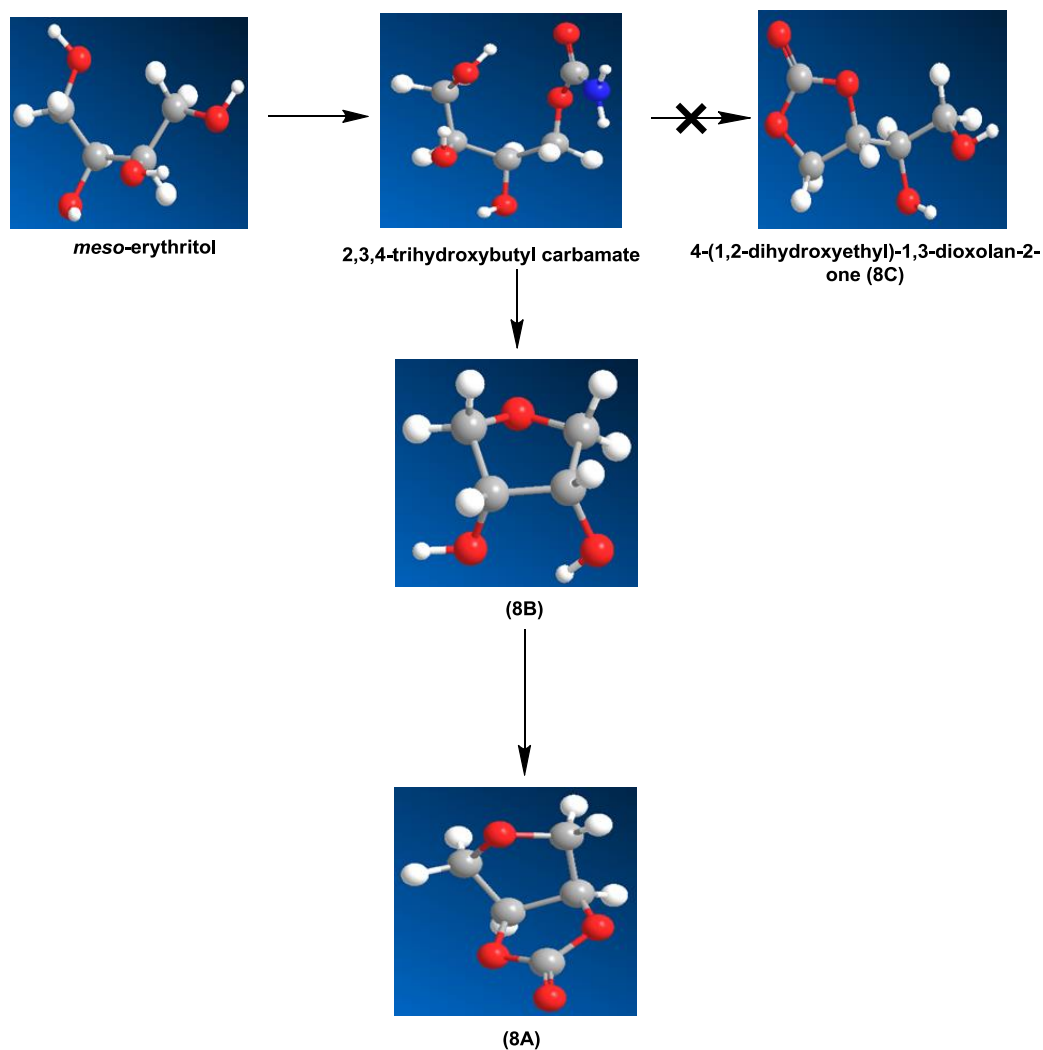


**Figure 2.20:** 3-D representation of formation of product **8A** and **8B**.

The results from the synthesis of **7A** were applied to other naturally occurring diol-monosaccharides such as d-glucose and d-fructose. However, there was no conversion to any isolatable product and in both cases only starting material was observed.

## 2.4 Conclusion

A green, solvent free approach was developed for scalable production of glycerol carbonate. Glycerol carbonate was obtained in 83% yield with 98% conversion under optimal conditions involving glycerolysis of urea using zinc monoglycerolate (ZMG) as catalyst. The key intermediate in the catalytic cycle was an isocyanate ligand coordinated to the metal glycerolate.

Transesterification using dimethyl carbonate provides an efficient way to synthesize various cyclic carbonates, although the commercial production of dimethyl carbonate is expensive. A suitable alternative involves urea and ZMG under similar conditions developed for the synthesis of glycerol carbonate. In all of the products **1A-8A**, comparative yields for the cyclization between two methods were obtained except with product **5A**. The yield of **5A** with ZMG/urea was lower because of the low conversion of diglycerol. Overall, using ZMG as a catalyst resulted in high diol conversion with excellent selectivity for the cyclic carbonates.

## 2.5 References

- ARESTA, M., DIBENEDETTO, A., NOCITO, F. & PASTORE, C. 2006. A study on the carboxylation of glycerol to glycerol carbonate with carbon dioxide, the role of the catalyst, solvent and reaction conditions. *J. Mol. Catal. A: Chem.*, 257, 149-153.
- BEATTIE, C., NORTH, M., VILLUENDAS, P. & YOUNG, C. 2013. Influence of Temperature and Pressure on Cyclic Carbonate Synthesis Catalyzed by Bimetallic Aluminum Complexes and Application to Overall syn-Bis-hydroxylation of Alkenes. *J. Org. Chem.*, 78, 419-426.

- CLIMENT, M. J., CORMA, A., DE, F. P., IBORRA, S., NOY, M., VELTY, A. & CONCEPCION, P. 2010. Chemicals from biomass: Synthesis of glycerol carbonate by transesterification and carbonylation with urea with hydrotalcite catalysts. The role of acid-base pairs. *J. Catal.*, 269, 140-149.
- DIBENEDETTO, A., PASTORE, C. & ARESTA, M. 2006. Direct carboxylation of alcohols to organic carbonates: Comparison of the Group 5 element alkoxides catalytic activity: An insight into the reaction mechanism and its key steps. *Catalysis Today*, 115, 88-94.
- FUJITA, S.-I., YAMANISHI, Y. & ARAI, M. 2013. Synthesis of glycerol carbonate from glycerol and urea using zinc-containing solid catalysts: A homogeneous reaction. *Journal of Catalysis*, 297, 137-141.
- GABRIELE, B., MANCUSO, R., SALERNO, G., VELTRI, L., COSTA, M. & DIBENEDETTO, A. 2011. A General and Expedient Synthesis of 5- and 6-Membered Cyclic Carbonates by Palladium-Catalyzed Oxidative Carbonylation of 1,2- and 1,3-Diols. *ChemSusChem*, 4, 1778-1786.
- HAMMOND, C., LOPEZ-SANCHEZ, J. A., RAHIM, M. H. A, DIMITRATOS, N., JENKINS, R. L., CARLEY, A. F., HE, Q., KIELY, C. J., KNIGHT, D. W. & HUTCHINGS, G. J. 2011. Synthesis of glycerol carbonate from glycerol and urea with gold-based catalysts. *Dalton Trans.*, 40, 3927-3937.
- MOULOINGUI, Z., YOO, J.-W., GACHEN, C.-A., GASET, A. & VERMEERSCH, G. 1996. Process for the preparation of glycerol carbonate from glycerol and ethylene or propylene carbonates. *EP Patent 739888A1*.

- OCHOA-GÓMEZ, J. R., GÓMEZ-JIMÉNEZ-ABERASTURI, O., RAMÍREZ-LÓPEZ, C. & BELSUÉ, M. 2012. A Brief Review on Industrial Alternatives for the Manufacturing of Glycerol Carbonate, a Green Chemical. *Organic Process Research & Development*, 16, 389-399.
- RADOSLOVICH, E. W., RAUPACH, M., SLADE, P. G. & TAYLOR, R. M. 1970. Crystalline cobalt, zinc, manganese, and iron alkoxides of glycerol. *Aust. J. Chem.*, 23, 1963-1971.
- RAHIM, M. H. A., HE, Q., LOPEZ-SANCHEZ, J. A., HAMMOND, C., DIMITRATOS, N., SANKAR, M., CARLEY, A. F., KIELY, C. J., KNIGHT, D. W. & HUTCHINGS, G. J. 2012. Gold, palladium, and gold-palladium supported nanoparticles for the synthesis of glycerol carbonate from glycerol and urea. *Catal. Sci. Technol.*, 2, 1914-1924.
- ROKICKI, G. & KURAN, W. 1984. Cyclic Carbonates Obtained by Reactions of Alkali Metal Carbonates with Epihalohydrins. *Bulletin of The Chemical Society of Japan*, 57, 1662-1666.
- SONNATI, M. O., AMIGONI, S., TAFFIN DE GIVENCHY, E. P., DARMANIN, T., CHOULET, O. & GUITTARD, F. 2013. Glycerol carbonate as a versatile building block for tomorrow: synthesis, reactivity, properties and applications. *Green Chemistry*, 15, 283-306.
- STRAIN, F. 1948. Carbonate-haloformates of glycerol. *US Patent 2446145*.
- TOMCZYK, K. M., GUNKA, P. A., PARZUCHOWSKI, P. G., ZACHARA, J. & ROKICKI, G. 2012. Intramolecular etherification of five-membered cyclic carbonates bearing hydroxyalkyl groups. *Green Chemistry*, 14, 1749-1758.
- TUNDO, P. & SELVA, M. 2002. The Chemistry of Dimethyl Carbonate. *Accounts of Chemical Research*, 35, 706-716.

- TURNEY, T. W., PATTI, A., GATES, W., SHAHEEN, U. & KULASEGARAM, S. 2013. Formation of glycerol carbonate from glycerol and urea catalysed by metal monoglycerolates. *Green Chemistry*, 15, 1925-1931.
- VIEVILLE, C., YOO, J. W., PELET, S. & MOULOINGUI, Z. 1999. Synthesis of glycerol carbonate by direct carbonatation of glycerol in supercritical CO<sub>2</sub> in the presence of zeolites and ion exchange resins. *Catal. Lett.*, 56, 245-247.
- WHITEOAK, C. J., NOVA, A., MASERAS, F. & KLEIJ, A. W. 2012. Merging Sustainability with Organocatalysis in the Formation of Organic Carbonates by Using CO<sub>2</sub> as a Feedstock. *ChemSusChem*, 5, 2032-2038.
- YILDIRIM, O. A. & DURUCAN, C. 2010. Synthesis of zinc oxide nanoparticles elaborated by microemulsion method. *J. Alloys Compd.*, 506, 944-949.
- YOO, J. W. & MOULOINGUI, Z. 2003. Catalytic carbonylation of glycerin by urea in the presence of zinc mesoporous system for the synthesis of glycerol carbonate. *Stud. Surf. Sci. Catal.*, 146, 757-760.

# **Chapter 3      Interaction of glycerol carbonate and other cyclic carbonates with Na- smectite**

## **3.1 Introduction**

Smectite has been known to form complexes with various organic compounds by adsorption and cation exchange. Interlayer cations play a significant role in the intercalation of organic compounds and can result in stability of these intercalated complexes through cation dipole interaction and co-ordination mechanisms (Yamanaka et al., 1975). Orientation of organic molecules in smectite can be affected by the presence of interlayer water molecules (Yamanaka et al., 1974, Slade and Gates, 2004b, Gates, 2004). Propylene carbonate (PC) is currently the only candidate studied for intercalation into smectite (Kondo, 1996). PC/smectite complexes have been prepared by mixing an aqueous solution of smectite with propylene carbonate to study swell test properties (Kondo, 1996). It was found that the smectite activated with PC exhibited high swelling power in aqueous alkali solution [0.5N] and as a result, smectite modified with propylene carbonate has been used as an alternative barrier material for liner systems (Katsumi et al., 2008, Katsumi et al., 2007, Katsumi, 2010).

PC/montmorillonite complexes have been prepared by mixing Na-montmorillonite powder with PC using an agate mortar at room temperature and these complexes maintained osmotic swelling at high concentrations in NaCl solutions [1M] (Onikata et al., 1999) and CaCl<sub>2</sub> solutions [0.5M] (Onikata., 2002, Katsumi et al., 2008) comparable

to unmodified Na-bentonite in distilled water. Solvation of the interlayer cation is considered to be the driving force for intercalation of PC into montmorillonite. The interactions of the propylene carbonate molecules with the interlayer cations take place through the interlayer water as described by Onikata et al. (1999). Previously reported work (Katsumi et al., 2008, Onikata., 2002, Onikata et al., 1999) shows that the use of PC is limited to low saline waters equivalent to seawater (0.5-1M) and until now, there are no other published research reports on organic/smectite complexes, especially those of cyclic carbonates, describing the swelling of smectite in saline solutions having >1M total salt loads.

In this chapter, the intercalation of various amounts (wt%) of glycerol carbonate (GC) (synthesized previously in Chapter 2) into Na-smectite was studied and the interaction of glycerol carbonate with Na-smectite based on model FTIR studies was proposed. In addition, the intercalation of other previously synthesized (Chapter 2) cyclic carbonates with Na-smectites was achieved and will be discussed.

### **3.2 Objective**

The objective of this phase of the project was to synthesize GC intercalated Na-smectite complexes, to characterize these complexes using powder XRD and FTIR spectroscopy and to propose the mechanism of interaction of GC with sodium smectite. The mechanism of intercalation proposed was based on the results of model FTIR studies performed on GC with varying amounts of water, sodium chloride and a combination of water/sodium chloride. Stability studies of GC in alkali solutions (at various pH) were also undertaken.

A second important objective was to synthesize cyclic carbonate intercalated clay complexes and to characterize these complexes by powder XRD and FTIR spectroscopy.

### **3.3 Results and discussion**

#### **3.3.1 Interaction of glycerol carbonate with Na-smectite**

Glycerol carbonate (GC)(synthesized in chapter 2) was intercalated into sodium smectite from aqueous solution of glycerol carbonate (5 wt%). The GC solution was applied directly onto a film of sodium smectite prepared on a ceramic tile (4.6 mg smectite per  $\text{cm}^2$ ) using suction. X-ray diffraction spectra (XRD) of Na-smectite and GC intercalated complexes were obtained. The most notable difference in the XRD spectra of Na-smectite and GC/Na-smectite was found in the location of the basal (001) reflection. The intercalated complex was also characterized by FTIR.

##### **3.3.1.1 Study of glycerol carbonate by XRD**

GC was loaded into Na-smectite on a wt% basis to determine the effect on d-spacing and hence the intercalation behaviour. The *d*-spacing values ( $d(001)$ ), distance between the layers, were estimated by using the Bragg's equation ( $d = \lambda/2\sin\theta$ ). The basal spacing of air-dried Na-smectite was 1.29 nm. The gallery height was determined by subtracting the thickness of the silicate layer (0.960 nm) (Seki and Ogawa, 2010, Deeds and Van Olphen, 1963) from the observed basal spacing (1.29 nm) as 0.33 nm. Disordered stacking or imperfect alignment of clay platelets within the film resulted in broadening of the 001 reflection.

The amount of disorder can be estimated from the full width at half maximum height of the 001 reflection. FWHM is expressed by Scherrer equation,

$$L = \frac{K\lambda}{\beta\cos\theta}$$

Where,

L = Mean size of the ordered (crystalline) domains; K = constant normally with a value close to unity;  $\lambda$  = wavelength of the X-ray source (Cu K 0.154 nm);  $\beta$  = the line broadening at half the maximum intensity (FWHM), after subtracting the instrumental line broadening, in radians (also sometimes denoted as  $\Delta$  ( $^{\circ}2\theta$ )); and  $\theta$  = Bragg' s angle.

The basal spacing (001) of the GC intercalates varied depending on the amount of GC adsorbed. Glycerol carbonate (GC, **1A**) enters the interlayer space of Na-smectite, presumably by replacing some of the interlayer water surrounding sodium ions (Onikata et al., 1999). When the amount of GC was 10 wt% (0.1 g/ 0.9 g clay), the gallery height of the hydrated sample remained at 0.5 nm and is either wide enough to occupy GC molecule with the cyclic carbonate ring plane parallel to clay surface or the amount of intercalation was too disordered to significantly appear in 001 reflection and observed by XRD (Figure 3.1, Table 3.1).

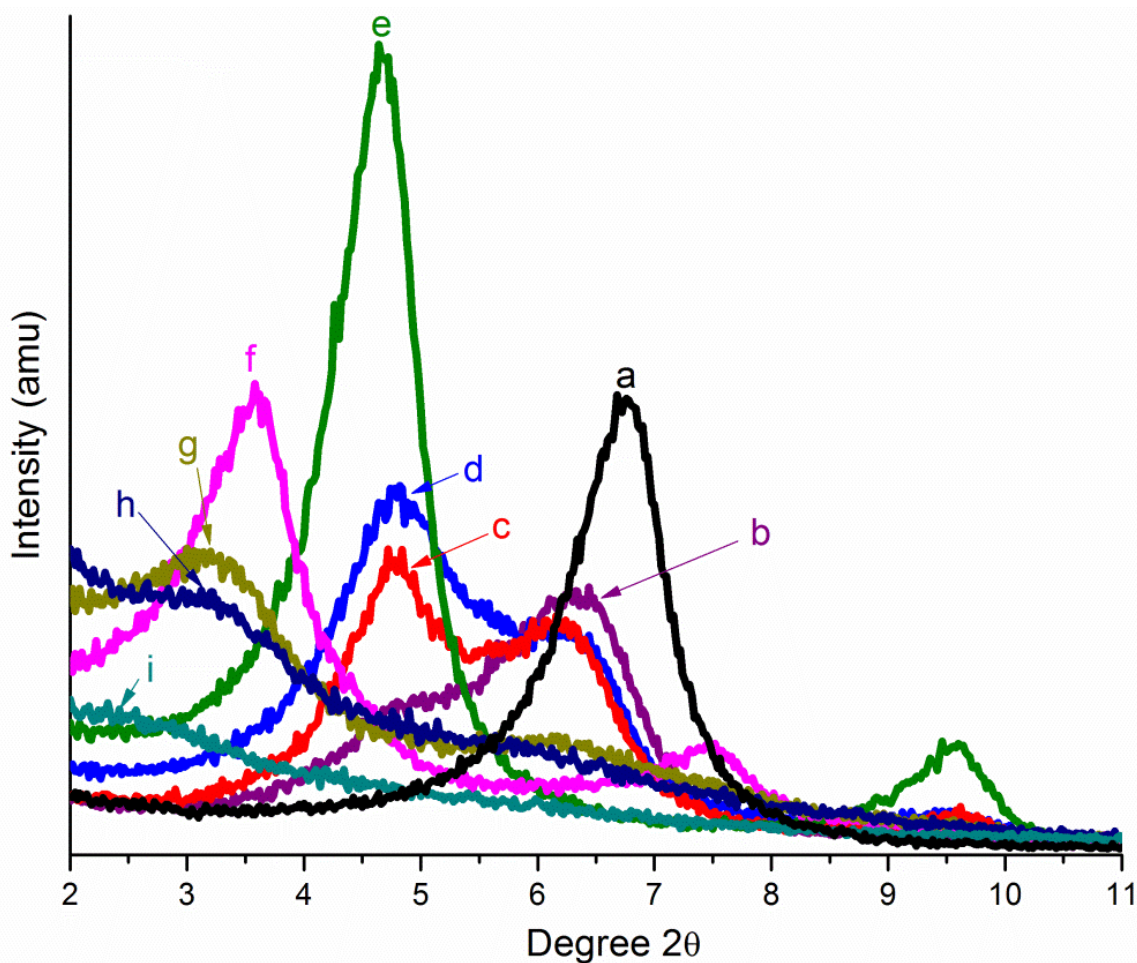


**Figure 3.1:** XRD traces of a) Na-smectite, and varying amounts of glycerol carbonate/Na-smectite as b) 20 wt% c) 30 wt% d) 40 wt% e) 50 wt% f) 60 wt% g) 70 wt% h) 80 wt% and i) 90 wt% of glycerol carbonate in Na-smectite.

The second possibility was more plausible i.e., disordered intercalation, as found by a change in the FWHM value of 001 reflection from  $1.16^\circ 2\theta$  of Na-smectite to  $1.56^\circ 2\theta$ . When the amount of **1A** increased to 20 wt% (0.2 g/ 0.8 g clay), the 001 reflection was split with  $d$ -values of 0.50 and 0.88 nm with a FWHM value of  $2.01^\circ 2\theta$ . The splitting of the diffraction trace for the GC/Na smectite complex indicated that a segregation between Na-water interlayer layer and Na-GC interlayer may have occurred, where only some layers intercalated **1A**. When the amounts of **1A** were 30 and 40 weight percent (0.3 g/ 0.7 g clay and 0.4 g/ 0.6 g clay), partial intercalation was still observed as the

splitting of the 001 reflection, with gallery heights of 0.5 and 0.95 nm with FWHM values of 2.58 and 2.47 °2 $\theta$ .

**Table 3.1:** Full width at half maximum (FWHM) values and  $d(001)$  spacing for **1A** intercalated Na-smectite complexes

Amount of glycerol carbonate (wt%)	$d(001)$ spacing (nm)	FWHM value (°2 $\theta$ )
00	1.29	1.16
10	1.40	1.56
20	1.78, 1.40	2.01
30	1.84, 1.42	2.58
40	1.85, 1.42	2.47
50	1.99	0.96
60	2.47	1.59
70	2.83	2.02
80	2.89	3.44
90	3.70	4.80

On loading an amount of 50 wt% GC (0.5/0.5 g clay), the basal spacing was 1.09 nm, and no splitting in the basal reflection was observed along with a narrower FWHM (0.96 °2 $\theta$ ) (Figure 3.1). With further increase in **1A** loading, the basal gallery height and the FWHM increased, although no further splitting was observed. When the amount of **1A** was increased from 60 to 70 wt%, the gallery height increased from 1.57-1.93 nm, after which a slight increase to 1.98 nm was observed by using 80 wt% amount of glycerol carbonate. The 001 reflection of Na-smectite was broadened (FWHM 4.8 °2 $\theta$ ) upon

further addition of glycerol carbonate i.e, 90 wt%. Note that above 50 wt% loading of **1A** the intensity of the basal reflections significant decreased. Above 50 wt% GC addition, intercalation disorder (explained in more detail in Section 3.3.2.1) appeared to dominate the intercalates.

A comparison of the gallery height of Na-smectite with the loading amount of glycerol carbonate is shown in Figure 3.2. A 10 wt% of GC was insufficient to observe any change in gallery height. However, by using 20 and 30 wt%, two  $d(001)$  reflections were present. An increase in gallery height was seen with increasing amounts of glycerol carbonate.

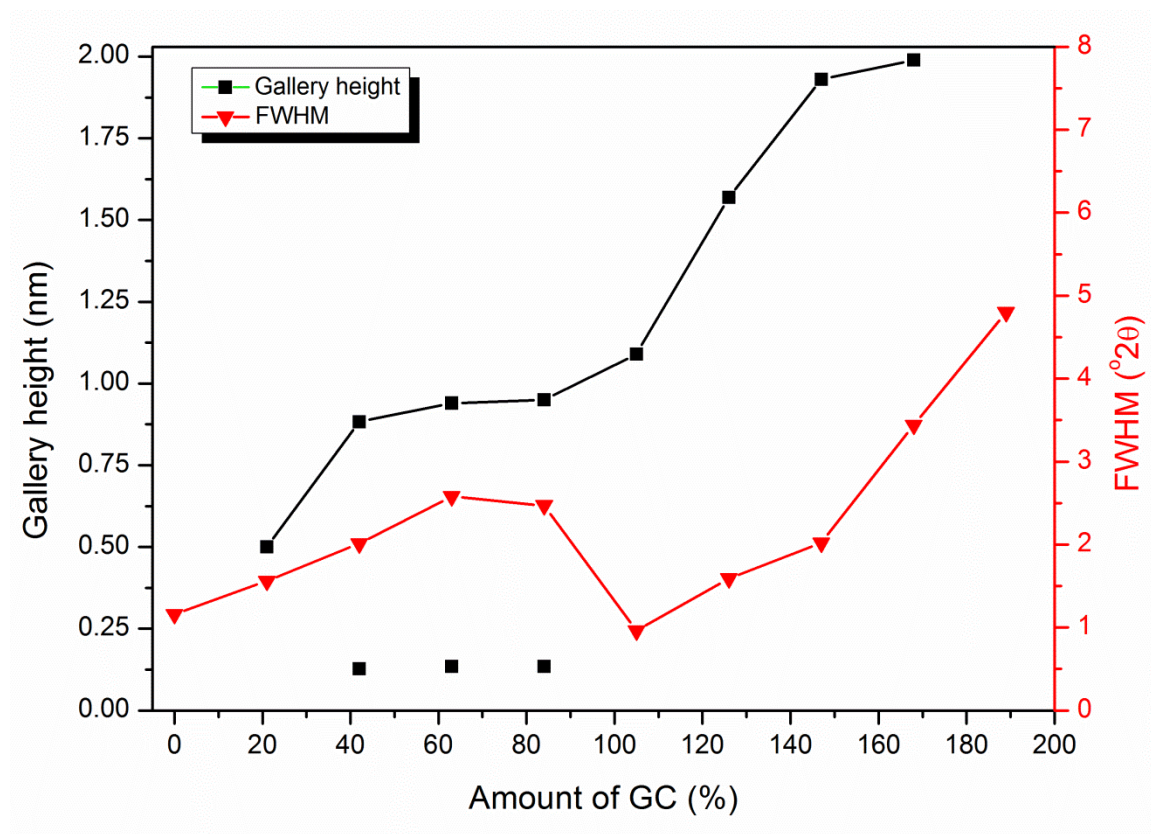


**Figure 3.2:** Change in gallery height and FWHM values of Na-smectite by varying the amount of glycerol carbonate (For 20-40 wt%, two reflections were present and gallery height calculated for each reflection).

Figure 3.2 also showed the effect of the amount of glycerol carbonate on FWHM values (broadening of 001 reflection). Na-smectite showed a narrow reflection with FWHM 1.16 °2θ. Adding 20 and 30 wt% amounts of GC into Na-smectite resulted in increased FWHM values. A narrow reflection was observed for 50 wt% amount of GC, which was comparable with FWHM value of Na-smectite suggesting an ordered arrangement of clay platelets upon intercalation. However, increasing further amounts of glycerol carbonate resulted in broadening of the 001 reflection due to disordered arrangement of clay platelets (the 001 reflection without the loss of intensity was observed suggesting that the clay particles were not delaminated).

From the basal spacing and the molecular size of GC (0.63 nm), the possible occupancy of the intercalated glycerol carbonate can be deduced. As an example, a representative diagram of Na-smectite showing mono- and bi-layer arrangements of glycerol carbonate by using 84 and 90 wt% amount of GC is shown in Figure 3.3. A basal spacing of 2.94 nm was achieved by adsorption of glycerol carbonate at an amount of 84 wt%.



### 3.3.1.2 Study of glycerol carbonate by FTIR

The FTIR spectrum in the range 4000-600  $\text{cm}^{-1}$  of GC/Na-smectite complex is shown in Figure 3.4 together with Na-smectite and glycerol carbonate (**1A**).

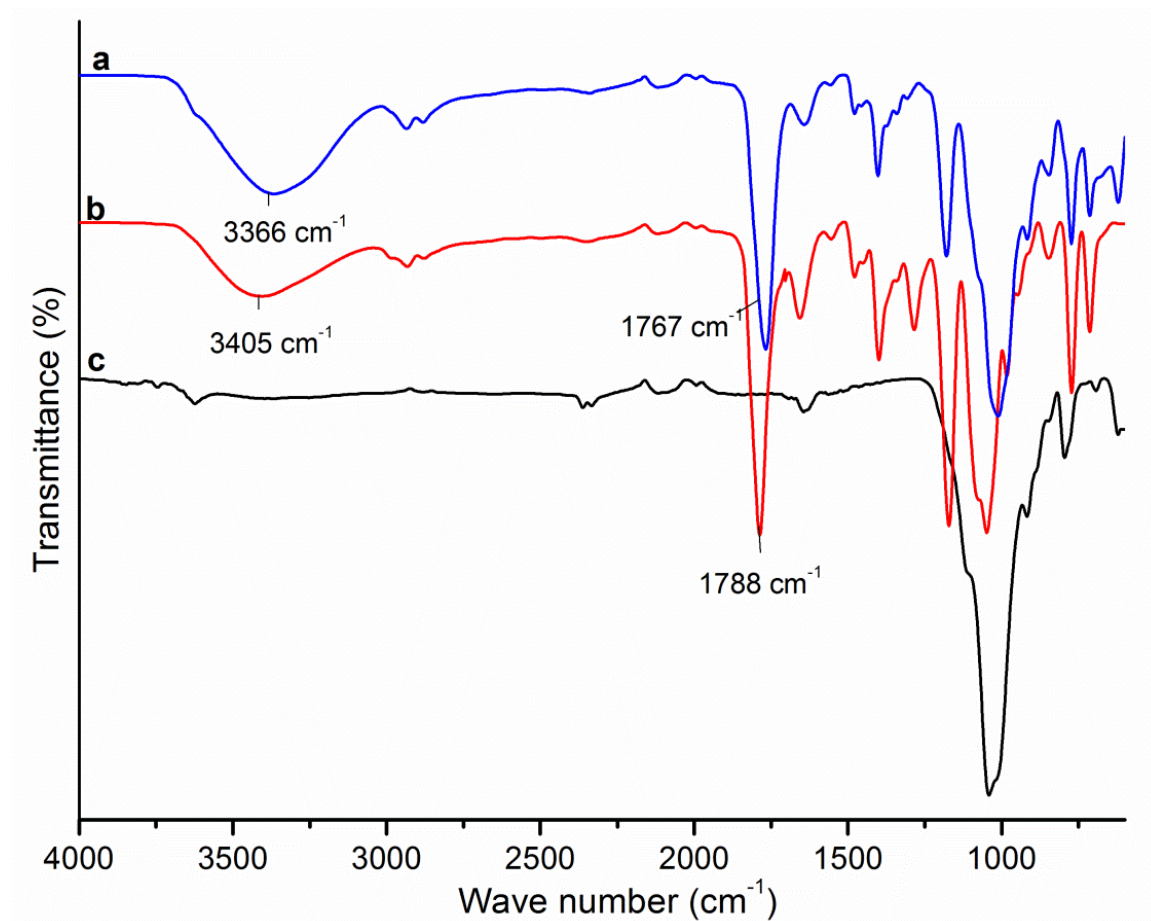


**Figure 3.4:** FTIR spectra of a) glycerol carbonate intercalated sodium smectite b) glycerol carbonate, and c) Na-smectite.

A spectral shift towards higher wavelengths (i.e. lower wavenumber, lower energy and lower frequency) is called a red-shift or a bathochromic shift, whereas, a spectral shift towards lower wavelengths (i.e. higher wavenumber, higher energy and higher frequency) is termed as blue-shift or hypsochromic shift. A significant red shift (about 21  $\text{cm}^{-1}$ ) for the characteristic cyclic carbonyl (C=O) stretch and a larger red shift (39  $\text{cm}^{-1}$ ) for  $\nu(\text{O}-$

$\text{H})_{\text{str}}$  was observed for glycerol carbonate when intercalated with sodium smectite. In the case of sodium smectite, a blue shift (about  $6 \text{ cm}^{-1}$ ) for  $\nu(\text{O-H})_{\text{str}}$  and red shift of (about  $8 \text{ cm}^{-1}$ ) for  $\nu(\text{Si-O})_{\text{str}}$  was observed upon intercalation of glycerol carbonate into sodium smectite. Bands of glycerol carbonate appearing in the region below  $1200 \text{ cm}^{-1}$  associated with C-O stretching were considered after the subtraction of Na-smectite spectra (Figure 3.5). Excess of GC was removed by washing the clay intercalated complex with water.

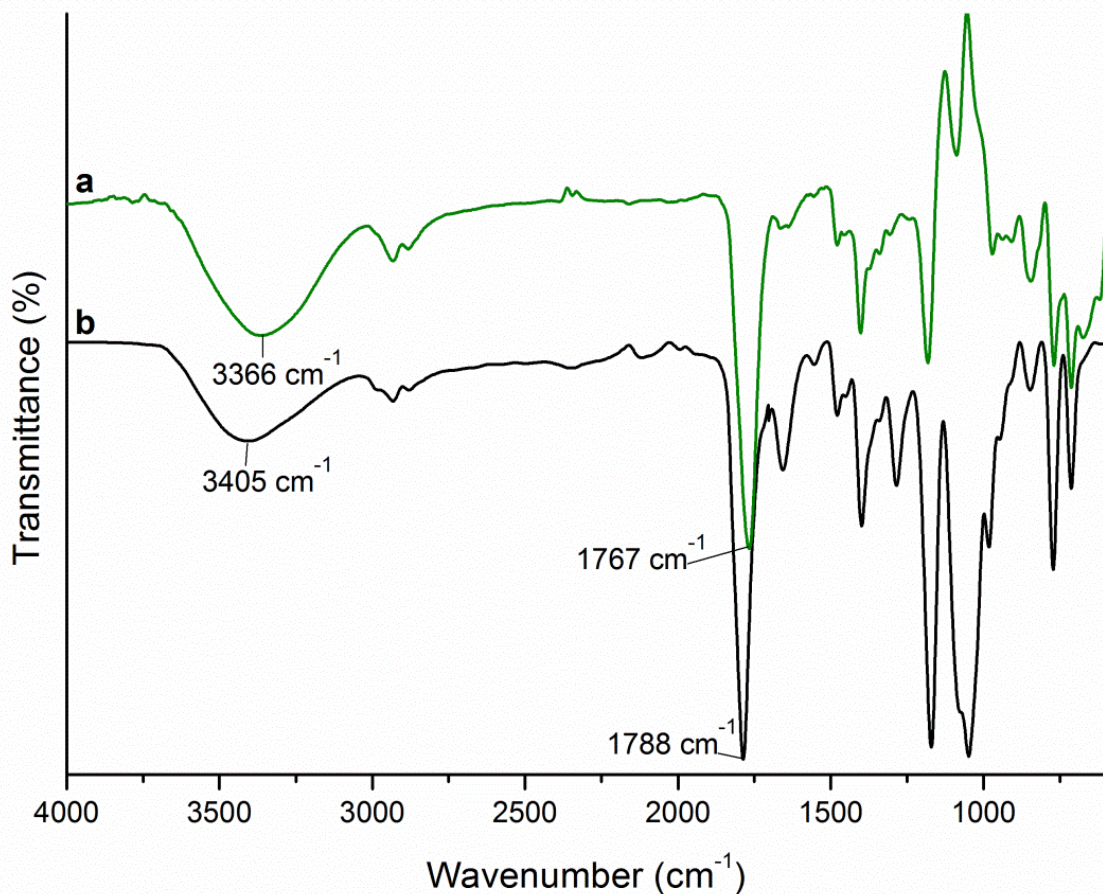


**Figure 3.5:** Figure showing comparison of FTIR spectra of a) subtracted glycerol carbonate (glycerol carbonate intercalated sodium smectite-Na-smectite), and b) glycerol carbonate.

A large red shift in the hydroxyl stretching of glycerol carbonate suggests that in addition to the interaction of the carbonyl group with sodium cations (Onikata et al., 1999), the

hydroxyl of glycerol carbonate may be involved in co-ordination with the surface oxygen groups of smectite. Hydrogen bonding of glycerol carbonate with the surface oxygen of smectite resulted in a shift of  $(\text{Si-O})_{\text{str}}$  by increasing the electron density on Si-O (Sikdar et al., 2008).

### **3.3.1.3 Interaction of glycerol carbonate with Na-smectite**

The interaction of smectite with various organic molecules has been determined with the aid of X-ray diffraction and FTIR spectroscopy. Considering the clay structure, three active components of smectite may be involved in the interaction with organic molecules, which are

- 1) Na-cations in Na-smectite
- 2) Water molecules/Interlayer water
- 3) Surface oxygen of Na-smectite

Exchangeable cations (via co-ordination complexes) and surface oxygen (H-bonding with O-H containing compounds) of tetrahedral sheets are the possible adsorption sites in smectites (Sandi, 2005). However, interlayer water also affects and influences the adsorption of organics by facilitating their penetration.

An aqueous solution of glycerol carbonate was used for the preparation of intercalated complex. Air-drying samples for few hours at ambient conditions was insufficient to remove water from the hygroscopic glycerol carbonate.

In order to determine whether the water molecules were involved in the formation of the GC/Na-smectite intercalation complex, a study on 50 wt% glycerol carbonate (**1A**) (0.1/0.1 g, GC/clay) was performed. Weight loss (%) of Na-smectite and **1A** was calculated (Table 3.2) from weighing the samples before and after heating the samples

at 105 °C overnight with subsequent cooling under a nitrogen atmosphere. The weight loss was assumed to be water loss from samples. Intercalated **1A**/Na-smectite was prepared from non-oven dried glycerol carbonate and Na-smectite at atmospheric conditions and weight loss calculated from weighing the intercalated complex before heating at 105 °C overnight with subsequent cooling to room temperature under a nitrogen atmosphere.

**Table 3.2:** Percent weight loss in glycerol carbonate and its intercalated complexes and resulting *d*-spacing of intercalated complex

Sample	Weight loss (water loss) %	<i>d</i> (001) spacing (nm)	Gallery height (nm)
Glycerol carbonate (GC, <b>1A</b> )	9.2	-	-
Na-smectite	6.6	1.26	0.33
<b>1A</b> /Na-smectite	23.0	1.79	0.83

The powder XRD of the oven dried sodium smectite along with its glycerol carbonate intercalated complex is presented in Figure 3.6. For oven dried Na-smectite (rehydrated in atmosphere), the *d*(001) reflection appeared at 1.26 nm (*d*-space of one layer hydrate) and when intercalated with **1A** at 50 wt%, the basal reflection shifted to *d*(001) = 1.79 nm, whereas *d*(001) reflection of air dried 1A/Na-smectite complex was 1.99 nm.

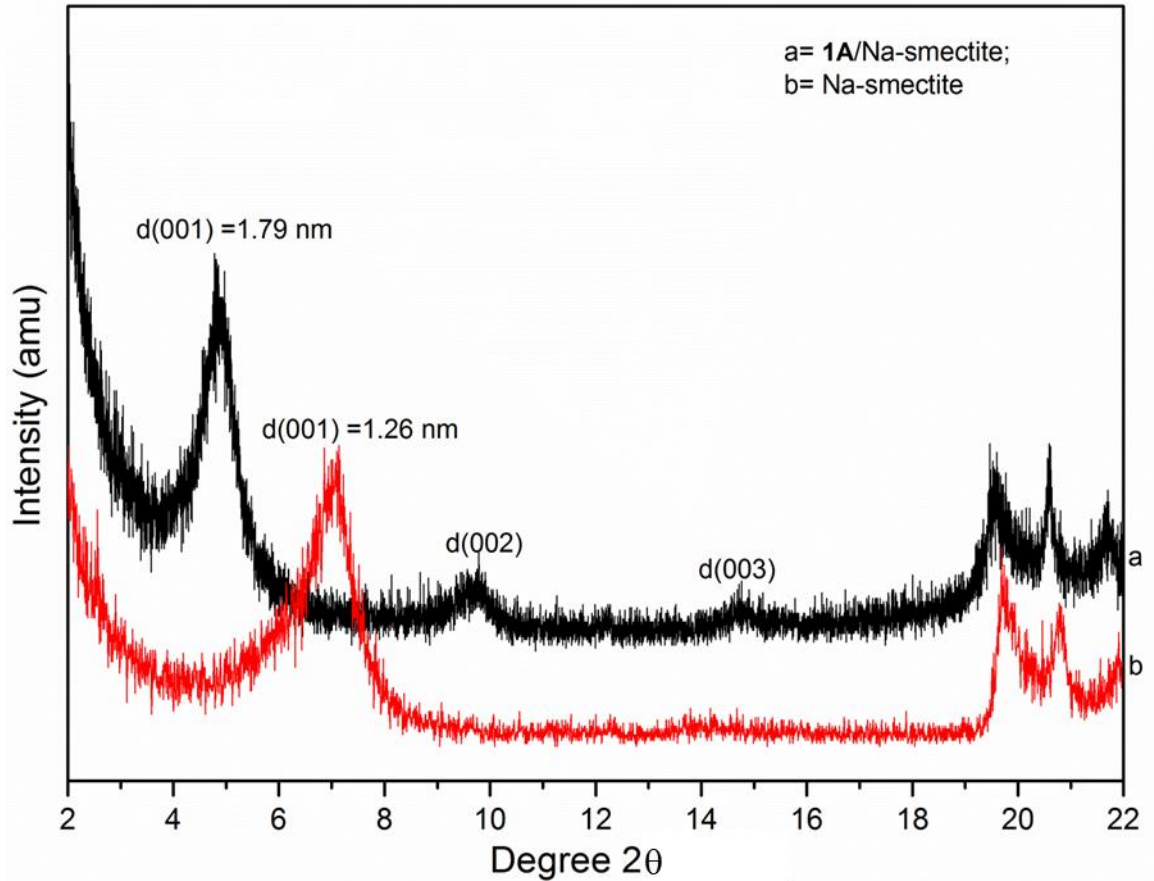


**Figure 3.6:** XRD spectra of Na-smectite along with 1A/Na-smectite complex.

Na-smectite has  $a$  and  $b$  unit cell dimensions of, respectively, 0.518 and 0.898 nm (Deeds and Van Olphen, 1963). Unit cell area of Na-smectite can be calculated as:

$$\text{Unit cell area} = A = a \times b = 0.518 \times 0.898 = 0.4652 \text{ nm}^2$$

Based on a reasonable assumption that all glycerol carbonate in the loadings used (up to 90 wt%) is present in the interlayer gallery, the gallery height for glycerol carbonate (50 wt%) ( $C_{GH}$ ) can be calculated experimentally from the XRD information  $d(001)$  and clay layer thickness,

$$C_{(001)} = C_{GH} + C_{CLT}$$

$$C_{GH} = C_{(001)} - C_{CLT}$$

$$C_{GH} = 1.79 - 0.96 = 0.83 \text{ nm}$$

On assuming that six water molecules are present as a hydration shell surrounding the sodium cation, the volume of GC occupying the unit cell gallery of clay can be calculated from the unit cell area,  $C_{GH}$  and volume of hydrated sodium cation as:

$$\begin{aligned} \text{GC unit volume occupied} &= (A \times C_{GH}) - (\text{volume of hydrated Na} \times \text{Net charge per unit cell}) \\ &= (0.4652 \text{ nm} \times 0.83 \text{ nm}) - (0.0510 \text{ nm}^3 \times 0.8) = 0.3861 \text{ nm}^3 - 0.0408 \text{ nm}^3 = 0.3453 \text{ nm}^3 \end{aligned}$$

Hence, number of GC molecules per unit cell can be calculated from the GC mass, where the GC density is  $1.4 \text{ g/cm}^3$ .

$$\text{Mass of GC} = \text{Density} \times \text{Volume}$$

$$\text{Mass of GC} = 1.4 \times 0.3453 \times 10^{-21} = 4.8 \times 10^{-22} \text{ g}$$

$$\text{Moles of GC/unit cell} = n = 4.8 \times 10^{-22} \text{ g} / 118 \text{ g/mol} = 4.1 \times 10^{-24} \text{ mol}$$

Number of molecules of GC/unit cell =  $n \times N_A = 4.1 \times 10^{-24} \times 6.02 \times 10^{23} = 2.5$  molecules, where  $N_A$  is Avogadro's number (constant =  $6.02 \times 10^{23}$ ).

**Table 3.3:** Information about Na-smectite (Trugel) and number of glycerol carbonate molecules per unit cell of Na-smectite. Data on Trugel chemistry and crystallography provided by Dr. W.P.

Gates (Monash University)

Information	Result
Chemical analysis (%)	SiO <sub>2</sub> , 66; Al <sub>2</sub> O <sub>3</sub> , 24.2; Fe <sub>2</sub> O <sub>3</sub> , 3.34; MgO, 3.3; CaO, 3.1.
Cation exchange capacity (CEC) of Na-smectite	105 cmol <sub>c</sub> /Kg
Unit cell formula*	(Si <sub>7.79</sub> Al <sub>0.21</sub> ) <sup>IV</sup> (Al <sub>3.09</sub> Fe <sub>0.29</sub> Mg <sub>0.63</sub> ) <sup>VI</sup> O <sub>20</sub> (OH) <sub>4</sub>
Unit cell dimensions	<i>a</i> = 0.518 nm, <i>b</i> = 0.898 nm, <i>c</i> = 0.96 nm
Unit cell area ( <i>axb</i> )	0.4652 nm <sup>2</sup>
Gallery height with glycerol carbonate (C <sub>GH</sub> )	0.83 nm
Gallery Unit volume occupied by glycerol carbonate	0.3453 nm <sup>3</sup>
Net total charge/unit cell	-0.81
Formula weight of Na-smectite	747.4 g/mol
Formula weight of glycerol carbonate	118 g/mol
No of Na cations/unit cell	0.81
Glycerol carbonate molecule/unit cell	2.5

\* Assuming no interlayer water (normally 4-8 water molecules per unit cell under ambient conditions i-e., 12-15% water content).

The information in Table 3.3 can be used to suggest models for possible arrangements of the 2.5 GC molecules intercalated within a unit cell of sodium smectite giving rise to a gallery height of 0.89 nm (Figure 3.7b). The model in Figure 3.7c indicates minimal

interactions among glycerol carbonate molecules (predicted by GAMESS software) and suggests that the cyclic carbonate ring may lie inclined to the silicate layer in the interlayer space.

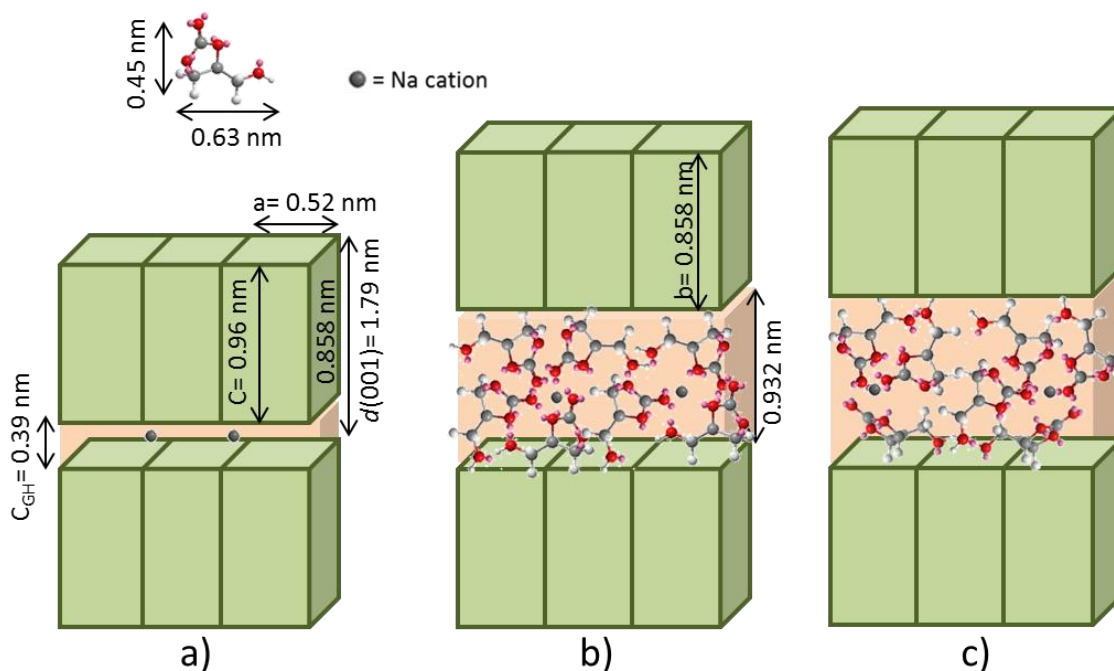


**Figure 3.7:** A representative figure suggesting possible arrangement of glycerol carbonate molecules within interlayer gallery of Na-smectite along with the molecular length of glycerol carbonate, where  $a$  = Na-smectite without any glycerol carbonate,  $b$  and  $c$  = arrangement of 2.5 molecules of glycerol carbonate per unit cell of smectite.

FTIR spectra (Figure 3.8) of the oven dried glycerol carbonate intercalated complex show a change in frequencies ( $< 20 \text{ cm}^{-1}$ ) of the hydroxyl stretch as well as the carbonyl stretch. A red shift of about  $15 \text{ cm}^{-1}$  for hydroxyl and  $4 \text{ cm}^{-1}$  for the carbonyl stretch was observed when intercalated, whereas, a blue shift of about  $9 \text{ cm}^{-1}$  and a red shift of  $20 \text{ cm}^{-1}$  were observed for cyclic  $(\text{C-O})_{\text{str}}$ . For acyclic  $(\text{C-O})_{\text{str}}$ , no change was observed in FTIR. The Na-smectite showed a blue shift of  $5 \text{ cm}^{-1}$  in  $(\text{Si-O})$  stretch upon formation of glycerol carbonate/Na-smectite.

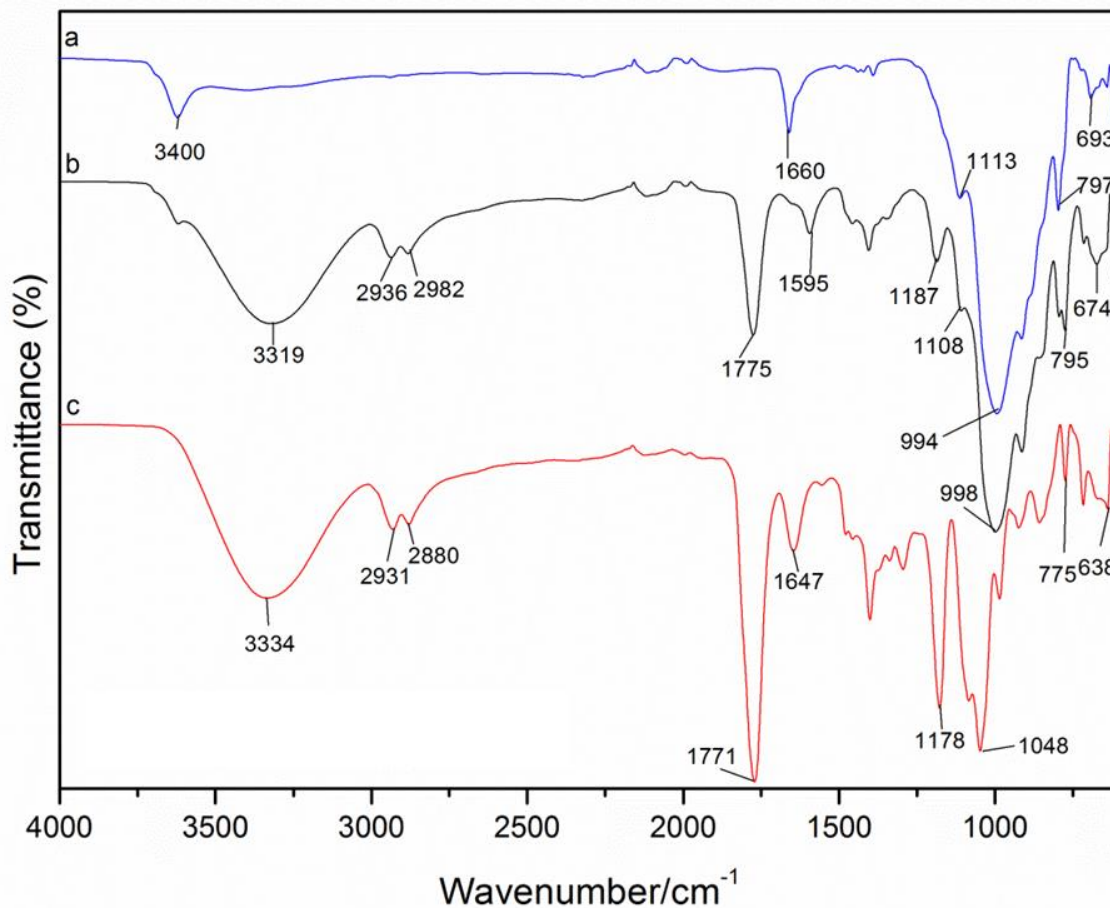


**Figure 3.8:** FTIR spectra of a) Na-smectite b) oven dried glycerol carbonate/Na-smectite and c) oven dried glycerol carbonate.

The presence of interlayer water was also evident by observing stretching around 1647 cm<sup>-1</sup> in FTIR (Figure 3.8). This showed that the GC/Na-smectite complex held interlayer water even on heating at 105 °C.

### 3.3.1.4 Model FTIR spectroscopic study for predicting interactions of glycerol carbonate

The main driving force for intercalation of propylene carbonate into Na-smectite is solvation of interlayer sodium cations (Onikata et al., 1999). In order to probe the interaction of GC with sodium cations and interlayer water in Na-smectite, a model study was performed by employing water, sodium chloride and water-sodium chloride solutions, each with glycerol carbonate. The interaction of GC with these components was studied with FTIR spectroscopy by observing the change (red or blue shift) in wavenumber of specific functionality. There are five main functionalities present in glycerol carbonate (Figure 3.9) which can be possibly affected due to the interactions with these components, i.e.,  $(\text{O-H})_{\text{str}}$ ,  $(\text{C=O})_{\text{str}}$ , two cyclic  $(\text{C-O})_{\text{str}}$  and one acyclic  $(\text{C-O})_{\text{str}}$ .

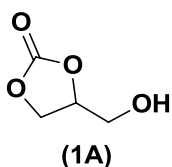


**Figure 3.9:** Structure of glycerol carbonate.

### 3.3.1.4.1 Interaction of glycerol carbonate with water

Water was added in a consecutive manner to glycerol carbonate and the most significant change was observed for  $\nu(\text{O-H})_{\text{str}}$  of glycerol carbonate as seen in Figure 3.10.

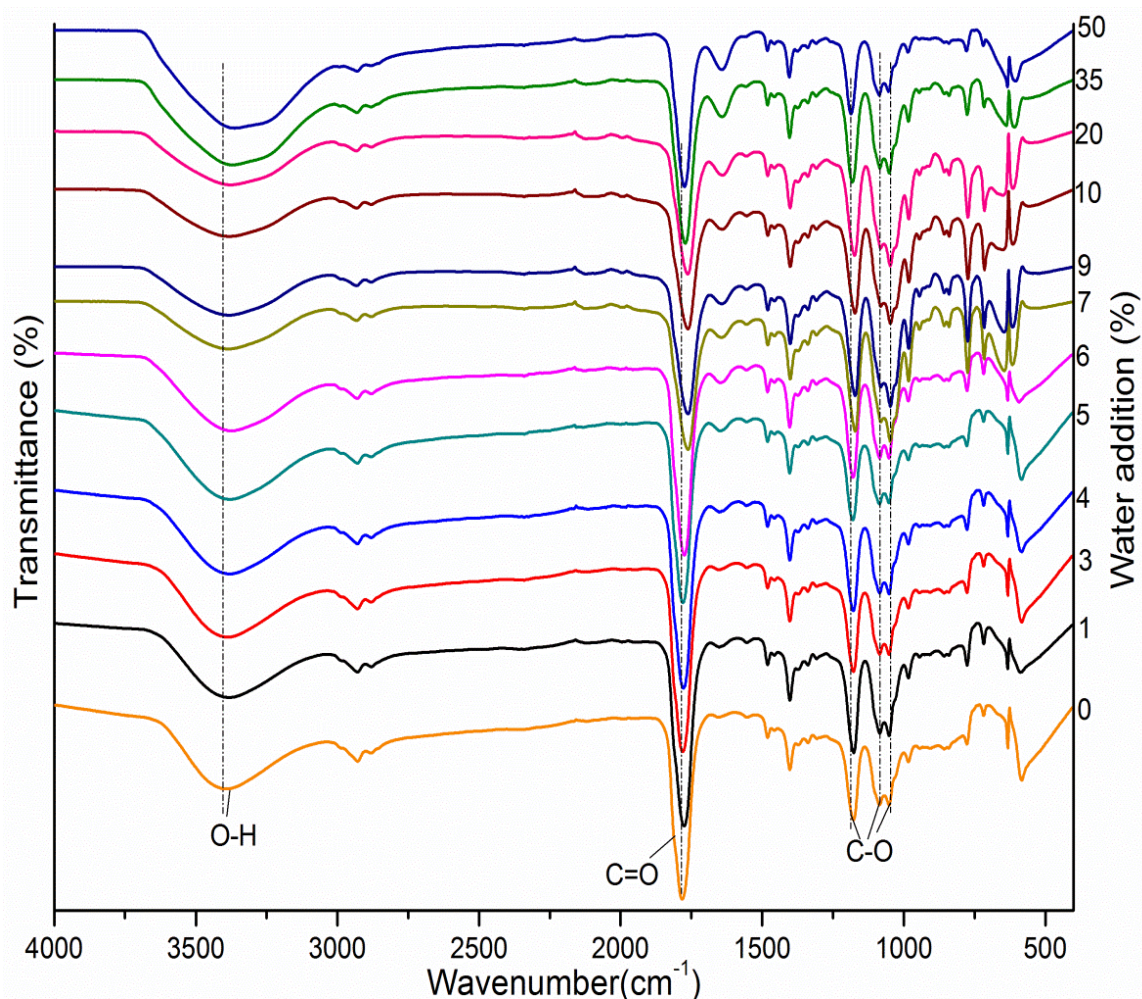


**Figure 3.10:** Stacked FTIR spectra of glycerol carbonate with varying the percentage of water.

It can be clearly seen in Figure 3.11 that with the addition of 1% water,  $\nu(\text{O-H})_{\text{str}}$  (assigned to hydroxyl group of glycerol carbonate) was shifted from  $3334 \text{ cm}^{-1}$  to  $3327 \text{ cm}^{-1}$  (a red shift of  $7 \text{ cm}^{-1}$ ). This red shift can be due to the hydrogen bonding among glycerol carbonate molecules which was affected upon water addition. Increasing red

shift ( $7\text{-}27\text{ cm}^{-1}$ ) of the  $\nu(\text{O-H})_{\text{str}}$  (Figure 3.11) of GC was observed with higher amounts of water. At higher concentration of water such as 50%, a shoulder was detected for O-H stretching. The second major group affected by addition of water was the cyclic carbonyl stretch ( $\text{C=O}$ ) and a variable pattern was observed. The shifts in hydroxyl and carbonyl stretching can be possibly explained as a breakdown of hydrogen bonding among glycerol carbonate molecules as it is diluted with water.

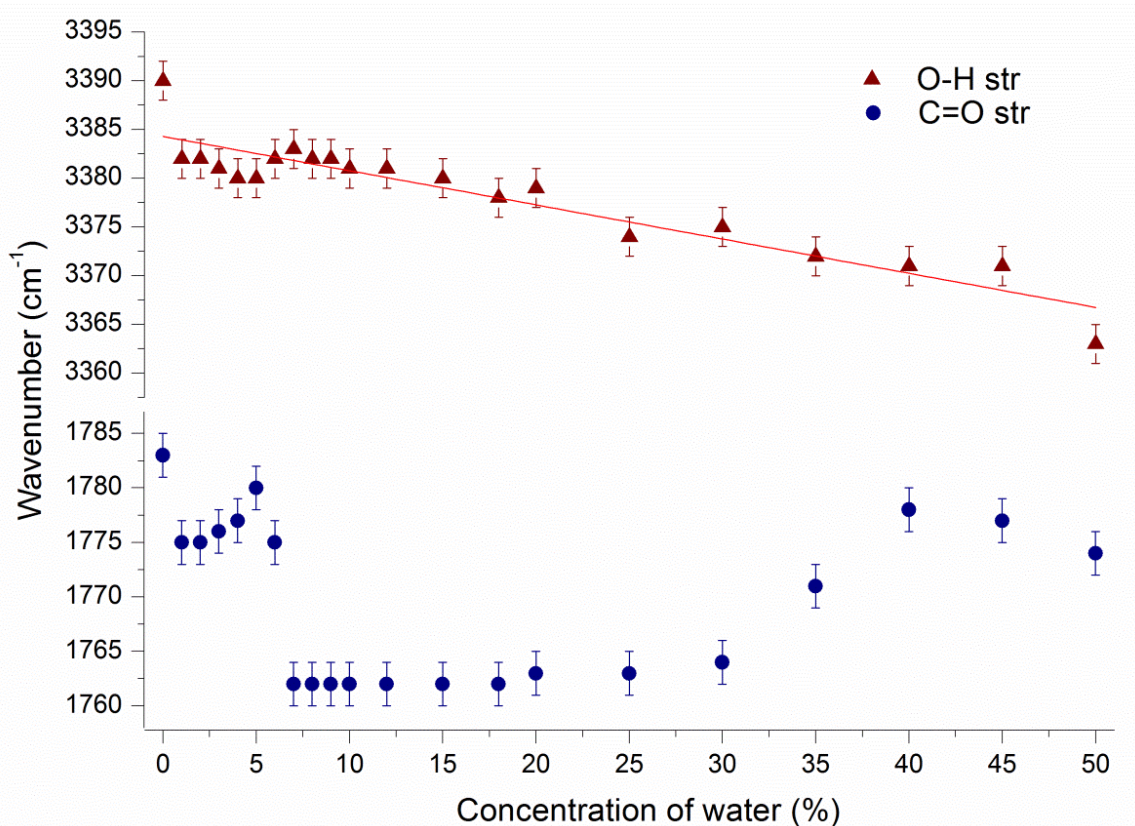


**Figure 3.11:** Effect of concentration of water on hydroxyl and carbonyl stretch of glycerol carbonate. Error bars for the FTIR are in the range of  $\pm 2\text{ cm}^{-1}$  after triplicate measurements.

### 3.3.1.4.2 Interaction of glycerol carbonate with sodium chloride

FTIR wavenumbers of main functionalities of glycerol carbonate affected upon addition of sodium chloride are presented in Figure 3.12. A low concentration of sodium chloride (2000 ppm) as well as higher concentration of sodium chloride (10,000 ppm i-e., this

step is from 0.2 to 1.0% salt levels (5 times) and capable of dissolving in glycerol carbonate to make a saturated solution) was used. It can be clearly seen that the salt has an impact on hydroxyl as well as carbonyl stretching of GC. A blue shift in  $\nu(\text{O-H})_{\text{str}}$  was seen with little amounts of added salt whereas, adding significant amounts resulted in a red shift. For carbonyl stretching, a small blue shift up to  $4 \text{ cm}^{-1}$  was observed. The blue shifts may explain the interaction of sodium salt with the carbonyl as well as hydroxyl groups of glycerol carbonate.

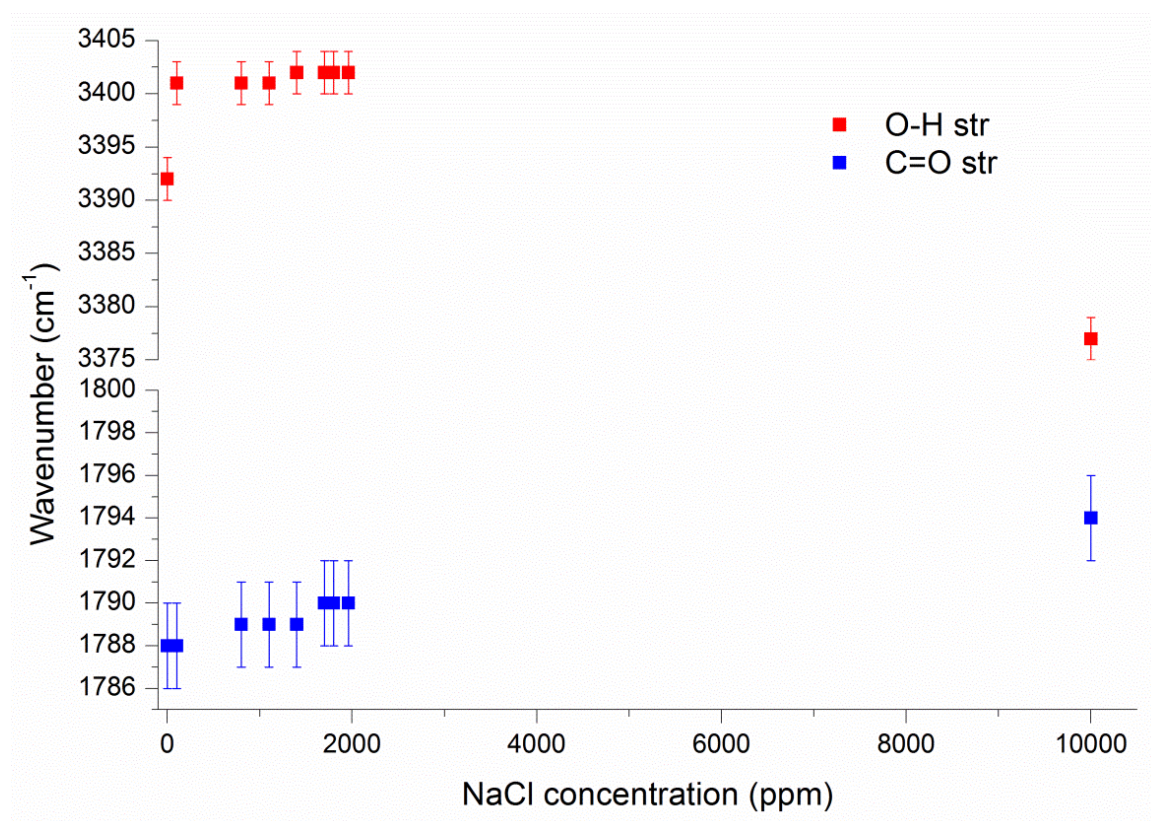


**Figure 3.12:** Plot of concentration of sodium chloride versus wavenumbers of  $\nu(\text{O-H})_{\text{str}}$  and  $\nu(\text{C=O})_{\text{str}}$  of glycerol carbonate. Error bars for the FTIR are in the range of  $\pm 2 \text{ cm}^{-1}$  after triplicate measurements.

#### **3.3.1.4.3      *Interaction of glycerol carbonate with sodium chloride and water***

In the previous Sections (3.3.1.4.1 & 3.3.1.4.2), it has been shown that water as well as salt interacted with glycerol carbonate. The interactions of GC with a mixture of salt and water were studied by using a 10,000 ppm solution of sodium chloride (in glycerol carbonate) and then varying the percentage amount of water (with respect to salt concentration).

Figure 3.13 shows a little/no change in  $\nu(\text{O-H})_{\text{str}}$  for up to 50% water compared to the reference salt solution (in glycerol carbonate). However, from 60% water and onwards, a red shift of  $8 \text{ cm}^{-1}$  was observed. A complicated effect (red shift as water was increased to 30% followed by no distinct change upto 50% water content and a subsequent blue shift when water percentage was increased from 50% to 60%) was observed for the  $\nu(\text{C=O})_{\text{str}}$  upon water addition. Water affects the H-bonding between glycerol carbonate molecules producing a change in the hydroxyl stretch frequency. The interaction of  $\nu(\text{C=O})_{\text{str}}$  with sodium chloride changed upon water addition as the salt became associated with water. However, the influence of salt on the cyclic carbonyl did not diminish out by addition of water, which suggests the existence of interaction between the carbonyl group and the salt through water.

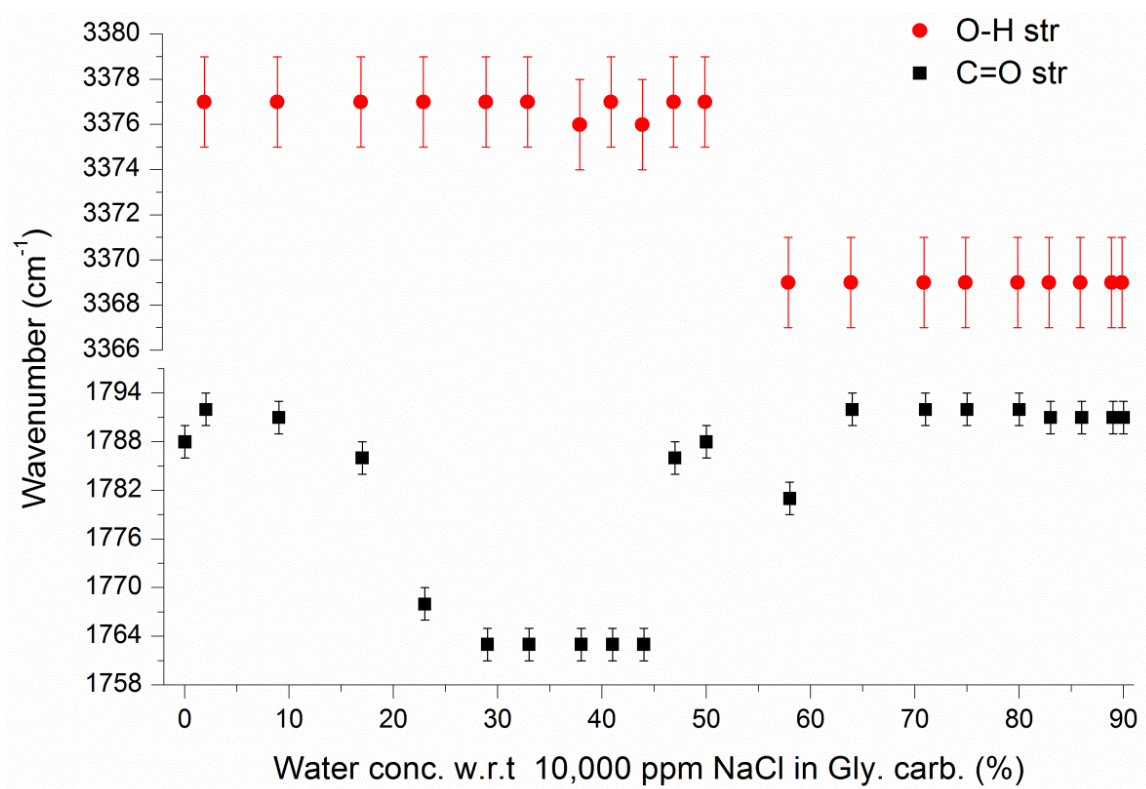


**Figure 3.13:** Influence of concentration of water on O-H and C=O stretching of glycerol

carbonate (with 10,000 ppm sodium chloride). Error bars for the FTIR are in the range of  $\pm 2 \text{ cm}^{-1}$  after triplicate measurements.

When the findings of this model FTIR study were applied to the FTIR result of intercalated glycerol carbonate/Na-smectite complex, a distinct red shift ( $15 \text{ cm}^{-1}$ ) for hydroxyl and a blue shift ( $4 \text{ cm}^{-1}$ ) for carbonate was seen. This suggests the possible interaction or complexation of the carbonate functionality of GC with sodium cations and influence of interlayer water. Glycerol carbonate competes with water for the coordination sites around the sodium cation and either results in:

- 1) Replacement of water by glycerol carbonate around sodium cation and strong coordination of the cyclic component of GC with the salt. The lower percentage of water in the system under study resulted in a greater shift ( $>4 \text{ cm}^{-1}$ ) for  $\nu(\text{C=O})$  as observed by FTIR study, or

- 2) Occupation of sites in the second sphere of co-ordination around the cation via bridging water molecules. As the percentage of water was increased, it resulted in a smaller shift ( $<4\text{ cm}^{-1}$ ) of  $\nu(\text{C}=\text{O})$  for GC intercalated complex and observed using FTIR spectroscopy.

Relatively small shifts of the  $\nu(\text{C}=\text{O})_{\text{str}}$  for GC/Na-smectite complexes are proposed to be indicative of the interaction of the glycerol carbonate functionality with the interlayer cation via water bridging which is in accordance with the published work on propylene carbonate (Onikata et al., 1999).

### **3.3.1.5 Stability studies of glycerol carbonate**

The stability, physical and chemical compatibility is the primary concern for the synthesis of cyclic organic carbonates. A stability study for the synthesized glycerol carbonate was carried out, under conditions that mimick the leachate from industrial or mining waste streams (Hornsey et al., 2010).

The stability test on glycerol carbonate was undertaken at standard temperature and pressure in 1M NaCl and 1M  $\text{CaCl}_2$  aq. Solution at different pH. The results from IR and  $^{13}\text{C}$ -NMR obtained are shown below in Table 3.4.

**Table 3.4:** Stability data (IR and  $^{13}\text{C}$ -NMR) of glycerol carbonate at different pH values

pH	Salt solution		IR data C=O <sub>str</sub> (carbonyl) $\nu/\text{cm}^{-1}$	$^{13}\text{C}$ -NMR (95% H <sub>2</sub> O+5%D <sub>2</sub> O) $\delta$ (ppm)	Test Duration
	NaCl	CaCl <sub>2</sub>			
7	✗	✗	1780	157.78, 78.1, 66.8, 61.0.	1.5 year
2	✓	✗	No change	No change	1.5 year
3	✓	✗	No change	No change	1.5 year
4	✓	✗	No change	No change	1.5 year
7	✓	✗	No change	No change	1.5 year
2	✗	✓	No change	No change	1.5 year
3	✗	✓	No change	No change	1.5 year
4	✗	✓	No change	No change	1.5 year
8	✗	✓	No change	No change	1.5 year

The results obtained from  $^{13}\text{C}$ -NMR and IR data indicated that the cyclic ring of glycerol carbonate is stable under the conditions tested, for a period up to 18 months. From these studies, it can be concluded that glycerol carbonate is potentially suitable to be used effectively in geosynthetic clay liners due to its non-volatile nature and stability at high boiling point and different pH values.

### 3.3.2 Preparation of cyclic carbonates intercalated Na-smectites complexes

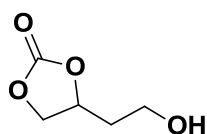
The previously synthesized cyclic carbonates were used for the preparation of intercalated complexes with sodium smectite. Films of samples (on a ceramic tile) were prepared as mentioned previously in Section 3.3.1. The films were air dried for three hours and characterized by X-ray diffraction (XRD) and FTIR spectroscopies.

#### 3.3.2.1 Intercalation of hydroxyl containing cyclic carbonate into Na-smectite

The 50 weight percent amount of cyclic carbonate was used for the preparation of cyclic carbonate/Na-smectite complexes. The  $d(001)$  reflection of Na-smectite appeared at 1.29 nm with a gallery height of 0.39 nm as determined by powder XRD (employing Bragg's equation). The gallery height was determined as

Gallery height =  $C_{GH} = d(001)$  spacing – thickness of silicate layer (0.898 nm).

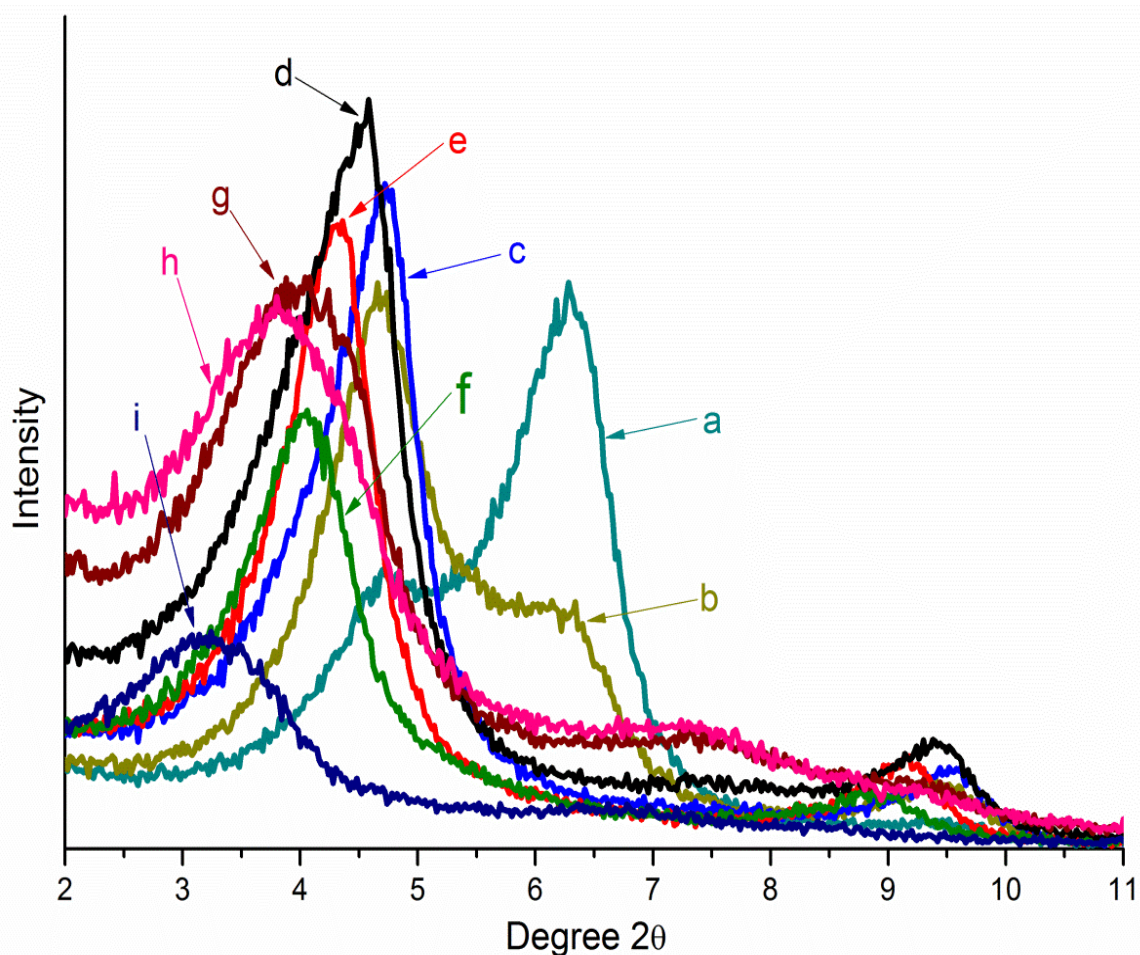
XRD patterns of different amounts (10 wt%-90 wt%) of 4-(2-ethyl)1-3-dioxolan-2-one (**2A**) intercalated with Na-smectite are shown in Figure 3.15.



**Figure 3.14:** Structure of 4-(2-ethyl)1-3-dioxolan-2-one (**2A**).

It is clear that two basal reflections were present until 20 wt% ( $1.38^\circ 2\theta$ ) which suggests segregation of the intercalates formed between the Na-water interlayer and Na-cyclic carbonate interlayer. For 30-80 wt%, a single reflection with an increase in gallery height of Na-smectite was observed (0.99-1.44 nm). A narrow FWHM ( $1.17^\circ 2\theta$ ) was seen for 30 wt% amount of **2A**, while a broader FWHM ( $2.01^\circ 2\theta$ ) was observed at 80 wt%. By

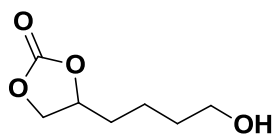
increasing the amount of **2A** from 80 to 90 wt%, the gallery height increased to 1.88 nm indicating further expansion of smectite galleries. Above 40 wt% the intensity of the 001 band diminished, and coupled with the increased FWHM, intercalation rates above 40 wt% of **2A** appeared to result in increased disorder of the intercalate.



**Figure 3.15:** XRD diffraction patterns of various amounts (10-90 wt%) of **2A** in **2A/Na-smectite** complexes, where a) 10 wt% b) 20 wt% c) 30 wt% d) 40 wt% e) 50 wt% f) 60 wt% g) 70 wt% h) 80 wt% and i) 90 wt% of **2A** in Na-smectite.

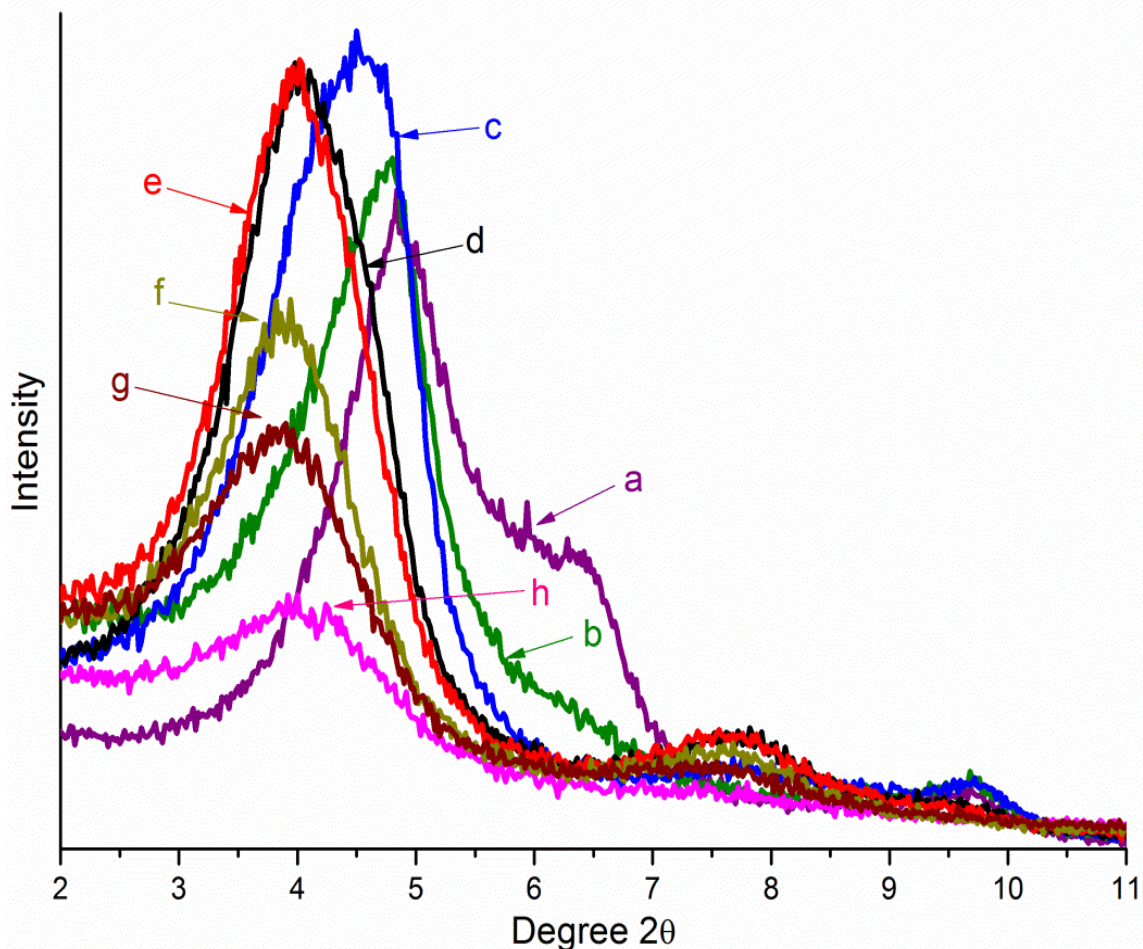
When 4-(4-butyl)-1,3-dioxolan-2-one (**3A**) (Figure 3.16), was intercalated using 20 wt% (0.2 g/ 0.8 g clay) into Na-smectite, two distinct reflections were observed with a gallery height of 0.48 and 0.93 nm and with a FWHM value of 1.93 °2θ. This suggests that an

insufficient amount of **3A** was intercalated for uniform monolayer adsorption into Na-smectite (Figure 3.17).



**Figure 3.16:** Structure of 4-(4-butyl)-1,3-dioxolan-2-one (**3A**).

The gallery height was increased to 1.32 nm using 50 wt% (narrow FWHM of 1.53 °2 $\theta$ ), after which a maximum expansion of 1.37 nm was achieved at 90 wt% amount (broader FWHM, 2.96 °2 $\theta$ ). However, above 40 wt% the intensity of the 001 band was significantly diminished, and coupled with the increased FWHM, intercalation rates above 40 wt% of **3A** resulted in increased levels of disorder.



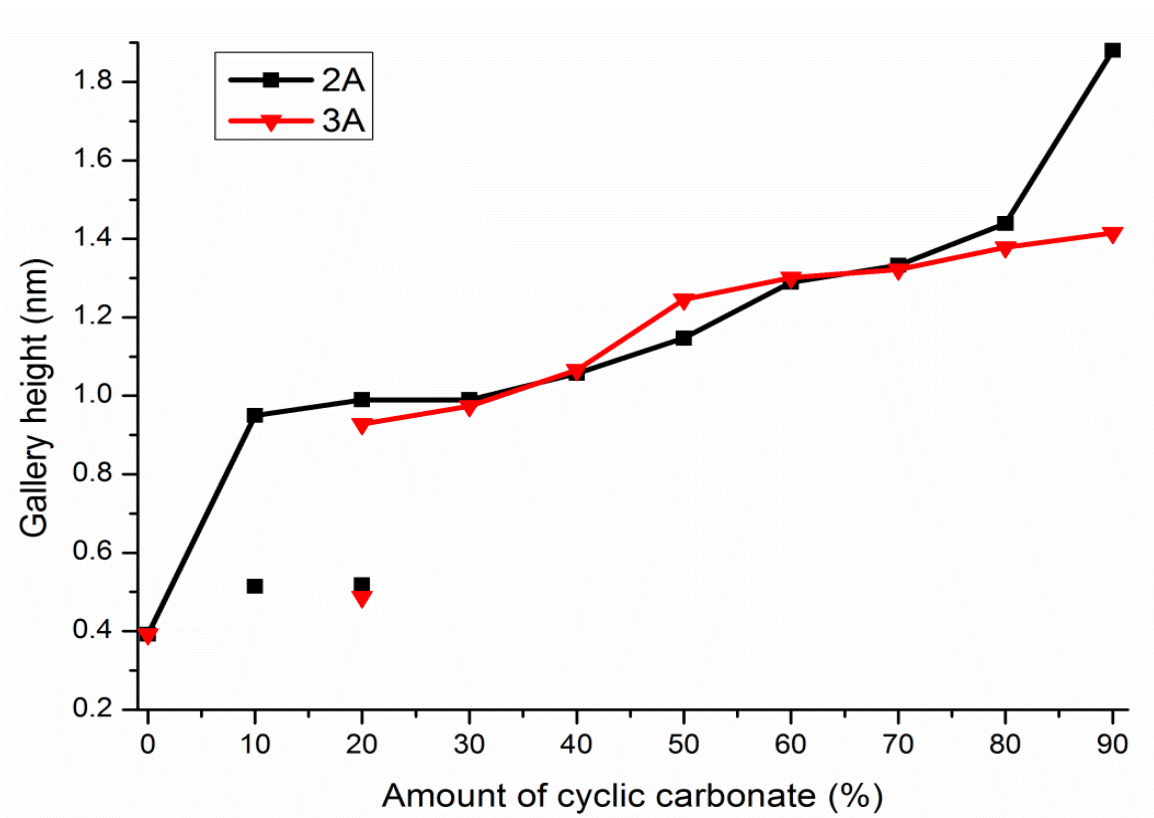
**Figure 3.17:** XRD spectra of various amounts of **3A** in **3A/Na-smectite**, where, a) 20 wt% b) 30 wt% c) 40 wt% d) 50 wt% e) 60 wt% f) 70 wt% and g) 80 wt%.

Table 3.5 shows the results of broadening (FWHM), calculated for the 001 reflection. It was observed that FWHM values decreased with an increased concentration indicating adsorption of cyclic carbonate into Na-smectite. However, further increase in amount of these GC derivatives resulted in increased line broadening due to intercalation disorder. Intercalation disorder as described here is disorder within the interlayer resulting from multiple gallery heights being present within the intercalate. Thus at intercalation loadings above ~40 wt % (**2A**, **3A**) or ~50 wt% (**1A**), multiple gallery heights lacking sufficient long range order were prevalent in the intercalates.

**Table 3.5:** Full width at half maximum (FWHM) values for **2A** and **3A** intercalated Na-smectite complexes

Amount of cyclic carbonate (wt%)	FWHM value ( $^{\circ}2\theta$ )	
	<b>2A</b> /Na-smectite	<b>3A</b> /Na-smectite
10	1.55	-
20	1.83	1.93
30	1.17	1.51
40	1.06	1.46
50	1.40	1.53
60	1.41	1.59
70	1.77	1.87
80	2.01	2.28
90	2.43	2.96

A comparison of the gallery height of cyclic carbonates (**2A-3A**) with their loading amount is shown in Figure 3.18. The only difference in these cyclic carbonates is the variable length of the carbon side chain affecting the molecular length of molecule. Two types of complexes or gallery heights were observed with using 20 wt% amounts for **2A** and **3A**. An expansion in gallery height of Na-smectite was observed with increasing the amount of cyclic carbonate. Intercalation disorder was observed when the amount of cyclic carbonate was increased from 40 wt%.



**Figure 3.18:** Change in gallery height of Na-smectite by varying amounts of **2A** & **3A** (For some amounts of cyclic carbonates, two reflections were present and gallery heights calculated for each reflection).

Adding cyclic carbonate, **3A** (4-carbon side chain) to sodium smectite, resulted in a random interstratification of smectite platelets due to the aliphatic 4-carbon chain. When the amounts were increased to 90 wt%, for **3A**, less expansion of the smectite layers (Figure 3.18) was observed, whereas, **2A** (2-carbon chain) showed a behavior similar to GC.

FTIR wavenumbers of characteristic absorption peaks of the adsorbed **2A**/Na-smectite and **3A**/Na-smectite complexes are summarized in Table 3.6, together with those of cyclic carbonates, **2A** and **3A**. The samples were dried in a vacuum oven prior to FTIR analysis. A small blue shift (about 2-5  $\text{cm}^{-1}$ ) in the characteristic  $\nu(\text{C}=\text{O})_{\text{str}}$  and a larger red

shift (16-17  $\text{cm}^{-1}$ ) for  $\nu(\text{O-H})_{\text{str}}$  was observed upon intercalation (Table 3.6). In addition, the acyclic  $\nu(\text{C-O})_{\text{st}}$  in the molecule showed a blue shift of 3-9  $\text{cm}^{-1}$  when intercalated.

**Table 3.6:** Infrared absorption peaks for sodium smectite complexes with compounds **2A-3A**

Code	FTIR frequencies ( $\text{cm}^{-1}$ )					
	Cyclic carbonate			Cyclic carbonate/Na-smectite		
	$\nu(\text{O-H})_{\text{str}}$	$\nu(\text{C=O})_{\text{st}}$	$\nu(\text{C-O})_{\text{st}}$	$\nu(\text{O-H})_{\text{str}}$	$\nu(\text{C=O})_{\text{st}}$	$\nu(\text{C-O})_{\text{st}}$
<b>2A</b>	3406	1770	1169	3390	1775	1178
<b>3A</b>	3395	1780	1168	3378	1782	1171

A large red shift (16-17  $\text{cm}^{-1}$ ) in the hydroxyl stretching suggests the interaction of side chain whereas, electrostatic interaction of the carbonyl with sodium smectite was suggested by a blue shift in carbonyl stretch via interlayer water. The behaviour of compounds **2A** and **3A** intercalated with sodium smectite was found to be similar to GC/Na-smectite.

### 3.3.2.2 Intercalation of other cyclic carbonates into Na-smectite

Monolayer adsorption was achieved by using a 50 wt% of GC and 40 wt% of compounds **2A** and **3A**. Therefore, other cyclic carbonates were intercalated at a loading of 50 wt% amount. When 50 wt% of compounds **2C**, **3C**, **4A**, **5A**, **6A**, and **8A** (Figure 3.19) were intercalated, the XRD showed a shift of  $d(001)$  reflection to a lower degree as compared with Na-smectite (Figure 3.20) suggesting an expansion of gallery height due to insertion of organic molecules in to the lamellae of smectite.

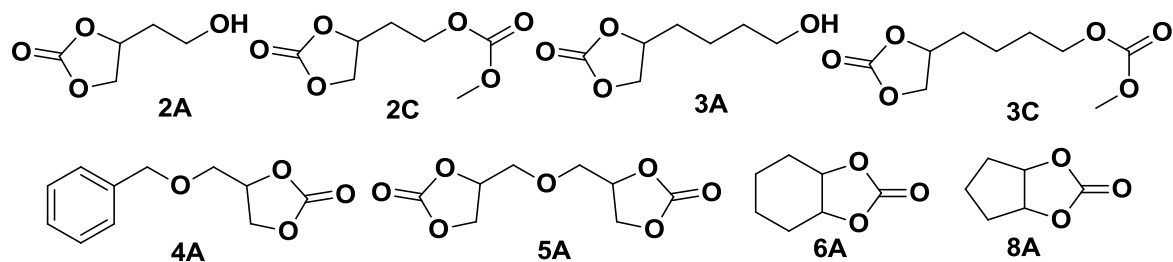


**Figure 3.19:** Structure of various cyclic carbonates, **2A**) 4-(2-hydroxyethyl)-1,3-dioxolan-2-one, **2C**) methyl (2-(2-oxo-1,3-dioxolan-4-yl)ethyl) carbonate, **3A**) 4-(4-hydroxybutyl)-1,3-dioxolan-2-one, **3C**) methyl (4-(2-oxo-1,3-dioxolan-4-yl)butyl) carbonate, **4A**) 4-((benzyloxy)methyl)-1,3-dioxolan-2-one, **5A**) 4,4'-(oxybis(methylene))bis(1,3-dioxolan-2-one), **6A**) hexahydrobenzo[d][1,3]dioxol-2-one and **8A**) tetrahydrofuro[3,4-d][1,3]dioxol-2-one.

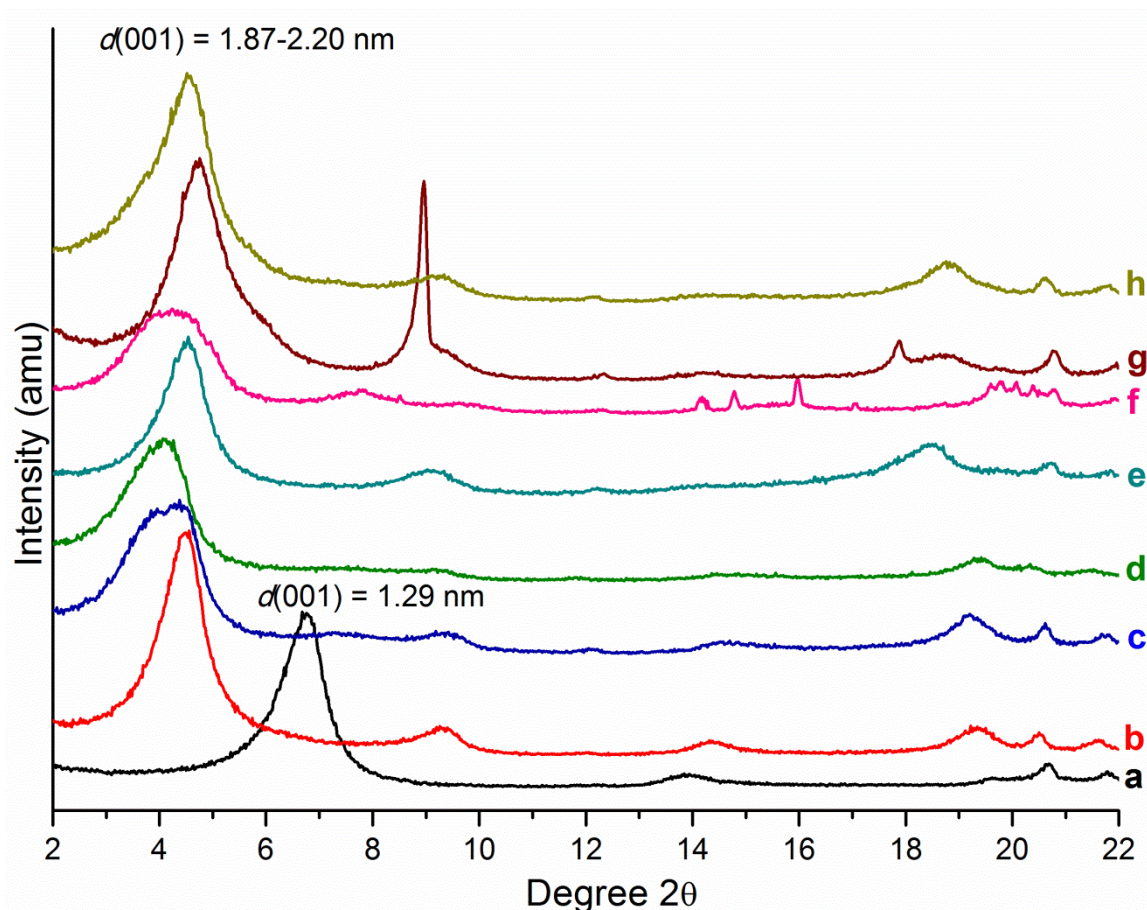


**Figure 3.20:** XRD spectra of various cyclic carbonates intercalated Na-smectite complexes, a) Na-smectite, b) PC/Na-smectite, c) **2C**/Na-smectite, d) **3C**/Na-smectite, e) **4A**/Na-smectite, f) **5A**/Na-smectite, g) **6A**/Na-smectite, and h) **8A**/Na-smectite.

In the case of **6A**/Na-smectite intercalated complex, neat organic material formed a separate phase, hence, a strong reflection at  $8.9^\circ 2\theta$  was observed in XRD trace. A disordered intercalation pattern was seen for **2C**/Na-smectite and **5A**/Na-smectite, whereas, ordered intercalation was observed for PC/Na-smectite, **3C**/Na-smectite, **4A**/Na-smectite and **8A**/Na-smectite complexes.

In the FTIR spectra, more noticeable shifts in  $\nu(\text{C=O})_{\text{str}}$  ( $6\text{-}18\text{ cm}^{-1}$ ) and cyclic  $\nu(\text{C-O})_{\text{str}}$  ( $4\text{-}12\text{ cm}^{-1}$ ) were observed for intercalated complexes (Figure 3.21 and Table 3.7). A smaller shift in  $\nu(\text{C=O})_{\text{str}}$  indicated that the cyclic carbonate moiety is coordinated via interlayer water to the sodium cations. This observation was in accordance with glycerol carbonate intercalated sodium smectite and propylene carbonate intercalated sodium smectite complex as reported in the literature (Onikata et al., 1999).

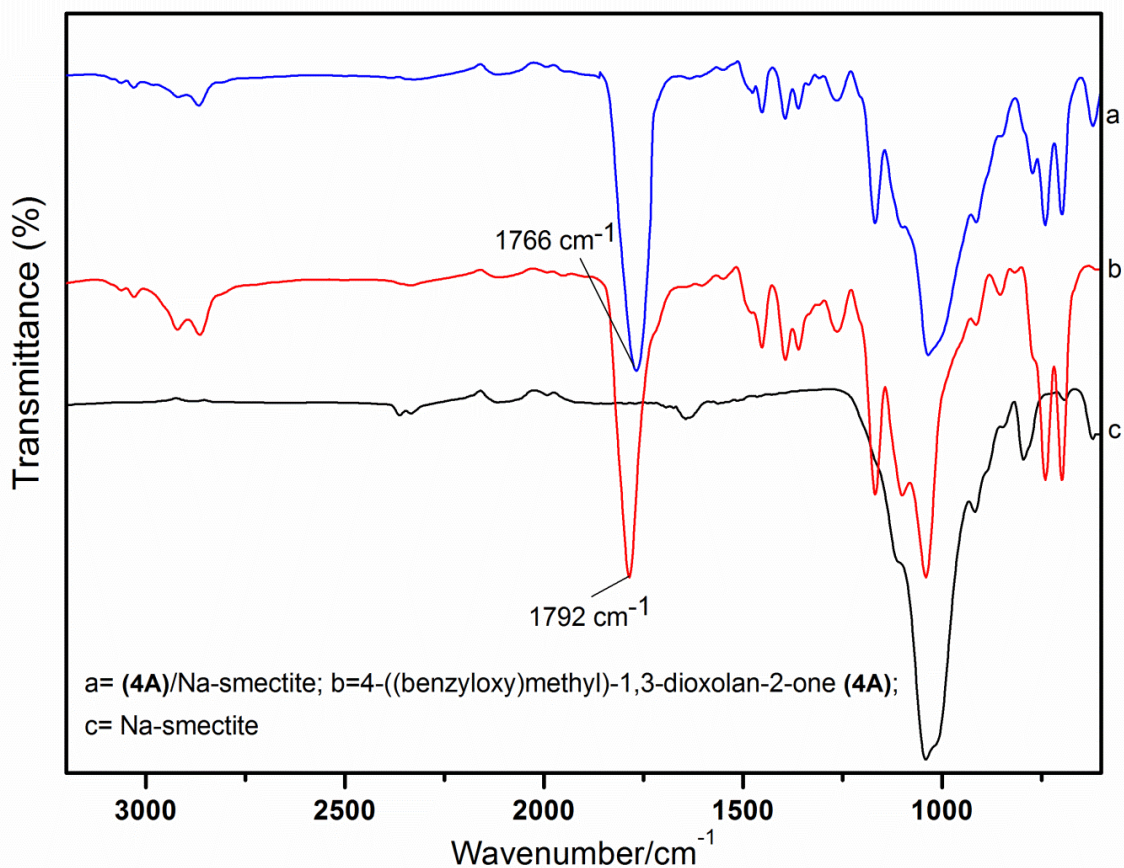


**Figure 3.21:** FTIR spectra of 4-((benzyloxy)methyl)-1,3-dioxolan-2-one (**4A**) intercalated sodium smectite, sodium smectite and **4A**.

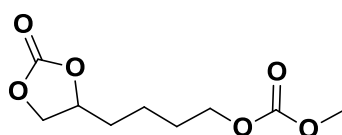


**Figure 3.22:** Structure of methyl (4-(2-oxo-1,3-dioxolan-4-yl)butyl) carbonate (**3C**).

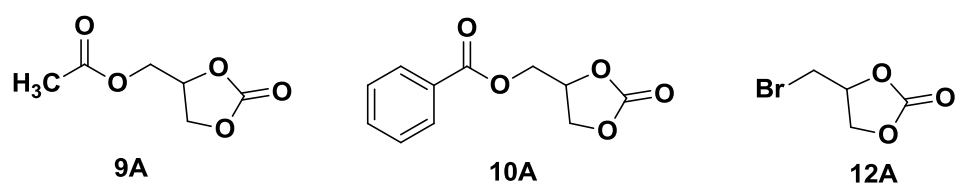
However, in the case of methyl (4-(2-oxo-1,3-dioxolan-4-yl)butyl) carbonate (**3C**), a greater red shift (27 cm<sup>-1</sup>) was observed for  $\nu(\text{C}=\text{O})_{\text{str}}$  linear carbonate which suggested electrostatic interaction of linear carbonate with sodium smectite as well.

**Table 3.7:** FTIR frequencies of main functional groups in cyclic carbonate upon smectite complex formation

Code	FTIR frequencies (cm <sup>-1</sup> )			
	Cyclic carbonate		Cyclic carbonate/Na-smectite	
	$\nu(\text{C=O})_{\text{str}}$	$\nu(\text{C-O})_{\text{str}}$	$\nu(\text{C=O})_{\text{str}}$	$\nu(\text{C-O})_{\text{str}}$
PC	1792	1191	1780	1179
<b>2C</b>	1797	1272	1782	1266
	1749		1749	
<b>3C</b>	1789	1373	1792	1395
	1746	1261	1719	1269
		1166		1172
<b>4A</b>	1796	1177	1781	1169
<b>5A</b>	1780	1170	1772	1162
<b>6A</b>	1788	1172	1796	1169
<b>8A</b>	1776	1174	1782	1165
<b>12A</b>	1792	1164	1774	1168

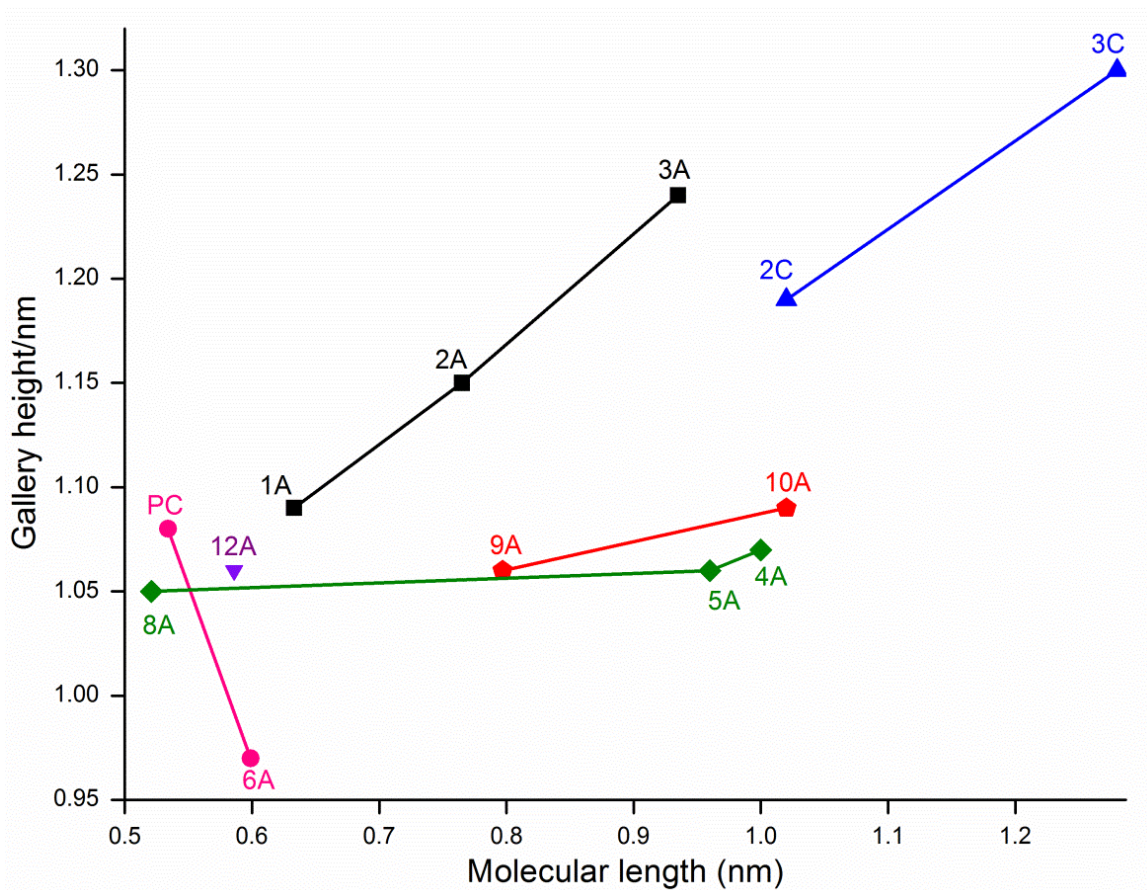
### 3.3.2.3 Effect of molecular length of cyclic carbonates on gallery height of intercalated complexes

Figure 3.24 showed that cyclic carbonates (**4A**, **5A**, **6A**, **8A**, **9A** and **12A**) (Figure 3.19) resulted in a less expansion of smectite galleries when compared with PC. Whereas, cyclic carbonate, **1A**, **2A**, **3A**, **10A**, **2C** and **3C** (Figure 3.23) resulted in a greater expansion of the Na-smectite interlayer gallery due to formation of stronger intercalates.



**Figure 3.23:** Various derivatives of glycerol carbonate.

When the gallery heights of intercalated cyclic carbonates were compared with the molecular length of respective cyclic carbonates, it was observed that an increase in molecular length of cyclic carbonate resulted in an increase in the expansion of the smectite galleries (Figure 3.24).



**Figure 3.24:** Gallery height relationship between hydroxyl, linear, alkyl and alkoxy cyclic carbonates.

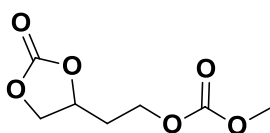


**Figure 3.25:** Cyclic carbonate with additional linear carbonate, methyl (4-(2-oxo-1,3-dioxolan-4-yl)ethyl) carbonate (**2C**).

The gallery height rule also appeared to apply for the cyclic carbonates with an additional functional group, such as a linear carbonate. This suggests that in addition to molecular length, the expansion of smectite galleries is also dependent on the kind and type of functionality. Interestingly, the increase in gallery height with molecular length and functionality occurs where the organic intercalate (GC and its derivatives) act as

solvents within the interlayer, whereas compared to other organic intercalates (e.g. hexadecyltrimethylammonium (HDTMA)) the organic molecule replaced the interlayer sodium cation and layer spacings of the resulting intercalates vary with layer charge of the smectite (Slade and Gates, 2004b). Lagaly et al. (1976) showed that the HDTMA in clay minerals with low charge densities ( $<0.5 e^-$  per unit cell), the aliphatic chains lay parallel to the layer planes and form monolayers. Above  $0.5 e^-$  per cell, bilayer configurations begin to form with the aliphatic chains flat-lying and paraffin-like structures have been postulated for charges greater than  $1.0 e^-$  (Lagaly and Weiss, 1976) and confirmed by Slade and Gates (Slade and Gates, 2004a, Slade and Gates, 2007). A similar change in orientation of the cyclic carbonates as a function of smectite layer charge could thus also be expected.

Among different functionalities, linear carbonates were most effective in providing greater expansion of smectite interlayers due to their increased molecular length (Table 3.8). The numbers of molecules per unit cell calculated for all the intercalated cyclic carbonates were similar to the result obtained for glycerol carbonate.

Expansion of sodium smectite galleries was also dependent on the molecular length of the molecule employed for intercalation with the exception of the cyclic carbonate fused with another ring such as cyclohexane (**6A**) and tetrahydrofuran (**8A**).

**Table 3.8:**  $d(001)$  spacing of cyclic carbonates/Na-smectite, molecular length of respective cyclic carbonates with number of molecules calculated per unit cell for each system

Code	Molecular length (nm)	$d(001)$ spacing (nm)	Gallery height, $C_{GH}$ (nm)	Molar volume <sup>a</sup> , $M_V$ ( $\text{cm}^3/\text{mol}$ )	No. of molecule/unit cell <sup>b</sup>
<b>1A</b>	0.63	1.99	1.09	$85.8 \pm 3.0$	2.5
<b>2A</b>	0.76	2.05	1.15	$102.3 \pm 3.0$	2.9
<b>3A</b>	0.93	2.22	1.24	$135.3 \pm 3.0$	2.4
<b>PC</b>	0.53	1.98	1.08	$87.2 \pm 3.0$	3.2
<b>6A</b>	0.60	1.87	0.97	$119.2 \pm 3.0$	2.1
<b>8A</b>	0.52	1.95	1.05	$92.5 \pm 3.0$	2.9
<b>5A</b>	0.96	1.96	1.06	$154.5 \pm 3.0$	1.8
<b>4A</b>	1.00	1.97	1.07	$171.9 \pm 3.0$	1.6
<b>2C</b>	1.02	2.09	1.19	$147.7 \pm 3.0$	2.1
<b>3C</b>	1.28	2.20	1.30	$180.7 \pm 3.0$	2.0

<sup>a</sup>Calculated using Advanced Chemistry Development (ACD/Labs) Software V11.02.

<sup>b</sup>Based on assumption that all of material is present in the interlayer gallery along with hydrated sodium cation. Calculated from number of moles (unit volume of gallery cyclic carbonate occupy/molar volume).

### 3.4 Conclusions

Intercalation of glycerol carbonate into Na-smectite was investigated by XRD and FTIR. Various wt% amounts of glycerol carbonate were used to probe intercalation into Na-smectite and an ordered complex was obtained with  $\leq 50$  wt% amount of glycerol carbonate. Above 50 wt% disorder in the intercalation resulted.

The main driving force for intercalation of glycerol carbonate was the solvation of interlayer sodium cations. A model study based on FTIR spectroscopy was performed to predict the interactions of glycerol carbonate with sodium smectite employing water, sodium chloride and water-sodium chloride. The FTIR results showed that water affected the H-bonding between glycerol carbonate molecules, whereas,  $(\text{C}=\text{O})_{\text{str}}$  indicated strong interactions with sodium chloride. For the intercalated complex formed, the possible interaction or complexation of the carbonate functionality in glycerol carbonate with sodium cations was suggested via water bridges based on reported work on PC (Onikata et al., 1999). Long term stability studies on glycerol carbonate indicated it to be stable in saline solutions under ambient conditions and potentially compatible with applications in high saline waste facilities.

Intercalation of synthesized cyclic carbonates into Na-smectite was also performed successfully as studied by XRD and FTIR spectroscopy. Various wt% amounts of cyclic carbonates were used for hydroxyl containing cyclic carbonates intercalation, while other cyclic carbonates were intercalated employing 50 wt% amounts. For electrostatic interaction with the Na-smectite, the cyclic carbonate carbonyl (i.e., PC), linear carbonate carbonyl (i.e., **3C**) as well as other functional groups such as hydroxyl (e.g., **2A**) also participated if present. It was also found that the expansion of the gallery of

Na-smectite was dependent on the molecular length of the cyclic carbonate (for a specific functionality) with the exception of hexahydrobenzo[d][1,3]dioxol-2-one (**6A**).

### 3.5 References

ARESTA, M., DIBENEDETTO, A., NOCITO, F. & PASTORE, C. 2006. A study on the carboxylation of glycerol to glycerol carbonate with carbon dioxide, the role of the catalyst, solvent and reaction conditions. *J. Mol. Catal. A: Chem.*, 257, 149-153.

BEATTIE, C., NORTH, M., VILLUENDAS, P. & YOUNG, C. 2013. Influence of Temperature and Pressure on Cyclic Carbonate Synthesis Catalyzed by Bimetallic Aluminum Complexes and Application to Overall syn-Bis-hydroxylation of Alkenes. *J. Org. Chem.*, 78, 419-426.

CLIMENT, M. J., CORMA, A., DE, F. P., IBORRA, S., NOY, M., VELTY, A. & CONCEPCION, P. 2010. Chemicals from biomass: Synthesis of glycerol carbonate by transesterification and carbonylation with urea with hydrotalcite catalysts. The role of acid-base pairs. *J. Catal.*, 269, 140-149.

DEEDS, C. T. & VAN OLPHEN, H. 1963. Density studies in clay-liquid systems. II. Application to core analysis. *Clays Clay Minerals, Proc. Natl. Conf. Clays Clay Minerals*, 10, 318-28.

DIBENEDETTO, A., PASTORE, C. & ARESTA, M. 2006. Direct carboxylation of alcohols to organic carbonates: Comparison of the Group 5 element alkoxides catalytic activity: An insight into the reaction mechanism and its key steps. *Catalysis Today*, 115, 88-94.

- FUJITA, S.-I., YAMANISHI, Y. & ARAI, M. 2013. Synthesis of glycerol carbonate from glycerol and urea using zinc-containing solid catalysts: A homogeneous reaction. *Journal of Catalysis*, 297, 137-141.
- GABRIELE, B., MANCUSO, R., SALERNO, G., VELTRI, L., COSTA, M. & DIBENEDETTO, A. 2011. A General and Expedient Synthesis of 5- and 6-Membered Cyclic Carbonates by Palladium-Catalyzed Oxidative Carbonylation of 1,2- and 1,3-Diols. *ChemSusChem*, 4, 1778-1786.
- GATES, W. P. 2004. Crystalline swelling of organo-modified clays in ethanol–water solutions. *Applied Clay Science*, 27, 1-12.
- HAMMOND, C., LOPEZ-SANCHEZ, J. A., RAHIM, M. H. A., DIMITRATOS, N., JENKINS, R. L., CARLEY, A. F., HE, Q., KIELY, C. J., KNIGHT, D. W. & HUTCHINGS, G. J. 2011. Synthesis of glycerol carbonate from glycerol and urea with gold-based catalysts. *Dalton Trans.*, 40, 3927-3937.
- HORNSEY, W. P., SCHEIRS, J., GATES, W. P. & BOUAZZA, A. 2010. The impact of mining solutions/liquors on geosynthetics. *Geotextiles and Geomembranes*, 28, 191-198.
- KATSUMI, T. 2010. Hydraulic conductivity of geosynthetic clay liners. *Geosynthetic Clay Liners for Waste Containment Facilities*. CRC Press, 55-83.
- KATSUMI, T., ISHIMORI, H., OGAWA, A., YOSHIKAWA, K., HANAMOTO, K. & FUKAGAWA, R. 2007. Hydraulic conductivity of nonprehydrated geosynthetic clay liners permeated with inorganic solutions and waste leachates. *Soils and Foundations*, 47(1), 79-96.
- KATSUMI, T., ISHIMORI, H., ONIKATA, M. & FUKAGAWA, R. 2008. Long-term barrier performance of modified bentonite materials against sodium and calcium permeant solutions. *Geotextiles and Geomembranes*, 26, 14-30.

- KONDO, M. 1996. Activation of smectite clays for swellability and dispersibility. *EP Patent 718237A2*.
- LAGALY, G. & WEISS, A. 1976. The layer charge of smectitic layer silicates. *Appl. Publ. Ltd.*, 157-172.
- MOULOINGUI, Z., YOO, J.-W., GACHEN, C.-A., GASET, A. & VERMEERSCH, G. 1996. Process for the preparation of glycerol carbonate from glycerol and ethylene or propylene carbonates. *EP Patent 739888A1*.
- OCHOA-GÓMEZ, J. R., GÓMEZ-JIMÉNEZ-ABERASTURI, O., RAMÍREZ-LÓPEZ, C. & BELSUÉ, M. 2012. A Brief Review on Industrial Alternatives for the Manufacturing of Glycerol Carbonate, a Green Chemical. *Organic Process Research & Development*, 16, 389-399.
- ONIKATA, M. 2002. General Review (Japanese), Swelling properties of layered clay mineral montmorillonite and interaction with organic compounds. *Hyomen*, 40, 203-214.
- ONIKATA, M. KONDO, M., NAOKI HAYASHI, N. & YAMANAKA, S. 1999. Complex Formation of Cation-Exchanged Montmorillonites with Propylene Carbonate: Osmotic Swelling in Aqueous Electrolyte Solutions. *Clays and Clay Minerals*, 47, 672-677.
- RADOSLOVICH, E. W., RAUPACH, M., SLADE, P. G. & TAYLOR, R. M. 1970. Crystalline cobalt, zinc, manganese, and iron alkoxides of glycerol. *Aust. J. Chem.*, 23, 1963-71.
- RAHIM, R. M. A., HE, Q., LOPEZ-SANCHEZ, J. A., HAMMOND, C., DIMITRATOS, N., SANKAR, M., CARLEY, A. F., KIELY, C. J., KNIGHT, D. W. & HUTCHINGS, G. J. 2012.

- Gold, palladium, and gold-palladium supported nanoparticles for the synthesis of glycerol carbonate from glycerol and urea. *Catal. Sci. Technol.*, 2, 1914-1924.
- ROKICKI, G. & KURAN, W. 1984. Cyclic Carbonates Obtained by Reactions of Alkali Metal Carbonates with Epihalohydrins. *Bulletin of The Chemical Society of Japan*, 57, 1662–1666.
- ROKICKI, G., RAKOCZY, P., PARZUCHOWSKI, P. & SOBIECKI, M. 2005. Hyperbranched aliphatic polyethers obtained from environmentally benign monomer: glycerol carbonate. *Green Chemistry*, 7, 529-539.
- SANDI, G. 2005. S. M. Auerbach, K. A. Carrado, P.K. Dutta (EDs.), Handbook of Layered Materials, Marcel Dekker, New York, 2004, 650 pp. *Microporous Mesoporous Mater.*, 81, 375-376.
- SEKI, Y. & OGAWA, M. 2010. The removal of 2-phenylphenol from aqueous solution by adsorption onto organoclays. *Bull. Chem. Soc. Jpn.*, 83, 712-715.
- SIKDAR, D., KATTI, K. S. & KATTI, D. R. 2008. Molecular interactions alter clay and polymer structure in polymer clay nanocomposites. *J. Nanosci. Nanotechnol.*, 8, 1638-1657.
- SLADE, P. G. & GATES, W. P. 2004a. The ordering of HDTMA in the Interlayers of Vermiculite and the Influence of Solvents. *Clays and Clay Minerals*, 52, 204-210.
- SLADE, P. G. & GATES, W. P. 2004b. The swelling of HDTMA smectites as influenced by their preparation and layer charges. *Applied Clay Science*, 25, 93-101.
- SLADE, P. G. & GATES, W. P. 2007. HDTMA In the Interlayers of High-Charged Llanio Vermiculite. *Clays and Clay Minerals*, 55, 131-139.
- SONNATI, M. O., AMIGONI, S., TAFFIN DE GIVENCHY, E. P., DARMANIN, T., CHOULET, O. & GUITTARD, F. 2013. Glycerol carbonate as a versatile building block for

- tomorrow: synthesis, reactivity, properties and applications. *Green Chemistry*, 15, 283-306.
- STRAIN, F. 1948. Carbonate-haloformates of glycerol. *US Patent 2446145*.
- TOMCZYK, K. M., GUNKA, P. A., PARZUCHOWSKI, P. G., ZACHARA, J. & ROKICKI, G. 2012. Intramolecular etherification of five-membered cyclic carbonates bearing hydroxyalkyl groups. *Green Chemistry*, 14, 1749-1758.
- TUNDO, P. & SELVA, M. 2002. The Chemistry of Dimethyl Carbonate. *Accounts of Chemical Research*, 35, 706-716.
- TURNER, T. W., PATTI, A., GATES, W., SHAHEEN, U. & KULASEGARAM, S. 2013. Formation of glycerol carbonate from glycerol and urea catalysed by metal monoglycerolates. *Green Chemistry*, 15, 1925-1931.
- VIEVILLE, C., YOO, J. W., PELET, S. & MOULOINGUI, Z. 1999. Synthesis of glycerol carbonate by direct carbonatation of glycerol in supercritical CO<sub>2</sub> in the presence of zeolites and ion exchange resins. *Catal. Lett.*, 56, 245-247.
- WHITEOAK, C. J., NOVA, A., MASERAS, F. & KLEIJ, A. W. 2012. Merging Sustainability with Organocatalysis in the Formation of Organic Carbonates by Using CO<sub>2</sub> as a Feedstock. *ChemSusChem*, 5, 2032-2038.
- YAMANAKA, S., KANAMARU, F. & KOIZUMI, M. 1974. Role of interlayer cations in the formation of acrylonitrile-montmorillonite complexes. *The Journal of Physical Chemistry*, 78, 42-44.
- YAMANAKA, S., KANAMARU, F. & KOIZUMI, M. 1975. Studies on the orientation of acrylonitrile adsorbed on interlamellar surfaces of montmorillonites. *Phys. Chem*, 79(13), 1285-1288.

YILDIRIM, O. A. & DURUCAN, C. 2010. Synthesis of zinc oxide nanoparticles elaborated by microemulsion method. *J. Alloys Compd.*, 506, 944-949.

YOO, J. W. & MOULOUGUI, Z. 2003. Catalytic carbonylation of glycerin by urea in the presence of zinc mesoporous system for the synthesis of glycerol carbonate. *Stud. Surf. Sci. Catal.*, 146, 757-760.

# Chapter 4 Derivatization of glycerol carbonate and polymerization of cyclic carbonates

## carbonates

### 4.1 Introduction

Having developed an efficient process to access glycerol carbonate from glycerol (Turney et al., 2013), the synthesis of a range of derivatives of glycerol carbonate was explored. The presence of a cyclic carbonate group along with the pendant hydroxyl functionality allows glycerol carbonate to behave as a nucleophile as well as an electrophile. Glycerol carbonate can react with carboxylic acids, acid halides, anhydrides, isocyanates and diamines (Pfaendler and Müller, 1992, Olivero et al., 1993) to form esters (Sonnati et al., 2013), ethers and urethanes (Gillis et al., 1997).

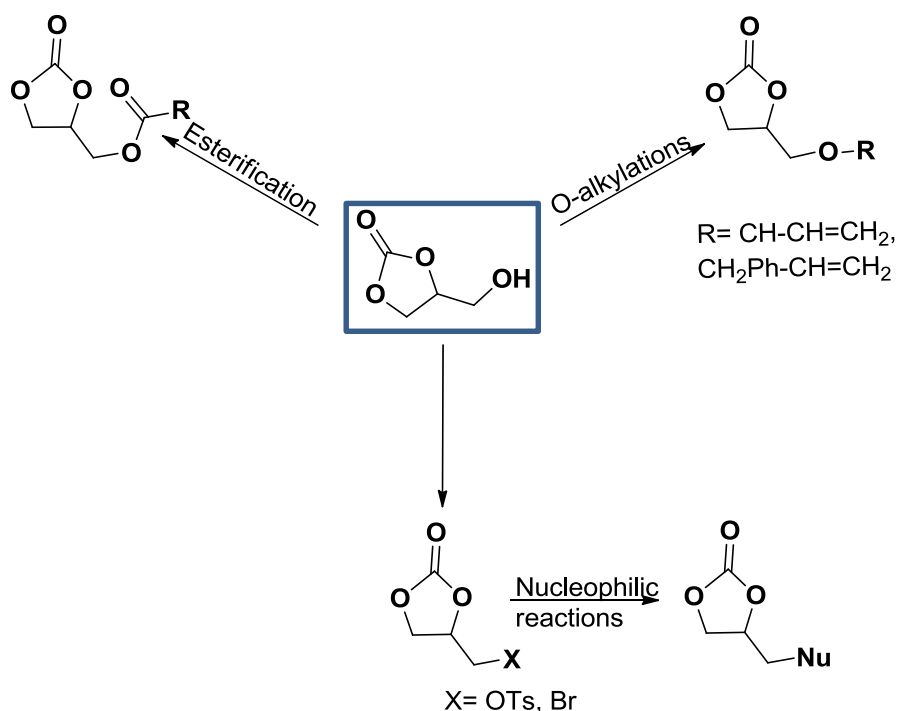


**Figure 4.1:** Functionalization of glycerol carbonate to synthesize cyclic carbonate precursors.

Replacement of the pendant hydroxyl group with either a sulfonyl or a bromide group can improve the options for selective derivatisation of the original glycerol carbonate. Rousseau et al. (2009) have shown the polymorphic reactivity of tosylated glycerol 1,2-carbonate in the presence of nucleophiles (Simao et al., 2006, Rousseau et al., 2009) to generate glycidol analogs protected with carbonate or carbamate groups. Higher yields of nucleophilic products can also be obtained by substituting the hydroxyl group with a bromide, which is a better leaving group compared to the tosyl group in  $S_N2$  reactions.

A new approach to access several monomers with pendant cyclic carbonates was used, based on directly reacting glycerol carbonate with double-bond containing electrophiles (Benyahya et al., 2011). The double bond allows further reaction to give an epoxide group. A variety of monomers that contained either an epoxide or a double bond were thus prepared in this manner from GC synthesized previously (Chapter 2). The monomers with pendant cyclic carbonate were subsequently polymerized via ring opening polymerization of an epoxide group or radical photopolymerization of the double bond.

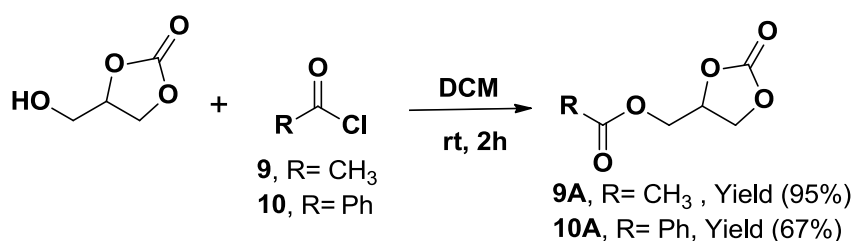
## 4.2 Objective

The main objective of this part of the project was to prepare a range of derivatives of glycerol carbonate for potential intercalation into Na-smectite that would subsequently be useful in clay-liner applications where resistance to high osmotic stress is required. In addition, an important aim was also to synthesize cyclic carbonate monomers that contained reactive groups capable of being polymerized through ring opening polymerization and radical photopolymerization, while preserving the pendant cyclic carbonate moiety.

## 4.3 Results and discussion

### 4.3.1 Functionalization of glycerol carbonate

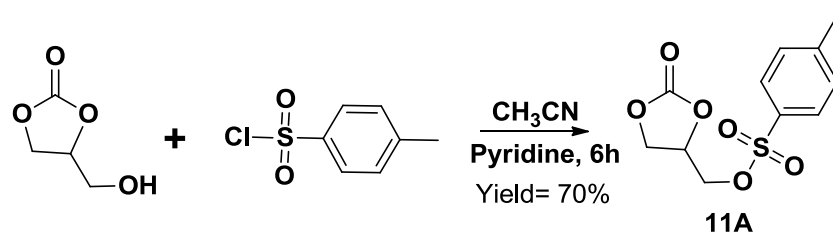
A variety of functionalized glycerol carbonate derivatives that included ester, tosyl and bromo groups were synthesized in order to prepare their intercalated complexes with Na-smectite.



**Scheme 4.1:** Synthesis of ester derivatives of glycerol carbonate.

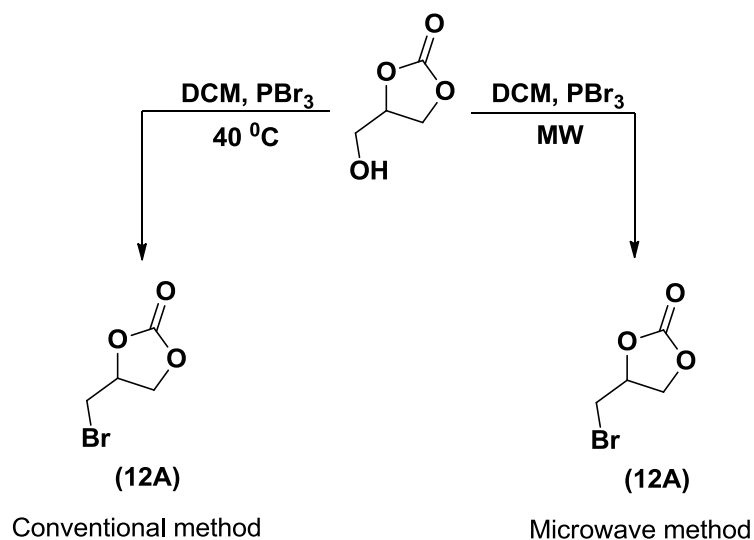
The ester derivatives of glycerol carbonate were obtained by the reaction of glycerol carbonate with acetyl chloride or benzoyl chloride in equivalent molar ratios (Scheme 4.1). The reactions were carried out under nitrogen in dichloromethane and pyridine was employed as a catalyst in the reaction. The (2-oxo-1,3-dioxolan-4-yl)methyl acetate (**9A**) was obtained after extraction with water in 95% yield, whereas 4-methylbenzoate-1,3-dioxolan-2-one (**10A**) was obtained as a white solid in 67% yield after purification by column chromatography.

The tosyl derivative of glycerol carbonate was prepared in 70% yield from tosyl chloride (Giardi et al., 2010) as illustrated below in Scheme 4.2.



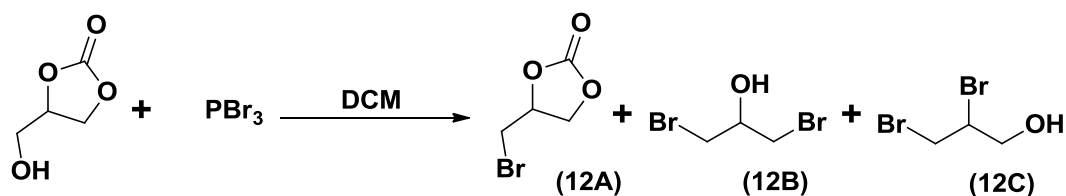
**Scheme 4.2:** Synthesis of tosylated glycerol carbonate.

A modification of glycerol carbonate undertaken was the conversion of the hydroxyl group of glycerol carbonate into a better leaving group, in the form of a bromide (4-bromomethyl-1,3-dioxolan-2-one (**12A**)). The reported methods for this synthesis involved coupling epibromohydrin with carbon dioxide employing *N*-heterocyclic carbenes-ZnBr<sub>2</sub> as a catalyst (Liu et al., 2012) and from reaction of tosyl glycerol carbonate with tetra-*n*-butylammonium iodide or bromide (Bensemhoun and Condon, 2012). Hence, the conversion was optimized using conventional and microwave methods (Scheme 4.3).



**Scheme 4.3:** Conventional and microwave method to synthesize 4-bromomethyl-1,3-dioxolan-2-one (**12A**).

Employing the conventional method resulted in a low selectivity (33%) for **12A** and a poor yield (18%). The microwave reaction was conducted by irradiation at 300W using dichloromethane (1 mL) as solvent. After completion of the reaction, the product (**12A**) was extracted with toluene and the solvent evaporated under reduced pressure. The microwave reaction was performed at various temperatures from 20 to 40 °C and at irradiation times of 2 to 6 minutes. It was observed that with an increase in temperature, the conversion to 4-bromomethyl-1,3-dioxolan-2-one improved (up to 99% at 40 °C). However, at longer reaction times, the selectivity for **12A** decreased, with corresponding formation of side products **12B** and **12C** by attack of phosphorous tribromide on **12A** itself (Scheme 4.4).



**Scheme 4.4:** Reaction showing different products obtained from the reaction of glycerol carbonate with phosphorus tribromide.

**Table 4.1:** Comparison between conventional and microwave assisted synthesis of 4-bromomethyl-1,3-dioxolan-2-one (**12A**)

Method	Temp (°C)	Time (min)	Conv. %	% Selectivity			% Yield <sup>a</sup>
				<b>12A</b>	<b>12B</b>	<b>12C</b>	
MW	20	2	15	50	50	-	8
	20	4	18	65	35	-	12
	25	2	30	92	8	-	28
	30	2	19	87	13	-	16
	30	4	22	65	35	-	14
	40	2	32	98	2	-	31
	40	4	40	99	1	-	40
	40	6	42	68	24	8	29
Conventional	40	180	55	33	61	6	18
	-78	45	100	95	3	2	95

<sup>a</sup>Yield determined with the gas chromatography.

This unfavourable attack on the carbonyl carbon (loss of cyclic carbonate moiety) can be prevented by decreasing the reactivity of PBr<sub>3</sub> if the reaction was conducted at a lower temperature. As this could not be achieved by microwave irradiation, a conventional approach was used. Phosphorus tribromide was added to a solution of glycerol carbonate in (equivalent molar ratios) dichloromethane at -78 °C, followed by warming to ambient temperature over 30 minutes. After workup, the product, 4-bromomethyl-1,3-dioxolan-2-one (**12A**) was then isolated in 95% yield (Table 4.1).

### 4.3.2 Intercalation of ester and bromo functional cyclic carbonates

A 50 wt% amount of functionalized cyclic carbonate was used to prepare the intercalated complexes with Na-smectite. Figure 4.2 shows the XRD traces of Na-smectite along with ester and bromo functionalized cyclic carbonates/Na-smectite. The XRD of ethanol/Na-smectite under similar conditions is also shown for reference. The gallery height of Na-smectite was found to be 0.35 nm ( $d(001) = 1.29$  nm). When these carbonates were intercalated, the gallery height increased from 0.35 nm to 1.0-1.03 nm ( $d(001) = 1.96-1.99$  nm). This increase in gallery height of Na-smectite confirmed that successful intercalation of cyclic carbonates into Na-smectite occurred, which was also suggested by FTIR.

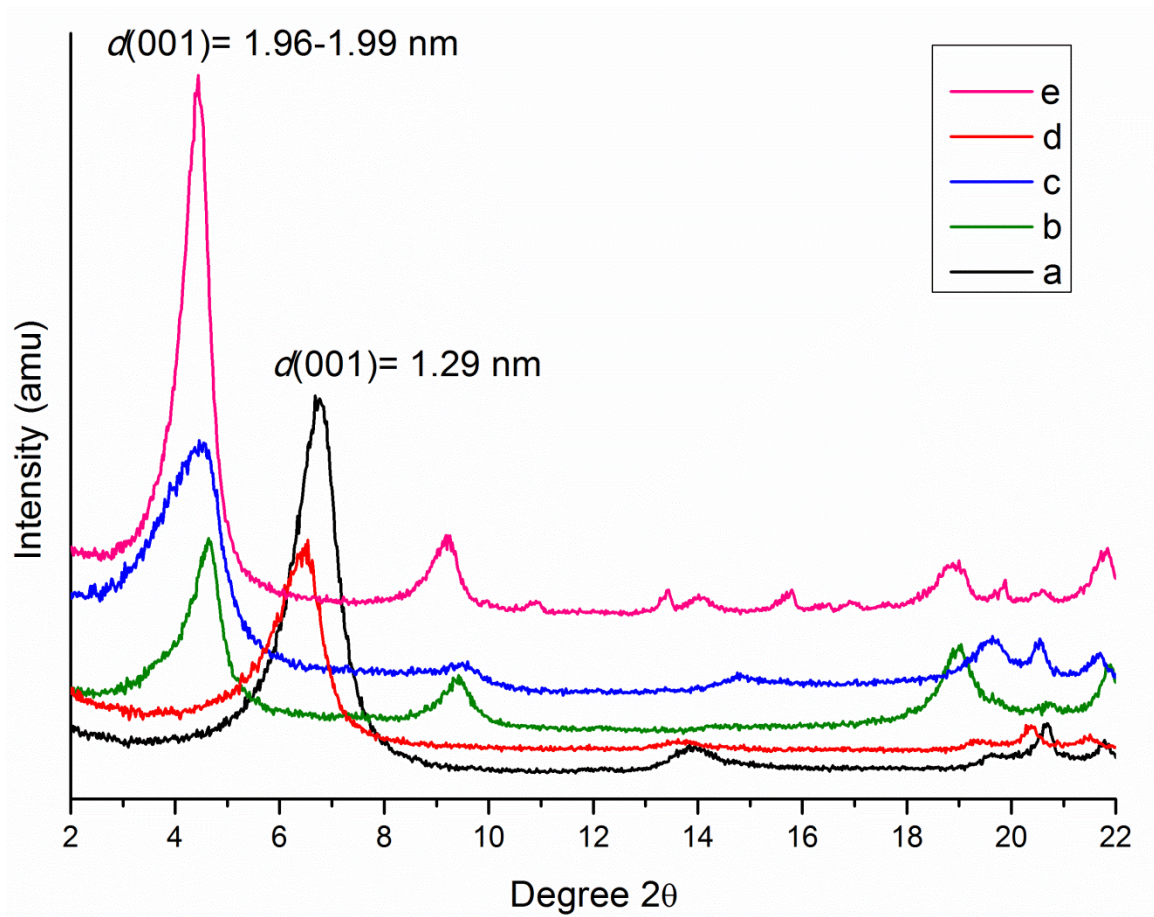


**Figure 4.2:** XRD traces of, a) Na-smectite, b) **12A**/Na-Smectite, c) **9A**/Na-smectite, d) ethanol/Na-smectite, and e) **10A**/Na-smectite.

In the case of esters (**9A-10A**)/Na-smectite, relatively small shifts were observed in the FTIR for the characteristic cyclic carbonyl stretch when intercalated (Table 4.2). However, significant blue shifts ( $19\text{-}29\text{ cm}^{-1}$ ) in the  $\nu(\text{C=O})_{\text{str}}$  (ester) bands were seen along with red shifts ( $4\text{-}11\text{ cm}^{-1}$ ) in the  $\nu(\text{C-O})_{\text{str}}$  bands upon intercalation. This indicated that in addition to carbonyl ( $\text{C=O}$ ) of cyclic carbonates, the ester ( $\text{C=O}$ ) may also participate in coordination with sodium cations.

**Table 4.2:** Major FTIR absorption frequencies of intercalated cyclic carbonate complexes

Code	FTIR absorption frequencies (cm <sup>-1</sup> )			
	Cyclic carbonate		Cyclic carbonate/Na-smectite	
	$\nu(\text{C=O})_{\text{str}}$	$\nu(\text{C-O})_{\text{str}}$	$\nu(\text{C=O})_{\text{str}}$	$\nu(\text{C-O})_{\text{str}}$
<b>9A</b>	1792	1280	1789	1269
	1714	1172	1743	1173
<b>10A</b>	1794	1274	1792	1271
	1720	1178	1739	1170
<b>12A</b>	1792	1164	1774	1168

For **12A**/Na-smectite, a bromo derivative of glycerol carbonate, a greater (18 cm<sup>-1</sup>) red shift was observed for  $\nu(\text{C=O})_{\text{str}}$  which inferred the electrostatic interaction of C=O with the sodium smectite.

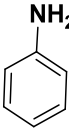
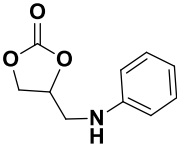
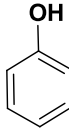
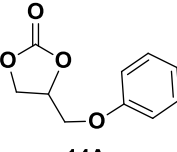
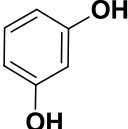
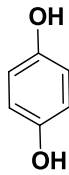
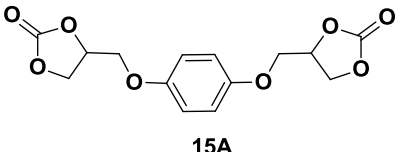
### 4.3.3 Reactions of cyclic carbonates

#### 4.3.3.1 Nucleophilic substitution reactions of tosylated glycerol carbonate

Tosylated glycerol carbonate was separately reacted with aniline, phenol, resorcinol and hydroquinone (Table 4.3) in order to obtain various derivatives of glycerol carbonate (Simao et al., 2006, Rousseau et al., 2009). When aniline or phenol were reacted together with tosylated glycerol carbonate at 80 °C under solvent free conditions, the reaction was complete in 2 hours (Simao et al., 2006) giving 4-((phenylamino)methyl)-1,3-dioxolan-2-one (**13A**) and 4-(phoxymethyl)-1,3-dioxolan-2-one (**14A**), with 100% selectivity. Upon employing solvent free as well as literature conditions (Simao et al., 2006, Rousseau et al., 2009) (tosylated glycerol carbonate was reacted with resorcinol in

dimethyl formamide (DMF) employing potassium carbonate as a base at 80 °C) for resorcinol, mono- or di-substituted product was not formed. However, reaction with hydroquinone resulted in the formation of **15A** in poor yield (<10%). The products obtained were purified by column chromatography.

**Table 4.3:** Reactions of tosylated glycerol carbonate with different nucleophiles

Nucleophile	Temp (°C)	Product	% Yield <sup>a</sup> (Lit)
	160	 <b>13A</b>	29(31)
	70	 <b>14A</b>	32(30)
	80 80 <sup>b</sup>	- -	- -
	80 80 <sup>b</sup>	 <b>15A</b>	7 8

Reaction conditions:  $K_2CO_3$  was used as a base, 1 mole equivalent of tosylated glycerol carbonate/potassium carbonate was used. <sup>a</sup>Isolated yield. <sup>b</sup>DMF was used as a solvent.

It was observed that the phenols with two potentially nucleophilic hydroxyl groups behaved completely differently compared with a single hydroxyl. Rousseau et al. (2009) explained that the reactivity of tosylated glycerol carbonate with *O*-nucleophiles was governed by hard and soft acids and bases criteria. For resorcinol, the two hydroxyls at

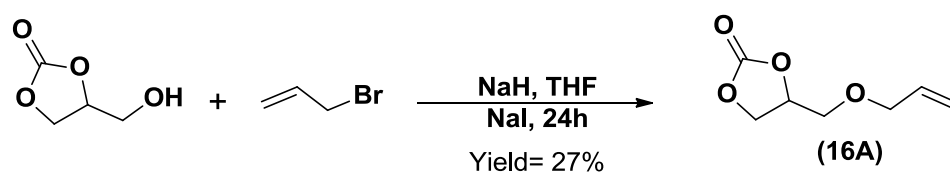
the *meta*-position experience steric hindrance which made it difficult for the nucleophilic hydroxyl to attack the electrophilic carbon of tosylated glycerol carbonate and most likely resulted in the formation of the sodium alkoxide (Simao et al., 2006, Rousseau et al., 2009). As a result, resorcinol failed to react with tosylated glycerol carbonate. In the case of hydroquinone, however, the two hydroxyls were at a maximum distance and experience less hindrance, and the substrate was comparatively more reactive than resorcinol due to resonance donating and inductive electron withdrawing effect towards electrophilic agent and a low yield of product was obtained. Low yields were also due to the dissociation of the tosylated derivative into glycerol carbonate and *p*-toluene sulfonic acid in the presence of potassium carbonate and were recovered.

#### **4.3.3.2 O-alkylation of hydroxyl containing cyclic carbonates to obtain monomeric precursors**

A wide range of derivatives of glycerol carbonate with a functionality to enable polymerization can be obtained via O-alkylation of the pendant hydroxyl containing cyclic carbonate with various double bond containing electrophiles.

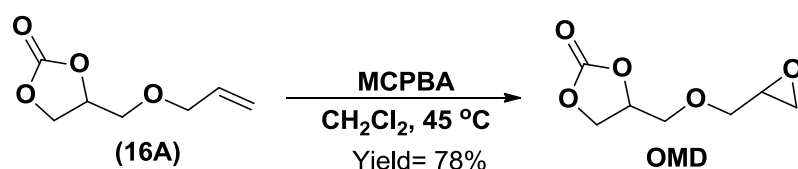
##### ***4.3.3.2.1 O-alkylation of glycerol carbonate with allyl bromide and 4-bromomethyl-1,3-dioxolan-2-one***

A suitable candidate that possesses polymerizing capabilities has been identified: 4-((allyloxy)methyl)-1,3-dioxolan-2-one (**16A**). This compound was synthesized using a literature method (Benyahya et al., 2011). The liquid was purified and characterized by NMR spectroscopy.



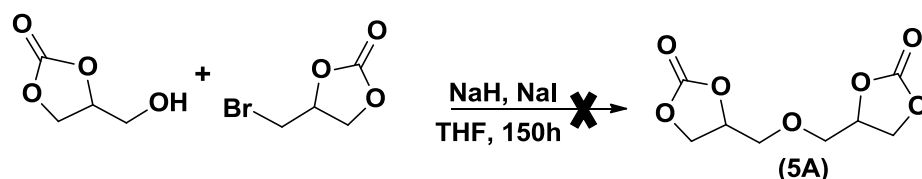
**Scheme 4.5:** Synthesis of 4-((allyloxy)methyl)-1,3-dioxolan-2-one (**16A**).

The double bond in 4-((allyloxy)methyl)-1,3-dioxolan-2-one (**16A**) was easily converted to an epoxide ring by reacting with meta-chloroperoxy benzoic acid (MCPBA) (Scheme 4.6). 4-((Oxiran-2-ylmethoxy)methyl)-1,3-dioxolan-2-one (**OMD**) was obtained using a literature method (He et al., 2010) in 78% yield after purification and characterized further.



**Scheme 4.6:** Oxidation of double bond in 4-((allyloxy)methyl)-1,3-dioxolan-2-one.

O-alkylation of glycerol carbonate with 4-bromomethyl-1,3-dioxolan-2-one (**12A**) under similar conditions (Scheme 4.7) failed to produce a dimer of cyclic carbonate (**5A**).

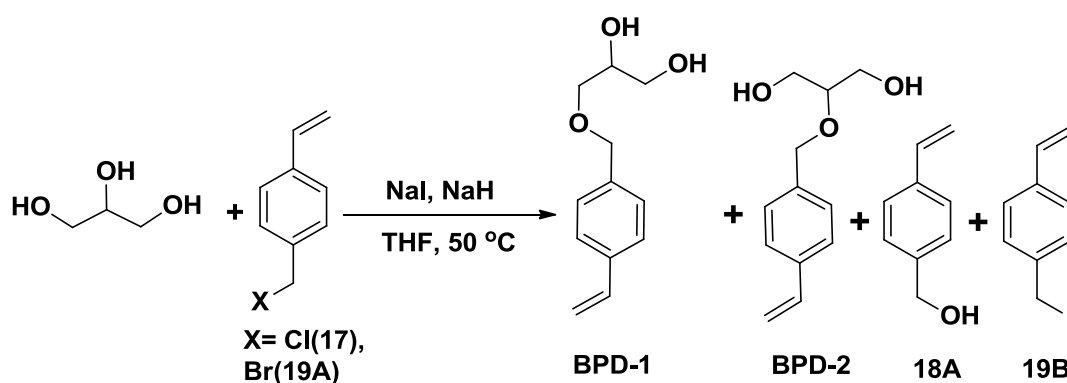


**Scheme 4.7:** Attempted synthesis of dimer of glycerol carbonate.

The reactants were isolated at the end of reaction after workup. The non-reactivity of 4-bromomethyl-1,3-dioxolan-2-one towards glycerol carbonate may be due to the lack of an activated system, such as double bond, which is present in allyl bromide.

#### 4.3.3.2.2 O-Alkylation of glycerol

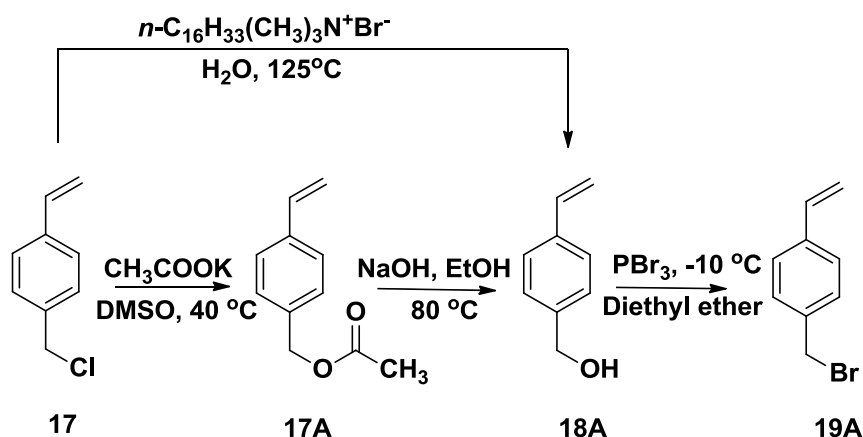
The O-alkylation of glycerol was also performed in order to obtain monomers with a pendant hydroxyl functionality, 3-((4-vinylbenzyl)oxy)propane-1,2-diol (**BPD-1**), which can be potentially converted into five-membered cyclic carbonate. Glycerol was dried using calcium chloride with subsequent heating at 150 °C prior to use. 4-Vinylbenzyl chloride was reacted with glycerol in THF with sodium hydride as a base to introduce a 1,2-diol group on styrene (Scheme 4.8), which can be potentially cyclized in second step to form a cyclic carbonate. However, in addition to **BPD-1**, the formation of 3-((4-vinylbenzyl)oxy)propane-1,3-diol (**BPD-2**) was also observed.



**Scheme 4.8:** O-alkylation of glycerol with 4-vinylbenzyl chloride and bromide.

The conversion of glycerol was low (39%) due to the lack of reactivity of the electrophile. Hence, the chloride was converted by substitution to provide the bromide as a better leaving group (**19A**).

Synthesis of these derivatives was performed using literature methods (Shimomura et al., 2005, Gao et al., 2011) (Scheme 4.9).



**Scheme 4.9:** Synthesis of 4-vinylbenzyl bromide from 4-vinylbenzyl chloride.

The reaction of glycerol with 4-vinylbenzyl chloride resulted in the formation of both isomers (**BPD-1** and **BPD-2**) along with **18A** and **19B** (Scheme 4.8). However, higher conversion (86%) was obtained by the employing the analogous benzylbromide (Table 4.4). Formation of a side product (**18A**) suggests that the glycerol was contaminated with water. A moderate yield of monomeric diol (**BPD-1**) was obtained after purification. Conversion of **BPD-1** into respective cyclic carbonate was not attempted due to the low conversion of glycerol.

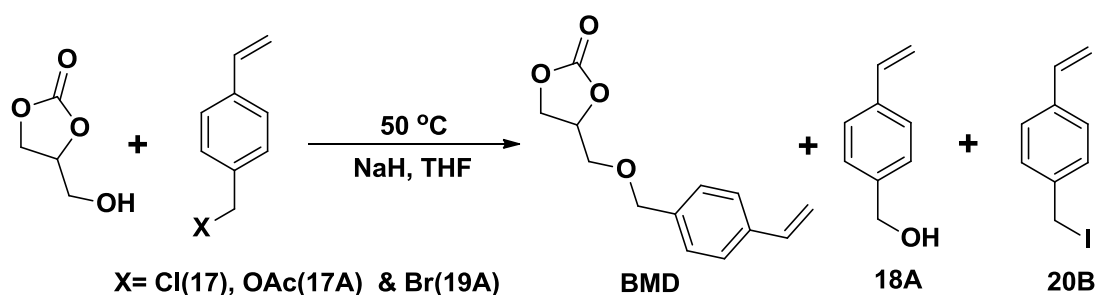
**Table 4.4:** Conversion and selectivity of different products obtained by reaction of glycerol with 4-vinylbenzyl derivatives

X	Time (h)	Conv. %	% Selectivity				Yield %
			<b>BPD-1</b>	<b>BPD-2</b>	<b>18A</b>	<b>19B</b>	
Cl	96	39	51	20	23	6	20
Br	24	86	62	9	21	8	53

Reaction conditions: 1 mole equivalent of glycerol/4-vinylbenzyl derivative, 1.2 mole equivalents of NaH and 0.1 mole equivalent of NaI was used.

### 4.3.3.2.3 *O*-Alkylation of glycerol carbonate with 4-vinylbenzyl derivatives

A low yield of **BPD-1** was obtained, an alternative approach to provide the desired monomer with a pendant cyclic carbonate in good yield was to perform the *O*-alkylation directly on glycerol carbonate. 4-Vinylbenzyl acetate (**17A**), 4-vinylbenzyl bromide (**19A**) and 4-vinylbenzyl chloride (**17**) were reacted with glycerol carbonate (Scheme 4.10) under similar conditions as mentioned in Section 4.3.3.2.2. The reactivity of 4-vinylbenzyl chloride, acetate and bromide with glycerol carbonate is presented in the Table 4.5.



**Scheme 4.10:** Synthesis of alkyl-aryl ether containing cyclic carbonate (**BMD**) from glycerol carbonate.

**Table 4.5:** Conversion and selectivity of products using 4-vinylbenzyl derivatives

X	Catalyst	Time (h)	Conv. %	% Selectivity			% Yield <sup>a</sup>
				<b>BMD</b>	<b>18A</b>	<b>20B</b>	
Cl	NaI	96	39	95	-	5	37
Br	NaI	18	100	90	-	10	90
OAc	NaI	23	40	-	55	-	22 <sup>f</sup>
	Ni[P(OC <sub>2</sub> H <sub>5</sub> ) <sub>3</sub> ] <sub>4</sub> <sup>b</sup>	20	50	-	100	-	50 <sup>f</sup>
	Ni[P(OC <sub>2</sub> H <sub>5</sub> ) <sub>3</sub> ] <sub>4</sub> <sup>c</sup>	20	59	-	100	-	59 <sup>f</sup>
	Ni[P(OC <sub>2</sub> H <sub>5</sub> ) <sub>3</sub> ] <sub>4</sub> <sup>d</sup>	20	59	-	100	-	59 <sup>f</sup>
	Ni[P(OC <sub>2</sub> H <sub>5</sub> ) <sub>3</sub> ] <sub>4</sub> <sup>e</sup>	20	38	-	100	-	38 <sup>f</sup>

Reaction conditions: 1.2 moles equivalent of glycerol carbonate/vinylbenzyl derivative; 1.2 mole equivalents of NaH; 0.1 mole equivalent of NaI and 5 mole% of Ni[P(OC<sub>2</sub>H<sub>5</sub>)<sub>3</sub>]<sub>4</sub>.  
<sup>a</sup>Yield of **BMD**. <sup>b</sup>DMF/THF (1/2) was used as solvent. <sup>c</sup>2.5 mole equivalents of NaH was used. <sup>d</sup>20 mole% of Ni[P(OC<sub>2</sub>H<sub>5</sub>)<sub>3</sub>]<sub>4</sub> was used. <sup>e</sup>Amount of Ni[P(OC<sub>2</sub>H<sub>5</sub>)<sub>3</sub>]<sub>4</sub> was 50 mole%.  
<sup>f</sup>Yield of **18A**.

Upon reacting 4-vinylbenzyl bromide with glycerol carbonate, 100% conversion of 4-vinylbenzyl bromide was observed in 18h. In addition to the coupled product 4-(((4-vinylbenzyl)oxy)methyl)-1,3-dioxolan-2-one (**BMD**), 4-vinylbenzyl iodide (**19B**) was also isolated in small amounts indicating its formation as a reactive intermediate in the reaction mechanism (Figure 4.3). Analytically pure product (**BMD**) was obtained in 90% yield after purification by column chromatography and was characterized by IR, NMR and MS. The data for this compound is consistent with literature values where it was

synthesized using a different method from a styrene with pendant epoxide (Miyata, 2012).

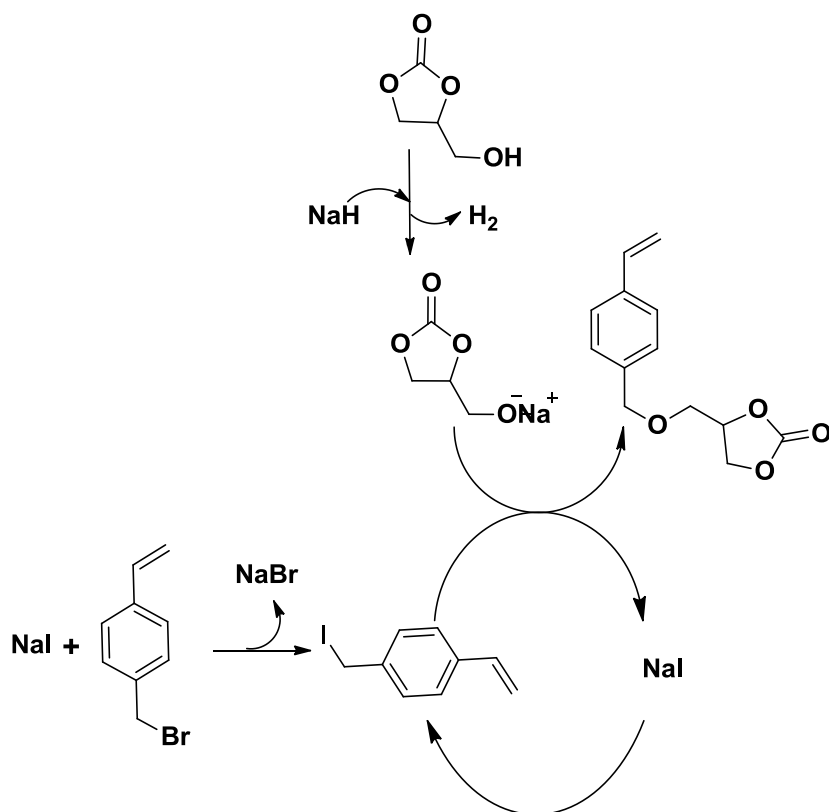


**Figure 4.3:** Mechanism for O-alkylation of glycerol carbonate with 4-vinylbenzyl bromide.

When 4-vinylbenzyl acetate was reacted under similar conditions, 4-vinylbenzyl alcohol (**18A**) was obtained selectively in all cases instead of the styrene derivative. The catalyst 5 to 50 mole% of tetrakis(triethyl phosphite)nickel(0) was used along with sodium hydride (1.2-1.5 mole) with non-dried as well as CaCl<sub>2</sub> dried glycerol carbonate (Yatsumonji et al., 2007). The desired product was not obtained by using the acetate derivative of glycerol carbonate. Under these conditions the 4-vinylbenzyl acetate was prone to hydrolysis (Figure 4.4).

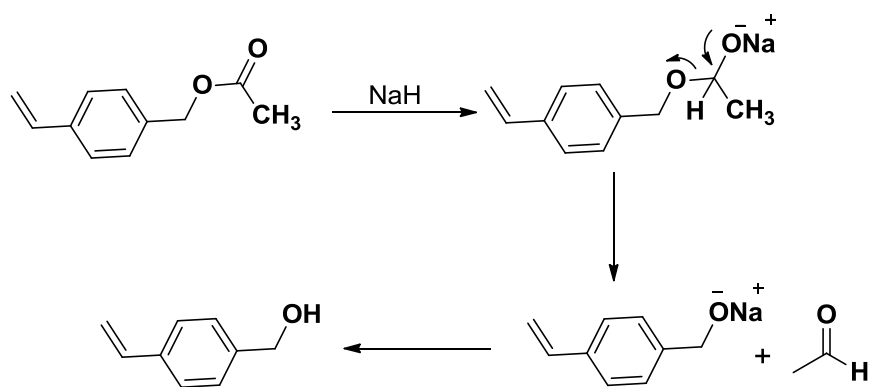
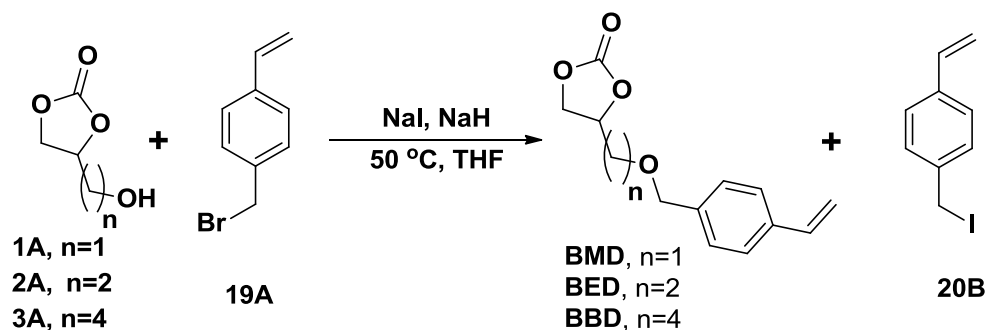


**Figure 4.4:** Hydrolysis of 4-vinylbenzyl acetate.

#### 4.3.3.2.4 O-Alkylation of other hydroxyl containing cyclic carbonates

Novel monomeric precursors containing cyclic carbonate functionalities (**BED** & **BBD**) were synthesized by reaction of 4-vinylbenzyl bromide with hydroxyl containing cyclic carbonates such as, 4-(2-hydroxyethyl)-1,3-dioxolan-2-one (**2A**) and 4-(2-hydroxybutyl)-1,3-dioxolan-2-one (**3A**) (Scheme 4.11). Reactions were completed in short times with excellent yields (Table 4.6). Formation of **18A** was not observed.



**Scheme 4.11:** O-alkylation to form alkyl-aryl ether containing cyclic carbonate.

**Table 4.6:** Table showing selectivity and yields of the monomeric products via O-alkylation

Substrate	Time (h)	Conv. %	% Selectivity		Yield %
			<b>BMD/BED/BBD</b>	<b>20B</b>	
<b>1A</b>	18	100	90	10	90
<b>2A</b>	24	100	89	11	89
<b>3A</b>	18	100	92	8	92

Reaction conditions: 1.2 mole equivalents of cyclic carbonate/4-vinylbenzyl bromide, 1.2 mole equivalents of NaH and 0.1 mole equivalent of NaI were used.

### 4.3.4 Polymerization of monomers containing pendant cyclic carbonate

#### 4.3.4.1 Ring opening polymerization of an epoxide with a pendant cyclic carbonate functionality

The ring opening polymerization (ROP) of 4-((oxiran-2-ylmethoxy)methyl)-1,3-dioxolan-2-one (**OMD**) (Figure 4.5) was achieved under various cationic and anionic conditions in order to obtain a polymer with a five-membered cyclic carbonate moiety.

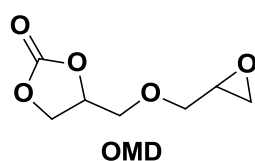
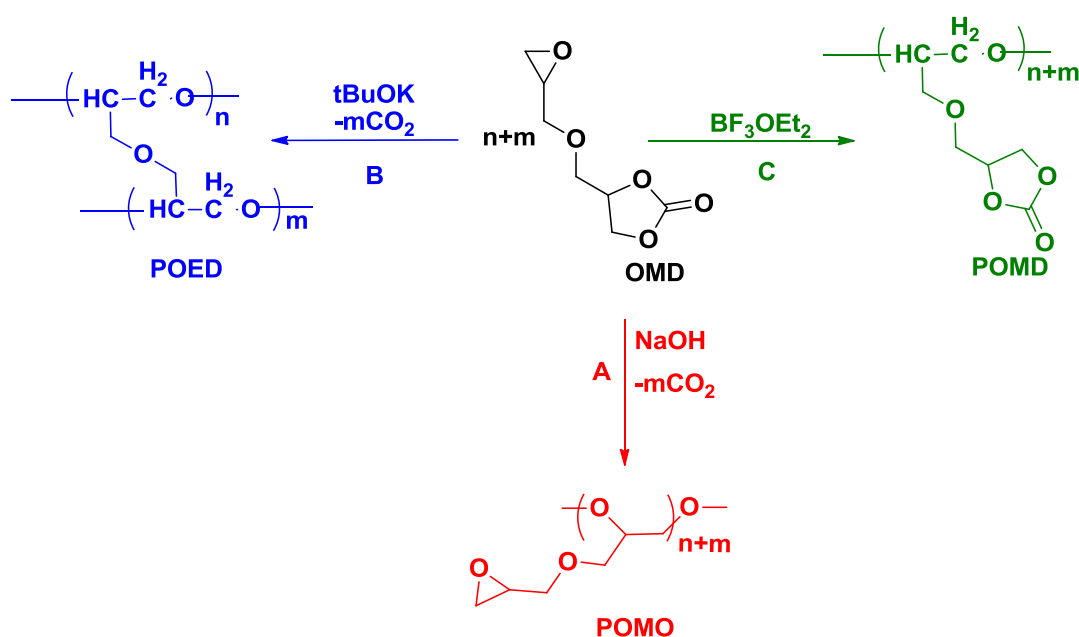


**Figure 4.5:** Structure of 4-((oxiran-2-ylmethoxy)methyl)-1,3-dioxolan-2-one (**OMD**).

A series of experiments was performed to develop optimal reaction conditions for anionic ring opening polymerization. **OMD** was quite stable with a strong base such as sodium hydride even at 110 °C. Employing sodium hydroxide resulted in a selective ring

opening of the cyclic carbonate functionality with the retention of epoxy group to form poly[oxy(ethane-1-(((methoxy)methyl)oxirane)-1,2-diyl)] (**POMO**) in 52% yield (Scheme 4.12). On reacting with a strong non-nucleophilic base such as potassium *t*-butoxide in toluene, the monomer showed no reactivity at or below 80 °C. However, increased reaction temperature (110 °C) resulted in ring opening of the epoxide functionality, as well as the cyclic carbonate, with the loss of carbon dioxide to yield a poly[oxy(ethane-1,2-diyl)] (**POED**) crosslinked via methoxy methyl bridge in 87% yield (Scheme 4.12). The anionic initiating conditions were not suitable for the selective ring opening of the epoxide, as it resulted in the loss of the cyclic carbonate moiety as well.



**Scheme 4.12:** Ring opening polymerization of 4-((oxiran-2-ylmethoxy)methyl)-1,3-dioxolan-2-one (**OMD**) to yield various polyethers at different conditions.

When the polymerization was carried out under cationic conditions, with boron trifluoride diethyl etherate as an initiator, selective formation of poly[oxy(ethane-1-((4-methoxymethyl)-1,3-dioxolan-2-one)-1,2-diyl)] (**POMD**) in 63% yield was observed, with

the cyclic carbonate retained as a pendant group (Scheme 4.12). The retention of the cyclic carbonate was evidenced by the presence of a strong  $\nu(\text{C=O})_{\text{str}}$  band at  $1779 \text{ cm}^{-1}$  in the FTIR and by the distinctive cyclic carbonate protons at  $\delta 4.83$ ,  $4.51\text{-}4.42$  and  $4.00\text{-}3.00$  ppm in the  $^1\text{H-NMR}$  spectrum. In order to optimize the conditions, the temperature of the reaction was varied. Conversion, as well as yield, increased from 63% to 76% when the temperature was decreased from  $80 \text{ }^\circ\text{C}$  to  $25 \text{ }^\circ\text{C}$ . Polyether (**POMD**) with molecular weight above  $8.0 \times 10^3 \text{ Da.}$ , and having low polydispersity (the polydispersity is a measure of the variation of molecular weight distributions), was obtained at room temperature (Table 4.7). Generally, it was observed that the polydispersity index increased from 1.3 to 6 on increasing the reaction temperature from  $25 \text{ }^\circ\text{C}$  to  $80 \text{ }^\circ\text{C}$ .

**Table 4.7:** Ring opening polymerization of 4-((oxiran-2-ylmethoxy)methyl)-1,3-dioxolan-2-one (**OMD**)

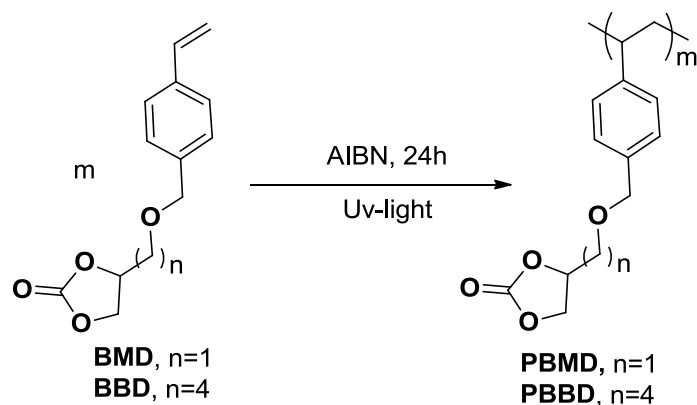
Polymerization	Polymer	Initiator	Temp ( $^\circ\text{C}$ )	Conv. (%)	Yield <sup>a</sup> (%)	$M_n \times 10^3$ ( $\text{g}\cdot\text{mol}^{-1}$ ) <sup>b</sup>	$M_w/M_n$
Anionic ROP <sup>c</sup>	<b>POMD</b>	NaOH	110	66	52	2.8	1.6
	<b>POED</b>	<i>t</i> -BuOK		100	87	1.4	1
Cationic ROP <sup>d</sup>	<b>POMD</b>	$\text{BF}_3\text{OEt}_2$	80	77	63	3.4	6
			50	69	42	1.1	3.1
			RT	94	76	8.1	1.3

<sup>a</sup>Isolated yield. <sup>b</sup>Molecular weight was calculated using GPC. <sup>c</sup>Ratio of monomer/initiator was 10/1, toluene was used as a solvent, time of polymerization was 24 h, conversion was calculated from DCM insoluble part. <sup>d</sup>Ratio of monomer/initiator was 20/1.

#### 4.3.4.2 Radical photopolymerization of cyclic carbonate containing

##### Styrene monomers

In order to attempt a different approach to polymerization, of cyclic carbonate, the five-membered cyclic carbonate containing-styrene monomers, 4-(((4-vinylbenzyl)oxy)methyl)-1,3-dioxolan-2-one (**BMD**) were subjected to radical photopolymerization using AIBN as an initiator (Scheme 4.13).



**Scheme 4.13:** Radical photopolymerization of styrene monomers retaining pendant five-membered cyclic carbonate moiety.

Photopolymerization in bulk without initiator resulted in a polymer with low molecular weight in moderate yield (52%) and conversion (59%) (Table 4.8).

**Table 4.8:** Effect of time on conversion of **BMD** and yield of **PBMD**

Time (h)	AIBN (%)	Conv. <sup>a</sup> (%)	Yield <sup>b</sup> (%)	$M_n^c \times 10^3$ (g.mol <sup>-1</sup> )	$M_w/M_n$
4	2	61	56	18	3.9
8	2	61	60	20	3.6
12	2	62	61	21	3.5
16	2	68	66	20	3.5
20	2	79	71	20	2.4
24	2	99	93	21	2.5
4 <sup>d</sup>	2	22	17	10	1.5
4	-	59	52	10	4.5

<sup>a</sup>Conversion determined from <sup>1</sup>H-NMR. <sup>b</sup>Isolated yield. <sup>c</sup>Molecular weight was calculated using RI detector in the GPC. <sup>d</sup>Acetonitrile was employed as a solvent.

It was observed that the conversion of **BMD** and yield of **PBMD** increased by ~40% with increasing reaction time from 4 hours to 24 hours (Table 4.8). Irradiation was stopped after 24 hours and the polymer (**PBMD**) was collected after precipitation with addition of methanol or water by filtration. Employing acetonitrile as a solvent for 4 hours resulted in lower conversion (22%) and therefore, low yield (17%) with a low molecular weight when compared with bulk photopolymerization.

The <sup>1</sup>H-NMR spectrum of the polymer, **PBMD** obtained after 24 hours is shown in Figure 4.6. The disappearance of vinyl proton signals at  $\delta$ 5.77 and  $\delta$ 5.26 ppm with the appearance of new aliphatic proton signals around  $\delta$ 0.9-2.1 ppm indicated that polymerization had occurred. Retention of the five membered cyclic carbonate was evidenced in the FTIR spectrum where the cyclic carbonate stretching band,  $\nu(\text{C=O})_{\text{str}}$ , at

1783  $\text{cm}^{-1}$  was retained, as well as in the  $^1\text{H-NMR}$  spectrum where five proton signals at  $\delta 4.90$  ppm,  $\delta 4.52$ - $3.9$  ppm and  $\delta 3.59$  ppm, consistent with the cyclic carbonate ring, are present.

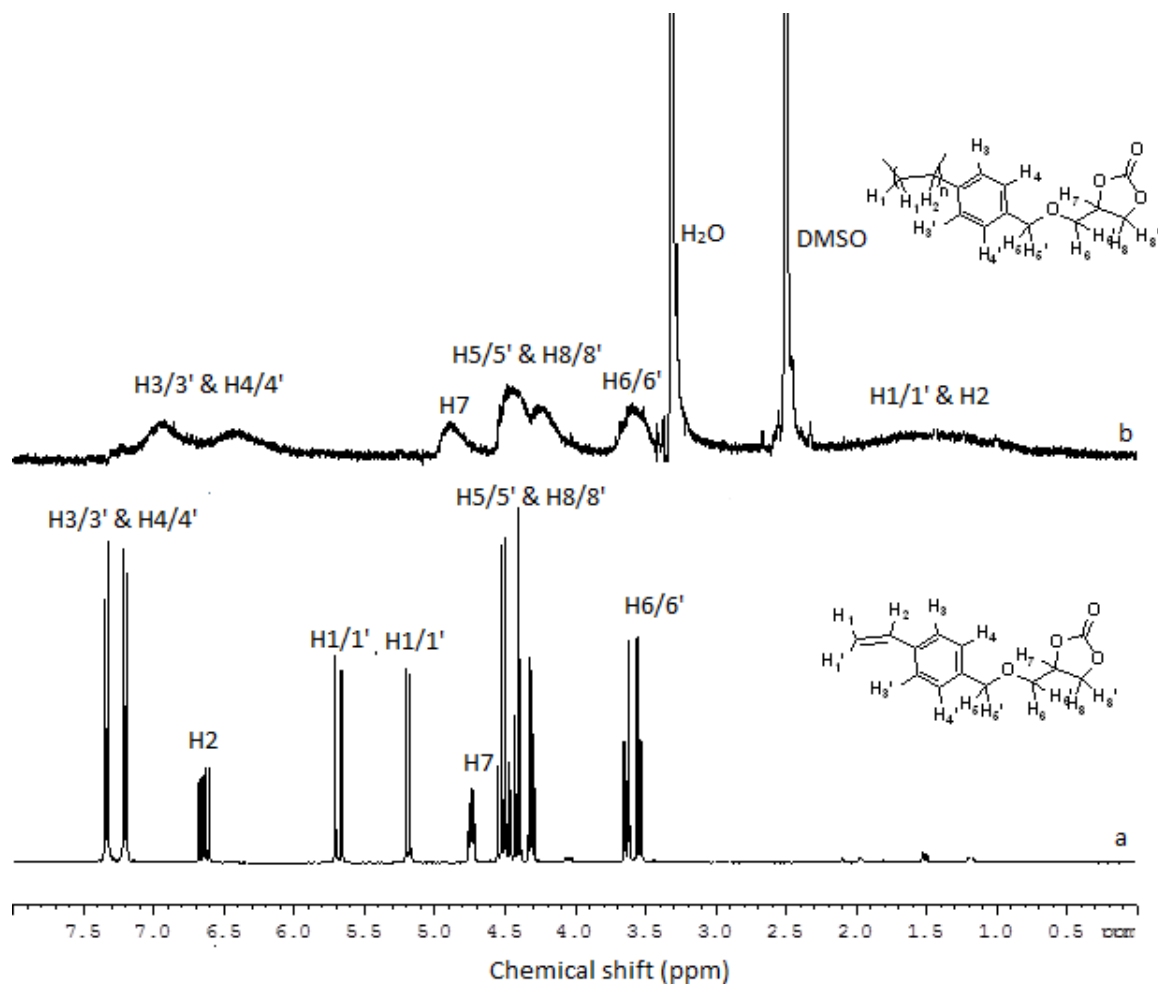


**Figure 4.6:** Assignment of signals in  $^1\text{H-NMR}$  spectra of a) monomer, **BMD** and b) polymer, **PBMD**.

4-(((4-vinylbenzyl)oxy)butyl)-1,3-dioxolan-2-one (**BBD**) was also subjected to radical photopolymerization employing the optimal conditions for **BMD** (Scheme 4.13 and Table 4.9).

**Table 4.9:** Yield and molecular weight of polymers with a pendant cyclic carbonate obtained via radical photopolymerization of pendant cyclic carbonate monomers with styrene functionality

Monomer	Polymer	Conv. (%)	Yield <sup>a</sup> (%)	$M_n \times 10^3$ (g.mol <sup>-1</sup> ) <sup>b</sup>	$M_w/M_n$
<b>BMD</b>	<b>PBMD</b>	99	93	21	2.5
<b>BBD</b>	<b>PBBD</b>	91	74	12	2.4

<sup>a</sup>Polymerization conditions: 2 wt% of initiator (AIBN) were used, time of irradiation was 24h, polymerization was performed at room temperature, conversion was calculated from <sup>1</sup>H-NMR.

Figure 4.7 shows the <sup>1</sup>H-NMR spectrum of polymer (**PBBD**) along with the starting material (**BBD**). Three signals at  $\delta$ 4.81-4.65 ppm,  $\delta$ 4.55-4.19 ppm and  $\delta$ 4.17-3.98 ppm assigned to the five membered cyclic carbonate protons were clearly observed and the broad signal around  $\delta$ 1.81-1.20 ppm was assigned to methyne, methylene and alkyl chain protons, which indicated that the vinyl polymerization occurred with the remaining five-membered cyclic carbonate structure intact.

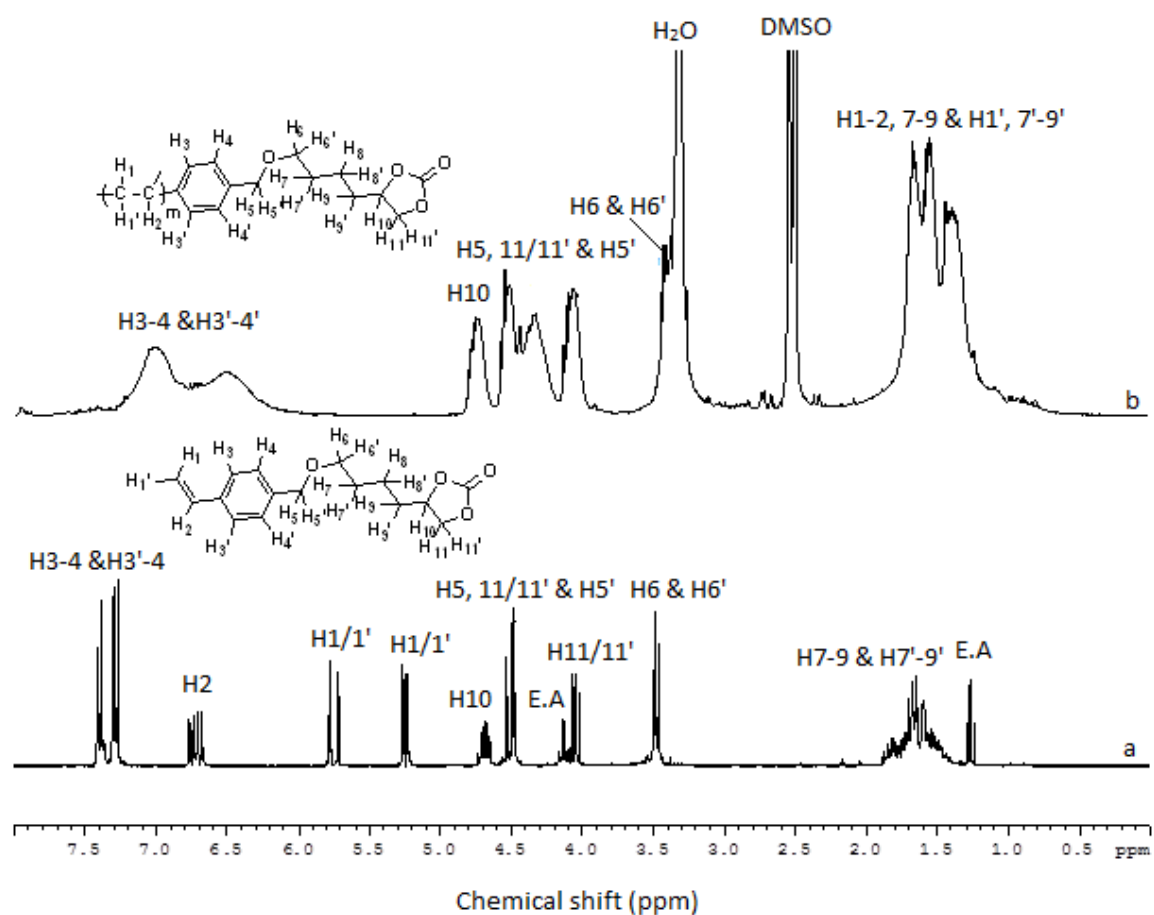


**Figure 4.7:** <sup>1</sup>H-NMR spectra of a) **BBD** (monomer), and b) **PBBD** (polymer).

The molecular weight distribution of **PBBD** was analysed by GPC. The polymer, **PBBD** formed had a molecular weight  $M_n = 1.2 \times 10^3 \text{ gmol}^{-1}$  (PDI= 2.4).

#### 4.4 Conclusion

Various derivatives of glycerol carbonate such as esters, tosyl and bromo were synthesized for the preparation of intercalated complexes with Na-smectite and investigated by XRD and FTIR spectroscopies. The tosyl derivative was reacted with various nucleophiles employing an alternative solvent free methodology, yielding comparable results with previously reported methods. O-Alkylation of hydroxyl containing pendant five-membered cyclic carbonates was performed to obtain precursor

monomers that could subsequently be used in polymerization reactions. Ring opening polymerization of the epoxy monomer with a pendant five-membered cyclic carbonate employing boron trifluoride diethyl etherate resulted in a selective opening of the epoxide ring to yield a polyether with retention of cyclic carbonate intact as part of the polymer structure. Radical photopolymerization for styrene monomers having pendant cyclic carbonate group were performed to successfully obtain styrene polymers retaining the pendant carbonate functionality.

## 4.5 References

- BENSEMHOUN, J. & CONDON, S. 2012. Valorization of glycerol 1,2-carbonate as a precursor for the development of new synthons in organic chemistry. *Green Chem.*, 14, 2595-2599.
- BENYAHYA, S., DESROCHES, M., AUVERGNE, R., CARLOTTI, S., CAILLOL, S. & BOUTEVIN, B. 2011. Synthesis of glycerin carbonate-based intermediates using thiol-ene chemistry and isocyanate free polyhydroxyurethanes therefrom. *Polym. Chem.*, 2, 2661-2667.
- GAO, Y., HE, C. & QING, F.-L. 2011. Polyhedral oligomeric silsesquioxane-based fluoroether-containing terpolymers: Synthesis, characterization and their water and oil repellency evaluation for cotton fabric. *J. Polym. Sci., Part A: Polym. Chem.*, 49, 5152-5161.
- GIARDI, C., LAPINTE, V., NIELLOUD, F., DEVOISSELLE, J.-M. & ROBIN, J.-J. 2010. Synthesis of polyoxazolines using glycerol carbonate derivative and end chains functionalization via carbonate and isocyanate routes. *J. Polym. Sci., Part A: Polym. Chem.*, 48, 4027-4035.

- GILLIS, H. R., STANSSENS, D., DE, V. R., POSTEMA, A. R. & RANDALL, D. 1997. Preparation of polyurethane rigid foam. *US Patent 5703136A*.
- HE, Y., GOEL, V., KEUL, H. & MOELLER, M. 2010. Synthesis, Characterization, and Selectivity of Bifunctional Couplers. *Macromol. Chem. Phys.*, 211, 2366-2381.
- LIU, X., CAO, C., LI, Y., GUAN, P., YANG, L. & SHI, Y. 2012. Cycloaddition of CO<sub>2</sub> to epoxides catalyzed by N-heterocyclic carbene (NHC)-ZnBr<sub>2</sub> system under mild conditions. *Synlett*, 23, 1343-1348.
- OLIVERO, A. G., CASSEL, J. M. & POULSEN, J. R. 1993. Process of preparing enriched enantiomers of glycerol carbonate and derivatives thereof for synthesis of (beta)-blockers. *WO Patent 9322451A1*.
- PFAENDLER, H. R. & MÜLLER, F. X. 1992. A Simple Preparation of Enol Ether Lipids. *Synthesis*, 1992, 350-352.
- ROUSSEAU, J., ROUSSEAU, C., LYNKAITE', B., ŠAČKUS, A., DE LEON, C., ROLLIN, P. & TATIBOUËT, A. 2009. Tosylated glycerol carbonate, a versatile bis-electrophile to access new functionalized glycidol derivatives. *Tetrahedron*, 65, 8571-8581.
- SHIMOMURA, O., LEE, B. S., METH, S., SUZUKI, H., MAHAJAN, S., NOMURA, R. & JANDA, K. D. 2005. Synthesis and application of polytetrahydrofuran-grafted polystyrene (PS-PTHF) resin supports for organic synthesis. *Tetrahedron*, 61, 12160-12167.
- SIMAO, A.-C., LYNKAITE-PUKLEVICIENE, B., ROUSSEAU, C., TATIBOUËT, A., CASSEL, S., SACKUS, A., RAUTER, A. P. & ROLLIN, P. 2006. 1,2-Glycerol carbonate: a versatile renewable synthon. *Lett. Org. Chem.*, 3, 744-748.
- SONNATI, M. O., AMIGONI, S., TAFFIN DE GIVENCHY, E. P., DARMANIN, T., CHOLET, O. & GUITTARD, F. 2013. Glycerol carbonate as a versatile building block for

tomorrow: synthesis, reactivity, properties and applications. *Green Chemistry*, 15, 283-306.

MIYATA, T., Matsumoto, K., ENDO, T., YONEMORI, S., & WATANABE, S. 2012. Synthesis and Radical Polymerization of Styrene-Based Monomer Having a Five-Membered Cyclic Carbonate Structure. *Journal of Polymer Science PART A: Polymer Chemistry*, 50, 3046–3051.

TURNEY, T. W., PATTI, A., GATES, W., SHAHEEN, U. & KULASEGARAM, S. 2013. Formation of glycerol carbonate from glycerol and urea catalysed by metal monoglycerolates. *Green Chemistry*, 15, 1925-1931.

YATSUMONJI, Y., ISHIDA, Y., TSUBOUCHI, A. & TAKEDA, T. 2007. Nickel(0) Triethyl Phosphite Complex-Catalyzed Allylic Substitution with Retention of Regio- and Stereochemistry. *Org. Lett.*, 9, 4603-4606.

# **Chapter 5      Preparation of polymer Na-smectite nanocomposites containing pendant cyclic carbonate**

## **5.1 Introduction**

Polymer/layered silicate nanocomposites have attracted attention as low cost fillers for plastics, exhibiting excellent physical properties such as gas barrier performance, thermal stability, flame retardance and mechanical strength when compared to the unmodified polymer (Giannelis, 1996, Okamoto, 2006, Sinha Ray and Okamoto, 2003). Smectite clays, such as montmorillonite, as a component of nanocomposite are of interest because of their high surface area, high aspect ratio of the silicate layers and ease of intercalation with organic compounds. The intercalation of polymers, such as nylon-6 (Cho and Paul, 2001), polypropylene (Tarapow et al., 2009), polyimides (Abdalla et al., 2002), polystyrene (Nazarenko et al., 2007), unsaturated polyesters (Maji et al., 2009) and polyurethanes (Maji et al., 2009) into montmorillonite has formed the basis of most common nanocomposites.

Three methods have been developed for the synthesis of polymer/clay nanocomposites; solution intercalation, melt intercalation and *in-situ* intercalative polymerization (Alexandre and Dubois, 2000). Polymer solution intercalation is based on a solvent system in which polymer is soluble. The layered silicate is then dispersed into a solvent such as water or chloroform and mixed with the polymer. The polymer layers intercalate by displacing solvent. Upon solvent removal, the intercalated polymer remains within interlayer. Melt intercalation is a method enabling mixing of the layered silicate with the

polymer matrix in the molten state. In the *in-situ* polymerization intercalative technique, the monomer along with the initiator, is intercalated within silicate layers and polymerization is initiated chemically *in-situ* (within the interlayer). A variety of interlayer polymerizations have been studied (Kelly et al., 1994, Lan and Pinnavaia, 1994, Lan et al., 1995, LeBaron et al., 1999). The reaction is usually started by initiator molecules, e.g. polymerization of acrylonitrile by initiation with benzoyl peroxide (Bergaya and Kooli, 1991) or by enhanced temperature, e.g.,  $\epsilon$ -caprolactam into poly-6-amide at 250 °C (Fukushima et al., 1988) and acrylonitrile in kaolinite (Sugahara et al., 1988). For nanocomposite synthesis, polymer chains must diffuse into the interlayer space to produce structures ranging from intercalated to exfoliated (Tjong, 2006). Often the ordered silicate stacking is mostly retained resulting in an intercalated nanocomposite which can therefore be observed by XRD.

Traditional polymer/smectite nanocomposites use between 1 and 5% smectite doped into polymer (Chen et al., 2008) to prevent formation of complex morphologies of nanocomposite. In this chapter, the five-membered cyclic carbonate containing polymers prepared in chapter 4 were used for the preparation of Na-smectite nanocomposites using as much as 50 wt% of unmodified smectite. These nanocomposites potentially create more effective hydraulic barriers for saline leachates. Two effective routes for synthesis of polymer/Na-smectite nanocomposites were used, namely by solution intercalation and by *in-situ* intercalative polymerization (consisting of activated ring opening polymerization and radical polymerization within the interlayer space of Na-smectite). These two routes are schematically presented in Figure 5.1.

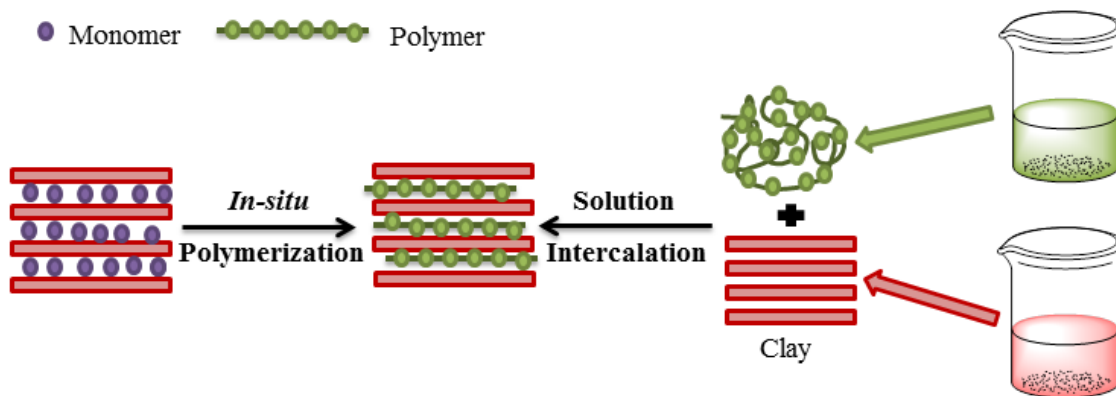


**Figure 5.1:** Approaches used for synthesis of polymer-smectite nanocomposites.

## 5.2 Objectives

The objective was to prepare nanocomposites of Na-smectite with polyether and polystyrene, having pendant five-membered cyclic carbonate moieties, via clay *in-situ* polymerization and solution intercalation methods. The nanocomposites formed were characterized by XRD and FTIR. Another objective was to study the thermal properties, such as the glass transition temperature, of the nanocomposites obtained from solution intercalation and *in-situ* polymerization approaches. A range of characterization techniques including using differential scanning calorimetry and thermogravimetric analysis were applied. In addition, the polymers formed by the *in-situ* technique were separated from the clay and characterized.

## 5.3 Results and discussion

### 5.3.1 Formation of polymers/Na-smectite nanocomposites by solution intercalation and clay *in-situ* polymerization

For the preparation of poly[oxy(ethane-1-(((methoxy)methyl)oxirane)-1,2-diyl)] (**POMD-1**)/Na-smectite by the *in-situ* polymerization method, the Na-smectite was intercalated with 4-((oxiran-2-ylmethoxy)methyl)-1,3-dioxolan-2-one (**OMD**) using 50 wt% amount and characterized by XRD [ $d(001) = 2.29$  nm] (Figure 5.2). Initiator ( $\text{BF}_3 \cdot \text{OEt}_2$ ) was added to the **OMD**/Na-smectite and subjected to ultrasonic treatment, followed by stirring at room temperature for 24h. **POMD-1**/Na-smectite was then precipitated by the addition of water. Powder XRD was used to determine whether polymer intercalation occurred from changes in the gallery height, as measured by the position of the basal reflections, of the resulting smectite-polymer mixture. The broadness of the basal reflection, as measured by the full width at half maximum (FWHM) intensity, gives an indication of the intercalation disorder. Intercalation disorder is a result of variable hydration, stacking disorder and/or polymer orientation differences that occur during intercalation. A narrow reflection (smaller FWHM value) indicates less intercalation disorder. The *in-situ* nanocomposite (**POMD-1**/Na-smectite) shows a small change in  $d$ -space value as compared to **OMD**/Na-smectite, but significant broadening of the 001 reflection was observed. The broadening can be attributed to formation of polymer within the interlayer gallery which pushes clay platelets apart, and results in a range of gallery heights and partial loss of the ordered layer stacking.

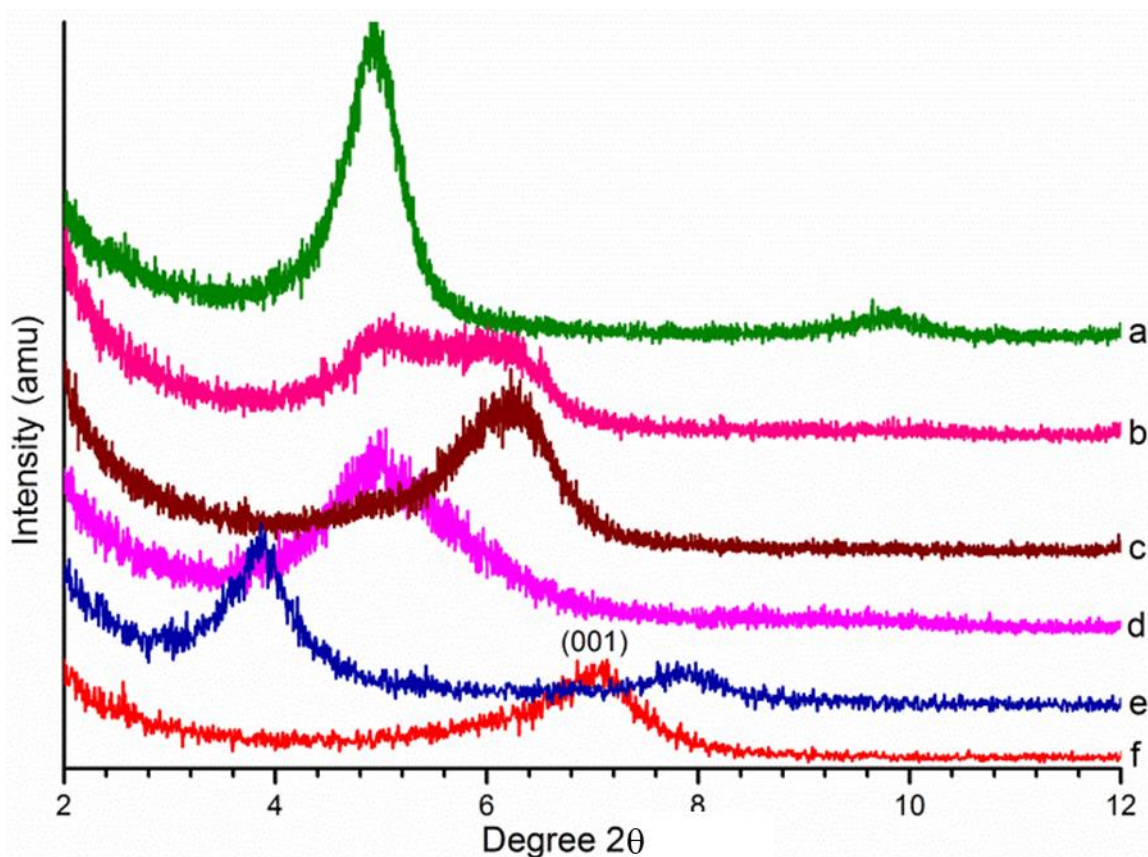


**Figure 5.2:** XRD patterns of the nanocomposites with different **POMD** amounts obtained via solution intercalation (in acetone) and *in-situ* polymerization a) **POMD** (50 wt%)/Na-smectite after solution intercalation, b) **POMD** (20 wt%)/Na-smectite after solution intercalation, c) **POMD** (10 wt%)/Na-smectite after solution intercalation, d) **POMD-1**/Na smectite after *in-situ* polymerization, e) **OMD** (50 wt%)/Na-smectite, and f) Na-smectite.

In addition to the *in-situ* polymerization, solution intercalation was used for the preparation of **POMD**/Na-smectite nanocomposites. Acetone was used as a solvent for solution intercalation. Various amounts of **POMD** with Na-smectite (10, 20 and 50 wt% with respect to Na-smectite) were used and excess polymer was removed using methanol. In the XRD spectra (Figure 5.2), the original Na-smectite shows a 001 diffraction maximum corresponding to a *d* value of 1.25 nm. After the separate intercalation of **POMD** in 10, 20 and 50 wt%, the nanocomposite had 001 reflections

corresponding to  $d$  values of 1.43, 1.74 (1.46) and 1.79 nm, respectively, and with FWHM values of 2.27, 5.86 and 2.58 nm, respectively (Table 5.1). This increase in  $d$ -value is ascribed to the intercalation of **POMD** within the galleries of smectite, and importantly, an ordered intercalated nanocomposite is obtained by using **POMD** at a loading of 50 wt%.

**Table 5.1:** XRD characterization of polymer nanocomposites containing cyclic carbonate obtained via *in-situ* polymerizations and solution intercalation method

Sample	d(001) spacing (nm)	Peak width (nm)	CHN analysis (%)			Organic content <sup>e</sup> (%)
			C	H	N	
Na-smectite	1.25	1.66	0.46	1.33	-	-
<b>OMD</b>	-	-	48.0	5.91	-	-
<b>OMD/Na-smectite</b>	2.29	2.99	18.8	4.07	-	39.7(38.9)
<b>POMD</b>	-	-	48.3	5.80	-	-
<b>POMD-1/Na-smectite<sup>a</sup></b>	1.77	4.90	25.5	3.60	-	51.8(52.8)
<b>POMD (10, 20 &amp; 50 wt%)/Na-smectite<sup>b</sup></b>	1.43,1.46	2.27	4.82	1.23		9.32(9.90)
	1.74	5.86	10.4	2.32		21.9(21.6)
	1.79	2.58	25.7	3.76		56.4(53.2)
<b>BMD</b>	-	-	66.6	6.02	-	-
<b>BMD/Na-smectite</b>	3.30	8.55	31.5	4.20	0.9	47.3(47.3)
<b>PBMD</b>	-	-	67.8	6.30	-	-
<b>PBMD-1/Na-smectite<sup>c</sup></b>	2.46	9.66	35.9	3.95	0.5	43.0(42.8)
<b>PBMD (10, 20 &amp; 50 wt%)/Na-smectite<sup>d</sup></b>	1.26	1.43	5.97	1.43	-	8.90(9.00)
	1.30	2.38	10.9	1.92	-	16.0(16.6)
	1.53	3.64	33.5	3.58	0.2	51.2(50.3)
<b>BBD</b>	-	-	70.6	7.50	-	-
<b>PBBD (10, 20 &amp; 50 wt%)/Na-smectite<sup>d</sup></b>	1.29	1.87	10.7	1.75	-	15.0(16.1)
	1.56	3.68	15.9	2.99	0.1	23.7(24.0)
	1.58	6.06	33.2	4.43	0.3	50.3(50.2)

<sup>a</sup>Prepared by *in-situ* method. <sup>b</sup>Acetone was used as solvent for solution intercalation.

<sup>c</sup>Dimethylformamide (DMF) as solvent was used for thermal radical *in-situ* polymerization. <sup>d</sup>Solution intercalation was performed using acetonitrile. <sup>e</sup>Calculated

from TGA analysis, in parenthesis calculated from CHN analysis (experimental error =  $\pm$  2). Organic (%) = [(Calculated value – Observed value) / Calculated value] x 100%.

Figure 5.3 shows the FTIR spectra from 4000-600  $\text{cm}^{-1}$  for Na-smectite, **POMD**, **OMD**/Na-smectite complex, **POMD** nanocomposites obtained via either *in-situ* polymerization or solution intercalation. Note that the bands appearing in region 2360-2340  $\text{cm}^{-1}$  were due to overtone absorbancies of gaseous carbon dioxide which originated from the air environment.

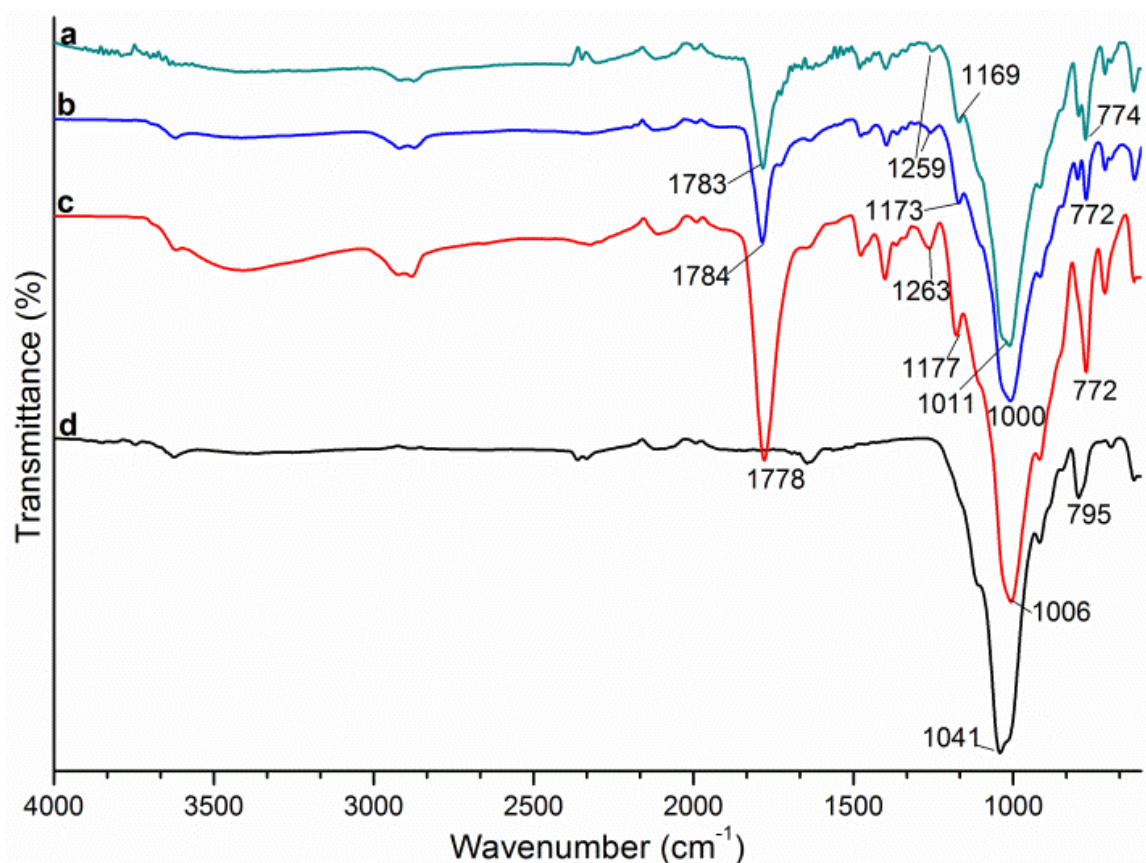


**Figure 5.3:** Comparison of FTIR spectra between 1400 and 600  $\text{cm}^{-1}$  of a) **POMD**-1/Na-smectite nanocomposites obtained via *in-situ* polymerization, b) **POMD** (50 wt%)/Na-smectite prepared by solution intercalation, c) **OMD**/Na-smectite, and d) Na-smectite.

The most significant changes upon nanocomposite formation corresponded to (C=O) and (C-O) stretching vibrations of the cyclic carbonate moiety (Figure 5.3). Pure **POMD** exhibited the characteristic carbonyl stretching band at 1780  $\text{cm}^{-1}$  and  $\nu(\text{C-O})_{\text{str}}$

stretching bands at 1255, 1166 and 1039  $\text{cm}^{-1}$ . In both the solution intercalated and *in-situ* intercalation nanocomposites, the cyclic carbonyl stretching band shifted to  $\sim 1784 \text{ cm}^{-1}$  along with a shift of acyclic  $\nu(\text{C-O})_{\text{str}}$  to  $1259 \text{ cm}^{-1}$ . A blue shift of 4-9  $\text{cm}^{-1}$  was observed for the cyclic  $\nu(\text{C-O})_{\text{str}}$  stretching band upon intercalation. The observed shifts can be interpreted in terms of interactions between the oxygen atoms of **POMD** and the interlayer cations.

The *in-situ* formation of polyether (**POMD**) within smectite galleries is also inferred by comparing the FTIR spectra of pure **POMD** and **OMD** with the Na-smectite subtracted spectra of **POMD-1/Na-smectite** (Figure 5.4). Ring opening of epoxide can be seen by disappearance of the characteristic  $\nu(\text{C-O})_{\text{str}}$  epoxide stretching band, which is present in monomer (**OMD**) at 910 and 826  $\text{cm}^{-1}$ . Furthermore, practically identical FTIR spectra for pure polyether **POMD** as well as *in-situ* polymer **POMD-1** were obtained indicating that clay *in-situ* polymerization resulted in the formation of a similar polymer.

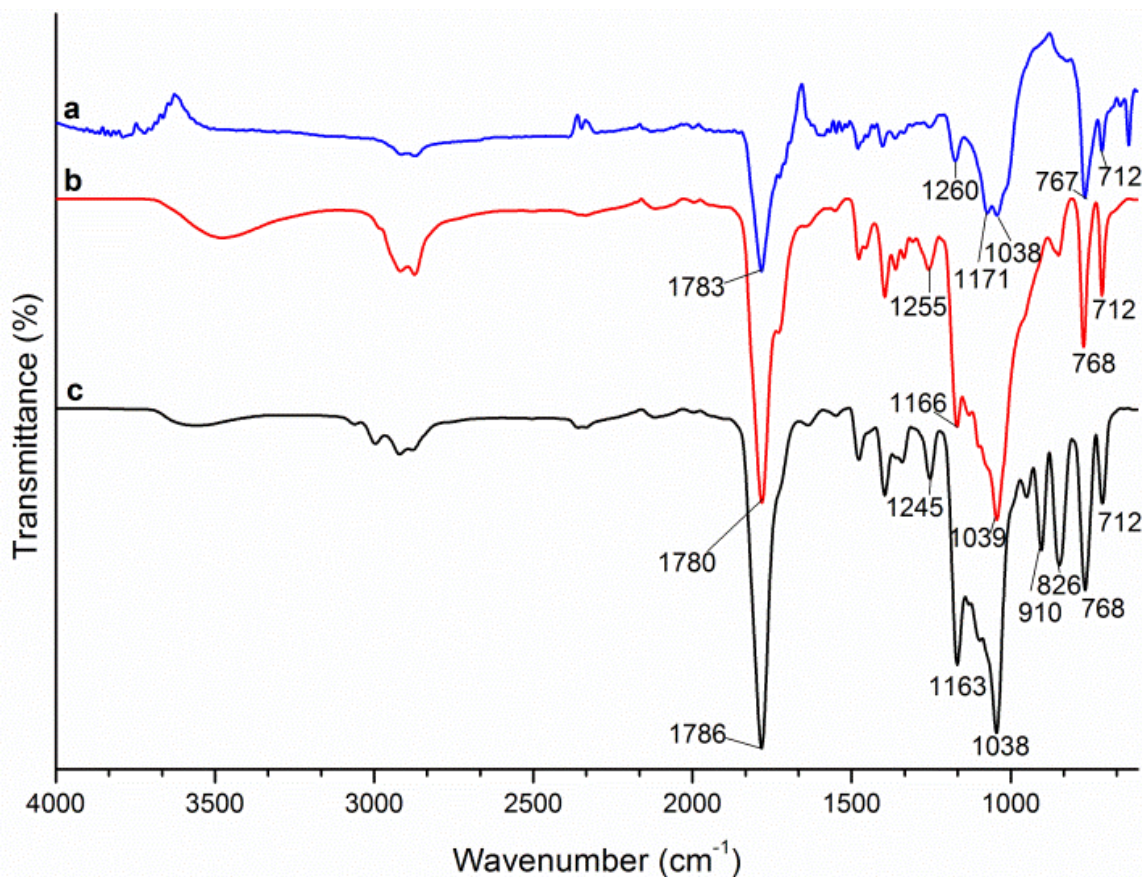


**Figure 5.4:** FTIR spectra of a) **POMD-1** obtained after subtracting FTIR of Na-smectite from **POMD-1/Na-smectite**, b) **POMD** obtained from ring opening polymerization, and c) **OMD** (monomer).

Figure 5.5 shows the XRD result for the poly[4-(((4-vinylbenzyl)oxy)methyl)-1,3-dioxolan-2-one] (**PBMD**)/Na-smectite obtained via solution intercalation in acetonitrile and poly[4-(((4-vinylbenzyl)oxy)methyl)-1,3-dioxolan-2-one] (**PBMD-1**)/Na-smectite via *in-situ* thermal radical polymerization in DMF along with monomer, 4-(((4-vinylbenzyl)oxy)methyl)-1,3-dioxolan-2-one (**BMD**)/Na-smectite and Na-smectite.

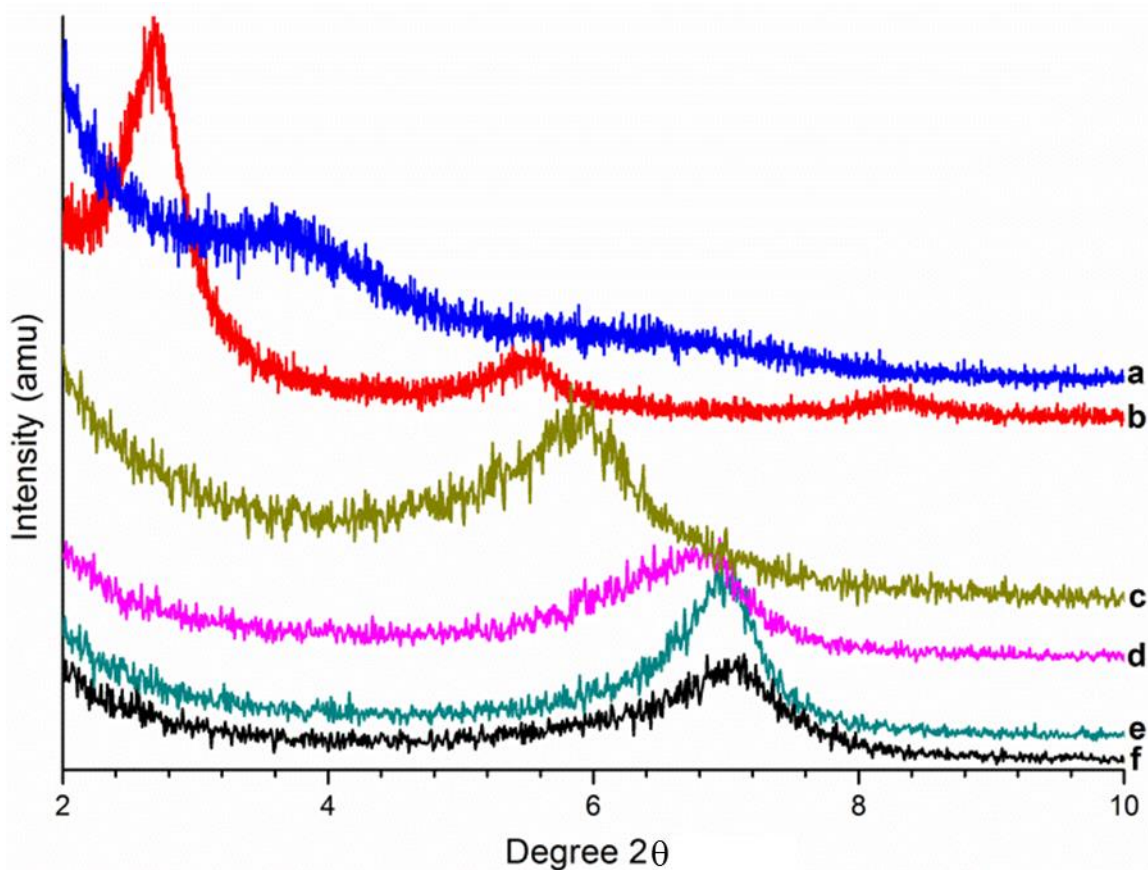


**Figure 5.5:** XRD patterns of a) **PBMD-1**/Na-smectite prepared by *in-situ* method, b) **BMD**/Na-smectite, c) **PBMD (50 wt%)**/Na-smectite, d) **PBMD (20 wt%)**/Na-smectite obtained via solution, e) **PBMD (10 wt%)**/Na-smectite, and f) pure Na-smectite.

The  $d(001)$  information obtained from XRD patterns in the above Figure 5.5 can be plotted in two graphs as shown in Figure 5.6. When monomer **BMD** is intercalated (Figure 5.6a), the  $d$  value for the 001 reflection is shifted to 3.3 nm indicating intercalation within smectite galleries. Upon *in-situ* polymerization, the  $d(001)$  reflection in **PBMD-1**/Na-smectite was at a lower position (to 2.46 nm) as compared to **BMD**/Na-smectite (3.3 nm), and a lower intensity and wider FWHM (9.66 nm) were obtained (Figure 5.5), suggesting polymer formation within the smectite galleries. This indicates substantial disruption of the original interlayer spacing of Na-smectite with the formation of intercalated polymer within silicate layers. An increase in the distribution of

gallery heights, loss of parallel stacking of the clay layers due to inconsistent or uneven polymer intercalation, or both may be the reasons for the broadness of  $d(001)$  reflection.

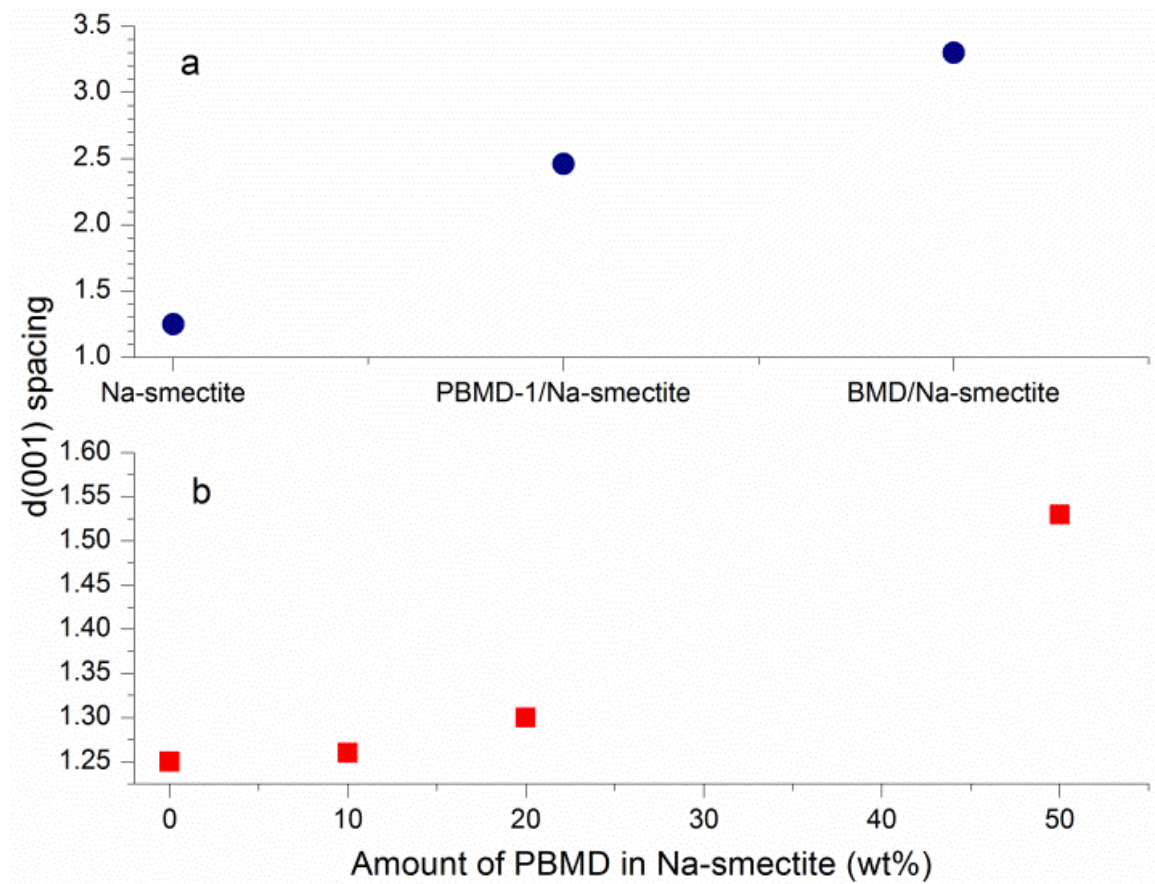
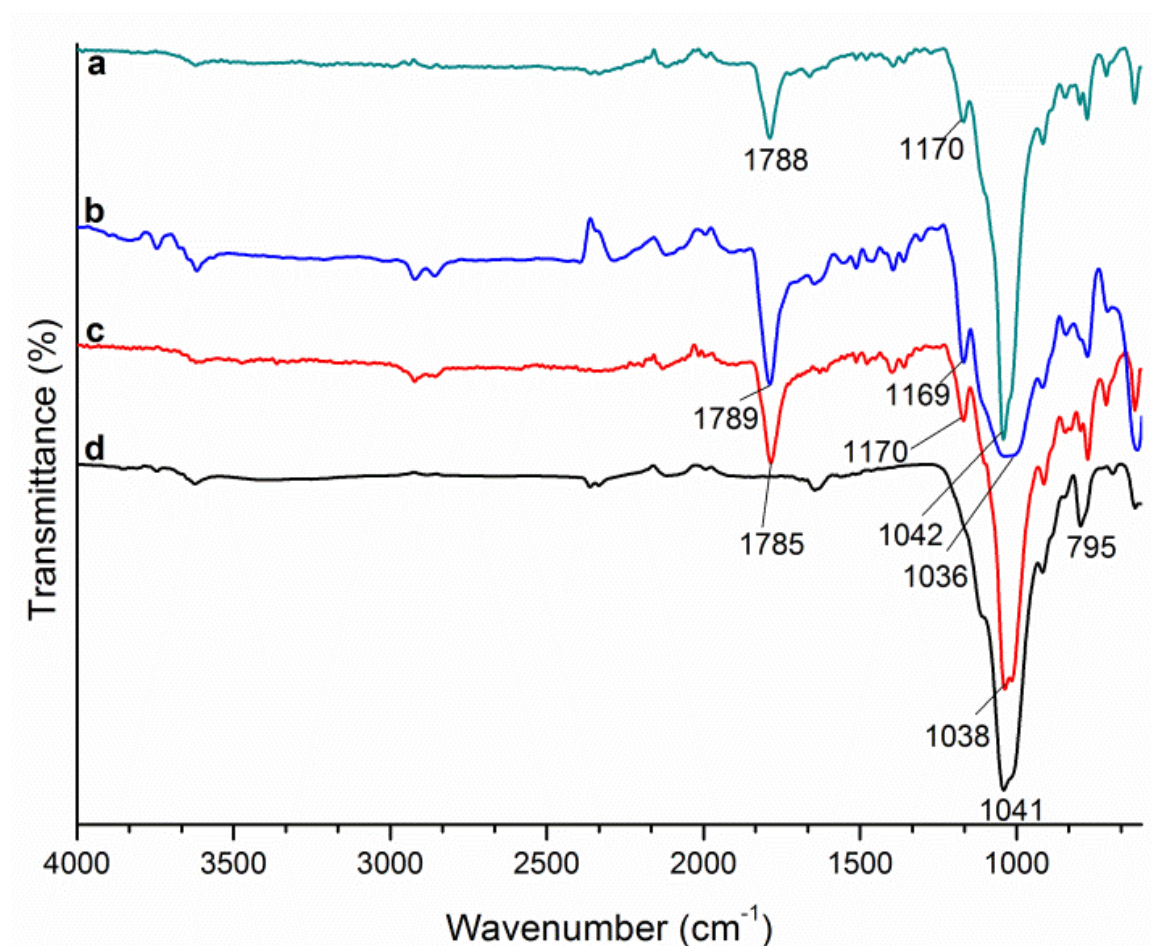


**Figure 5.6:** a) Plot of  $d(001)$  spacing versus Na-smectite, **PBMD-1/Na-smectite** obtained via *in-situ* polymerization along with monomer, **BMD/Na-smectite**, b) Plot of  $d$ -spacing of nanocomposites with varying (wt%) amount of **PBMD** in Na-smectite obtained via solution intercalation.

Figure 5.6b shows that by varying amounts of **PBMD** (10, 20 and 50 wt%) during solution intercalation, the  $d(001)$  reflection increased from 1.25 nm to 1.53 nm, whereas the intensity decreased with a corresponding increase in broadness (FWHM = 1.43-1.64 nm) was observed (Figure 5.5). As more polymer entered the galleries, the layer stacking

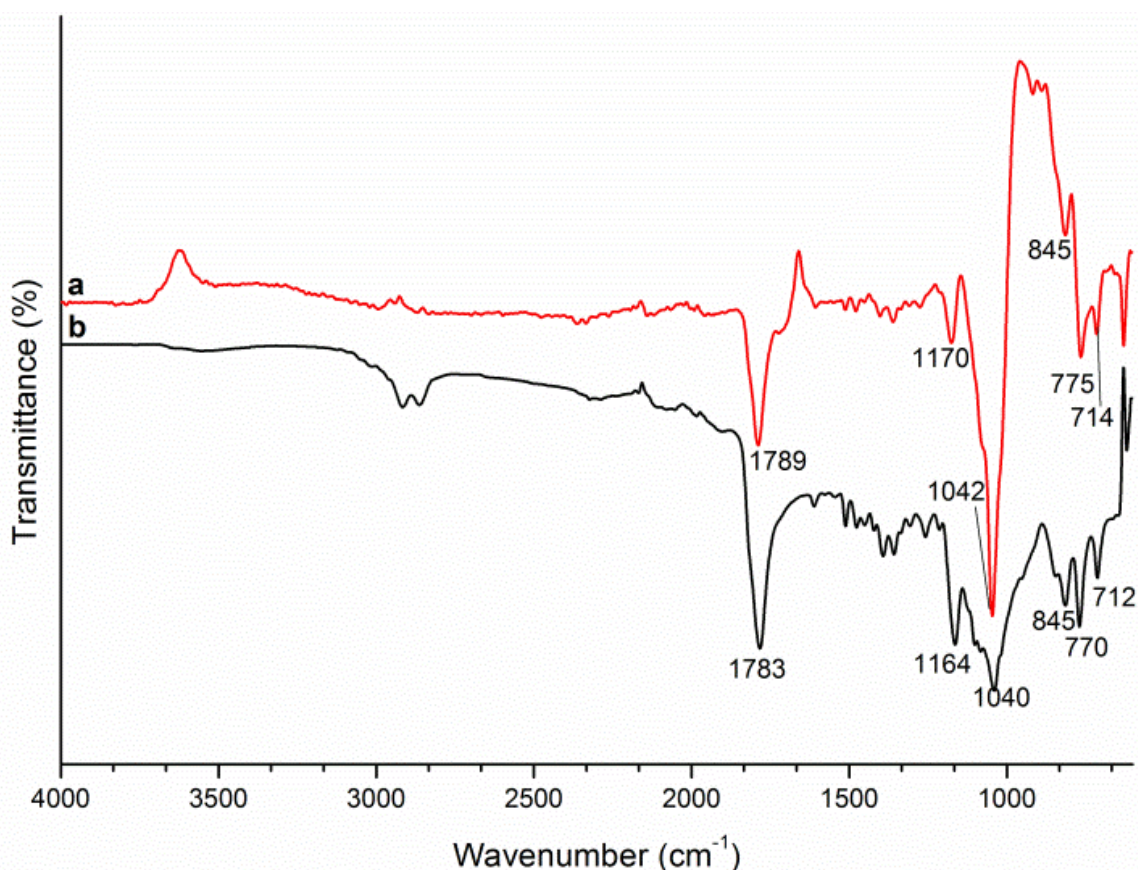
becomes disordered due to a larger range in gallery heights, resulting in a broader 001 reflection (intercalation disorder).

Figure 5.7 summarizes the characteristic frequency of C=O and C-O bands in the FTIR spectra of **PBMD**/Na-smectite and of **PBMD-1**/Na-smectite. Similar spectra with the characteristic carbonyl stretching band appearing at  $1788\text{ cm}^{-1}$  were obtained for nanocomposites prepared by both approaches. A red shift of about  $6\text{ cm}^{-1}$  for cyclic  $\nu(\text{C=O})_{\text{str}}$  from  $1783\text{ cm}^{-1}$  and a blue shift of cyclic  $\nu(\text{C-O})_{\text{str}}$  of  $6\text{ cm}^{-1}$  from  $1164\text{ cm}^{-1}$  was observed for the nanocomposites indicating interaction of cyclic carbonate moiety in polymer with Na-smectite.



**Figure 5.7:** Stacked FTIR spectra of a) **PBMD-1**/Na-smectite, b) **PBMD** (50 wt%)/Na-smectite obtained via solution and *in-situ* polymerization, c) **BMD**/Na-smectite, and d) Na-smectite.

Formation of *in-situ* **PBMD-1**/smectite was also noted by comparing the subtracted FTIR spectra along with pure **PBMD** (Figure 5.8). Disappearance of olefin  $\nu(\text{C}=\text{C})_{\text{str}}$  at  $1628\text{ cm}^{-1}$  and the appearance  $\nu(\text{C}-\text{H})_{\text{str}}$  in the range  $2900\text{--}3000\text{ cm}^{-1}$ , due to formation of alkyl groups, are the major indications for polymerization via the *in-situ* process.



**Figure 5.8:** Comparison of FTIR spectra of a) **PBMD-1** obtained from subtraction of Na-smectite from **PBMD-1/Na-smectite**, and b) pure **PBMD**.

Figure 5.9 shows the  $d(001)$  spacing and FWHM values plotted against the wt% amount of poly[4-(((4-vinylbenzyl)oxy)butyl)-1,3-dioxolan-2-one] (**PBBD**) used for solution intercalation. Addition of greater amounts of **PBBD** into Na-smectite consistently resulted in broader FWHM values. The  $d$  value of the 001 reflection of Na-smectite at 1.25 nm (FWHM 1.66 nm), upon loading of **PBBD** in 20-50 wt% the  $d$  value increased to

1.58 nm with slight broadening (FWHM 3.68-6.06 nm) as illustrated by the Figure 5.9 for the **PBBD**/Na-smectite samples, which attests to the degree of disorder of clay platelets at 50 wt% loading.

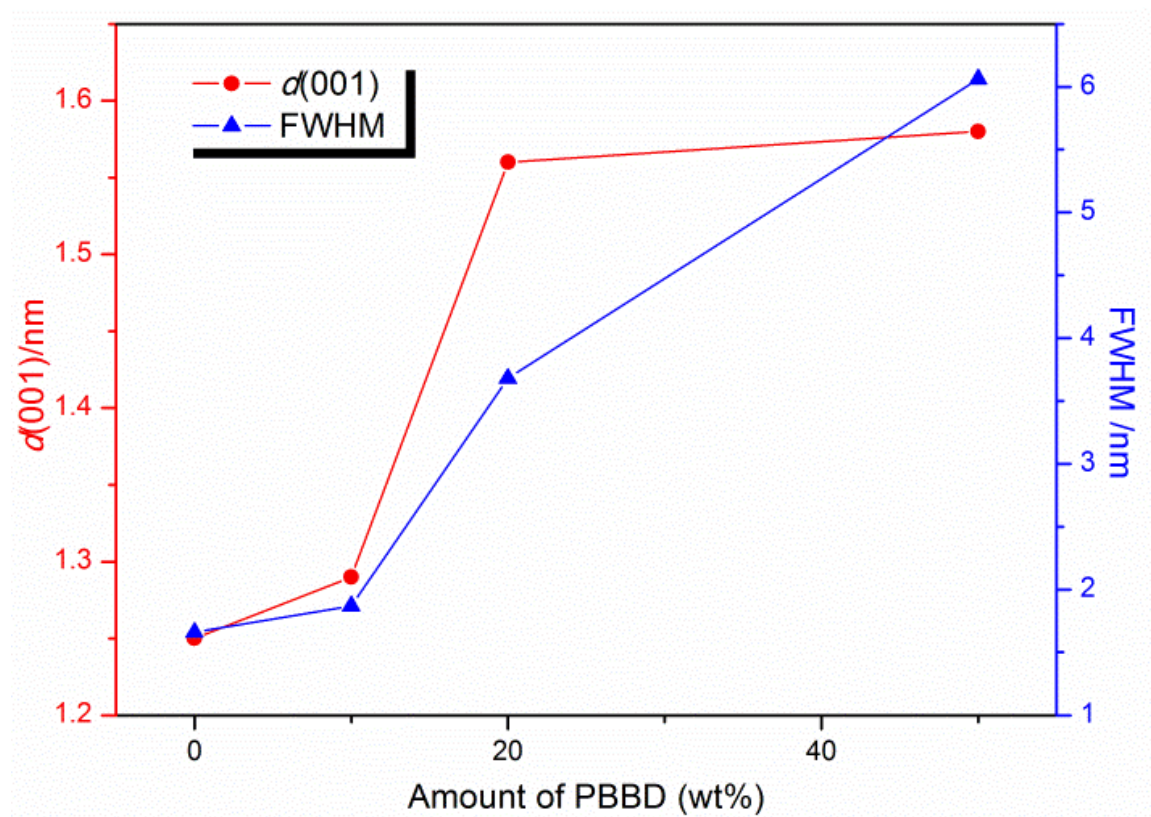


**Figure 5.9:** Plot of  $d(001)$  as well as full width at half maximum (FWHM) versus amount of addition of **PBBD** to Na-smectite.

Characteristic absorbance frequencies in the FTIR of neat polymer (**PBBD**) and of **PBBD**/Na-smectite nanocomposites obtained by solution intercalation are presented in Table 5.2. A small blue shift of about  $4\text{ cm}^{-1}$  was observed for the cyclic carbonyl group stretching in nanocomposites. There was no significant change in other FTIR absorbance bands.

**Table 5.2:** Infrared frequencies of the main characteristic absorbance bands of pure **PBBD** and **PBBD/Na-smectite** obtained via solution intercalation

Sample	FTIR stretching (cm <sup>-1</sup> )				
	(C-H)	(C=O)	(C-O) acyclic	(C-O) cyclic	(C-O)
<b>PBBD</b>	2920, 2853	1788	1260	1166	1093, 1057
<b>PBBD (10 wt%)/Na-smectite</b>	-	1792	-	-	997
<b>PBBD (20 wt%)/Na-smectite</b>	2925	1793	-	-	998
<b>PBBD (50 wt%)/Na-smectite</b>	2921, 2858	1792	1262	1167	1004

Different types of the nanocomposites were obtained as evaluated by XRD studies using clay *in-situ* polymerization and the solution intercalation method. A brief summary is listed in Table 5.3. The morphologies of nanocomposites obtained for polyether, **POMD** via *in-situ* polymerization were disordered intercalates. However, solution intercalation resulted in formation of intercalated nanocomposites. The *in-situ* polymerization of polystyrene, **PBMD-1** resulted in disordered intercalated nanocomposites; however, partially disordered intercalated nanocomposites were obtained by using the solution intercalation approach for styrene polymers (**PBMD/Na-smectite** & **PBBD/Na-smectite**). Intercalated morphologies of nanocomposites were obtained with both approaches; however, the *in-situ* intercalative polymerization method was preferred when compared with the solution intercalation for the one pot process, where no solvent was required and which also lended itself to easy purification.

**Table 5.3:** Types of nanocomposites obtained via *in-situ* method and solution intercalation approach

Sample	Method	Type
<b>POMD-1/Na-smectite</b>	<i>in-situ</i> polymerization	Disordered intercalates
<b>POMD/Na-smectite</b>	Solution intercalation	Intercalated
<b>PBMD-1/Na-smectite</b>	<i>in-situ</i> polymerization	Disordered intercalates
<b>PBMD/Na-smectite</b>	Solution intercalation	Partially disordered intercalates
<b>PBBD/Na-smectite</b>	Solution intercalation	Partially disordered intercalates

### 5.3.2 Isolation of polymers formed by *in-situ* polymerization

The molecular weight and properties of polymer formed from the *in-situ* polymerization method were determined by removing the polymer from the clay galleries using an appropriate solvent (acetone or acetonitrile). The isolated solutions containing the free polymers were collected, concentrated, washed and were fully characterized by FTIR, <sup>1</sup>H-NMR, GPC, DSC and TGA (POMD-A and POMD-B) whereas, the solid residue (PBMD-A and PBMD-B) were characterized by powder XRD, FTIR and TGA (Table 5.4).

**Table 5.4:** Characterization of extracted polymers from *in-situ* polymerized sample

Sample	Organic content <sup>a</sup> (%)	<i>d</i> (001) spacing (nm)	$M_n \times 10^3$ (g.mol <sup>-1</sup> ) <sup>b</sup>	$M_w/M_n$
<b>POMD-A</b>	25.2	1.96	-	-
<b>POMD-B</b>	100	-	5.6	1.6
<b>PBMD-A</b>	41.5	1.36	-	-
<b>PBMD-B</b>	100	-	15.5	2.7

<sup>a</sup>Calculated from TGA analysis. <sup>b</sup>Molecular weight was calculated on filtrate using GPC.

After washing the **POMD-1**/Na-smectite with acetone, reflections in the XRD trace broadened and decreased in intensity. The reflection for the **POMD-A**/Na-smectite did not shift to a lower position (Figure 5.10) indicating that while most of the polymer attached to the surface of clay was removed, high molecular weight polymer was still present in the nanocomposites and was not fully removed using this washing method.

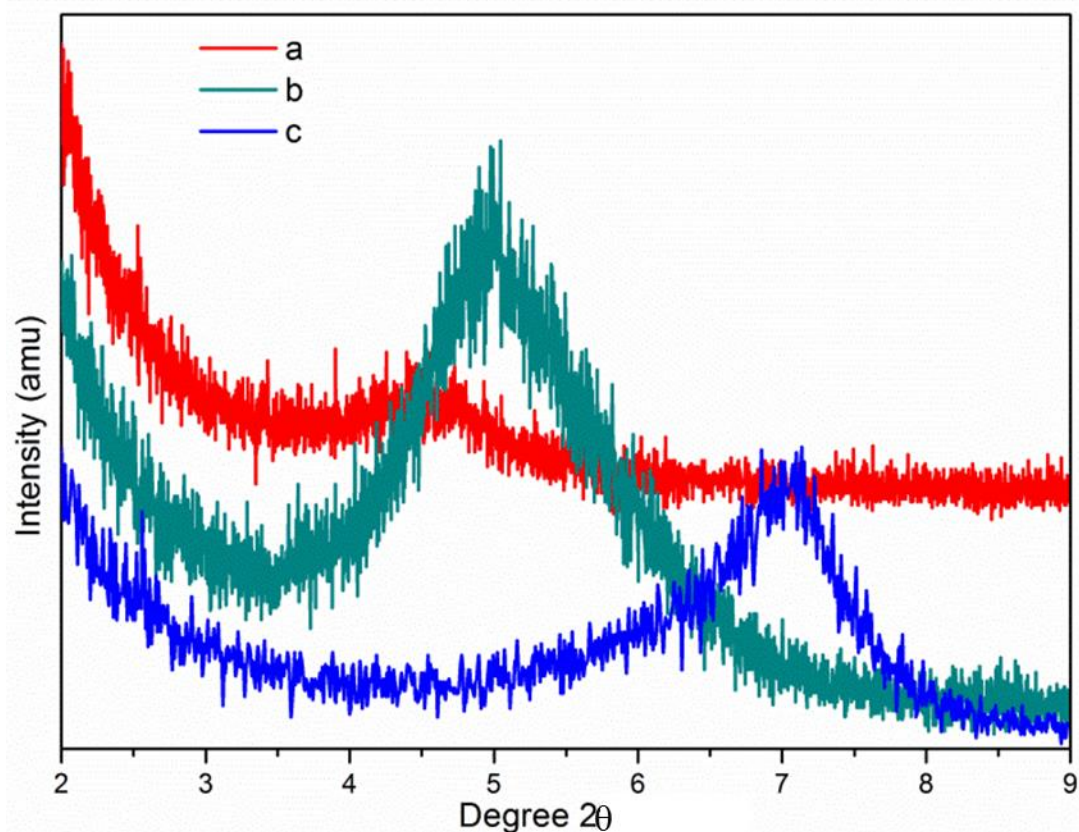


**Figure 5.10:** Stacked XRD patterns of a) **POMD-A**, b) **POMD-1/Na-smectite** prepared by *in-situ* method, and c) **Na-smectite**.

In the XRD diffraction pattern of **PBMD-A**, the reflection at 3.5 °2θ was lost and the *d*-space value was shifted to a higher °2θ value and lower position (from 2.46 to 1.36 nm) with a broader distribution attributed to irregular stacking of clay platelets or the possible presence of multiple solvation states of acetonitile-**PBMD-1/Na-smectite** (Figure 5.11).

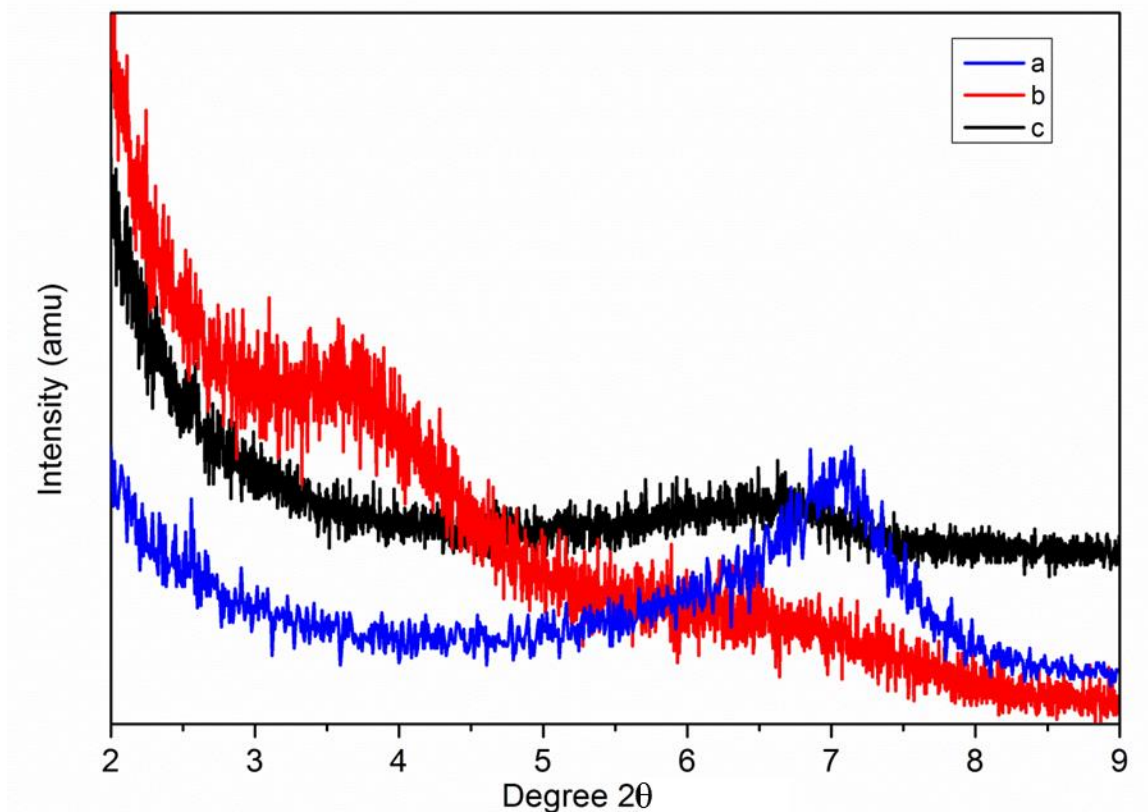


**Figure 5.11:** XRD traces of a) Na-smectite, b) **PBMD/Na-smectite**, and c) **PBMD-A** obtained after washing with acetonitrile.

TGA analysis indicated the presence of polymeric content in **PBMD-A** and **POMD-A**, which was retained strongly in nanocomposite even after acetone or acetonitrile washing (Table 5.4). When FTIR and  $^1\text{H-NMR}$  of neat polyether **POMD** were compared with extracted polymer **POMD-B**, no differences were observed in the spectral data (Figure 5.12 & Figure 5.13).

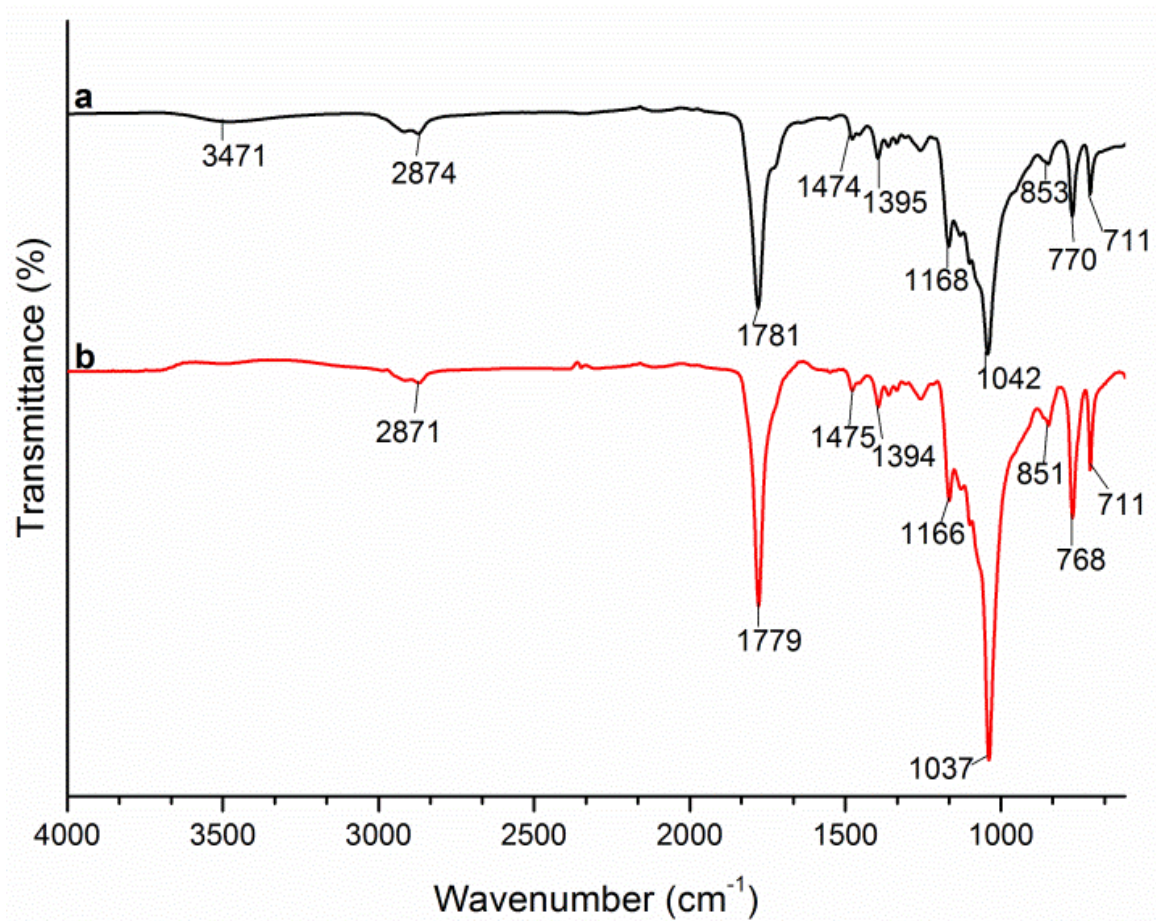


**Figure 5.12:** FTIR spectra of a) **POMD**, neat polymer, and b) **POMD-B** (extracted polymer).

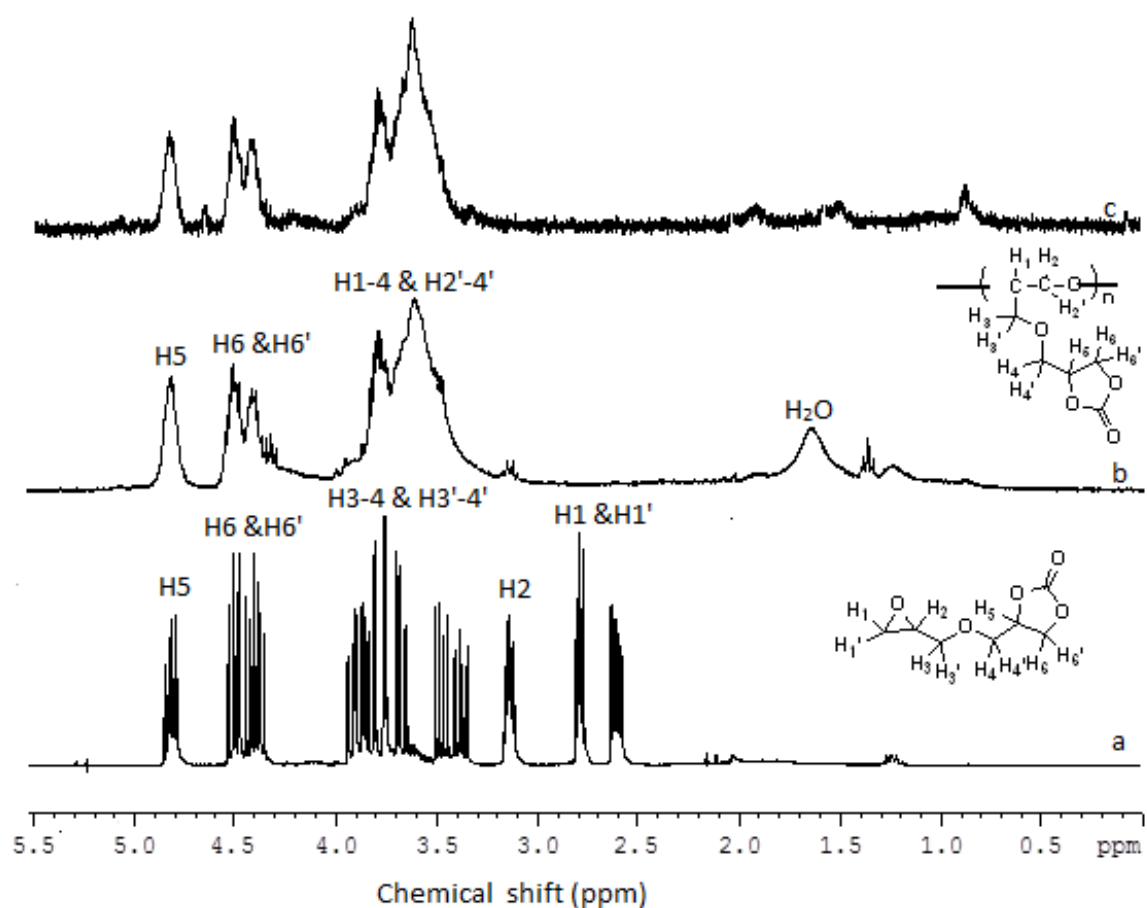


**Figure 5.13:** Comparison of  $^1\text{H-NMR}$  spectra in  $\text{CDCl}_3$  of a) **OMD**, monomer, b) Neat polyether (**POMD**), and c) extracted polymer, **POMD-B**.

FTIR and  $^1\text{H-NMR}$  data proved the formation of a similar polymer within the clay interlayer galleries as could be synthesized by other methods. Furthermore, the GPC data showed comparable molecular weights of extracted polymers when compared with their respective neat polymer (Chapter 4). These results suggest that a polymer containing cyclic carbonate was formed within the clay during the *in-situ* polymerization method.

### 5.3.3 Treatment of polymer nanocomposites with sodium chloride

An investigation into the possible leaching of the **OMD**/Na-smectite (monomer complex) and polyether with pendant five membered cyclic carbonate/sodium smectite nanocomposites (**POMD**/Na-smectite prepared via solution intercalation method using 50 wt% amount of **POMD**) was performed with a 3M sodium chloride aqueous solution. After treatment of the monomer complex, **OMD**/Na-smectite with saline solution, the  $d(001)$  reflection shifted from 22.7 nm to 13.9 nm (Figure 5.14). The  $d(001)$  spacing of 13.9 nm represented the loss of organic content.

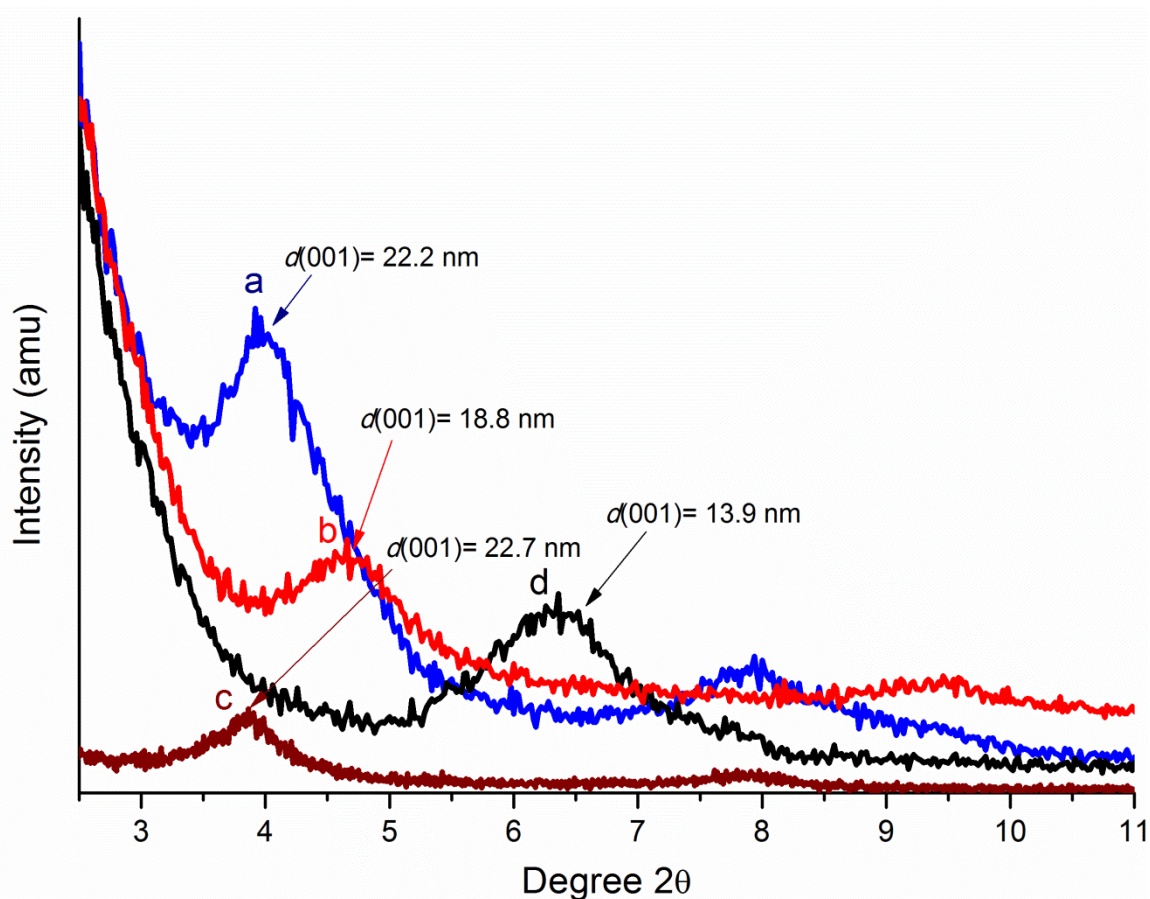


**Figure 5.14:** XRD diffraction patterns of a) **POMD**/Na-smectite, b) **POMD**/Na-smectite after treatment with 3M NaCl, c) **OMD**/Na-smectite (XRD trace was run at a different parameters), and d) **OMD**/Na-smectite after treatment with 3M sodium chloride.

When compared with polyether nanocomposite, the same saline solution treatment resulted in a shift of the  $d(001)$  reflection peak from 22.2 nm to 18.8 nm. The polymer nanocomposite (**POMD**/Na-smectite) showed a small change in  $d(001)$  reflection suggesting a better retention of polymer in the smectite nanocomposites as compared with its monomer (**OMD**/Na-smectite) upon interaction with the saline solution.

#### **5.3.4 Thermal properties of intercalated polymer/Na-smectite nanocomposites**

The thermal properties of the nanocomposites were analysed by differential scanning calorimetry (DSC). The increment in the glass transition temperature ( $T_g$ ) is associated with the immobilization of the polymer in the presence of inorganic nanocomposites. The neat polymer exhibit low temperature behavior showing a  $T_g$  around 56.3, 56.5 and 82.4 °C respectively, which is assigned to glass transition in these polymers. The addition of Na-smectite caused only a slight decrease in  $T_g$  for polymers with styrene functionality (Figure 5.15 & Table 5.5). However, a significant decrease in  $T_g$  was observed for polyether polymer (**POMD**) when intercalated into Na-smectite (Figure 5.15).

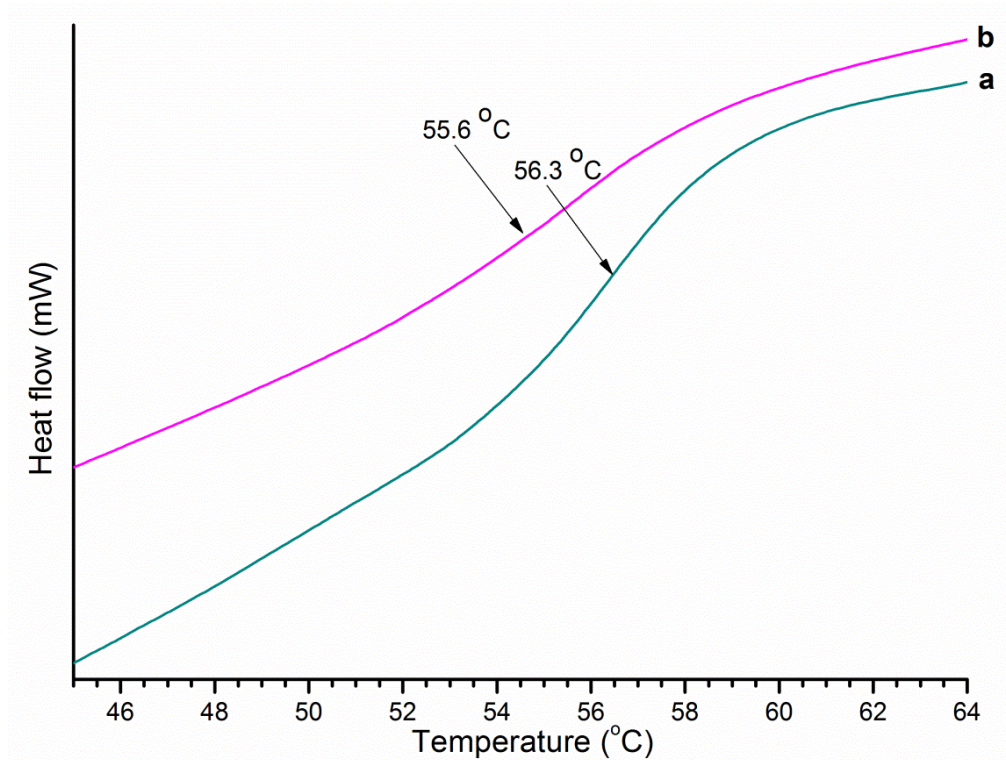


**Figure 5.15:** Glass transition temperature of a) neat polystyrene with pendant cyclic carbonate, PBBD and b) PBBD (50 wt%)/Na-smectite nanocomposite.

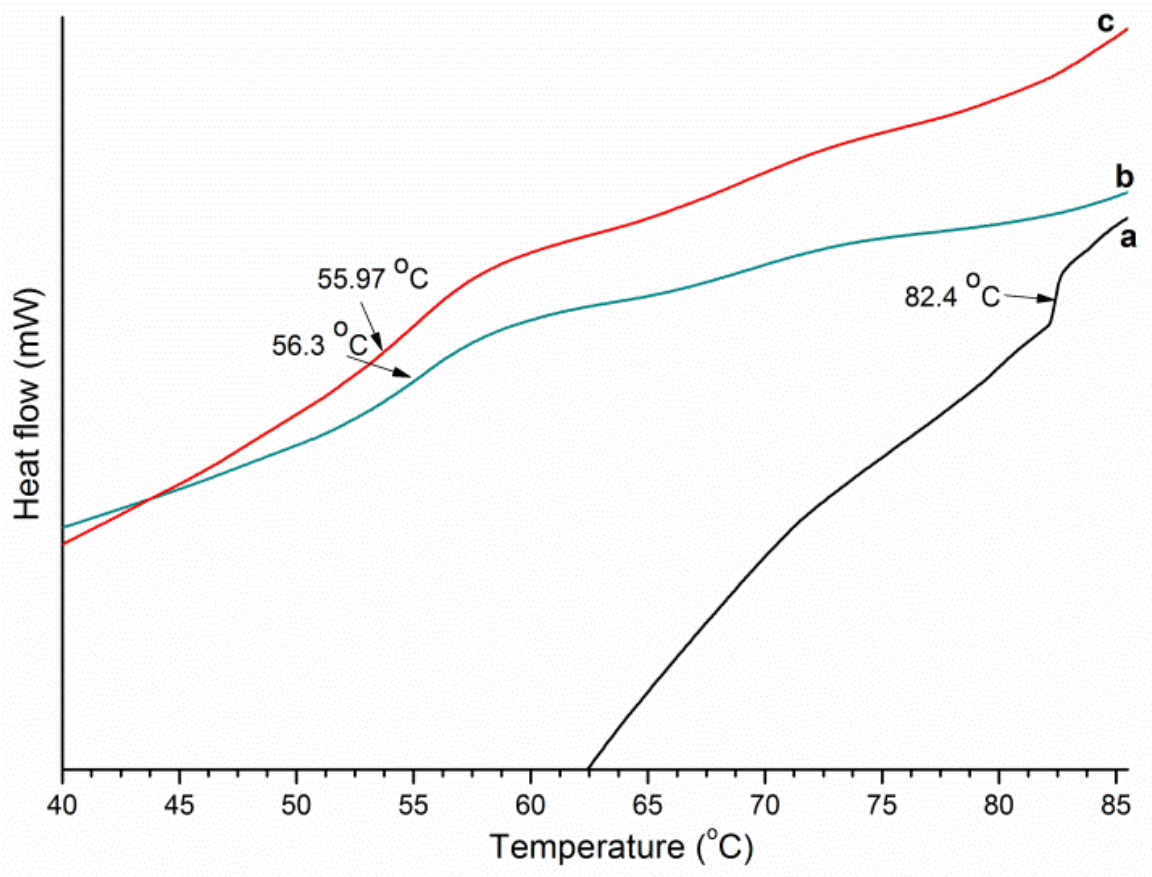


**Figure 5.16:** Glass transitions temperature of the a) neat polyether **POMD**, b) **POMD/Na-smectite** obtained via solution intercalation, and c) **POMD-1/Na-smectite** prepared by *in-situ* method. The arrows indicate the glass transition temperatures.

**Table 5.5:** Glass transition temperature of pure polymers along with their nanocomposites

Sample	$T_g^a$ (°C)
<b>POMD</b>	82.4± 0.2
<b>POMD-1/Na-smectite<sup>b</sup></b>	55.9± 0.4
<b>POMD/Na-smectite<sup>c</sup></b>	56.3± 0.7
<b>POMD-A</b>	55.2± 0.1
<b>POMD-B</b>	82.8± 0.3
<b>PBMD</b>	56.5± 0.1
<b>PBMD-1/Na-smectite<sup>b</sup></b>	54.8± 0.3
<b>PBMD/Na-smectite<sup>c</sup></b>	54.6± 0.4
<b>PBMD-A</b>	54.7± 0.2
<b>PBMD-B</b>	56.4± 0.1
<b>PBBD</b>	56.3± 0.2
<b>PBBD/Na-smectite<sup>c</sup></b>	55.6± 0.5

<sup>a</sup>Mean ± standard deviation of each analysis, n=3. <sup>b</sup>Prepared by *in-situ* method.

<sup>c</sup>Nanocomposite prepared via solution intercalation approach.

The reduction in  $T_g$  of the polymer intercalated within the Na-smectite may be caused by the confinement within the silicate interlayer galleries. Such confinement may prevent the segmental motion of the polymer chains and allow the glass phase transition to proceed at lower temperatures.

The organic content in the intercalated materials can be calculated from their thermogravimetric analysis (TGA) and CHN analysis (Table 5.1). The results for percent organic matter in the nanocomposites calculated via both methods was comparable and

in close agreement with the experimentally added amounts. Figure 5.17 clearly shows two main weight losses with ascending temperature, attributed respectively, to the release of adsorbed water (near 100 °C) and dehydroxylation of the Al/Mg-OH groups in Na-smectite (near 650 °C). Water adsorbed on the external surface of smectite is removed around 80 °C. Water adsorbed within the interlayer space is removed at higher temperatures (around 100 °C, see Appendix 2 for derivative curve).

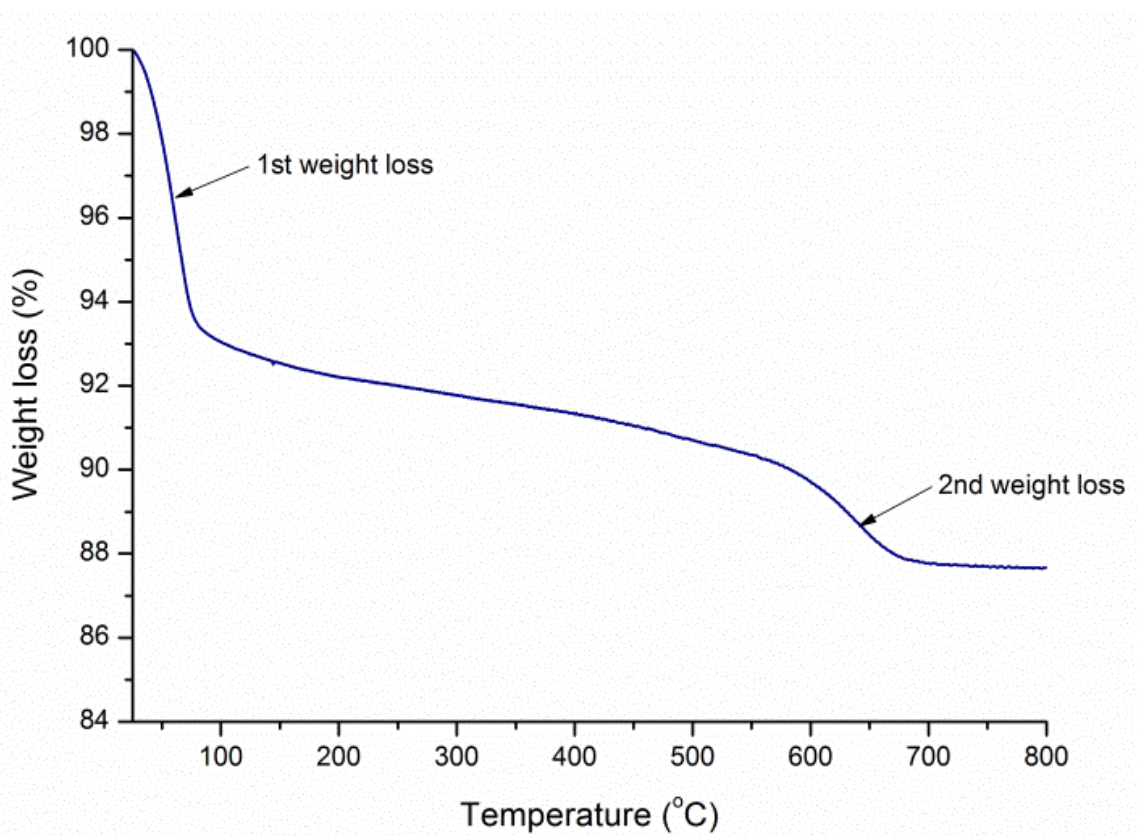


**Figure 5.17:** TGA curve of Na-smectite showing weight losses.

In Figure 5.18, thermograms of **POMD-1/Na-smectite** and **POMD/Na-smectite** are presented, for nanocomposites prepared by *in-situ* as well as solution intercalation. All nanocomposites exhibited higher thermal stabilities compared to virgin polymer. These results confirm that the quantitative anchoring of polymer within the interlayer galleries of Na-smectite was obtained by solution as well as by the *in-situ* method.

TGA results (Figure 5.18) for **POMD** nanocomposites show that in most cases, nearly all the interlayer water has been replaced by the polymer as the loading increases probably by the way the polymer was intercalated (using acetone for solution intercalation and the solvent-mixture for *in-situ* method). In addition, the increased temperature of polymer degradation with decreasing polymer loading may suggest that at higher polymer loading, the polymer behaves more like a bulk polymer. Alternatively, at lower polymer loading, the polymer is bound very strongly to the clay surface, is highly protected and therefore has a higher decomposition temperature.

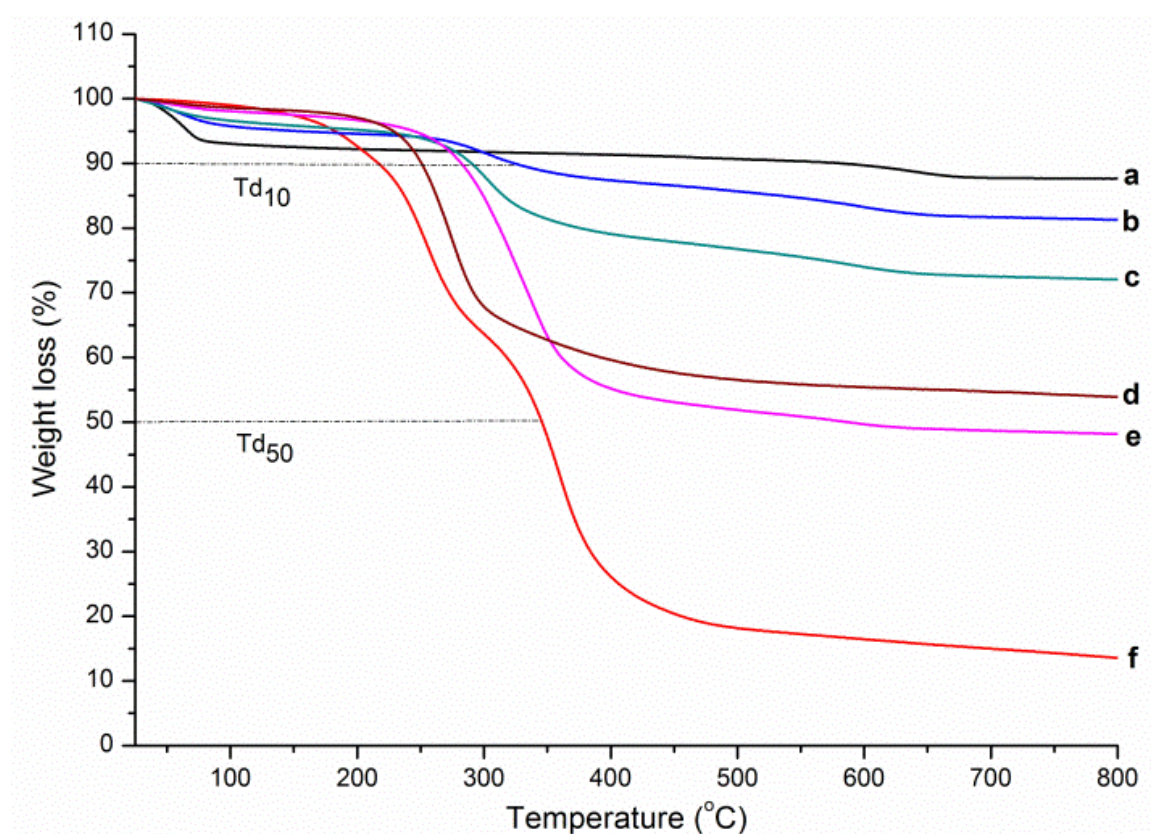


**Figure 5.18:** A comparison of thermogravimetric analysis (TGA) of the a) Na-smectite, b) **POMD** (10 wt%)/Na-smectite, c) **POMD** (20 wt%)/Na-smectite, d) **POMD-1**/Na-smectite prepared by *in-situ* method, e) **POMD** (50 wt%)/Na-smectite, and f) neat polyether, **POMD** (b,d & e prepared by solution intercalation approach, see Appendix 2 for derivative curve).

From TGA data (Table 5.6), it is clear that the decomposition onset and midpoint degradation temperatures of all intercalated complexes shifted significantly when compared with neat polymer (**POMD**). The increase in degradation onset of the *in-situ* complexes (**POMD-1/Na-smectite**), when compared with the monomer intercalated complex (**OMD/Na-smectite**), confirmed *in-situ* polymer formation. However, nanocomposites prepared by the *in-situ* approach were thermally less stable (a slight difference of 35 degrees) than those prepared by solution intercalation technique. This suggests either that fewer polymer chains might adhere to clay layers, thus losing the protective nature of surface absorption or the polymers formed might be inherently less stable when formed from the *in-situ* method. Either would cause a lower thermal stability.

In Section 5.3.1 it has been shown that the *in-situ* prepared nanocomposite was intercalate disordered, whereas the nanocomposite obtained by solution was intercalated ordered. This may also have an effect on the resulting onset temperature as well as the broadness of the decomposition event. For example, if all interlayers were uniformly spaced, then the onset of decomposition would be related to the amount of polymer and the broadness would be related to the distribution of gallery heights, which would be narrow. In the *in-situ* prepared nanocomposite, there may be multiple overlapping decomposition onsets due to the heterogeneity of the polymer formed from one interlayer to the next and this will affect the broadness. Broadness will also be impacted by the distribution of gallery heights.

However, the polymer formed by *in-situ* technique was not that different from the polymer formed in solution intercalation method so differences in the polymer formed are not likely to be the only explanation.

Whereas, nanocomposites containing the styrene functionality, such as, **PBMD-1/Na-smectite**, **PBMD/Na-smectite** and **PBBD/Na-smectite** exhibit lower thermal stabilities when compared with their neat polymer **PBMD** and **PBBD**, respectively.

**Table 5.6:** Information of thermal degradation of Na-smectite, neat polymers and nanocomposites obtained by thermogravimetric analysis

Sample	Mass Loss <sup>a</sup>			$Td_{10}$ <sup>b</sup> (°C)	$Td_{50}$ <sup>c</sup> (°C)
	$T_{initial}$ (°C)	$T_{final}$ (°C)	Loss (%)		
Na-smectite	25.0 555	95.0 703	6.90 2.50	-	-
<b>OMD/Na-smectite</b> <sup>d</sup>	65.0	500	39.7	229	-
<b>POMD</b> <sup>d</sup>	135	534	81.0	216	346
<b>POMD-1/Na-smectite</b> <sup>d</sup>	189	590	42.0	250	-
<b>POMD-B</b> <sup>d</sup>	184	477	21.6	265	353
<b>POMD-A</b> <sup>d</sup>	134	527	85.0	201	357
<b>POMD (10, 20 &amp; 50 wt%)/Na-smectite</b> <sup>d</sup>	214	689	12.7	320	-
	211	682	22.3	290	-
	224	675	47.2	282	565
<b>BMD/Na-smectite</b>	141	385	47.3	236	-
<b>PBMD</b>	228	555	83.0	291	391
<b>PBMD-1/Na-smectite</b>	185	537	34.5	257	-
<b>PBMD-A</b>	183	630	19.9	281	-
<b>PBMD-B</b>	179	645	79.0	297	396
<b>PBMD (10, 20 &amp; 50 wt%)/Na-smectite</b>	194	471	7.30	352	-
	198	481	13.4	282	-
	177	630	51.9	257	-
<b>BBD</b>	227	524	88.4	299	392
<b>PBBD (10, 20 &amp; 50 wt%)/Na-smectite</b>	197	651	13.6	306	-
	201	617	30.5	279	-
	200	615	48.0	265	-

<sup>a</sup>Mean value is presented, n=2 except where specified, experimental errors fall between 0-2. <sup>b</sup>10% Degradation temperature. <sup>c</sup>Temperature at which 50% decomposition occurred. <sup>d</sup>n= 3.

Extracted polymers (**POMD-B** & **PBMD-B**) from *in-situ* nanocomposites showed a similar degradation pattern to their neat polymers. The degradation pattern of **POMD-B** along with its neat polymer, **POMD**, is presented in Figure 5.19. **POMD-A** showed the presence of water as well as the retention of polymeric content even on washing with acetone (the **POMD-1/Na-smectite** prepared by *in-situ* polymerization) when compared with **POMD-1/Na-smectite**.

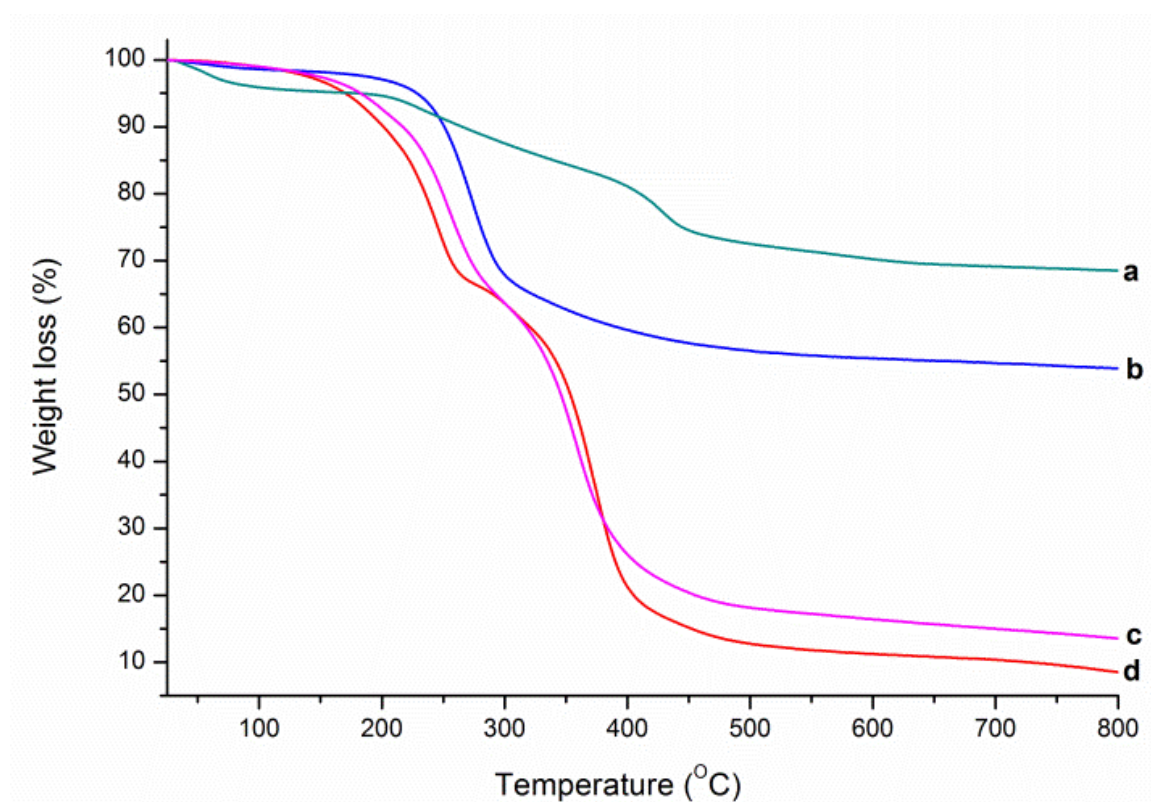


**Figure 5.19:** Thermogravimetric analysis (TGA) curves of the a) **POMD-B**, b) **POMD-1/Na-smectite** prepared by *in-situ* polymerization, c) **POMD** (neat polymer), d) **POMD-A** (acetone extracted polymer).

## 5.4 Conclusions

Clay *in-situ* polymerization resulted in the formation of a polymer, **POMD-1** inside smectite galleries which was similar to the pure **POMD**. The synthesis of polyether nanocomposites via solution intercalation and *in-situ* ring opening polymerization resulted in intercalated and intercalated-disordered nanocomposites, respectively. Polystyrene cyclic carbonate nanocomposites obtained via an *in-situ* polymerization and a solution intercalation approach were intercalated-disordered and partially intercalated-disordered on the basis of XRD studies. The different morphologies of the nanocomposites resulted in significant changes in thermal properties compared with the pure polymer. The nanocomposites exhibited lower  $T_g$  when compared to the neat polymers as determined by DSC. The TGA results confirmed the quantitative anchoring of polymer within Na-smectite by solution intercalation as well as by the clay *in-situ* polymerization method. The onset decomposition temperature ( $T_{d10}$ ) for the polyether nanocomposites measured by TGA increased to 250 °C and 282 °C for nanocomposites via solution and *in-situ* polymerization, respectively. However, for polystyrene cyclic carbonate nanocomposites,  $T_{d10}$  decreased to 257 °C and 265 °C. In addition, the *in-situ* polymer formed was separated and found to be similar to that of pure polymer on the basis of characterization data. The polyether nanocomposite was more stable than its monomer/smectite complex upon treatment with saline solution, where leaching of the monomer from the clay was observed.

## 5.5 References

- ABDALLA, M. O., DEAN, D. & CAMPBELL, S. 2002. Viscoelastic and mechanical properties of thermoset PMR-type polyimide–clay nanocomposites. *Polymer*, 43, 5887-5893.
- ALEXANDRE, M. & DUBOIS, P. 2000. Polymer-layered silicate nanocomposites: preparation, properties and uses of a new class of materials. *Materials Science and Engineering: R: Reports*, 28, 1-63.
- BERGAYA, F. & KOOLI, F. 1991. Acrylonitrile-smectite complexes. *Clay Minerals*, 26, 33-41.
- CHEN, B., EVANS, J. R. G., GREENWELL, H. C., BOULET, P., COVENEY, P. V., BOWDEN, A. A. & WHITING, A. 2008. A critical appraisal of polymer-clay nanocomposites. *Chem. Soc. Rev.*, 37, 568-594.
- FUKUSHIMA, Y., OKADA, A., KAWASUMI, M., KURAUCHI, T. & KAMIGAITO, O. 1988. Swelling behaviour of montmorillonite by poly-6-amide. *Clay Minerals*, 23, 27-34.
- GIANNELIS, E. P. 1996. Polymer Layered Silicate Nanocomposites. *Advanced Materials*, 8, 29-35.
- KELLY, P., AKELAH, A., OUTUBUDDIN, S. & MOET, A. 1994. Reduction of residual stress in montmorillonite/epoxy compounds. *J. Mater. Sci.*, 29, 2274-80.
- LAN, T., KAVIRATNA, P. D. & PINNAVAIA, T. J. 1995. Mechanism of Clay Tactoid Exfoliation in Epoxy-Clay Nanocomposites. *Chem. Mater.*, 7, 2144-50.
- LAN, T. & PINNAVAIA, T. J. 1994. Clay-Reinforced Epoxy Nanocomposites. *Chem. Mater.*, 6, 2216-19.
- LEBARON, P. C., WANG, Z. & PINNAVAIA, T. J. 1999. Polymer-layered silicate nanocomposites: an overview. *Appl. Clay Sci.*, 15, 11-29.

- MAJI, P., GUCHHAIT, P. & BHOWMICK, A. 2009. Effect of nanoclays on physico-mechanical properties and adhesion of polyester-based polyurethane nanocomposites: structure–property correlations. *Journal of Materials Science*, 44, 5861-5871.
- NAZARENKO, S., MENEGHETTI, P., JULMON, P., OLSON, B. G. & QUTUBUDDIN, S. 2007. Gas barrier of polystyrene montmorillonite clay nanocomposites: Effect of mineral layer aggregation. *Journal of Polymer Science Part B: Polymer Physics*, 45, 1733-1753.
- OKAMOTO, M. 2006. Recent advances in polymer/layered silicate nanocomposites: an overview from science to technology. *Material Science and Technology*, 22, 756-779.
- SINHA RAY, S. & OKAMOTO, M. 2003. Polymer/layered silicate nanocomposites: a review from preparation to processing. *Progress in Polymer Science*, 28, 1539-1641.
- SUGAHARA, Y., SATOKAWA, S., KURODA, K. & KATO, C. 1988. Evidence for the formation of interlayer polyacrylonitrile in kaolinite. *Clays and Clay Minerals*, 36, 343-348.
- TARAPOW, J. A., BERNAL, C. R. & ALVAREZ, V. A. 2009. Mechanical properties of polypropylene/clay nanocomposites: Effect of clay content, polymer/clay compatibility, and processing conditions. *Journal of Applied Polymer Science*, 111, 768-778.
- TJONG, S. C. 2006. Chapter 10 - Synthesis and Structure-Property Characteristics of Clay-Polymer Nanocomposites. *In: TJONG, S. C. (ed.) Nanocrystalline Materials*. Oxford: Elsevier Science Ltd.

## Chapter 6 Experimental

### 6.1 Materials and methods

#### 6.1.1 Gas chromatography (GLC)

Gas chromatography (GLC) was performed on an Agilent 6850 Series II Network GC System, equipped with an FID detector and an HP-1 column (30 m × 0.32 mm ID). Helium was used as a carrier gas at a flow-rate of 2.0 mL/min, and a temperature program of 40–250 °C at 10 °C/min was employed. Multiple point calibration curves were developed to determine detector response factors for all of the starting materials and reaction products.

#### 6.1.2 Gas chromatography-mass spectrometry (GC-MS)

Gas chromatography-mass spectrometry was used to confirm the identity of products employing a ThermoQuest TRACE DSQ GC-MS using an SGE BP5 column (30 m × 0.22 mm ID) and an Electron Impact (EI) detector with ionization energy of 70 eV. Helium was used as carrier gas at a flow-rate of 0.8 mL/min. The temperature program used involved: 50 °C for 2 min and then increased the temperature at a rate of 20 °C/min to 250 °C, after which the temperature was held for 16 min.

#### 6.1.3 Electrospray ionization mass spectrometry (ESI-MS)

Electrospray ionization mass spectrometry (ESI-MS) was performed on an Agilent 6220 series Time of Flight Liquid chromatography mass spectrometry (LC/MS) (TOF) system with Agilent 1200 Series HPLC.

#### **6.1.4 Infrared spectroscopy (IR)**

Infrared spectra (IR) were obtained using an ATR-Perkin Elmer Spectrum RX1 series Fourier Transform infrared spectrometer with samples presented as a liquid film or ground powder. An infrared background is collected, from the clean ATR (diamond) crystal. The sample is placed on to the small crystal area and transmittance measured. The spectrum was processed for base line correction. Eighty co-added IR spectral scans were recorded in the mid-IR region ( $400\text{-}4000\text{ cm}^{-1}$ ) at a resolution of  $2\text{ cm}^{-1}$ .

#### **6.1.5 Nuclear magnetic resonance (NMR) spectroscopy**

Nuclear Magnetic Resonance ( $^1\text{H}$  and  $^{13}\text{C}$ -NMR) spectra were recorded using either a Bruker DRK-400 or DRK-300 operating at 400 and 300 MHz (100 and 75 MHz for carbon) respectively, on samples dissolved in deuterated acetone, chloroform, methanol and dimethyl sulfoxide with tetramethylsilane (TMS) as the internal standard. Chemical shifts ( $\delta$ ) were measured in parts per million (ppm) relative to TMS. Each resonance was assigned according to the following convention: chemical shift; multiplicity; number of protons and assignment. Multiplicity was denoted as singlet (s), broad singlet (br s), doublet (d), doublet of doublets (dd), triplet (t), quartet (q) or multiplet (m). Integrated area of specific resonance signal is used to determine conversion.

#### **6.1.6 Powder X-ray diffraction (XRD)**

Powder X-ray diffraction (XRD) spectra were acquired on a Philips PW1140 diffractometer having a computerized stepper motor control. Scans were conducted from  $2\text{-}22^\circ 2\theta$  at  $4^\circ\text{ min}^{-1}$  at steps of  $0.02^\circ$  using a Cu  $K\alpha$  source ( $\lambda = 1.54\text{ nm}$ ). A  $1^\circ$  divergence slit,  $1^\circ$  receiving slit and  $0.2^\circ$  scatter aperture were used. Samples were prepared either as oriented films on ceramic tile or as front loaded packed powders in

aluminium sample holders. In order to determine the  $d(001)$  lattice spacing ( $d$ -values), the degree  $2\theta$  for the centre of gravity of the 001 reflection was determined instead of maximum height of reflection. The  $d$ -space values of the 001 reflection ( $d(001)$ ), which corresponded to the distance between adjacent mineral layers, were estimated by using the Bragg equation ( $d = \lambda/2\sin\theta$ ).

The disordered stacking or alignment of clay platelets resulted in broadening of 001 reflection. The amount of broadening can be determined from the full width at half maximum (FWHM) of the reflections. FWHM is expressed by Scherrer equation,

$$L = \frac{K\lambda}{\beta\cos\theta}$$

Where, FWHM =  $L$  = Mean size of the ordered (crystalline) domains;  $K = 1$ ;  $\lambda$  = wavelength of the X-ray source (Cu K 0.154 nm);  $\beta$  = the line broadening at half the maximum intensity (FWHM), after subtracting the instrumental line broadening, in radians (also sometimes denoted as  $\Delta$  ( $^{\circ}2\theta$ )); and  $\theta$  = Bragg's angle.

### **6.1.7 Gel permeation chromatography (GPC)**

The molecular weight of synthesized polymers were determined by gel permeation chromatography (GPC) using GPC system Tosoh EcoSec HLC-8320GPC equipped with both refractive index (RI) and ultraviolet UV detectors (UV detection at 280 nm) using Tosoh alpha 2000 and 4000 columns. Calibration curves were obtained by using polystyrene standards ranging between  $M_n$  500-2.89 x 10<sup>6</sup> gmol<sup>-1</sup>. DMF (with 10 mM LiBr) was used as the mobile phase with a flow rate of 1.0 mL/min. The polymers were dissolved in DMF (2 mg/mL) and the solution was filtered to remove any insoluble solid

prior to analysis. The molecular mass was calculated using the software Eco data analysis (ver. 1.03).

### **6.1.8 Differential scanning calorimetry (DSC)**

Differential scanning calorimetry (DSC) was performed on A TA-Q100 DSC to determine the glass transition temperature of polymers and the polymer nanocomposites. The module was calibrated using indium/zinc method (an indium and zinc sample is used to quantify enthalpy and melt temperature and results entered into the calibration file). The samples were oven dried at 40 °C overnight prior to measurement and were accurately weighed (3 mg) into aluminium pans. The sample was heated from -40 °C to 110 °C at a rate of 10 °C/min in the first cycle to remove any traces of water present and then cooled back to -10 °C. In the second cycle, the sample was heated to the 180, 190 or 200 °C as indicated, while collecting calorimetric data. Glass-transition temperature ( $T_g$ ) values were determined using the software 'TA Universal Analysis' from temperature versus heat flow plots.

### **6.1.9 Thermogravimetric analysis (TGA)**

Thermogravimetric analysis (TGA) was performed on samples (Na-smectite, monomer/Na-smectite, polymer/Na-smectite) using a Mettler Toledo TGA/DSC instrument under air atmosphere at heating rate of 5 °C/min between 25-800° C. Samples (1-5 mg) were accurately weighed into alumina pans (70 µL) with a lid. StarE software was used to measure the changes in mass of materials as a function of temperature.

### **6.1.10 Elemental Analysis**

Determination of C, H and N of the nanocomposites was done using a Perkin Elmer 2400 Series II CHNS Elemental Analyzer by Perkin Elmer. Sample (2-3 mg) was weighed into a tin capsule and triplicate measurements were performed. EA 2400 Data Manager (SQL-based software package) was used to collect and store the data retrieved from Perkin Elmer 2400 Series II CHNS Elemental Analyzer.

### **6.1.11 Microwave irradiation reactor and ultrasonic bath**

Microwave irradiation was carried out in CEM Focused Microwave™ Synthesis System, Discover; employing maximum power of 300 watts with 2455 MHz frequency. An Elmasonic S100 ultrasound bath ( $P = 150 \text{ W}$ ,  $f = 37 \text{ kHz}$ ) was used for sonication and dispersion of samples in various solvents.

### **6.1.12 Photochemical reactions**

A 450 Watt photochemical ACE-Hanovia 7883-14 reflector type mount UV-lamp, which is capable of irradiating broad UV wavelengths, a 7883-02 reflector (reflects 85% of spectral rays) and a 450 watt 7830-61 power supply (230V, 50 Hz) were purchased from Ace Glass Incorporated (Vineland, NJ, USA) and used for photopolymerization reactions. The sample tube was placed at a distance of 12 cm from the lamp at room temperature.

### **6.1.13 Molecular dimensions measurements**

Molecular models of cyclic carbonate were drawn using the GAMESS program after minimizing the energy using Chem3D software. The molecular dimensions of cyclic carbonates were calculated using the GAMESS program.

#### **6.1.14 Melting point determination**

Melting points were determined using a Buchi B-545 melting point apparatus with a digital thermometer.

#### **6.1.15 Reagents and Solvents**

All reagents and materials were purchased from Sigma-Aldrich (Castle Hill, NSW, Australia) in the laboratory reagent grade. Solvents were purchased from Merck (Kilsyth, VIC, Australia) and used as received. Commercial samples of zinc monoglycerolate (ZMG) and nanoparticulate ZnO were obtained from Micronisers Pty Ltd (Dandenong, VIC, Australia). Na-bentonite was supplied from the Ebenezer coal mine, Bentonite Products, Ipswich, Queensland. The cation exchange capacity (CEC) of the Na-smectite is reported to be 105 meq/100 g clay (data provided by Dr. W.P. Gates, Monash University).

#### **6.1.16 Thin Layer Chromatography (TLC)**

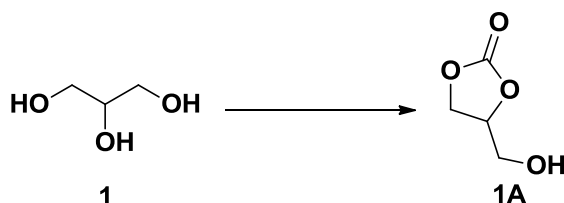
Thin layer chromatography was carried out using silica gel 60 as a stationary phase using chloroform, EA, hexane and toluene as eluents. Visualization of compounds was undertaken by using *p*-anisaldehyde stain or under a UV lamp at 254 nm and/or 365 nm wavelengths.

#### **6.1.17 Silver nitrate test**

A silver nitrate ( $\text{AgNO}_3$ ) test was used to determine the presence of chloride ions in washing supernatants after treatment of the clay samples. A few drops of 0.1 M aqueous solution of silver nitrate was used to test for the presence of  $\text{Cl}^-$ . If halide ions were present, the insoluble precipitate  $\text{AgCl}$  was formed and could be visually detected.

## 6.2 Experimental for Chapter 2- Production of glycerol carbonate and other cyclic carbonates

### 6.2.1 Reaction of glycerol with dimethyl carbonate (Rokicki et al., 2005)



Glycerol (10.00 g, 0.108 mol), dimethyl carbonate (29.40 mL, 0.326 mol) and potassium carbonate (0.45 g, 3.240 mmol) were added to a one-neck round bottom flask fitted with a condenser. The reaction was carried out at 77 °C for 3h and monitored by FTIR. After 3h, methanol and dimethyl carbonate were evaporated and potassium carbonate was precipitated by adding acetone. The solution was filtered and the filtrate concentrated. The product, glycerol carbonate (96% yield, 9.60 g) was analysed by gas chromatography. <sup>1</sup>H-NMR (400 MHz, CDCl<sub>3</sub>): δ<sub>H</sub> 5.27 (br s, 1H, OH), 4.82-4.77 (m, 1H, CHCH<sub>2</sub>), 4.49 (t, 1H, J= 8.4 Hz, CH<sub>2</sub>OC), 4.28 (dd, 1H, J= 8.4 Hz, 6 Hz, CH<sub>2</sub>OC), 3.66 (dd, 1H, J= 12.6, 2.8 Hz, CH<sub>2</sub>OH), 3.51 (dd, 1H, J= 12.6, 3.6 Hz, CH<sub>2</sub>OH). FTIR (neat): ν/cm<sup>-1</sup> 3418(O-H<sub>str</sub>), 2930, 1780(C=O<sub>str</sub> cyclic), 1402, 1179, 1054 (consistent with reported data). GC-MS: m/z 118(M-1, 3), 87.1(M-CH<sub>2</sub>OH, 75), 71(5), 61(7), 55(10).

### 6.2.2 Reaction of glycerol with urea using ZnO (Climent et al., 2010)

Glycerol (10.00 g, 0.108 mol) was added to a 250 mL round bottom flask. 5 wt% of ZnO (0.50 g) with respect to glycerol and urea (6.53 g, 0.108 mol) were then added and the reaction mixture heated to 150 °C. The reaction flask was connected to a HCl trap and the reaction allowed to run for 6h. The catalyst was precipitated by adding methanol

and the filtrate concentrated. The yield (37%) of glycerol carbonate was determined by GLC and the product was not isolated.

### **6.2.3 Reaction of glycerol with urea using ZnSO<sub>4</sub> (Yoo and Mouloungui, 2003)**

Glycerol (1.00 g, 0.0108 mol) and urea (0.97 g, 0.0108 mol) were heated using 5 wt% ZnSO<sub>4</sub> as a catalyst at 140 °C for 6h in a round bottom flask fitted with a condenser and HCl trap. Acetone was added to separate the catalyst and GLC was performed on the final product (36% yield). Product was not further purified.

### **6.2.4 Reaction of glycerol with urea using ZMG in *iso*-propanol**

Urea (1.00 g, 0.017 mol), glycerol (3.00 g, 0.017 mol) and 5 wt% ZMG (0.15 g) with respect to glycerol were added to a round bottom flask along with 5 mL of *iso*-propanol. The mixture was heated at 170 °C for 4h. The solution was filtered to separate the solid catalyst and the solvent evaporated. GC (30% yield) was analysed by gas chromatography and purified by distillation using a Kugelrohr apparatus.

### **6.2.5 Reaction of glycerol and urea using ZMG**

All the reactions were performed in a 100 mL round bottom flask fitted with a condenser. In a typical experiment, glycerol (10.0 g, 0.108 mol) was combined with urea (6.5 g, 0.108 mol) and ZMG. The amount of catalyst used was always 5% by weight with respect to glycerol. The reaction was stirred at a constant rate of 630 rpm and heated in an oil bath at the desired temperature (see below). Reactions were conducted under reduced pressure (40 mbar) and in the absence of solvent. After the reaction, methanol was added and the catalyst was removed by filtration. The catalyst was washed with acetone to remove any adsorbed products. The filtrate was concentrated under reduced

pressure and the products identified by GC-MS. The reaction was monitored by gas chromatography (GLC) and the final yield also determined by GLC.

#### **Reaction of glycerol and urea at different temperatures (Table 2.2)**

The reaction mixture containing glycerol, urea and zinc monoglycerolate were heated at 100, 110, 120, 130, 140 and 150 °C under constant stirring of 630 rpm for 7h, while the ammonia liberated during the reaction was removed in vacuo. At the end of each reaction, the mixture was cooled to room temperature, the catalyst was separated and yield was determined as above.

#### **Uncatalysed and catalysed reactions (Table 2.3)**

Using the same method as reported in Section 6.2.5, the reaction of glycerol and urea were performed with or without catalyst at 150 °C for 3, 4, 5, 6 and 7h. At the end of each time interval, an aliquot of the reaction mixture was taken, methanol added, centrifuged and analysed by gas chromatography.

#### **Reaction of glycerol and urea at different molar ratios (Table 2.4)**

The reaction of glycerol and urea was performed in a molar ratio (1:1.5; glycerol: urea) at 150 °C for 3, 4, 5, 6 and 7h. At the end of each time interval, an aliquot was analysed by GLC.

#### **ZMG re-cycling experiment (Table 2.5)**

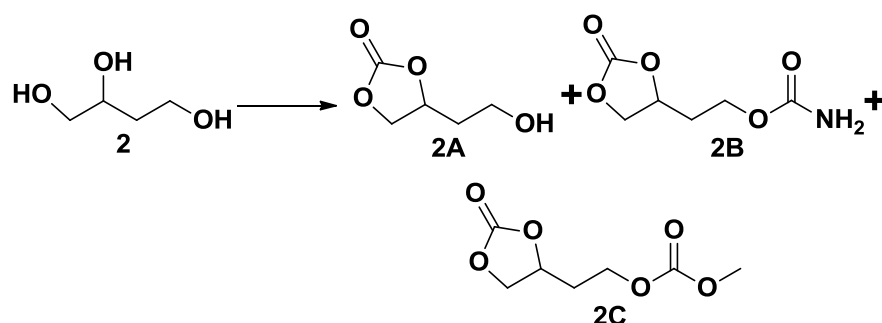
Glycerol (10.0 g, 0.110 mol), urea (6.5 g, 0.110 mol) and ZMG (5 wt%, 0.5 g) were heated at 140 °C/40 mbar. Reaction aliquots were sampled at t = 3, 4, 5 and 6h and analysed by gas chromatography. The final mixture was taken-up in 45 mL methanol and the solid filtered and dried in a vacuum oven (at 60 °C). The identity of this solid was confirmed by IR to be ZMG (0.45 g, 90% recovery). This was used as 5 wt% to glycerol (9.0 g, 0.098

mol) with urea (5.9 g, 0.098 mol) at 140 °C/40 mbar and monitored at similar time intervals as above. The workup to recover ZMG (0.38 g, 84% recovery) was as above.

### 6.2.6 Reaction of glycerol and urea using ZnO (Table 2.6, Figures 2.11 and 2.12)

Glycerol (15.00 g, 0.162 mol), urea (14.70 g, 0.244 mol) and ZnO (5 wt%, 0.75 g) were heated at 140 °C/40 mbar. Reaction aliquots were sampled at a t = 1, 2, 3, 4, 5 and 6 hour by gas chromatography. After the reaction, methanol was added and the catalyst was removed by filtration. The catalyst was washed with acetone to remove any adsorbed products and dried in a vacuum oven (at 40 °C). The washed and dried solid was analysed by FTIR and XRD.

### 6.2.7 Reaction of 1, 2, 4-butanetriol (2) with urea and DMC



#### 4-(2-Hydroxyethyl)-1,3-dioxolan-2-one (2A) (Tomczyk et al., 2012)

**Urea/ZMG method:** 1,2,4-Butanetriol (2.50 g, 0.024 mol), urea (2.10 g, 0.034 mol) and ZMG 5% (0.12 g) were heated for 7h at 140 °C in a 100 mL round bottom flask at 40 mbar (reduced pressure). The reaction was monitored by GLC. After 7h, the catalyst was precipitated out by adding methanol and filtered. The crude mixture was concentrated under reduced pressure and purified by column chromatography (EA) to afford a colorless liquid. Yield = 47% (1.40 g). <sup>1</sup>H-NMR (300 MHz, CDCl<sub>3</sub>): δ<sub>H</sub> 4.98-4.88 (m, 1H,

CHCH<sub>2</sub>), 4.59 (dd, 1H, J= 8.4, 7.8 Hz, CH<sub>2</sub>OC), 4.20 (dd, 1H, J= 8.4, 7.5 Hz, CH<sub>2</sub>OC), 3.84-3.79 (m, 2H, CH<sub>2</sub>OH), 2.12 (br s, 1H, OH), 2.04-1.94 (m, 2H, CH<sub>2</sub>CH). FTIR (neat):  $\nu/\text{cm}^{-1}$  3406(O-H<sub>str</sub>), 2966(C-H<sub>str</sub>), 2925(C-H<sub>str</sub>), 1770(C=O<sub>str</sub> cyclic), 1481, 1386, 1262, 1170, 1051, 774, 717 (data was consistent with Tomczyk et al., 2012). GC-MS: m/z 131.1(M-1, 3), 114.1(M-H<sub>2</sub>O, 6), 101.1(M-CH<sub>2</sub>OH, 5), 90.1(M-CH<sub>2</sub>CO, 14), 87.1(M-C<sub>2</sub>H<sub>4</sub>OH, 2), 70.1(M-HOCO<sub>2</sub>H, 19), 59.1(87-CO, 39), 55.1(13). ESI-MS: m/z 133.1 (5%) [M+H]<sup>+</sup> and m/z 155.1 (100%) [M+Na]<sup>+</sup>.

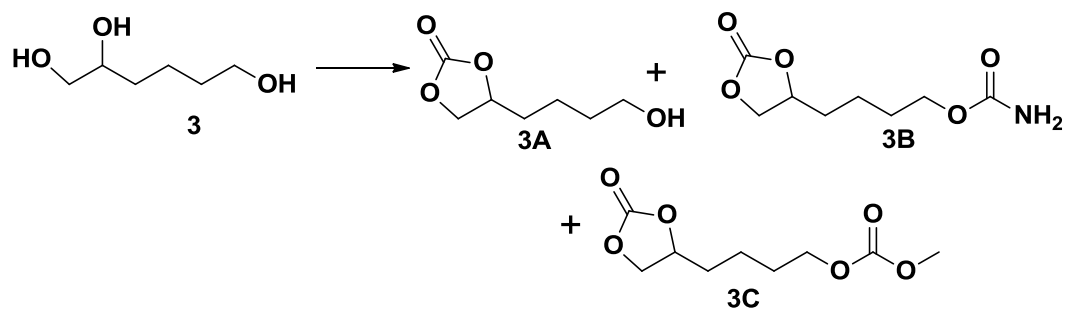
**DMC/K<sub>2</sub>CO<sub>3</sub> method** (Tomczyk et al., 2012): 1,2,4-Butanetriol (2.50 g, 0.024 mol), dimethyl carbonate (2.10 g, 0.024 mol) and potassium carbonate (0.10 g, 0.720 mmol) were mixed in a 100 mL round bottom flask and heated for 3h at 90 °C. The reaction was monitored by GLC. After 3h, the methanol formed in the reaction was removed under reduced pressure and the product was purified by column chromatography (EA). Yield = 72% (2.6 g).

**Methyl (2-(2-oxo-1,3-dioxolan-4-yl)ethyl) carbonate (2C)** (Tomczyk et al., 2012)

2.5 g of 1,2,4-butanetriol (0.024 mol) with 3 equivalents of dimethyl carbonate (6.5 g, 0.072 mol) and potassium carbonate (0.099 g, 0.72 mmol) were used. Reaction conditions and workup were similar to the method described above. Acetone was added to the concentrate to precipitate out potassium carbonate and then filtered. The pure product was obtained on evaporating the acetone. Yield = 93% (4.30 g). <sup>1</sup>H-NMR (400 MHz, CDCl<sub>3</sub>):  $\delta_{\text{H}}$  4.91-4.82 (m, 1H, CHCH<sub>2</sub>), 4.63-4.57 (m, 1H, CH<sub>2</sub>OC), 4.37-4.23 (m, 2H, OCH<sub>2</sub>CH<sub>2</sub>), 4.15 (dd, 1H, J= 9.6, 1.6 Hz, CH<sub>2</sub>OC), 3.79 (s, 3H, OCH<sub>3</sub>), 2.16-2.14 (m, CH<sub>2</sub>CH<sub>2</sub>), FTIR (neat):  $\nu/\text{cm}^{-1}$  2964(C-H<sub>str</sub>), 2925(C-H<sub>str</sub>), 1797(C=O<sub>str</sub> cyclic), 1749(C=O<sub>str</sub> linear), 1272, 1177, 1063 (data was consistent to reported literature (Tomczyk et al., 2012)).

GC-MS:  $m/z$  190(M, 0.2%), 163(8), 103(M-C<sub>3</sub>H<sub>3</sub>O<sub>3</sub>, 3), 87(M-C<sub>2</sub>H<sub>4</sub>OCOCH<sub>3</sub>, 5.8), 77(103-C<sub>2</sub>H<sub>2</sub>, 26), 70(M-CH<sub>3</sub>OCO<sub>2</sub>H & CO<sub>2</sub>, 28), 59(M-C<sub>2</sub>H<sub>4</sub>OCO<sub>2</sub>CH<sub>3</sub> & CO, 27).

### 6.2.8 Reaction of 1,2,6-hexanetriol (3)



#### 4-(4-Hydroxybutyl)-1,3-dioxolan-2-one (3A) (Tomczyk et al., 2012)

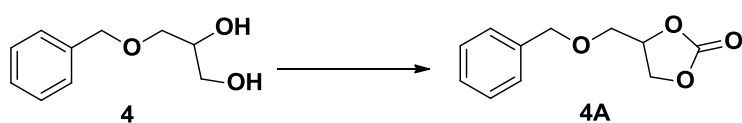
**Urea/ZMG method:** 1,2,6-Hexanetriol (1.00 g, 7.45 mmol), urea (0.67 g, 11.17 mmol) and 5 wt% ZMG (0.05 g) were heated under similar conditions to Section 6.2.7. The product was purified by column chromatography (MeOH/EA = 1/4) to afford a colorless liquid. Yield = 61% (0.75 g). <sup>1</sup>H-NMR (400 MHz, CDCl<sub>3</sub>):  $\delta_{\text{H}}$  4.74-4.69 (m, 1H, CHCH<sub>2</sub>), 4.54 (t, 1H, J = 8 Hz, CH<sub>2</sub>OC), 4.09 (dd, 1H, J = 8.4, 7.2 Hz, CH<sub>2</sub>OC), 3.68-3.67 (m, 3H, CH<sub>2</sub>OH), 1.87-1.47 (m, 6H, CH<sub>2</sub>CH<sub>2</sub>CH<sub>2</sub>). <sup>13</sup>C-NMR (100 MHz, CDCl<sub>3</sub>):  $\delta_{\text{C}}$  155.3 (C=O), 76.9 (CH), 69.3 (CH<sub>2</sub>OC), 62.3 (CH<sub>2</sub>OH), 33.8 (CH<sub>2</sub>CH), 32.7 (CH<sub>2</sub>OH) and 21.6 (CH<sub>2</sub>CH<sub>2</sub>). FTIR (neat):  $\nu/\text{cm}^{-1}$  3395(O-H<sub>str</sub>), 1785(C=O<sub>str</sub> cyclic), 1450, 1392, 1268, 1169, 1055, 776, 714. GC-MS:  $m/z$  (3A) 160.1(M, 1), 142.1(M-H<sub>2</sub>O, 6), 130.1(M-CH<sub>2</sub>O, 4), 98.1(142-C<sub>3</sub>H<sub>8</sub>, 8), 80.1(142-HOCO<sub>2</sub>H, 41), 67.1(10), 57.1(M-C<sub>3</sub>H<sub>6</sub>OH & CO<sub>2</sub>, 22); (3B) 202.4(M, 0.3), 116.1(M-C<sub>3</sub>H<sub>2</sub>O<sub>3</sub>, 2), 87(M-(CH<sub>2</sub>)<sub>4</sub>-OCONH<sub>2</sub>, 41), 71.1(M-C<sub>2</sub>H<sub>4</sub>OCONH<sub>2</sub>, 17), 55.1(116-HOCONH<sub>2</sub>, 40). ESI-MS:  $m/z$  160.9 (100%) [M+H]<sup>+</sup> and  $m/z$  182.7 (18%) [M+Na]<sup>+</sup>. Analysis of the isolated product was consistent with Tomczyk et al., 2012.

**DMC/K<sub>2</sub>CO<sub>3</sub> method** (Tomczyk et al., 2012): 1,2,6-Hexanetriol (1.00 g, 7.40 mmol), dimethyl carbonate (0.65 g, 7.30 mmol) and potassium carbonate (0.03 g, 0.22 mmol) were used as in 6.2.7. The product was purified by column chromatography (MeOH/EA = 1/4). Yield = 72% (0.87 g).

**Methyl (4-(2-oxo-1,3-dioxolan-4-yl)butyl) carbonate (3C)** (Tomczyk et al., 2012)

1,2,6-Hexanetriol (1.00 g, 7.50 mmol), dimethyl carbonate (2.00 g, 22.4 mmol) and potassium carbonate (0.03 g, 0.22 mmol) were reacted as in 6.2.7. Yield = 91% (1.50 g). <sup>1</sup>H-NMR (400 MHz, CDCl<sub>3</sub>): δ<sub>H</sub> 4.74-4.67 (m, 1H, CHCH<sub>2</sub>), 4.53 (t, 1H, J= 7.2 Hz, CH<sub>2</sub>OC), 4.15 (t, 2H, J= 6 Hz, CH<sub>2</sub>OH), 4.07 (dd, 1H, J= 8.4, 7.2 Hz, CH<sub>2</sub>OC), 3.78 (s, 3H, OCH<sub>3</sub>), 1.88-1.41 (m, 6H, CH<sub>2</sub>CH<sub>2</sub>CH<sub>2</sub>). <sup>13</sup>C-NMR (100 MHz, CDCl<sub>3</sub>): δ<sub>c</sub> 155.7 (C=O, cyclic), 154.8 (C=O, acyclic), 76.7 (OCH), 69.2 (OCH<sub>2</sub>), 67.3 (OCH<sub>2</sub>CH), 54.7 (OCH<sub>3</sub>), 33.5 (OCHCH<sub>2</sub>), 28.2 (CH<sub>2</sub>CH<sub>2</sub>O) and 21.0 (CH<sub>2</sub>CH<sub>2</sub>CH<sub>2</sub>O). FTIR (neat): ν/cm<sup>-1</sup> 2957(C-H<sub>str</sub>), 1788(C=O<sub>str</sub> cyclic), 1740(C=O<sub>str</sub> linear), 1442, 1388, 1166, 1059, 941, 792, 774, 716. GC-MS: m/z 218(M, 1), 116(M-C<sub>2</sub>H<sub>2</sub>OCO<sub>2</sub>CH<sub>3</sub>, 7), 87(M-C<sub>2</sub>H<sub>4</sub>OCOCH<sub>3</sub>, 42), 71(M-C<sub>2</sub>H<sub>6</sub>OCO<sub>2</sub>CH<sub>3</sub> & CH<sub>2</sub>O, 15), 55(35) (data was consistent with Tomczyk et al., 2012).

**6.2.9 4-((Benzyloxy)methyl)-1,3-dioxolan-2-one (4A)** (Whiteoak et al., 2012)

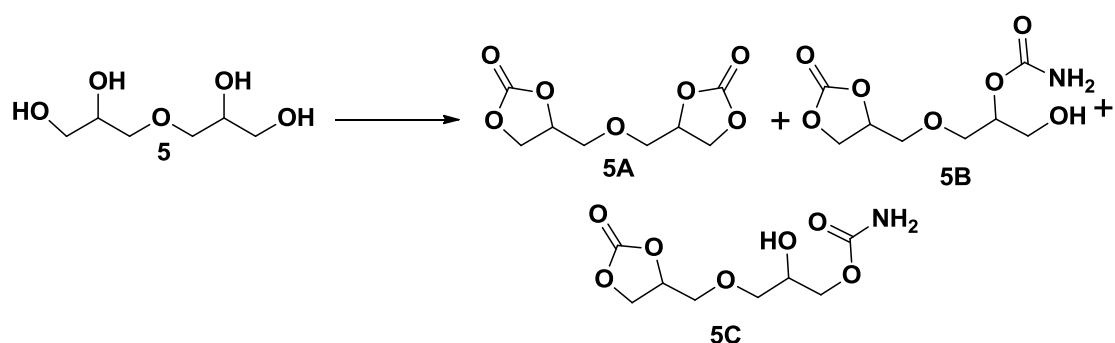


**Urea/ZMG method:** 3-(Benzyloxy)propane-1,2-diol (2.00 g, 0.011 mol), urea (0.99 g, 0.016 mol) and 5 wt% ZMG (0.10 g) were combined and reacted at 140 °C/40 mbar for 7h. Catalyst was separated by adding methanol, filtered and the filtrate was concentrated to afford colorless oil. Yield = 71% (1.60 g). <sup>1</sup>H-NMR (400 MHz, CDCl<sub>3</sub>): δ<sub>H</sub> 7.40-7.30 (m, 5H, C<sub>6</sub>H<sub>5</sub>), 4.85-4.79 (m, 1H, CH), 4.68-4.56 (m, 2H, CH<sub>2</sub>OPh), 4.49 (t, 1H, J=

8.4 Hz, OCH<sub>2</sub>CH), 4.40 (dd, 1H, J= 8.4, 6 Hz, OCH<sub>2</sub>CH), 3.72 (dd, 1H, J= 10.8, 4.0 Hz, OCHCH<sub>2</sub>), 3.63 (dd, 1H, J= 11.2, 3.6 Hz, OCHCH<sub>2</sub>). FTIR (neat):  $\nu/\text{cm}^{-1}$  3032(C-H<sub>str</sub>), 1792(C=O<sub>str</sub> cyclic), 1637, 1496, 1453, 1395, 1275, 1174, 1105, 1088, 776, 742, 700 (the data obtained was consistent to Whiteoak et al., 2012).

**DMC/K<sub>2</sub>CO<sub>3</sub> method:** 3-(benzyloxy)propane-1,2-diol (0.480 g, 2.63 mmol), dimethyl carbonate (0.710 g, 7.9 mmol) and potassium carbonate (0.011 g, 0.79 mmol) were heated at 90 °C for 3h. Methanol and excess dimethyl carbonate were evaporated to obtain pure product. Yield = 92% (0.500 g).

**6.2.10 4'-(Oxybis(methylene))bis(1,3-dioxolan-2-one) (5A)** (Rokicki and Kuran, 1984)



**From urea/ZMG:** Diglycerol (5.00 g, 0.03 mol), urea (5.40 g, 0.09) and ZMG (0.25 g) were used as previously. Addition of ice to the viscous mixture resulted in the precipitation of 4'-(oxybis(methylene))bis(1,3-dioxolan-2-one) (**5A**) as a white solid which was purified by re-crystallization in chloroform. Aqueous fraction was concentrated and the side products (**5B** and **5C**) were analysed by GC-MS. <sup>1</sup>H-NMR (400 MHz, CDCl<sub>3</sub>):  $\delta_{\text{H}}$  4.87-4.81 (m, 2H, 2CH), 4.52 (t, 2H, J= 8.4 Hz, 2OCH<sub>2</sub>CH), 4.40 (dd, 2H, J= 8.4, 5.6 Hz, 2OCH<sub>2</sub>CH), 3.86 (dd, 2H, J= 11.2, 3.2 Hz, 2OCHCH<sub>2</sub>), 3.79 (dd, 2H, J= 11.2, 2.9 Hz, 2OCHCH<sub>2</sub>). <sup>13</sup>C-NMR (100 MHz, CDCl<sub>3</sub>):  $\delta_{\text{C}}$  154.7 (C=O), 74.7 (CH), 70.9 (OCH<sub>2</sub>CH) and 65.9 (OCHCH<sub>2</sub>).

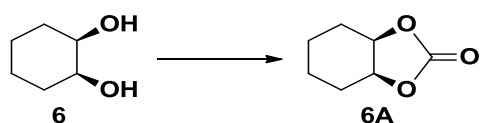
FTIR (neat):  $\nu/\text{cm}^{-1}$  2924(C-H<sub>str</sub>), 2879(C-H<sub>str</sub>), 1780(C=O<sub>str</sub> cyclic), 1478, 1396, 1274, 1170, 1045, 852, 712. GC-MS: m/z **(5A)** 218(M, 0.4), 129.9(M-2CO<sub>2</sub>, 3), 117.1(M-CH<sub>2</sub>C<sub>3</sub>H<sub>3</sub>O<sub>3</sub>, 22), 105(5), 87.1(M-CH<sub>2</sub>OCH<sub>2</sub>C<sub>3</sub>H<sub>3</sub>O<sub>3</sub>, 5), 73(129.9-CHO & C<sub>2</sub>H<sub>4</sub>, 8.4), 57.1(87-CO<sub>2</sub>, 57); **(5B)** 235(M, 0.4), 217(M-H<sub>2</sub>O, 1), 205.1(M-CH<sub>2</sub>O, 1), 132.1(2.5), 117.1(M-CH<sub>2</sub>CH(OCONH<sub>2</sub>)CH<sub>2</sub>OH, 8), 87.1(117-CH<sub>2</sub>O, 15), 70.1(9), 57.1(87-CO<sub>2</sub>, 63); **(5C)** 235(M, 0.3), 219(M-NH<sub>2</sub>, 0.5), 191(M-CONH<sub>2</sub>, 2), 161.1(M-CH<sub>2</sub>OCONH<sub>2</sub>, 1), 132.1(5), 117.1(M-CH<sub>2</sub>CH(OH)CH<sub>2</sub>OCONH<sub>2</sub>, 9), 93.1(11), 87.1(M-CH<sub>2</sub>OCH<sub>2</sub>C<sub>3</sub>H<sub>3</sub>O<sub>3</sub>, 3), 70.1(18), 57.1(87-CO<sub>2</sub>, 52).

**From DMC/K<sub>2</sub>CO<sub>3</sub>:** Diglycerol (5.0 g, 0.03 mol), dimethyl carbonate (15.6 g, 0.17 mol) and potassium carbonate (0.01 g, 0.90 mmol) were reacted and isolated as above. Yield = 88% (5.90 g).

### **2-Hydroxy-3-((2-oxo-1,3-dioxolan-4-yl)methoxy)propyl carbamate (5C)**

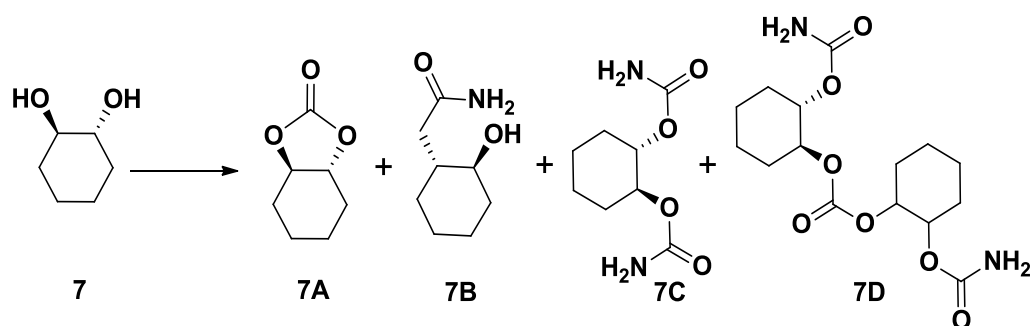
Diglycerol (2.00 g, 0.012 mol), urea (0.72 g, 0.012 mol) and ZMG (0.10 g) were combined and reacted as above, then ice was added to precipitate out **5A**. Once filtered, the filtrate was concentrated to afford **5C**. Yield = 39% (1.10 g). FTIR (neat):  $\nu/\text{cm}^{-1}$  3356(O-H<sub>str</sub>), 2924(C-H<sub>str</sub>), 2877(C-H<sub>str</sub>), 1778(C=O<sub>str</sub> cyclic), 1647(C=O<sub>str</sub> linear), 1473, 1398, 1175, 1039, 857, 771, 712. GC-MS: **5C** 235(M, 0.3), 219(M-NH<sub>2</sub>, 0.5), 191(M-CONH<sub>2</sub>, 2), 161.1(M-CH<sub>2</sub>OCONH<sub>2</sub>, 1), 132.1(5), 117.1(M-CH<sub>2</sub>CH(OH)CH<sub>2</sub>OCONH<sub>2</sub>, 9)<sup>+</sup>, 93.1(11), 87.1(M-CH<sub>2</sub>OCH<sub>2</sub>C<sub>3</sub>H<sub>3</sub>O<sub>3</sub>, 3), 70.1(18), 57.1(87-CO<sub>2</sub>, 52); **(5B)** 235(M, 0.4), 217(M-H<sub>2</sub>O, 1), 205.1(M-CH<sub>2</sub>O, 1), 132.1(2.5), 117.1(M-CH<sub>2</sub>CH(OCONH<sub>2</sub>)CH<sub>2</sub>OH, 8), 87.1(117-CH<sub>2</sub>O, 15), 70.1(9), 57.1(87-CO<sub>2</sub>, 63).

### 6.2.11 Hexahydrobenzo[d][1,3]dioxol-2-one (6A) (Beattie et al., 2013)



*Cis*-1,2-cyclohexanediol (750 mg, 6 mmol), urea (580 mg, 9.6 mmol) and 5 wt% ZMG (38.0 mg) were combined and reacted as above. The product was purified by recrystallization from methanol. Yield = 56% (400 mg).  $^1\text{H-NMR}$  (400 MHz,  $\text{CDCl}_3$ ):  $\delta_{\text{H}}$  4.63 (t, 2H, 4 Hz, 2CHOC), 1.86 (m, 4H, 2CH<sub>2</sub>CH), 1.58-1.53 (m, 2H, 2CH<sub>2</sub>CH<sub>2</sub>CH), 1.38-1.34 (m, 2H, 2CH<sub>2</sub>CH<sub>2</sub>CH).  $^{13}\text{C-NMR}$  (100 MHz,  $\text{CDCl}_3$ ):  $\delta_{\text{C}}$  155.3 (C=O), 70.6 (CH), 26.7 (CH<sub>2</sub>CH), 19.1 (CH<sub>2</sub>CH<sub>2</sub>CH). FTIR (Nujol):  $\nu/\text{cm}^{-1}$  2852(C-H<sub>str</sub>), 1788(C=O<sub>str</sub> cyclic), 1673, 1620, 1462, 1376, 1172, 1076 (data was consistent with data reported by Beattie et al., 2013). GC-MS:  $m/z$  142(M, 2), 97.1(4), 81(M-OCO<sub>2</sub>H, 12), 69(M-HOCOCHO, 41), 55(40).

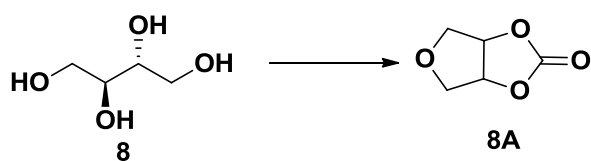
### 6.2.12 Reaction of *trans*-1,2-cyclohexanediol (7)



*Trans*-1,2-cyclohexanediol (5.00 g, 0.043 mol), urea (3.88 g, 0.065 mol) and 5 wt% ZMG (0.25 g) were reacted as above. Reaction mixture was analysed by GLC after removing ZMG catalyst and characterized.  $^1\text{H-NMR}$  (400 MHz, MeOD) of [7C]:  $\delta_{\text{H}}$  8.63 (br s, 4H, 2NH<sub>2</sub>), 4.39-4.33 (m, 2H, 2CH), 1.76-1.68 (m, 4H, 2CHCH<sub>2</sub>), 1.45-1.28 (m, 4H, 2CHCH<sub>2</sub>CH<sub>2</sub>). FTIR (film) of [7C]:  $\nu/\text{cm}^{-1}$  2943(C-H<sub>str</sub>), 2884(C-H<sub>str</sub>), 1753(C=O<sub>str</sub> linear), 1690(C=O<sub>str</sub> carbamate), 1491, 1389, 1229, 1068, 943. GC-MS:  $m/z$  (7C) 203(M+1, 0.4), 131(0.4), 116.1(1), 98.1(M-CONH<sub>2</sub> & OCONH<sub>2</sub>, 36), 83(10), 70.1(98-C<sub>2</sub>H<sub>4</sub>, 33), 57.1(98-

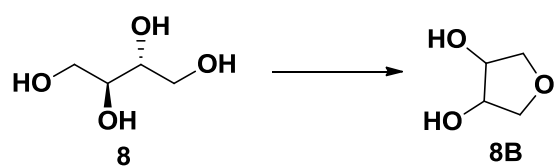
C<sub>3</sub>H<sub>5</sub>, 16); **(7A)** m/z 142(M, 2), 97.1(4), 81(M-OCO<sub>2</sub>H, 12), 69(M-HOCOCHO, 41), 55(40); **(7B)** 159.1(M, 1), 141(M-H<sub>2</sub>O, 1), 116.1(M-HNCO, 1), 98.1(M-HOCONH<sub>2</sub>, 54), 83(8), 70.1(98-C<sub>2</sub>H<sub>4</sub>, 4), 57.1(98-C<sub>3</sub>H<sub>5</sub>, 11); **(7D)** 344(M, 1), 328.8(M-NH<sub>2</sub>, 1), 300.4(M-CONH<sub>2</sub>, 1), 194.2(2), 98(M-NH<sub>2</sub>OCOC<sub>6</sub>H<sub>10</sub>OCONH<sub>2</sub>, 36), 83(11), 70.1(98-C<sub>2</sub>H<sub>4</sub>, 34), 57.1(98-C<sub>3</sub>H<sub>5</sub>, 15).

### 6.2.13 Tetrahydrofuro[3,4-d][1,3]dioxol-2-one (**8A**) (Tomczyk et al., 2012)



Meso-erythritol (5.00 g, 0.04 mol), urea (4.90 g, 0.08 mol) and ZMG (0.25 g) were combined and reacted as in Section 6.2.7. The solid product was purified by recrystallization with chloroform and methanol (5:3 mL). Yield = 97% (5.2 g). M.P = 77 °C (76-77.5 °C[lit]). <sup>1</sup>H-NMR (400 MHz, CDCl<sub>3</sub>): δ<sub>H</sub> 5.21-5.20 (m, 2H, CH), 4.27 (d, 2H, J= 12.4 Hz, 2OCH<sub>2</sub>), 3.57 (distorted d, 2H, J= 12.2 Hz, 2OCH<sub>2</sub>). <sup>13</sup>C-NMR (100 MHz, CDCl<sub>3</sub>): δ<sub>C</sub> 154.2 (C=O), 79.9 (CH), 73.0 (OCH<sub>2</sub>). FTIR (neat): ν/cm<sup>-1</sup> 2926(C-H<sub>str</sub>), 1776(C=O<sub>str</sub> cyclic), 1662, 1622, 1454, 1371, 1174, 1047, 899, 770 (analysis of the isolated product was consistent with that reported in the Tomczyk et al., 2012). GC-MS: m/z 130(M, 18), 101(M-CHO, 3), 73(101-CO, 5), 55 (M-HOCO & CH<sub>2</sub>O, 74).

### 6.2.14 Tetrahydrofuran-3,4-diol (8B) (Tomczyk et al., 2012)



Using the same method and conditions as in Section 6.2.7, *meso*-erythritol (500 mg, 4 mmol), urea (245 mg, 4 mmol) and ZMG (25 mg) were reacted as in 6.2.7. After separating ZMG by adding methanol, chloroform was added to the concentrate in order to crystallize out the remaining *meso*-erythritol, then separated by filtration. The filtrate was concentrated to afford a colorless oil. Yield = 76% (319 mg).  $^1\text{H-NMR}$  (400 MHz,  $\text{CDCl}_3$ ):  $\delta_{\text{H}}$  4.21-4.15 (m, 2H, 2CH), 3.93 (brs, 2H, 2OH), 3.83 (dd, 2H,  $J = 9.6, 5.6$  Hz, 2OCH<sub>2</sub>), 3.64 (dd, 2H,  $J = 9.6, 4$  Hz, 2OCH<sub>2</sub>).  $^{13}\text{C-NMR}$  (100 MHz,  $\text{CDCl}_3$ ):  $\delta_{\text{C}}$  72.9 (CH<sub>2</sub>OH), 71.3 (CH<sub>2</sub>O) FTIR (neat):  $\nu/\text{cm}^{-1}$  3562(O-H<sub>str</sub>), 2952(C-H<sub>str</sub>), 1334, 1182, 1112, 1053, 991, 904 (data obtained was consistent with the Tomczyk et al., 2012).

### 6.2.15 Attempted reactions of monosaccharides

#### Reaction of D-Glucose

**With urea only:** D-glucose (2.00 g, 0.011 mol) and urea (0.13 g, 0.022 mol) were combined in 3.00 mL of water and heated at 120 °C for 5h. The brownish yellow solution was diluted with ethanol to obtain precipitates which were found to be a mixture of urea and D-glucose.

**With urea/ZMG:** D-glucose (2.0 g, 0.011 mol) was heated with urea (1.3 g, 0.022 mol) and 5% ZMG (0.10 g) at 130 and 140 °C under 40 mbar pressure for 3h in two separate experiments. The reactions were cooled, methanol added and concentrated. D-glucose was recovered with some urethane formation. FTIR (film):  $\nu/\text{cm}^{-1}$  3353, 2944(C-H<sub>str</sub>), 2832(C-H<sub>str</sub>), 2216(NCO<sub>str</sub>), 1667(C=O<sub>str</sub> carbamate), 1454, 1028, 918, 875, 783.

**With DMC/K<sub>2</sub>CO<sub>3</sub>:** D-glucose (2.000 g, 0.011 mol) was heated along with dimethyl carbonate (3.000 g, 0.033 mol) and potassium carbonate (0.046 g, 0.33 mmol) at 77 °C for 3h. After evaporating excess dimethyl carbonate and methanol, starting material was obtained.

### **Reaction of D-Fructose**

**With DMC/K<sub>2</sub>CO<sub>3</sub>:** D-Fructose (2.000 g, 0.01 mol), dimethyl carbonate (3.000 g, 0.03 mol) and potassium carbonate (0.046 g, 0.33 mmol) were reacted as mentioned above. Only d-fructose was recovered.

**With urea/ZMG:** D-Fructose (2.0 g, 0.01 mol), urea (1.3 g, 0.02 mol) and 5 wt% ZMG (0.1 g) were heated at 95 °C/ambient pressure. In two separate reactions, similar amounts of d-fructose, urea and ZMG were used at 70 mbar pressure and heated at 105 and 140 °C for 3h. After 3h, the crude mixtures were analysed by IR. D-Fructose was recovered along with some urethane formation. FTIR (film):  $\nu/\text{cm}^{-1}$  3249(O-H<sub>str</sub>), 2920(C-H<sub>str</sub>), 2212(NCO<sub>str</sub>), 1660(C=O<sub>str</sub> carbamate), 1455, 1028, 791.

## **6.3 Experimental for Chapter 3- Interaction of glycerol carbonate and other cyclic carbonates with Na-smectite**

### **6.3.1 Preparation of Na-smectite**

The mineralogy of the bentonite was smectite (>80 %) as determined by X-ray diffraction and Reitfeld analysis (Mr M.D. Raven, CSIRO Land and Water, Adelaide, 2014). The following procedure was adopted for preparation of sodium smectite.

**Method A:** Na-smectite (20 g) was added to 130 mL of 1M NaCl solution and stirred for 24h at room temperature. The clay was recovered by centrifugation and the supernatant was discarded. The clay was subjected to numerous washing steps with water to remove

soluble salts as well as to remove non-swelling mineral impurities. Absolute ethanol was used in the final washing until halide ions could no longer be detected by a silver nitrate test. The sodium saturated smectite (Na-smectite) was then freeze dried giving a final weight of 13 g and was ground in a mortar prior to use.

**Method B:** De-ionised water (1L) was added to smectite (25 g) along with sodium chloride (100 g) and mixed thoroughly. After leaving stand for 12h, the suspension was decanted into a (glass) beaker avoiding any sediment transfer. This process was repeated three times (on sediment) until the suspension volume was reduced to 350 mL. Excess salts were removed by dialysis of the suspension for a week. The Na-smectite (16 g) was then freeze dried to a powder.

### **6.3.2 Preparation of glycerol carbonate (1A)/Na-smectite**

Na-smectite (variable, accurately weighed, from Section 6.3.1, method A) was dispersed in water (3 mL). The smectite suspension was deposited on a ceramic tile under suction to form an oriented film. An amount (variable, accurately weighed) of glycerol carbonate (**1A**) was dissolved in 1 mL of water. This **1A** solution was then filtered through the still-wet Na-smectite film and air dried for 3h.

For preparation of various amounts of **1A**/Na-smectite, the amounts of **1A** used were varied from 10-90 mg and that of Na-smectite was varied from 90-10 mg, yielding a range of GC wt% with respect to Na-smectite.

### **6.3.3 Calculation of water content (Table 3.1)**

Na-smectite (1 g) and glycerol carbonate (1 g) were weighed into two separate tared glass vials and heated in vacuum oven at 105 °C for 24h. The vials were cooled in a

desiccator under nitrogen for 1h. Once cooled, the contents were re-weighed to calculate the water content from the mass loss.

#### **6.3.4 Preparation of oven dried 1A/Na-smectite**

Na-smectite (90 mg, 50 wt% with respect to **1A**) was taken in a mortar and pestle and mixed with glycerol carbonate (**1A**) (90 mg, 50 wt% with respect to Na-smectite). The intercalated complex was dried in a vacuum oven at 105 °C for overnight, cooled under nitrogen and stored for further use.

#### **6.3.5 FTIR studies on glycerol carbonate (1A)**

Glycerol carbonate was oven dried under vacuum at 80 °C for 3 days prior to use. Various amounts of water (1-15  $\mu\text{L}$ ) were added stepwise to 100  $\mu\text{L}$  of glycerol carbonate and FTIR were run after each addition. Similarly, various amounts of sodium chloride (100-10,000 ppm) were dissolved in glycerol carbonate and an FTIR study was also performed. 10,000 ppm sodium chloride solution in glycerol carbonate was used and amounts of water (9-91%) were varied stepwise with respect to sodium chloride.

#### **6.3.6 Stability testing of glycerol carbonate (1A)**

The stability of glycerol carbonate (**1A**) was tested at ambient temperature and pressure in 1M NaCl and 1M  $\text{CaCl}_2$  aq. solution (95%  $\text{H}_2\text{O}$ + 5%  $\text{D}_2\text{O}$ ). The pH of solution was set to 2, 3, 4 and 7 for NaCl and 2, 3, 4 and 8 for  $\text{CaCl}_2$  by adding HCl. 1 mL of each salt solution was added to NMR sample tubes. Glycerol carbonate (32 mg) was dissolved in each sample in NMR tubes. A blank solution of glycerol carbonate was also prepared in 95%  $\text{H}_2\text{O}$ ; 5%  $\text{D}_2\text{O}$  without adding any salt. Samples were removed at predetermined time intervals. The stability of the cyclic carbonyl group was investigated by IR analysis and carbon-13 NMR spectroscopy. The stability was monitored by taking  $^{13}\text{C}$ -NMR of these

samples.  $^{13}\text{C}$ -NMR spectra were taken twice a week to confirm the stability for up to 1.5 years.

### **6.3.7 Preparation of PC intercalated Na-smectite**

Na-smectite (50 mg, 50 wt% with respect to PC) was dispersed in water and the smectite suspension was loaded onto a ceramic tile under suction. An amount of PC (50 mg, 50 wt% with respect to Na-smectite) was dissolved in water (1.0 mL). PC aqueous solution was loaded directly onto the top of the still-wet Na-smectite containing ceramic tile and air dried for 3h.

### **6.3.8 Synthesis of 2A intercalated Na-smectite**

Varying amounts of **2A** intercalated Na-smectite were prepared from Na-smectite and **2A** following the above mentioned method for **1A**/Na-smectite (method 6.3.2).

### **6.3.9 Preparation of 2C intercalated Na-smectite**

Amounts of Na-smectite (50 mg, 50 wt% with respect to **2C**) and **2C** (50 mg, 50 wt%) were used and the method described in Section 6.3.2 was followed.

### **6.3.10 Preparation of 3A intercalated Na-smectite**

Various amounts (10-90 wt% with respect to **3A**) of **3A**/Na-smectite were prepared by using variable amounts of **3A** as 10-90 mg and weight of Na-smectite was varied from 90-10 mg, respectively following the method 6.3.2.

### **6.3.11 Preparation of 3C intercalated Na-smectite**

Na-smectite (50 mg, 50 wt% with respect to **3C**) was loaded along with 50 mg of **3C** (50 wt% with respect to Na-smectite) according to the procedure as mentioned in Section 6.3.7.

### **6.3.12 Preparation of 4A intercalated Na-smectite**

Method 6.3.2 was used for 50 mg of Na-smectite (50 wt% with respect to **4A**) and 50 mg of **4A** (50 wt% with respect to smectite) dissolved in 1.0 mL of water.

### **6.3.13 Preparation of 5A intercalated Na-smectite**

Na-smectite (50 mg, 50 wt% with respect to **5A**) was dispersed in water and was loaded onto a ceramic tile under suction. 1.0 mL of methanolic solution of **5A** (25 mg, 25 wt%) was prepared and loaded directly onto the wet clay and air dried for 3h.

### **6.3.14 Preparation of 6A intercalated Na-smectite**

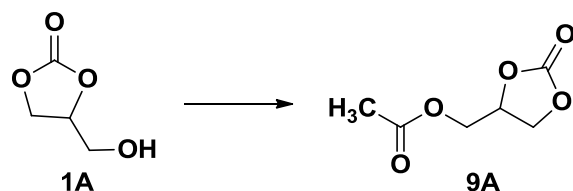
Na-smectite (75 mg, 50 wt% with respect to **6A**) and 75 mg of **6A** (50 wt% with respect to Na-smectite) was used employing the method described in Section 6.3.13.

### **6.3.15 Preparation of 8A intercalated Na-smectite**

Amounts of Na-smectite (60 mg, 50 wt% with respect to **8A**) and **8A** (60 mg, 50 wt% with respect to smectite) were used and the method described in Section 6.3.13 was adopted.

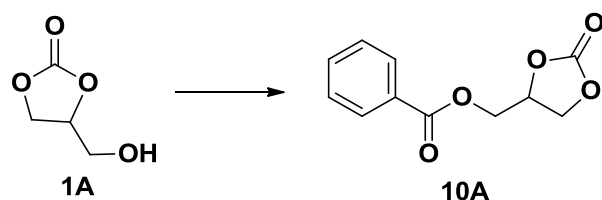
## 6.4 Experimental for Chapter 4- Derivatization of glycerol carbonate and polymerization of cyclic carbonates

### 6.4.1 (2-oxo-1,3-dioxolan-4-yl)methyl acetate (9A) (Dibenedetto et al., 2011)



Glycerol carbonate (1.00 g, 0.008 mol) was placed into a 100 mL round bottom flask and dichloromethane (10.00 mL) was added. The solution was stirred under nitrogen followed by the addition of acetyl chloride (0.72 mL, 0.008 mol). Three drops of pyridine were added and the resulting mixture was stirred for 2h at room temperature. Reaction progress was monitored by TLC (EA/hexane = 3/2). The mixture was extracted with water, dried over sodium sulfate and evaporated in vacuo. Yield = 95% (0.970 g). <sup>1</sup>H-NMR (400 MHz, CDCl<sub>3</sub>): δ<sub>H</sub> 4.97-4.91 (m, 1H, CH), 4.57 (t, 1H, J= 8.8 Hz, CH<sub>2</sub>O), 4.38-4.22 (m, 3H, CH<sub>2</sub>O), 2.11 (s, 3H, CH<sub>3</sub>). FTIR (neat): ν/cm<sup>-1</sup> 2953(C-H<sub>str</sub>), 2869, 1792(C=O<sub>str</sub> cyclic), 1714, 1447, 1395, 1280, 1172, 782, 718 (analysis of the isolated product was consistent with reported data (Dibenedetto et al., 2011)). GC-MS: 160(M, 7), 117(M-COCH<sub>3</sub>, 20), 101(5), 87(M-CH<sub>2</sub>OCOCH<sub>3</sub>, 68).

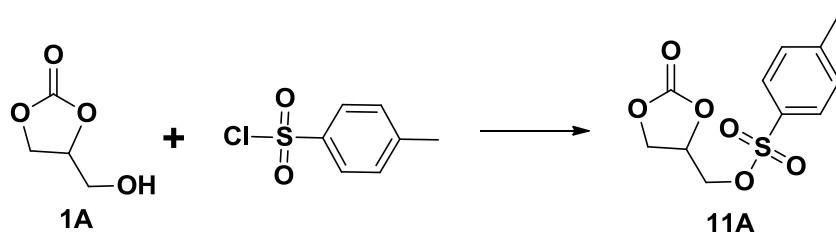
### 6.4.2 4-methylbenzoate-1,3-dioxolan-2-one (10A) (Dibenedetto et al., 2011)



Glycerol carbonate (5.0 g, 0.042 mol), benzoyl chloride (5.9 g, 0.042 mol) in dichloromethane (50.0 mL) with pyridine were reacted as above. The final product was

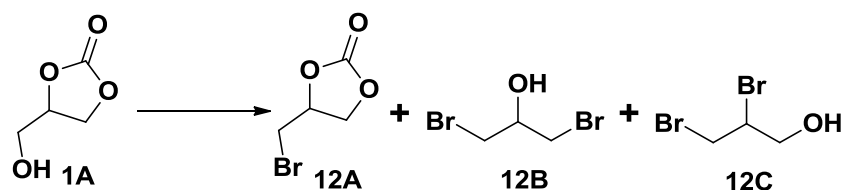
purified by column chromatography (chloroform/toluene = 1/1). Yield = 67% (6.3 g).  $^1\text{H-NMR}$  (400 MHz,  $\text{CDCl}_3$ ):  $\delta_{\text{H}}$  8.58 (d, 2H,  $J = 2$  Hz, 2Ar-H), 7.50 (t, 1H,  $J = 1.6$  Hz, 1Ar-H), 7.47 (t, 2H,  $J = 2$  Hz, 2Ar-H), 5.1-5.05 (m, 1H, CH), 4.65 (t, 1H,  $J = 8.6$  Hz,  $\text{CH}_2\text{O}$ ), 4.62-4.52 (m, 2H,  $\text{CH}_2\text{O}$ ), 4.44 (dd, 1H,  $J = 8.8, 5.6$  Hz,  $\text{CH}_2\text{O}$ ). FTIR (KBr):  $\nu/\text{cm}^{-1}$  3071( $\text{C-H}_{\text{str}}$ ), 2922( $\text{C-H}_{\text{str}}$ ), 2850, 1794( $\text{C=O}_{\text{str}}$  cyclic), 1720( $\text{C=O}_{\text{str}}$ , ester), 1553, 1402, 1324, 1274, 1178, 1120, 1071, 1027, 935, 804, 770, 709 (data was consistent to that reported in the Dibenedetto et al., 2011).

### 6.4.3 Tosylated glycerol carbonate (11A) (Giardi et al., 2010)



Glycerol carbonate (0.25 g, 2.200 mmol) and tosyl chloride (0.60 g, 0.003 mol) were dissolved in acetonitrile (1.00 mL) and added dropwise via a dropping funnel to a solution of pyridine (0.33 g, 0.004 mol) in acetonitrile (5 mL) at 0 °C. The mixture was stirred for 6h at room temperature. The reaction mixture was extracted with dichloromethane and water. Dichloromethane layer was dried over sodium sulfate and evaporated. Yield = 70% (0.38 g). M.P = 107 °C (108 °C[lit]).  $^1\text{H-NMR}$  (400 MHz,  $\text{DMSO-d}_6$ ):  $\delta_{\text{H}}$  7.8 (d, 2H,  $J = 9$  Hz, 2Ar-H), 7.5 (d, 2H,  $J = 1.6$  Hz, 2Ar-H), 5.05-4.98 (m, 1H, CH), 4.52 (t, 1H,  $J = 8.8$  Hz,  $\text{CH}_2\text{O}$ ), 4.33 (dd, 1H,  $J = 11.5, 2.5$  Hz,  $\text{CH}_2\text{O}$ ), 4.28 (dd, 1H,  $J = 11.5, 5.7$  Hz,  $\text{CH}_2\text{O}$ ), 4.17 (dd, 1H,  $J = 8.8, 6$  Hz,  $\text{CH}_2\text{O}$ ), 2.44 (s, 3H). FTIR (KBr):  $\nu/\text{cm}^{-1}$  3071( $\text{C-H}_{\text{str}}$ ), 2922( $\text{C-H}_{\text{str}}$ ), 1801( $\text{C=O}_{\text{str}}$  cyclic), 1616, 1595, 1475, 1395, 1247, 1170, 1098, 1047, 963, 951, 841, 809, 745, 664 (product data was consistent with Giardi et al., 2010).

**6.4.4 4-bromomethyl-1,3-dioxolan-2-one (12A)** (Bensemhoun and Condon, 2012)



**Method A (conventional method):** To a solution of glycerol carbonate (4.00 g, 0.034 mol) in dichloromethane (10.0 mL), the stoichiometric amount of phosphorus tribromide (3.1 g, 0.011 mol) was added drop-wise at  $-78\text{ }^{\circ}\text{C}$  and the temperature was increased slowly over 15 min to room temperature. The reaction mixture was stirred for a further 30 min. Progress of the reaction was monitored by TLC. The resultant reaction mixture was decanted using toluene and then evaporated under reduced pressure to obtain the desired product. Yield = 78% (4.8 g).  $^1\text{H-NMR}$  (400 MHz,  $\text{CDCl}_3$ ):  $\delta_{\text{H}}$  5.94-5.00 (m, 1H, CH), 4.58 (t, 1H,  $J = 8.4\text{ Hz}$ ,  $\text{CH}_2\text{O}$ ), 4.20 (dd, 1H,  $J = 8.4, 6\text{ Hz}$ ,  $\text{CH}_2\text{O}$ ), 3.64-3.53 (m, 2H,  $\text{CH}_2\text{Br}$ ). FTIR (film):  $\nu/\text{cm}^{-1}$  2966( $\text{C-H}_{\text{str}}$ ), 1792( $\text{C=O}_{\text{str}}$  cyclic), 1474, 1413, 1396, 1164, 1066, 846, 790, 715, 667 (Consistent with data reported by Bensemhoun and Condon, 2012). GC-MS:  $m/z$  (**12A**) 182( $\text{M}+2$ , 9), 180( $\text{M}$ , 10), 93(5), 87( $\text{M}-\text{CH}_2\text{Br}$ , 70) and 57(6); (**12B**) 218( $\text{M}$ , 1), 125(45), 123( $\text{M}-\text{CH}_2\text{Br}$ , 48), 93( $\text{M}-\text{CH}_2\text{Br}$ , 4) and 57(2).

**Method B (microwave method):** Glycerol carbonate (2.00 g, 0.017 mol) and stoichiometric amount of phosphorus tribromide (1.53 g, 0.006 mol) in 1.00 mL of dichloromethane was irradiated at 300W at various temperatures of 20, 25, 30 and  $40\text{ }^{\circ}\text{C}$  for time interval of 2 and 4 minutes in microwave. Pure product (**12A**) was obtained after workup with toluene, as described above.

#### 6.4.5 Preparation of 9A intercalated Na-smectite

Na-smectite (50 mg, 50 wt% with respect to **9A**) was added to water and loaded onto a ceramic tile under suction to prepare Na-smectite film. **9A** (50 mg, 50 wt% with respect to Na-smectite) was dissolved in methanol (1.0 mL). Solution of **9A** was loaded onto the wet clay on the ceramic tile and finally air dried for 3h.

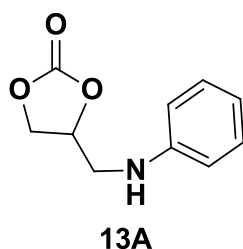
#### 6.4.6 Preparation of 10A intercalated Na-smectite

The method described in Section 6.4.5 was followed for amounts of Na-smectite (70 mg, 50 wt% with respect to **10A**) and **10A** (70 mg, 50 wt% with respect to Na-smectite).

#### 6.4.7 Preparation of 12A intercalated Na-smectite

Amounts of Na-smectite (60 mg, 50 wt%) and an aqueous solution (1.0 mL) of **12A** (60 mg, 50 wt% to Na-smectite) was used and the method described in Section 6.4.5 was repeated.

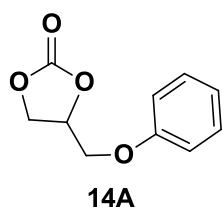
#### 6.4.8 Preparation of 4-((phenylamino)methyl)-1,3-dioxolan-2-one (**13A**) (Simao et al., 2006)



In a round bottom flask, tosylated glycerol carbonate (1.00 g, 3.6 mmol), aniline (0.34 g, 3.6 mmol) and potassium carbonate (0.50 g, 3.6 mmol) were reacted together at 80 °C in an oil bath for 3h under nitrogen. After completion of the reaction the crude mixture was purified by column chromatography (EA/hexane = 2/3) to yield pure **13A**. Yield =

29% (0.20 g).  $^1\text{H-NMR}$  (400 MHz,  $\text{CDCl}_3$ ):  $\delta_{\text{H}}$  7.17-7.12 (m, 2H, 2Ar H), 6.75-6.71 (m, 1H, Ar-H), 6.59-6.57 (m, 2H, 2Ar-H), 4.90-4.84 (m, 1H, CH), 4.49 (t, 1H,  $J = 8.5$  Hz,  $\text{CH}_2\text{O}$ ), 4.23 (dd, 1H,  $J = 8.5, 6.8$  Hz,  $\text{CH}_2\text{O}$ ), 3.5 (dd, 1H,  $J = 14.3, 4.2$  Hz,  $\text{CH}_2\text{NH}$ ), 3.37 (dd, 1H,  $J = 14.3, 5.6$  Hz,  $\text{CH}_2\text{NH}$ ).  $^{13}\text{C-NMR}$  (100 MHz,  $\text{CDCl}_3$ ):  $\delta_{\text{C}}$  156.1 (C=O), 147.4 (Ar-C-NH<sub>2</sub>), 129.5 (Ar-C), 119.0 (Ar-C), 113.3 (Ar-C), 75.2 (CH), 67.0 ( $\text{CH}_2\text{O}$ ), 46.0 ( $\text{CH}_2\text{NH}$ ). FTIR (KBr):  $\nu/\text{cm}^{-1}$  3389(N-H<sub>str</sub>), 2925(C-H<sub>str</sub>), 1787(C=O<sub>str</sub> cyclic), 1603, 1257, 1339, 1172, 1076, 753, 695 (data similar to Simao et al., 2006). GC-MS:  $m/z$  193(M, 15), 118(M-C<sub>6</sub>H<sub>3</sub>, 1), 106(M-C<sub>3</sub>H<sub>3</sub>O<sub>3</sub>, 73), 77(106-CH<sub>2</sub>NH, 8), 65(1), 51(2).

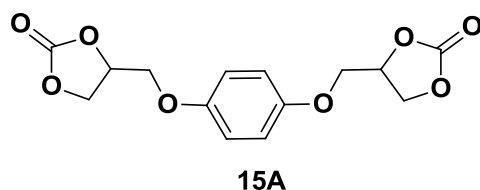
#### 6.4.9 4-(phenoxyethyl)-1,3-dioxolan-2-one (14A) (Simao et al., 2006)



The above method described in Section 6.4.8 was followed with tosylate glycerol carbonate (1.00 g, 3.6 mmol), phenol (0.34 g, 3.6 mmol) and potassium carbonate (0.50 g, 3.6 mmol). The product was purified by column chromatography (EA/hexane = 4/6) to yield pure **14A**. Yield = 32% (0.22 g).  $^1\text{H-NMR}$  (400 MHz,  $\text{CDCl}_3$ ):  $\delta_{\text{H}}$  7.82 (d, 2H,  $J = 8$  Hz, 2Ar-H), 7.40 (d, 2H,  $J = 8$  Hz, 2Ar-H), 6.85-6.83 (m, 1H, Ar-H), 4.93-4.87 (m, 1H, CH), 4.55 (t, 1H,  $J = 8.4$  Hz,  $\text{CH}_2\text{O}$ ), 4.38 (dd, 1H,  $J = 9.2, 6.8$  Hz,  $\text{CH}_2\text{O}$ ), 4.28-4.21 (m, 2H,  $\text{CH}_2\text{OPh}$ ).  $^{13}\text{C-NMR}$  (100 MHz,  $\text{CDCl}_3$ ):  $\delta_{\text{C}}$  157.1 (C=O), 155.3 (Ar-CO), 129.6 (Ar-C), 120.6 (Ar-C), 115.3 (Ar-C), 66.3 ( $\text{CH}_2\text{OPh}$ ), 65.5 (CH), 60.5 ( $\text{CH}_2\text{O}$ ). FTIR (film):  $\nu/\text{cm}^{-1}$  3021, 2954(C-H<sub>str</sub>), 2923, 2852, 1785(C=O<sub>str</sub> cyclic), 1458, 1396, 1339, 1168, 1073 (data was consistent with data reported by Simao et al., 2006). GC-MS:  $m/z$  194(M, 10), 107(M-C<sub>3</sub>H<sub>3</sub>O<sub>3</sub>, 71), 87(M-CH<sub>2</sub>OPh, 11), 77(87-CH<sub>2</sub>O, 7), 51(1).

#### 6.4.10 4,4'-((1,4-phenylenebis(oxy))bis(methylene))bis(1,3-dioxolan-2-one)

(15A)



**Method A:** Tosylated glycerol carbonate (2.45 g, 0.009 mol) was treated with hydroquinone (0.50 g, 0.005 mol) in DMF (20.00 mL) in the presence of excess potassium carbonate (1.25 g, 0.010 mol). The reaction mixture was heated at 80 °C for 4h. The reaction mixture was then extracted with EA and concentrated. The crude mixture was purified by column chromatography (EA/hexane = 2/3). Yield = 8% (0.22 g). <sup>1</sup>H-NMR (400 MHz, CDCl<sub>3</sub>): δ<sub>H</sub> 6.72 (s, 4H, 4Ar-H), 4.98-4.92 (m, 2H, 2CH), 4.59 (t, 2H, J= 8.8 Hz, 2CH<sub>2</sub>O), 4.42 (dd, 2H, J= 8.8, 6 Hz, 2CH<sub>2</sub>O), 3.77 (dd, 2H, J= 12.4, 2.8 Hz, 2CH<sub>2</sub>O), 3.73 (dd, 2H, J= 12, 3.2 Hz, 2CH<sub>2</sub>O). <sup>13</sup>C-NMR (100 MHz, CDCl<sub>3</sub>): δ<sub>C</sub> 159 (C=O), 156 (Ar-CO), 129.2 (Ar-C), 120.2 (Ar-C), 114.0 (Ar-C), 75.2 (CH), 71.0 (CH<sub>2</sub>O), 66.9 (CH<sub>2</sub>O). FTIR (film): ν/cm<sup>-1</sup> 2954(C-H<sub>str</sub>), 1801(C=O<sub>str</sub> cyclic), 1647, 1458, 1396, 1168, 1073. The unreacted materials (tosyl glycerol carbonate and hydroquinone) were separated by column chromatography and were characterized by IR and <sup>1</sup>H-NMR.

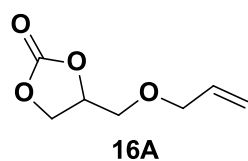
**Method B:** Method 6.4.9 was repeated with tosylated glycerol carbonate (2.45 g, 0.009 mol), hydroquinone (0.50 g, 0.005 mol) and potassium carbonate (1.25 g, 0.010 mol). Workup and purification was the same as before. The various fractions obtained by column chromatography (EA/hexane = 2/3) were: glycerol carbonate (10%), tosylated glycerol carbonate (27%), hydroquinone (26%), *p*-TSOH (31%) and **15A** (6%). In two separated reactions, using the similar amounts the reactants were heated at 50 and 60 °C. Fractions obtained by column chromatography (EA/hexane = 2/3) were: (**50 °C**

**reaction):** glycerol carbonate (15%), tosylated glycerol carbonate (33%), hydroquinone (29%), *p*-TSOH (18%) and **15A** (4%); **(60 °C reaction)** glycerol carbonate (18%), tosylated glycerol carbonate (29%), hydroquinone (24%), *p*-TSOH (21%) and **15A** (7%).

#### 6.4.11 Attempted reaction of tosylated glycerol carbonate with resorcinol

Methods A and B mentioned in Section 6.4.10 were used with tosylated glycerol carbonate (1.23 g, 0.045 mol), hydroquinone (0.25 g, 0.002 mol) and potassium carbonate (0.51 g, 0.005 mol). After the reaction, only reactants were isolated.

#### 6.4.12 Synthesis of 4-((allyloxy)methyl)-1,3-dioxolan-2-one (**16A**) (Benyahya et al., 2011)

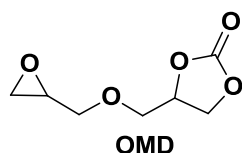


Glycerol carbonate (10.00 g, 0.09 mol) was taken into a three-neck round bottom flask and THF (90.00 mL) was added to it. Sodium hydride (2.43 g, 0.10 mol) was added to the solution cooled to -10 °C using ice-CaCl<sub>2</sub>·6H<sub>2</sub>O mixture and stirred for 10 minutes followed by the addition of allyl bromide (15.40 g, 0.13 mol) and sodium iodide (0.13 g, 84.70 mmol). The mixture was stirred for 24h at room temperature under nitrogen. The mixture was then filtered and the THF removed under reduced pressure. The crude liquid was extracted with EA and water. The organic fraction was concentrated to yield the pure product as a yellow oil. Yield = 27% (1.50 g). <sup>1</sup>H-NMR (400 MHz, CDCl<sub>3</sub>): δ<sub>H</sub> 5.85-5.75 (m, 1H, CH=CH<sub>2</sub>), 5.25-5.14 (m, 2H, CH<sub>2</sub>=CH), 4.78-4.72 (m, 1H, CH<sub>2</sub>O), 4.44 (t, 1H, J= 8.4 Hz, CH<sub>2</sub>O), 4.33 (dd, 1H, J= 8.4, 6.4 Hz, CH<sub>2</sub>O), 4.00-3.98 (m, 2H, CH<sub>2</sub>.CH=CH<sub>2</sub>), 3.62 (dd, 1H, J= 10.8, 4 Hz, CH<sub>2</sub>O), 3.55 (dd, 1H, J= 11.2, 4 Hz, CH<sub>2</sub>O). <sup>13</sup>C-NMR (100 MHz,

CDCl<sub>3</sub>):  $\delta_c$  154.9 (C=O), 133.7 (CH<sub>2</sub>=CH), 117.9 (CH=CH<sub>2</sub>), 74.5 (CH<sub>2</sub>O), 72.6 (CH), 68.9 (CH<sub>2</sub>-CH=CH<sub>2</sub>), 66.3 (CH<sub>2</sub>O)(data was consistent with cited by Benyahya et al., 2012).

#### 6.4.13 Synthesis of 4-((oxiran-2-ylmethoxy)methyl)-1,3-dioxolan-2-one (OMD)

(He et al., 2010)



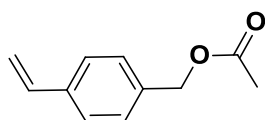
*m*-Chloroperoxybenzoic acid (13.00 g, 0.75 mol) was added to 4-((allyloxy)methyl)-1,3-dioxolan-2-one (**16A**) (6.82.00 g, 43.00 mmol) in dichloromethane (100.00 mL) under a nitrogen atmosphere, heated to 45 °C and stirred for 24h. The mixture was cooled in ice to precipitate out excess *m*-perchloroperoxybenzoic acid, which was removed by filtration. The filtrate then was diluted with CH<sub>2</sub>Cl<sub>2</sub> (100 mL) and washed with 10% NaHCO<sub>3</sub>, brine and water. The CH<sub>2</sub>Cl<sub>2</sub> fraction was collected, dried over sodium sulfate and concentrated to afford the desired product. Yield = 78% (7.10 g). <sup>1</sup>H-NMR (400 MHz, CDCl<sub>3</sub>):  $\delta_H$  5.85-5.76 (m, 1H, CH), 5.25-5.14 (m, 2H, CH<sub>2</sub>OC), 4.78-4.73 (m, 1H, CHO), 4.43 (t, 1H, J= 8.4 Hz, CHCH<sub>2</sub>O), 4.33 (dd, 1H, J= 8.4, 6.4 Hz, CHCH<sub>2</sub>O), 4.00-3.98 (m, 2H, CHCH<sub>2</sub>O), 3.62 (dd, 1H, J= 10.8, 4 Hz, CH<sub>2</sub>O), 3.55 (dd, 1H, J= 11.2, 4 Hz, CH<sub>2</sub>O). <sup>13</sup>C-NMR (100 MHz, CDCl<sub>3</sub>):  $\delta_c$  154.9 (C=O), 75.1 (CH<sub>2</sub>O), 72.6 (CH<sub>2</sub>O), 68.9 (CH<sub>2</sub>O), 66.3 (CH), 55.3 (CH<sub>2</sub>O). FTIR (film):  $\nu/cm^{-1}$  2985(C-H<sub>str</sub> aliphatic), 2922, 2867, 1782(C=O<sub>str</sub> cyclic), 1668(C=C<sub>str</sub>), 1477, 1396, 1360, 1262, 1166, 1044, 998, 931, 850 (data was consistent with the literature (He et al., 2010).

#### 6.4.14 Attempted synthesis of 4,4'-(oxybis(methylene))bis(1,3-dioxolan-2-one)

(5A) (Rokicki and Kuran, 1984)

The method described in Section 6.4.13 was used with glycerol carbonate (0.660 g, 5.55 mmol), sodium hydride (0.160 g, 6.64 mmol), 4-bromomethyl-1,3-dioxolan-2-one (1.5 g, 8 mmol) and sodium iodide (0.083 g, 0.55 mmol). Only the reactants were recovered from the reaction.

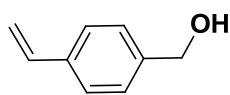
#### 6.4.15 4-Vinylbenzyl acetate (17A) (Shimomura et al., 2005)



17A

A mixture of 4-vinylbenzyl chloride (5.4 g, 0.036 mol) and potassium acetate (4.0 g, 0.040 mol) in dimethyl sulfoxide (15.0 mL) were stirred at 40 °C for 48h. The reaction mixture was poured into water (20.0 mL) and extracted three times with EA (40.0 mL). The organic fractions were combined, dried over sodium sulfate and concentrated. Yield = 96% (6.0 g). <sup>1</sup>H-NMR (400 MHz, CDCl<sub>3</sub>): δ<sub>H</sub> 7.43 (d, 2H, J= 8 Hz, 2Ar-H), 7.33 (d, 2H, J= 8 Hz, 2Ar-H), 6.74 (dd, 1H, J= 17.6, 10.8 Hz, CH=CH<sub>2</sub>), 5.77 (dd, 1H, J= 17.6, 0.8 Hz, CH=CH<sub>2</sub>), 5.27 (dd, 1H, J= 11.2, 0.8 Hz, CH=CH<sub>2</sub>), 4.99 (s, 2H, CH<sub>2</sub>), 2.01 (s, 3H, CH<sub>3</sub>) (data was the same as cited by Shimomura et al., 2005).

#### 6.4.16 4-Vinylbenzyl alcohol (18A)



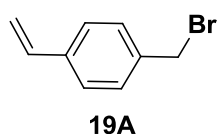
18A

**Method A** (Shimomura et al., 2005): Sodium hydroxide (2.7 g, 0.067 mol) and 4-vinylbenzyl acetate (7.9 g, 0.045 mol) were added to ethanol/water (15 mL/2.5 mL) and

refluxed for 2h. The reaction mixture was poured into water, extracted with EA, dried over sodium sulfate and concentrated. Crude was purified by vacuum distillation by using kugelrohr at 165 °C. Yield = 87% (4.1 g).  $^1\text{H-NMR}$  (400 MHz,  $\text{CDCl}_3$ ):  $\delta_{\text{H}}$  7.42 (d, 2H,  $J = 8$  Hz, 2Ar-H), 7.35 (d, 2H,  $J = 8$  Hz, 2Ar-H), 6.73 (dd, 1H,  $J = 17.6, 10.8$  Hz,  $\text{CH}=\text{CH}_2$ ), 5.76 (dd, 1H,  $J = 17.6, 0.8$  Hz,  $\text{CH}=\text{CH}_2$ ), 5.26 (dd, 1H,  $J = 11.2, 0.8$  Hz,  $\text{CH}=\text{CH}_2$ ), 4.69 (s, 2H,  $\text{CH}_2$ ), 1.65 (br s, 1H, OH) (data was consistent as reported by Shimomura et al., 2005).

**Method B** (Gao et al., 2011): Sodium hydroxide (0.08 g, 2.0 mmol) was dissolved in water (100.00 mL) and added to a round bottom flask. *n*-Hexyl decyl trimethyl ammoniumbromide (0.73 g, 20 mmol) and 4-vinylbenzyl chloride (3.00 g, 2.0 mmol) were added and heated at 125 °C for 1h. The reaction was cooled and extracted with three portions of EA (80 mL). This fraction was concentrated and purified by column chromatography (EA: hexane = 1:5). Yield = 60% (1.60 g).

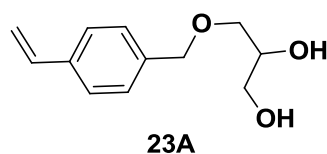
#### 6.4.17 4-Vinylbenzyl bromide (19A) (Shimomura et al., 2005)



Phosphorous tribromide (4.67 g, 0.017 mol) dissolved in diethyl ether (5.00 mL) was added in two portions over 30 minutes to 4-vinylbenzyl alcohol (6.95 g, 0.052 mol) dissolved in diethyl ether (80.00 mL) under nitrogen at -75 °C and then stirred for another hour on warming to room temperature. GLC was used to monitor the progress of the reaction. The mixture was cooled by adding ice-cold water and the reaction mixture was then extracted into diethyl ether. The organic layer was separately washed with sodium bicarbonate and then brine; then dried over anhydrous sodium sulfate. After evaporation of the solvent, pure product was obtained. Yield = 78% (7.82 g).  $^1\text{H-}$

NMR (300 MHz, CDCl<sub>3</sub>):  $\delta_{\text{H}}$  7.41-7.35 (m, 4H, 4Ar-H), 6.71 (dd, 1H, J= 17.6, 10.9 Hz, CH=CH<sub>2</sub>), 5.77 (dd, 1H, J= 17.6, 1 Hz, CH=CH<sub>2</sub>), 5.28 (dd, 1H, J= 10.9, 1 Hz, CH=CH<sub>2</sub>), 4.48 (s, 2H, CH<sub>2</sub>). <sup>13</sup>C-NMR (75 MHz, CDCl<sub>3</sub>):  $\delta_{\text{C}}$  139.8 (Ar-CH), 129.7 (Ar-CH<sub>2</sub>), 127.6 (CH=CH<sub>2</sub>), 125.0 (Ar-C), 33.1 (CH<sub>2</sub>Br) (data was consistent with literature (Shimumura et al., 2005)).

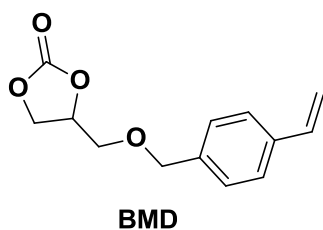
#### 6.4.18 3-((4-vinylbenzyl)oxy)propane-1,2-diol (23A) (Yokoi and Hironaka, 2012)



**4-Vinylbenzyl chloride method:** Sodium hydride (0.39 g, 9.8 mmol) was added slowly to a THF (20.0 mL) solution of glycerol (0.90 g, 9.8 mmol) in a three neck round bottom flask at -10 °C and was stirred for 10 min. 4-Vinylbenzyl chloride (1.50 g, 9.8 mmol) was added to the reaction mixture followed by addition of sodium iodide (0.15 g, 9.8 mmol). The reaction was stirred for 96h at 50 °C under nitrogen. Disappearance of 4-vinylbenzyl bromide was monitored by GLC. After 96h, the solution was filtered and remaining solvent was evaporated. The crude mixture was separated between EA and water. The organic layer was dried over anhydrous sodium sulfate and concentrated. The crude was purified by column chromatography (EA/hexane = 3/2). Yield = 18% (0.38 g). <sup>1</sup>H-NMR (400 MHz, CDCl<sub>3</sub>):  $\delta_{\text{H}}$  7.40 (d, 2H, J= 8 Hz, 2Ar-H), 7.28 (d, 2H, J= 8 Hz, 2Ar-H), 6.71 (dd, 1H, J= 17.6, 10.8 Hz, CH=CH<sub>2</sub>), 5.76 (d, 1H, J= 17.6 Hz, CH=CH<sub>2</sub>), 5.26 (d, 1H, J= 10.8 Hz, CH=CH<sub>2</sub>), 4.54 (s, 2H, CH<sub>2</sub>-C<sub>6</sub>H<sub>5</sub>), 3.89 (m, 1H, CH-OH), 3.71-3.53 (m, 4H, 2CH<sub>2</sub>CH), 2.59 (br s, 2H, 2OH). <sup>13</sup>C-NMR (100 MHz, CDCl<sub>3</sub>):  $\delta_{\text{C}}$  137.7 (Ar-C-CH), 137.6 (Ar-C-CH<sub>2</sub>), 136.8 (CH=CH<sub>2</sub>), 128.4 (Ar-C), 126.7 (Ar-C), 114.4 (CH<sub>2</sub>=CH), 73.6 (CH<sub>2</sub>O), 72.1 (CH<sub>2</sub>O), 71.0 (CHOH), 64.4 (CH<sub>2</sub>OH).

**4-Vinylbenzyl bromide method:** Method 6.4.18 was followed with glycerol (5.8 g, 0.063 mol), sodium hydride (2.5 g, 0.063 mol), 4-vinylbenzyl bromide (9.6 g, 0.05 mol) and sodium iodide (0.94 g, 6.3 mmol). After 24h, the reaction was stopped, worked up as described in 4-vinylbenzyl chloride method and purified by column chromatography (EA/hexane = 2/1). Yield = 51% (5.2 g).

**6.4.19 4-(4-((4-vinylbenzyl)oxy)methyl)-1,3-dioxolan-2-one (BMD)** (Miyata et al., 2012)



**From 4-vinylbenzyl chloride:** Method 6.4.18 was followed in reacting glycerol carbonate (5.00 g, 0.043 mol), sodium hydride (1.68 g, 0.043 mol), 4-vinylbenzyl chloride (6.50 g, 0.043 mol) and sodium iodide (0.64 g, 4.200 mmol). The reaction was continued for 96h at 50 °C. After workup as described in 6.4.18, column chromatography (EA/hexane = 2/1) was performed to purify the product. Yield = 25% (2.48 g). <sup>1</sup>H-NMR (400 MHz, CDCl<sub>3</sub>): δ<sub>H</sub> 7.40 (d, 2H, J= 7.6 Hz, 2Ar-H), 7.27 (dd, 2H, J= 8 Hz, 2Ar-H), 6.71 (dd, 1H, J= 17.6, 10.8 Hz, (CH=CH<sub>2</sub>)), 5.77 (dd, 1H, J= 17.6, 0.8 Hz, CH<sub>2</sub>=CH), 5.26 (dd, 1H, J= 10.8, 0.8 Hz, CH<sub>2</sub>=CH), 4.79-4.80 (m, 1H, CH), 4.58 (q, 2H, J= 9.6 Hz, CH<sub>2</sub>Ph), 4.47-4.37 (m, 2H, CH<sub>2</sub>O), 3.69-3.62 (m, 2H, CH<sub>2</sub>O). <sup>13</sup>C-NMR (75 MHz, CDCl<sub>3</sub>): δ<sub>C</sub> 154.9 (C=O), 137.5 (Ar-C-CH), 136.5 (Ar-C-CH<sub>2</sub>), 136.3 (CH=CH<sub>2</sub>), 128.0 (Ar-C), 126.4 (Ar-C), 114.2 (CH<sub>2</sub>=CH), 74.9 (CH<sub>2</sub>O), 73.4 (CH<sub>2</sub>Ph), 68.8(CH), 66.3 (CH<sub>2</sub>O). IR (film): ν/cm<sup>-1</sup> 3003(C-H<sub>str</sub> aromatic), 2864(C-H<sub>str</sub> aliphatic), 1789(C=O<sub>str</sub> cyclic), 1628(C=C<sub>str</sub>), 1476, 1395, 1359, 1250, 1165,

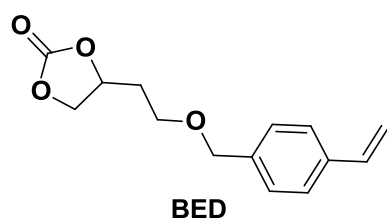
1102, 1041, 990, 827, 768, 714 (data consistent with reference (Miyata et al., 2012)).

ESI-MS:  $m/z$  257 (100%)  $[M+Na]^+$ .

**From 4-vinylbenzyl bromide:** Sodium hydride (1.9 g, 47 mmol) was added slowly to a solution of glycerol carbonate (5.5 g, 47.00 mmol) in THF (50 mL) at  $-10\text{ }^{\circ}\text{C}$  and the resulting mixture was stirred for 10 min. 4-Vinylbenzyl bromide (7.7 g, 0.39 mmol) was added to the mixture followed by addition of NaI (0.6 g, 3.90 mmol). The reaction was stirred for 18h at  $50\text{ }^{\circ}\text{C}$  under nitrogen. The disappearance of 4-vinylbenzyl bromide was monitored by GLC. After 18h, the solution was filtered and the remaining solvent was evaporated. The crude mixture was extracted between EA and water. The organic layer was dried over anhydrous sodium sulfate and concentrated. Column chromatography (EA/hexane = 2/1) of the residue gave pure product. Yield = 78% (7.1 g).

**Attempted synthesis from 4-vinylbenzyl acetate:** A two neck round bottom flask was charged with sodium hydride (0.34 g, 7.00 mmol), and glycerol carbonate (1.00 g, 8.00 mmol) in dimethyl formamide (10.00 mL) under nitrogen at room temperature. Tetrakis(triethylphosphite)nickel (0) (0.26 g, 0.35 mmol) and 4-vinylbenzyl acetate (1.20 g, 7.00 mmol) in dimethyl formamide (10.00 mL) were added along with THF (40.00 mL) and the mixture was heated to  $50\text{ }^{\circ}\text{C}$  for 20h. The reaction was monitored by GLC.

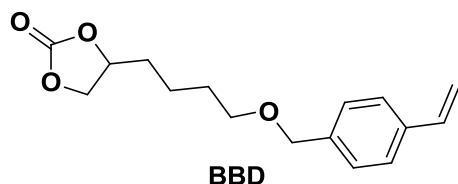
#### 6.4.20 4-(4-((4-vinylbenzyl)oxy)ethyl)-1,3-dioxolan-2-one (BED)



The method described in Section 6.4.18 was used for 4-(2-Hydroxyethyl)-1,3-dioxolan-2-one (1.50 g, 0.011 mol), sodium hydride (0.50 g, 0.011 mol), 4-vinylbenzyl bromide (1.70

g, 9.500 mmol) and sodium iodide (0.14 g, 0.950 mmol). After 24h, the crude product was purified by column chromatography (EA/hexane = 2/3). Yield = 65% (1.55 g).  $^1\text{H-NMR}$  (300 MHz,  $\text{CDCl}_3$ ):  $\delta_{\text{H}}$  7.41 (dd, 2H,  $J = 8.4, 2.4$  Hz, 2Ar-H), 7.28 (dd, 2H,  $J = 8.4, 2.4$  Hz, 2Ar-H), 6.72 (dd, 1H,  $J = 17.4, 10.8$  Hz, CH=CH<sub>2</sub>), 5.75 (dd, 1H,  $J = 17.4, 0.9$  Hz, CH<sub>2</sub>=CH), 5.25 (dd, 1H,  $J = 10.8, 0.9$  Hz, CH<sub>2</sub>=CH), 4.9-4.86 (m, 1H, CH), 4.53 (t, 1H,  $J = 7.8$  Hz, OCH<sub>2</sub>CH), 4.49 (s, 2H, CH<sub>2</sub>Ph), 4.19 (dd, 1H,  $J = 8.4, 7.2$  Hz, OCH<sub>2</sub>CH), 3.67-3.60 (m, 2H, CH<sub>2</sub>OCH<sub>2</sub>), 2.20-2.0 (m, 2H, CHCH<sub>2</sub>CH<sub>2</sub>).  $^{13}\text{C-NMR}$  (75 MHz,  $\text{CDCl}_3$ ):  $\delta_{\text{C}}$  155.3 (C=O), 137.6 (Ar-C-CH), 137.4 (Ar-C-CH<sub>2</sub>), 136.7 (CH=CH<sub>2</sub>), 128.2 (Ar-CH), 126.5 (Ar-CH), 114.4 (CH<sub>2</sub>=CH), 75.5 (CH<sub>2</sub>OPh), 73.2 (CH), 70.2 (OCH<sub>2</sub>CH), 65.9 (OCH<sub>2</sub>CH<sub>2</sub>), 34.4(OCH<sub>2</sub>CH<sub>2</sub>). FTIR (film):  $\nu/\text{cm}^{-1}$  3009(C-H<sub>str</sub> aromatic), 2934(C-H<sub>str</sub> aliphatic), 2860, 1791(C=O<sub>str</sub> cyclic), 1626(C=C<sub>str</sub>), 1465, 1396, 1360, 1215, 1168, 1059, 827, 775. ESI-MS:  $m/z$  271.0 (100%) [M+Na]<sup>+</sup>.

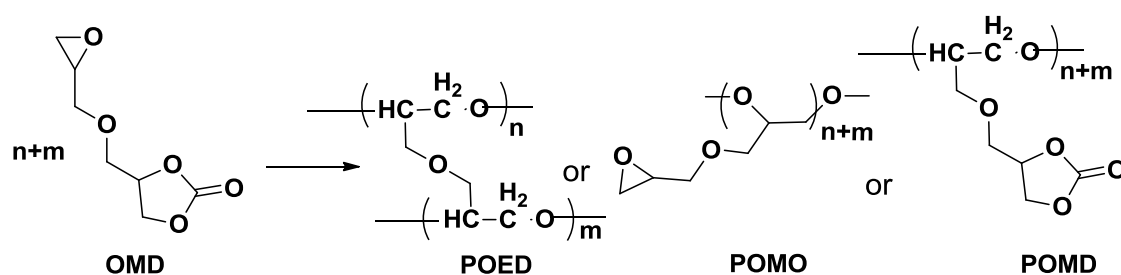
#### 6.4.21 4-(4-((4-vinylbenzyl)oxy)butyl)-1,3-dioxolan-2-one (BBD)



4-(2-Hydroxybutyl)-1,3-dioxolan-2-one (4.2 g, 24.00 mmol), sodium hydride (1.1 g, 24.00 mmol), 4-vinylbenzyl bromide (3.9 g, 12.00 mol) and sodium iodide (0.3 g, 1.96 mmol) were reacted using the method described in section 6.4.16. After isolation of the crude product by extraction with EA and water, the crude product was purified by column chromatography (EA/hexane = 2/3). Yield = 71% (4.0 g).  $^1\text{H-NMR}$  (300 MHz,  $\text{CDCl}_3$ ):  $\delta_{\text{H}}$  7.41 (dd, 2H,  $J = 8.4, 2.4$  Hz, 2Ar-H), 7.28 (dd, 2H,  $J = 8.4, 2.4$  Hz, 2Ar-H), 6.72 (dd, 1H,  $J = 17.4, 10.8$  Hz, CH=CH<sub>2</sub>), 5.75 (dd, 1H,  $J = 17.4, 0.9$  Hz, CH<sub>2</sub>=CH), 5.25 (dd, 1H,  $J = 10.8, 0.9$

Hz,  $\text{CH}_2=\text{CH}$ ), 4.71-4.67 (m, 1H, CH), 4.53-4.48 (m, 3H,  $\text{OCH}_2\text{CH}$ ,  $\text{CH}_2\text{Ph}$ ), 4.05 (dd, 1H,  $J=8.4, 7.2$  Hz,  $\text{OCH}_2\text{CH}$ ), 3.48 (t, 2H,  $J=6$  Hz,  $\text{OCH}_2\text{CH}_2$ ), 1.85-1.46 (m, 6H,  $\text{CHCH}_2\text{CH}_2\text{CH}_2\text{O}$ ).  $^{13}\text{C}$ -NMR (75 MHz,  $\text{CDCl}_3$ ):  $\delta_c$  155.3 (C=O), 138.3 (Ar-C $\text{CH}_2$ ), 137.4 (Ar-CCH), 136.8 ( $\text{CH}=\text{CH}_2$ ), 128.2 (Ar-CH), 126.5 (Ar-CH), 114.1 ( $\text{CH}_2=\text{CH}$ ), 76.9 ( $\text{CH}_2\text{Ph}$ ), 73.1 ( $\text{OCH}_2\text{CH}_2$ ), 69.9 (CH), 69.6 ( $\text{OCH}_2\text{CH}$ ), 34.0 ( $\text{CHCH}_2\text{CH}_2$ ), 29.5 ( $\text{OCH}_2\text{CH}_2$ ) and 21.7 ( $\text{OCH}_2\text{CH}_2\text{CH}_2$ ). FTIR (film):  $\nu/\text{cm}^{-1}$  3009(C-H $_{\text{str}}$  aromatic), 2934(C-H $_{\text{str}}$  aliphatic), 2860, 1794(C=O $_{\text{str}}$  cyclic), 1626(C=C $_{\text{str}}$ ), 1466, 1396, 1360, 1215, 1168, 1059, 827, 775. ESI-MS:  $m/z$  299.0 (100%)[M+Na] $^{+}$ .

#### 6.4.22 Ring opening polymerization of 4-((oxiran-2-ylmethoxy)methyl)-1,3-dioxolan-2-one (OMD)

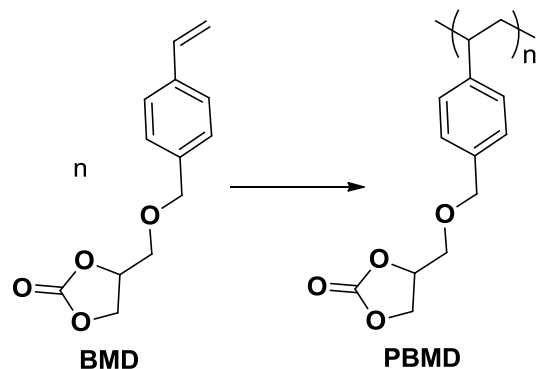


**Polyether (POED):** 4-((oxiran-2-ylmethoxy)methyl)-1,3-dioxolan-2-one (OMD) (750 mg, 4.30 mmol) was added to toluene (0.5 mL) under nitrogen. Potassium tertiary butoxide (021 mg, 0.17 mmol) was then added and the reaction mixture stirred for 24h at 110 °C. After 24h, polymerization was stopped by addition of one drop of acetic acid. Methanol (10 mL) was added to the mixture to precipitate a solid product, which was then filtered and vacuum dried at 40 °C. Yield = 87% (650 mg).  $^1\text{H}$ -NMR (400 MHz,  $\text{CDCl}_3$ ):  $\delta_H$  4.33-3.43 (m, 10H, aliphatic Hs), 2.22 (m, 2H, 2OH). IR (film):  $\nu/\text{cm}^{-1}$  3381, 2958, 2914, 2860(C-H $_{\text{str}}$ ), 1456, 1317, 1258(C-O $_{\text{str}}$ ), 1069, 1025(C-O $_{\text{str}}$ ), 799. GPC (10 mM LiBr in DMF):  $M_n = 1.4 \times 10^3$  Da.,  $M_w/M_n = 1$ .

**Polyether with pendant epoxide moiety (POMO):** 4-((oxiran-2-ylmethoxy)methyl)-1,3-dioxolan-2-one (**OMD**) (1.00 g, 5.70 mmol) was added to toluene (1.00 mL) in a 50.00 mL two neck round bottom flask under nitrogen. Sodium hydroxide (0.09 g, 0.23 mmol) was then added and the reaction mixture heated for 24h at 110 °C. After 24h, the toluene was removed under reduced pressure on a rotary evaporated. Methanol (20.00 mL) was added to the concentrated reaction mixture and the solid product was collected by filtration. Yield = 52% (0.52 g). <sup>1</sup>H-NMR (400 MHz, CDCl<sub>3</sub>): δ<sub>H</sub> 4.01-3.34 (m, 7H, aliphatic Hs), 3.17 (m, 1H, CH epoxide), 2.83 (m, 1H, OCH epoxide), 2.65 (m, 1H, OCH epoxide). IR (film): ν/cm<sup>-1</sup> 3386, 2923(C-H<sub>str</sub>), 1642, 1464, 1399, 1264(C-O<sub>str</sub>), 1050(C-O<sub>str</sub>), 909, 846, 759, 640. GPC (10mM LiBr in DMF):  $M_n = 2.8 \times 10^3$  Da.,  $M_w/M_n = 1.6$ .

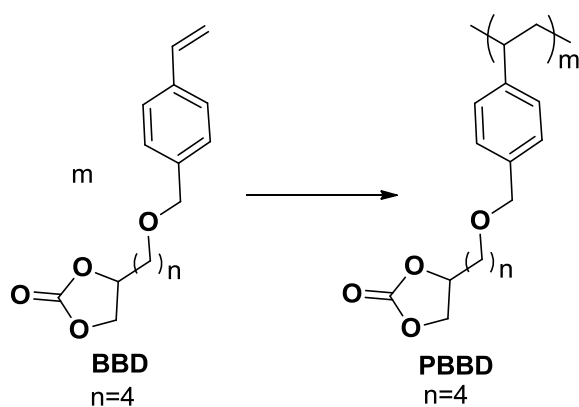
**Polyether with pendant cyclic carbonate (POMD):** 44-((oxiran-2-ylmethoxy)methyl)-1,3-dioxolan-2-one (**OMD**) (2.50 g, 0.01 mol) was transferred to a 50.00 mL two neck round bottom flask and purged with alternating cycles of vacuum and nitrogen. Boron trifluoride diethyl etherate (0.09 mL, 7.00 mmol) was added slowly under nitrogen. The reaction was stirred for 24h at room temperature to give a brown solid. Polymerization was stopped by addition of one drop of acetic acid. The crude was extracted with DCM and water, the organic phase was dried over sodium sulfate and concentrated to afford POMD. Yield = 94% (2.35 g). <sup>1</sup>H-NMR (300 MHz, CDCl<sub>3</sub>): δ<sub>H</sub> 4.83 (m, 1H, CH cyclic carbonate), 4.51-4.42 (m, 2H, OCH<sub>2</sub>CH), 4.00-3.30 (m, 7H, aliphatic Hs). IR (film): ν/cm<sup>-1</sup> 2871(C-H<sub>str</sub>), 1779(C=O<sub>str</sub> cyclic), 1475, 1394, 1258(C-O<sub>str</sub>), 1037(C-O<sub>str</sub>), 851, 768, 711. GPC (10mM LiBr in DMF):  $M_n = 8.1 \times 10^3$  Da.,  $M_w/M_n = 1.3$ .

#### 6.4.23 Radical photopolymerization of 4-(4-((4-vinylbenzyl)oxy)methyl)-1,3-dioxolan-2-one (BMD)



Azobisisobutyronitrile (0.03 g, 0.18 mmol) was added to 4-(4-((4-vinylbenzyl)oxy)methyl)-1,3-dioxolan-2-one (**BMD**) (1.40 g, 6.00 mmol) under a nitrogen atmosphere in a reaction tube. The sealed tube was placed under a UV-lamp at a distance of 12 cm at room temperature. Aliquots were taken at  $t = 0, 4, 8, 12, 16, 20$  and 24h. The polymer was precipitated by the addition of methanol (20 mL) and collected. Yield = 93% (1.30 g).  $^1\text{H-NMR}$  (400 MHz,  $\text{DMSO-d}_6$ ):  $\delta_{\text{H}}$  7.40-6.0 (m, 4H, 4Ar-H), 4.9 (m, 1H, CH), 4.52-3.9 (m, 5H,  $\text{OCH}_2\text{CH}$ ,  $\text{CH}_2\text{Ph}$ ), 3.59 (m, 1H,  $\text{CHCH}_2$ ), 2.0-0.9 (m, 3H,  $\text{CH}_2\text{CHPh}$ ). FTIR (film):  $\nu/\text{cm}^{-1}$  3009( $\text{C-H}_{\text{str}}$  aromatic), 2916( $\text{C-H}_{\text{str}}$  aliphatic), 2853, 1783( $\text{C=O}_{\text{str}}$  cyclic), 1564, 1550, 1511, 1475, 1392, 1358, 1255, 1213, 1165, 1040, 816, 768, 711, 675. GPC (10mM LiBr in DMF):  $M_n = 2.1 \times 10^4$  Da.,  $M_w/M_n = 2.5$ .

#### 6.4.24 Radical photopolymerization of 4-(4-((4-vinylbenzyl)oxy)butyl)-1,3-dioxolan-2-one (BBD)



The same photopolymerization method as described in Section 6.2.23 was used with 4-(4-((4-vinylbenzyl)oxy)butyl)-1,3-dioxolan-2-one (**BBD**) (1.900 g, 7.0 mmol) and AIBN (0.034 g, 0.2 mmol). The polymer was precipitated by the addition of water. Yield = 74% (1.400 g).  $^1\text{H-NMR}$  (400 MHz, acetone- $d_6$ ):  $\delta_{\text{H}}$  7.14 (m, 2H, 2Ar-H), 6.65 (m, 2H, 2Ar-H), 4.82 (m, 1H, CH), 4.62-4.58 (m, 3H,  $\text{CH}_2\text{Ph}$ ,  $\text{OCH}_2\text{CH}$ ), 4.15-4.12 (m, 1H,  $\text{OCH}_2\text{CH}$ ), 3.52-3.49 (m, 2H,  $\text{OCH}_2\text{CH}_2$ ), 1.79-1.52 (m, 9H,  $\text{CHCH}_2\text{CH}_2\text{CH}_2$ ,  $\text{PhCH-CH}_2$ ). FTIR (film):  $\nu/\text{cm}^{-1}$  3009( $\text{C-H}_{\text{str}}$  aromatic), 2921( $\text{C-H}_{\text{str}}$  aliphatic), 2853, 1789( $\text{C=O}_{\text{str}}$  cyclic), 1546, 1515, 1455, 1389, 1360, 1259, 1165, 1092, 1057, 817, 772, 712. GPC (10mM LiBr in DMF):  $M_n = 1.2 \times 10^4$  Da.,  $M_w/M_n = 2.4$ .

## 6.5 Experimental for Chapter 5- Preparation of polymer/Na-smectite nanocomposites

### 6.5.1 Preparation of POMD-1/Na-smectite by *in-situ* polymerization

Na-smectite (0.50 g, 50 wt% with respect to **OMD**) was placed in a mortar and pestle and manually ground with 4-((oxiran-2-ylmethoxy)methyl)-1,3-dioxolan-2-one (**OMD**) (0.50 g, 2.80 mmol, 50 wt% with respect to Na-smectite) for 2 minutes. The mixture was transferred to a two-neck round bottom flask and dried under vacuum for 1h. The initiator, boron trifluoride diethyl etherate (0.02 mL, 0.14 mmol) was added to the flask under a nitrogen atmosphere. The mixture was sonicated ( $P = 150 \text{ W}$ ,  $f = 37 \text{ kHz}$ ) for two hours and then subsequently stirred at room temperature for 24h. The polymerization was terminated by the addition of water, causing the polymer to precipitate, and washed with cold acetone to remove unreacted monomer and finally dried in vacuum oven at 40 °C.

### 6.5.2 Preparation of POMD/Na-smectite, PBMD/Na-smectite and PBBD/Na-smectite nanocomposites via solution intercalation

Separate samples (10, 20 and 50 mg) of polyether (**POMD**) (10, 20 and 50 wt% with respect to Na-smectite) and Na-smectite (90, 80 and 50 mg) were weighed according to the desired ratios. **POMD** was dissolved into acetone (7.0 mL), and Na-smectite was added to it. The mixture was sonicated ( $P = 150 \text{ W}$ ,  $f = 37 \text{ kHz}$ ) for 30 minutes and stirred at room temperature for 16h. Acetone was evaporated and the residue was washed thoroughly with water (5 mL), collected by centrifugation and dried in a vacuum oven for 48h at 40 °C.

With similar amounts of polymers, **PBMD** & **PBBD**, the above procedure was used for preparation of **PBMD/Na-smectite** and **PBBD/Na-smectite**. However, instead of acetone, acetonitrile was used for solution intercalation for **PBMD** and **PBBD**. The product was precipitated with methanol (5 mL), washed thrice with water (5 mL), centrifuged and vacuum dried at 40 °C for 48h to collect the polymer nanocomposite powder.

### 6.5.3 Preparation of **PBMD-1/Na-smectite** by clay *in-situ* polymerization

Na-smectite (0.50 g, 50 wt% with respect to **PBMD**) was mixed with 4-(4-((4-vinylbenzyl)oxy)methyl)-1,3-dioxolan-2-one (**PBMD**) (0.14 g, 0.6 mmol) in a mortar and pestle for 3 minutes. The mixture was transferred to a two-neck round bottom flask and dried under vacuum for 1h and purged with nitrogen. DMF (2.00 mL) was added and the mixture was stirred to form slurry. AIBN (3 mg, 0.2 mmol) was added to flask under a nitrogen atmosphere at 60 °C. The mixture was stirred at 70 °C for 24h. The polymerization was terminated by the addition of water (10.00 mL) and product was precipitated out, washed with cold acetone to remove unreacted monomer and finally dried in a vacuum oven at 40 °C for 48h.

### 6.5.4 Isolation of polymer in **POMD-1/Na-smectite** and **2PBMD-1/Na-smectite**

**POMD-1/Na-smectite** nanocomposite (80 mg) was weighed and mixed with ethanol. The suspension was deposited onto a ceramic tile, placed on a filtration flask and connected to a vacuum. While under suction, 50 mL of acetone was passed through the ceramic tile containing the **POMD-1/smectite**. The solid on ceramic tile as well as filtrate was collected, concentrated (if needed) and vacuum dried at 40 °C for 48h. The extracted polymer was characterized by <sup>1</sup>H-NMR, FTIR, GPC, DSC and TGA.

The same procedure was used for **POMD**-1/Na-smectite using acetonitrile for extraction of the polymer.

### **6.5.5 Treatment of POMD/Na-smectite and OMD/Na-smectite with sodium chloride**

Water (5.0 mL) was added to **OMD**/Na-smectite (30.0 mg) and loaded onto a ceramic tile under vacuum. The sample was air dried for 3h. NaCl aqueous solution (3M, 20.0 mL) was passed through the ceramic tile containing **OMD**/Na-smectite under vacuum allowing the system to saturate after addition of 10.0 mL of salt solution for 15 minutes. Finally, the addition of 10.0 mL of sodium chloride solution (3M) was continued followed by air drying for 3h.

The same procedure was used for treatment of polymer nanocomposite with saline solution employing 30.0 mg of **POMD**/Na-smectite nanocomposite.

## **6.6 References**

- BEATTIE, C., NORTH, M., VILLUENDAS, P. & YOUNG, C. 2013. Influence of Temperature and Pressure on Cyclic Carbonate Synthesis Catalyzed by Bimetallic Aluminum Complexes and Application to Overall syn-Bis-hydroxylation of Alkenes. *J. Org. Chem.*, 78, 419-426.
- BENSEMHOUN, J. & CONDON, S. 2012. Valorization of glycerol 1,2-carbonate as a precursor for the development of new synthons in organic chemistry. *Green Chem.*, 14, 2595-2599.
- BENYAHYA, S., DESROCHES, M., AUVERGNE, R., CARLOTTI, S., CAILLOL, S. & BOUTEVIN, B. 2011. Synthesis of glycerin carbonate-based intermediates using thiol-ene

- chemistry and isocyanate free polyhydroxyurethanes therefrom. *Polym. Chem.*, 2, 2661-2667.
- DIBENEDETTO, A., ANGELINI, A., ARESTA, M., ETHIRAJ, J., FRAGALE, C. & NOCITO, F. 2011. Converting wastes into added value products: from glycerol to glycerol carbonate, glycidol and epichlorohydrin using environmentally friendly synthetic routes. *Tetrahedron*, 67, 1308-1313.
- GAO, Y., HE, C. & QING, F.-L. 2011. Polyhedral oligomeric silsesquioxane-based fluoroether-containing terpolymers: Synthesis, characterization and their water and oil repellency evaluation for cotton fabric. *J. Polym. Sci., Part A: Polym. Chem.*, 49, 5152-5161.
- GIARDI, C., LAPINTE, V., NIELLOUD, F., DEVOISSELLE, J.-M. & ROBIN, J.-J. 2010. Synthesis of polyoxazolines using glycerol carbonate derivative and end chains functionalization via carbonate and isocyanate routes. *J. Polym. Sci., Part A: Polym. Chem.*, 48, 4027-4035.
- HE, Y., GOEL, V., KEUL, H. & MOELLER, M. 2010. Synthesis, Characterization, and Selectivity of Bifunctional Couplers. *Macromol. Chem. Phys.*, 211, 2366-2381.
- MIYATA, T., MATSUMOTO, K., ENDO, T., YONEMORI, S. & WATANABE, S. 2012. Synthesis and radical polymerization of styrene-based monomer having a five-membered cyclic carbonate structure. *J. Polym. Sci., Part A: Polym. Chem.*, 50, 3046-3051.
- ROKICKI, G. & KURAN, W. 1984. Cyclic Carbonates Obtained by Reactions of Alkali Metal Carbonates with Epihalohydrins. *Bulletin of The Chemical Society of Japan*, 57, 1662-1666.

- ROKICKI, G., RAKOCZY, P., PARZUCHOWSKI, P. & SOBIECKI, M. 2005. Hyperbranched aliphatic polyethers obtained from environmentally benign monomer: glycerol carbonate. *Green Chemistry*, 7, 529-539.
- SHIMOMURA, O., LEE, B. S., METH, S., SUZUKI, H., MAHAJAN, S., NOMURA, R. & JANDA, K. D. 2005. Synthesis and application of polytetrahydrofuran-grafted polystyrene (PS-PTHF) resin supports for organic synthesis. *Tetrahedron*, 61, 12160-12167.
- SIMAO, A.-C., LYNIKAITE-PUKLEVICIENE, B., ROUSSEAU, C., TATIBOUET, A., CASSEL, S., SACKUS, A., RAUTER, A. P. & ROLLIN, P. 2006. 1,2-Glycerol carbonate: a versatile renewable synthon. *Lett. Org. Chem.*, 3, 744-748.
- TOMCZYK, K. M., GUNKA, P. A., PARZUCHOWSKI, P. G., ZACHARA, J. & ROKICKI, G. 2012. Intramolecular etherification of five-membered cyclic carbonates bearing hydroxyalkyl groups. *Green Chemistry*, 14, 1749-1758.
- WHITEOAK, C. J., NOVA, A., MASERAS, F. & KLEIJ, A. W. 2012. Merging Sustainability with Organocatalysis in the Formation of Organic Carbonates by Using CO<sub>2</sub> as a Feedstock. *ChemSusChem*, 5, 2032-2038.
- YOKOI, K. & HIRONAKA, K. 2012. Ink compositions, ink-jet image formation method, and printed matter. *JP Patent 2012092330A*.

## Chapter 7 Concluding Remarks

Bentonite used in geosynthetic clay liners fails to act as a strong hydraulic barrier in hyper-saline conditions because the interlayer of the smectite phase contracts, as a result of removal of interlayer water. This behaviour can be mitigated by incorporation of appropriate organic molecules into the clay interlayer. In this research project, several five membered cyclic organic carbonates and a selection of their polymers were synthesized and characterized. Organoclay nanocomposites, formed from the intercalation of the cyclic organic carbonates and their polymers, were further studied for potential improvement of the barrier capabilities of clay-based liners. A strong analytical theme was a feature of this project, with GLC, FTIR, NMR, GC-MS/GPC used as tools for characterizing the cyclic carbonates and their polymers. FTIR, powder XRD, TGA, NMR and DSC were used to characterize the smectite complexes and polymer nanocomposites. Overall, the research described within this thesis contributes significantly to knowledge of cyclic carbonate – sodium smectite complexes and pendant cyclic carbonate polymer-clay nanocomposites.

### 7.1 Major Outcomes

- A method for the scalable production of glycerol carbonate (83% yield) was achieved via a green route from cheap substrates; glycerol and urea employing a novel zinc monoglycerolate (ZMG) catalyst. The yield is comparable to a more expensive method involving transesterification of dimethyl carbonate, described in the literature (Rokicki et al., 2005). A mechanism has been elucidated, involving an isocyanate ligand coordinated to the metal glycerolate as a key

reaction intermediate for this catalytic process. The ZMG methodology was extended to other 1,2-diols and resulted in comparative yields for the cyclic carbonate (transesterification and urea method) with the exception of 4,4'-(oxybis(methylene))bis(1,3-dioxolan-2-one) (**5A**) (54% yield from ZMG/urea method and 99% from the transesterification approach). A low yield of **5A** was obtained with ZMG/urea due to lower conversion of diglycerol. Generally, employing ZMG catalyst resulted in high 1,2-diol conversion with excellent selectivity for the desired cyclic carbonate (Turney et al., 2013).

- A range (10-90 wt%) of glycerol carbonate was intercalated into Na-smectite to investigate the properties of the complexes with varying glycerol carbonate proportions. An ordered glycerol carbonate/Na-smectite complex was formed at 50 wt% glycerol carbonate, with a  $d(001)$  spacing of 1.99 nm. Solvation of interlayer sodium cations is believed to be the main driving force for intercalation of glycerol carbonate. The interactions of glycerol carbonate with water or sodium chloride and water-sodium chloride mixtures were examined by FTIR and it was found that hydrogen bonding among glycerol carbonate molecules was affected by the addition of water. However, the cyclic carbonyl moiety in glycerol carbonate interacted strongly with sodium chloride salt as well. For the glycerol carbonate intercalated clay, the interaction of the carbonate functionality with interlayer sodium cations was suggested to occur via water bridges, as has been observed for propylene carbonate (Onikata et al., 1999). The glycerol carbonate intercalated complex was found to be stable in saline solutions (1M) for at least 18 months under ambient conditions. Thus, they

show potential applicability in geosynthetic clay liners for use in high saline waste facilities.

Intercalation of other synthesized cyclic carbonates into Na-smectite was also studied. FTIR results showed that for the electrostatic interaction of cyclic carbonate with the Na-smectite, cyclic carbonate carbonyl (i.e., PC,  $d(001) = 1.98$  nm), linear carbonate carbonyl (i.e., methyl (4-(2-oxo-1,3-dioxolan-4-yl)butyl) carbonate (**3C**),  $d(001) = 2.20$  nm) as well as other functional groups such as hydroxyl (i.e., 4-(2-hydroxyethyl)-1,3-dioxolan-2-one (**2A**),  $d(001) = 2.05$  nm) also participated when present. The expansion of the gallery of Na-smectite was dependent on the molecular length and size of the cyclic carbonate (for a specific functionality) with the exception of fused rings involving a cyclic carbonate.

- Several derivatives of glycerol carbonate, such as esters, tosylated glycerol carbonate and 4-bromomethyl-1,3-dioxolan-2-one were prepared as candidates for intercalation into Na-smectite. Long-term exposure of cyclic carbonate derivatives to saline wastes may result in leaching of the cyclic carbonates out of the clay interlayer. This possibility can be addressed by converting the cyclic carbonates into polymers with a pendant cyclic carbonate moiety that do not leach out of the clay interlayer. Precursor cyclic carbonate monomers were obtained in greater than 88% yield via O-alkylation of hydroxyl containing pendant five-membered cyclic carbonate. A polyether, poly[oxy(ethane-1-(((methyloxy)methyl)oxirane)-1,2-diyl)] (**POMD**) (76% yield,  $M_n = 8,100 \text{ g mol}^{-1}$ ) with retention of cyclic carbonate intact was obtained via selective ring opening polymerization of the epoxide ring of the epoxy monomer, 4-((oxiran-2-ylmethoxy)methyl)-1,3-dioxolan-2-one (**OMD**) with a pendant five-membered

cyclic carbonate using the initiator, boron trifluoride diethyl etherate. Polystyrene, (i.e., poly[4-(((4-vinylbenzyl)oxy)methyl)-1,3-dioxolan-2-one] (**PBMD**),  $M_n = 21,000 \text{ gmol}^{-1}$  and poly[4-(((4-vinylbenzyl)oxy)butyl)-1,3-dioxolan-2-one] (**PBBD**),  $M_n = 12,000 \text{ gmol}^{-1}$ ) with pendant carbonate functionalities were synthesized in good yield (**PBMD**, 94% and **PBBD**, 74%), by employing radical photopolymerization of the styrene monomers with a pendant cyclic carbonate functionality (4-(((4-vinylbenzyl)oxy)methyl)-1,3-dioxolan-2-one (**BMD**) & 4-(((4-vinylbenzyl)oxy)butyl)-1,3-dioxolan-2-one (**BBD**)).

- Solution intercalation and *in-situ* ring opening polymerization methods were used for preparation of polyether nanocomposites, resulting in intercalated and intercalated-disordered nanocomposites, respectively. Polystyrene cyclic carbonate nanocomposites, obtained via the above two approaches, were intercalated-disordered and partially intercalated-disordered, as determined by XRD. Nanocomposite formation resulted in significant changes in the thermal properties in comparison to their respective pure polymer. Nanocomposites exhibited lower glass transition temperature ( $T_g$ ) compared to the neat polymers, as determined by differential scanning calorimetry (DSC). An increase in decomposition temperature ( $Td_{10}$ ) for polyether nanocomposites was observed, however, for polystyrene cyclic carbonate nanocomposites, a decrease in  $Td_{10}$  was seen compared to their virgin polymers as measured by thermogravimetric analysis (TGA). The *in-situ* prepared polymers in (**POMD-1/Na-smectite** and **PBMD-1/Na-smectite**) smectite nanocomposites were characterized and were found to be similar to that of pure polymer. Polyether nanocomposite (**POMD/Na-smectite**) was also found to be comparatively stable than its

monomer sodium smectite complex (**OMD**/Na-smectite) when treated with saline solution (3M).

To conclude, several five membered cyclic organic carbonates and their polymers were synthesized and incorporated into sodium smectite for their potential applicability in geosynthetic clay liners to use in hyper-saline conditions.

## 7.2 Research Directions

A number of promising research areas were identified for further investigation.

- Single step *in-situ* preparation of glycerol carbonate/smectite complexes could be possibly achieved from reacting substrate such as glycerol intercalated smectite complex with urea employing ZMG catalyst. This methodology can be further applied to the *in-situ* synthesis of various cyclic carbonates/Na-smectite complexes starting from 1,2-diols and urea.
- The glycerol carbonate/Na-smectite complex synthesized in this study should be tested for its stability with saline solution over the long-term.
- The stability of the styrene polymer (**PBMD** and **PBBD**) smectite nanocomposites should be investigated with saline treatment along with its monomer smectite complexes. In addition to above future avenues, the long-term stability of polyether nanocomposite (**POMD**/Na-smectite) with salt solution should be further explored.
- The dynamics of water diffusion in the clay interlayer region of clay nanocomposites could be studied by using quasi-elastic neutron scattering (QENS) experiments and classical molecular dynamics (MD) simulations employing the MCY (Matsuoka-Clementi-Yoshimine) interaction model.

### 7.3 References

- ONIKATA, M., KONDO, M., HAYASHI, N. & YAMANAKA, S. 1999. Complex Formation of Cation-Exchanged Montmorillonites with Propylene Carbonate: Osmotic Swelling in Aqueous Electrolyte Solutions. *Clays and Clay Minerals*, 47, 672-677.
- ROKICKI, G., RAKOCZY, P., PARZUCHOWSKI, P. & SOBIECKI, M. 2005. Hyperbranched aliphatic polyethers obtained from environmentally benign monomer: glycerol carbonate. *Green Chemistry*, 7, 529-539.
- TURNEY, T. W., PATTI, A., GATES, W., SHAHEEN, U. & KULASEGARAM, S. 2013. Formation of glycerol carbonate from glycerol and urea catalysed by metal monoglycerolates. *Green Chemistry*, 15, 1925-1931.

## Appendix 1- Crystal structure and data for tetrahydrofuro[3,4-d][1,3]dioxol-2-one (**8A**)

(Single crystal X-ray analysis was performed by Craig Forsyth at Monash University).

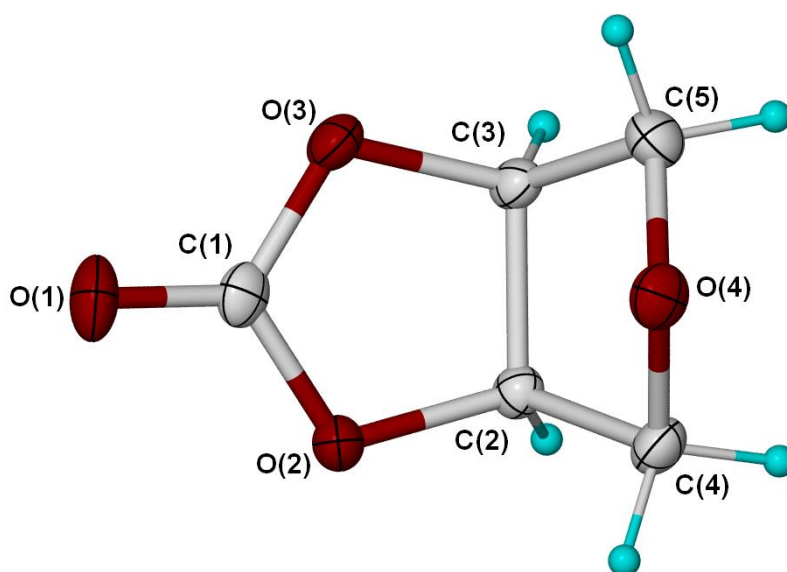


**Figure 1:** Molecular diagram with non-hydrogen atoms represented by 50% thermal ellipsoids and hydrogen atoms as spheres of arbitrary size.

**Table 1:** Crystal data and structure refinement for tetrahydrofuro[3,4-d][1,3]dioxol-2-one (**8A**)

Identification code	<b>8A</b>
Empirical formula	C <sub>5</sub> H <sub>6</sub> O <sub>4</sub>
Formula weight	130.10
Temperature	123(2) K
Wavelength	1.54178 Å
Crystal system, space group	Orthorhombic, P 21 21 21
Unit cell dimensions	a = 4.2717(2) Å    alpha = 90 deg. b = 10.2207(5) Å    beta = 90 deg. c = 12.2953(7) Å    gamma = 90 deg.
Volume	536.81(5) Å <sup>3</sup>
Z, Calculated density	4, 1.610 Mg/m <sup>3</sup>
Absorption coefficient	1.244 mm <sup>-1</sup>
F(000)	272
Crystal size	0.20 x 0.05 x 0.05 mm
Theta range for data collection	5.63 to 66.88 deg.
Limiting indices	-5<=h<=5, -10<=k<=12, -12<=l<=14
Reflections collected / unique	3562 / 591 [R(int) = 0.0263]
Completeness to theta = 66.88	100.0 %
Absorption correction	Semi-empirical from equivalents
Max. and min. transmission	1.00000 and 0.84722
Refinement method	Full-matrix least-squares on F <sup>2</sup>
Data / restraints / parameters	591 / 0 / 82
Goodness-of-fit on F <sup>2</sup>	1.085
Final R indices [I>2sigma(I)]	R1 = 0.0243, wR2 = 0.0637
R indices (all data)	R1 = 0.0264, wR2 = 0.0654
Largest diff. peak and hole	0.162 and -0.155 e.Å <sup>-3</sup>

**Table 2:** Atomic coordinates ( $\times 10^4$ ) and equivalent isotropic displacement parameters ( $\text{\AA}^2 \times 10^3$ )  $U(\text{eq})$  is defined as one third of the trace of the orthogonalized  $U_{ij}$  tensor

---

	x	y	z	$U(\text{eq})$
O(1)	3771(3)	2646(1)	7777(1)	33(1)
O(2)	913(3)	4491(1)	7767(1)	23(1)
O(3)	649(3)	3144(1)	9180(1)	23(1)
O(4)	2390(3)	5872(1)	9868(1)	25(1)
C(1)	1918(4)	3365(2)	8205(1)	22(1)
C(2)	-1108(4)	5172(2)	8530(1)	19(1)
C(3)	-1286(4)	4240(2)	9509(1)	20(1)
C(4)	552(4)	6371(2)	8977(2)	23(1)
C(5)	304(5)	4995(2)	10416(1)	25(1)

---

**Table 3:** Bond lengths [Å] and angles [deg] for tetrahydrofuro[3,4-d][1,3]dioxol-2-one (**8A**)

---

O(1)-C(1)	1.201(2)
O(2)-C(1)	1.341(2)
O(2)-C(2)	1.4528(19)
O(3)-C(1)	1.336(2)
O(3)-C(3)	1.4500(19)
O(4)-C(5)	1.432(2)
O(4)-C(4)	1.441(2)
C(2)-C(4)	1.518(2)
C(2)-C(3)	1.537(2)
C(3)-C(5)	1.517(2)
C(1)-O(2)-C(2)	110.04(12)
C(1)-O(3)-C(3)	110.54(11)
C(5)-O(4)-C(4)	103.89(13)
O(1)-C(1)-O(3)	123.85(16)
O(1)-C(1)-O(2)	124.08(16)
O(3)-C(1)-O(2)	112.06(13)
O(2)-C(2)-C(4)	110.07(14)
O(2)-C(2)-C(3)	103.76(12)
C(4)-C(2)-C(3)	103.86(13)
O(3)-C(3)-C(5)	110.03(14)
O(3)-C(3)-C(2)	103.45(12)
C(5)-C(3)-C(2)	103.80(13)
O(4)-C(4)-C(2)	104.15(12)
O(4)-C(5)-C(3)	104.56(12)

---

Symmetry transformations used to generate equivalent atoms .

**Table 4:** Anisotropic displacement parameters ( $\text{Å}^2 \times 10^3$ ) for tetrahydrofuro[3,4-d][1,3]dioxol-2-one (**8A**). The anisotropic displacement factor exponent takes the form:  $-2 \pi^2 [h^2 a^{*2} U_{11}$

$$+ \dots + 2 h k a^* b^* U_{12}]$$

	U11	U22	U33	U23	U13	U12
O(1)	32(1)	28(1)	38(1)	-15(1)	-1(1)	8(1)
O(2)	28(1)	20(1)	20(1)	-1(1)	3(1)	2(1)
O(3)	26(1)	16(1)	27(1)	2(1)	-1(1)	3(1)
O(4)	25(1)	22(1)	28(1)	-4(1)	-3(1)	-3(1)
C(1)	22(1)	18(1)	26(1)	-6(1)	-4(1)	-2(1)
C(2)	18(1)	18(1)	21(1)	0(1)	1(1)	2(1)
C(3)	20(1)	17(1)	22(1)	2(1)	2(1)	3(1)
C(4)	26(1)	16(1)	28(1)	1(1)	2(1)	1(1)
C(5)	29(1)	26(1)	20(1)	-1(1)	1(1)	0(1)

**Table 5:** Hydrogen coordinates ( $\times 10^4$ ) and isotropic displacement parameters ( $\text{Å}^2 \times 10^3$ ) for tetrahydrofuro[3,4-d][1,3]dioxol-2-one (**8A**)

	x	y	z	U(eq)
H(2)	-3211	5380	8217	22
H(3)	-3478	3978	9692	23
H(4A)	1910	6774	8417	28
H(4B)	-975	7030	9234	28
H(5A)	-1250	5485	10853	30
H(5B)	1475	4397	10901	30

## Appendix 2- TGA curves

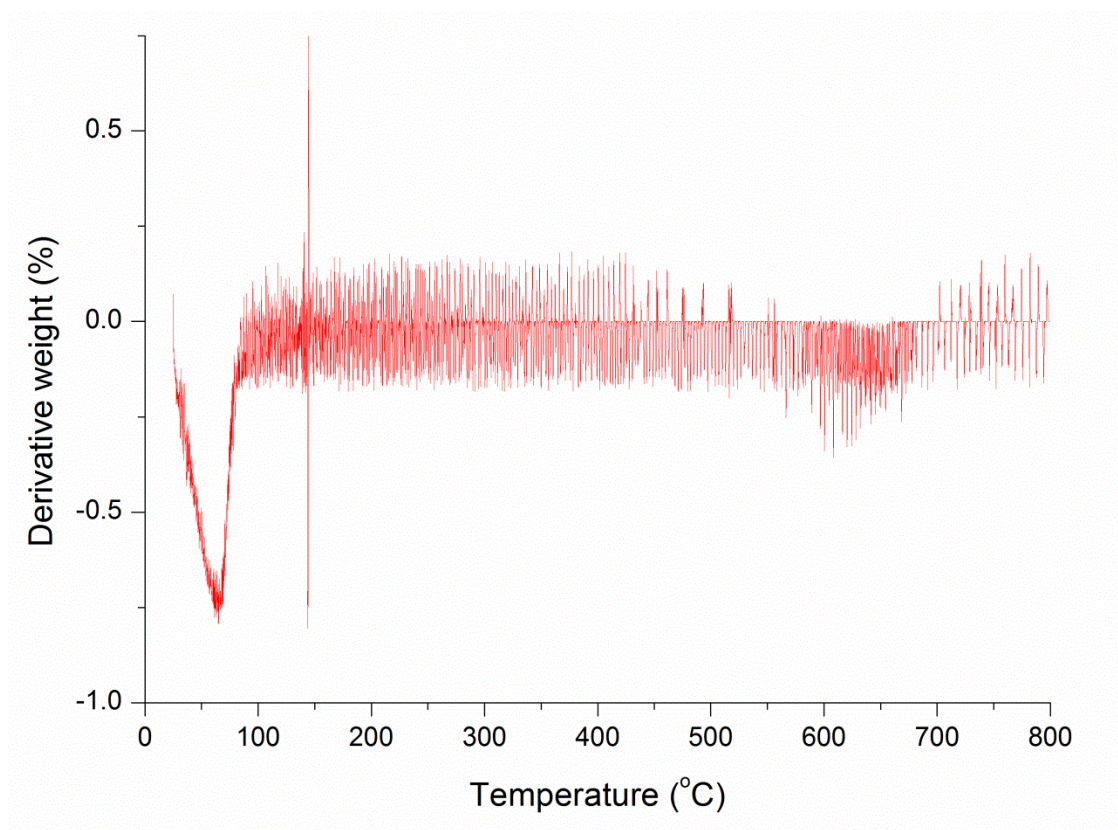


**Figure 1:** Derivative thermogravimetric curve of sodium smectite.

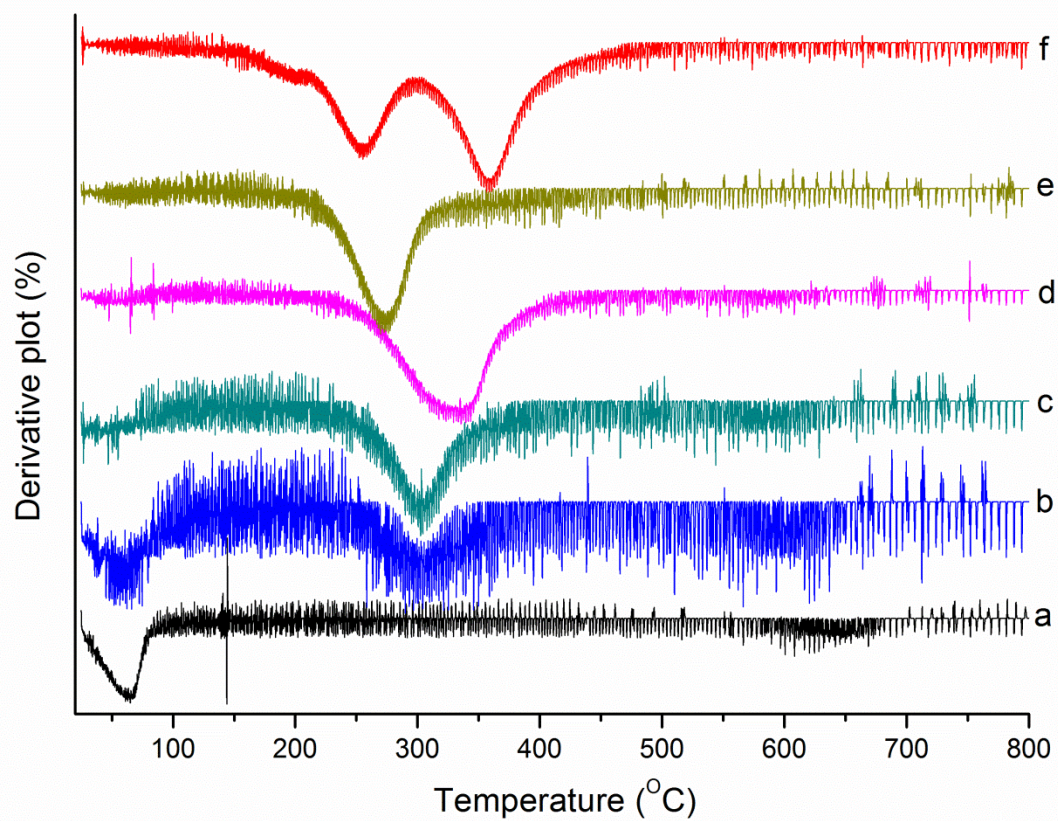


**Figure 2:** A comparison of derivative of thermogravimetric curve of the a) Na-smectite, b) **POMD** (10 wt%)/Na-smectite, c) **POMD** (20 wt%)/Na-smectite, d) **POMD** (50 wt%)/Na-smectite, e) **POMD-1**/Na-smectite prepared by *in-situ* method, and f) neat polyether, **POMD**.

## Formation of glycerol carbonate from glycerol and urea catalysed by metal monoglycerolates†

Cite this: *Green Chem.*, 2013, **15**, 1925

Terence W. Turney,<sup>\*a,b</sup> Antonio Patti,<sup>a</sup> Will Gates,<sup>c</sup> Uzma Shaheen<sup>a</sup> and Sanjitha Kulasegaram<sup>a</sup>

Polymeric monoglycerolate complexes of zinc and cobalt can act as homogeneous catalysts for the one-pot synthesis of glycerol carbonate from glycerol and urea. Effects of reaction temperature, time and glycerol to urea molar ratios on glycerol carbonate selectivity and glycerol conversion have been analysed, with yields reaching 83% at 98% glycerol conversion. The proposed mechanism involves competing catalysed and uncatalysed pathways. In the catalysed pathway, an intermediate isocyanate complex, formed from reaction of urea with the metal monoglycerolate, undergoes rearrangement to form glycerol carbonate and ammonia.

Received 14th December 2012,  
Accepted 9th May 2013

DOI: 10.1039/c3gc37028c

[www.rsc.org/greenchem](http://www.rsc.org/greenchem)

### Introduction

The formation of glycerol as a by-product from biodiesel production has resulted in a surplus over traditional requirements in the chemical, food, pharmaceutical and cosmetics industries. The need to find alternative commodity applications for glycerol and its derivatives has resulted in numerous options for use as a petrochemical replacement or as feedstock for aqueous reforming or bioconversions.<sup>1</sup> There has been recent interest in converting glycerol into glycerol carbonate, an environmentally attractive, biodegradable, polar solvent with low toxicity and good water miscibility. While progress has been made in limiting the use of halogenated or highly flammable solvents like diethyl ether, there is still a demand to replace polar, nonprotic solvents, such as *N,N*-dimethyl formamide and *N*-methyl-pyrrolidine-2-one, with more acceptable alternatives.<sup>2</sup> As polar solvents, cyclic carbonates possess relatively high boiling points and high dielectric constants and so may have the potential to replace more volatile organic solvents in industrial and pharmaceutical applications, without having a significant impact on reaction pathways.<sup>3</sup> We are interested in low-cost, cyclic organic carbonates for use in geosynthetic clay liners that contain leachates from landfills and mining operations.<sup>4</sup> Although, propylene carbonate, has been reported to

form stable interlayer complexes with hydrated Na-bentonite at moderate ionic strengths, we are currently seeking more environmentally acceptable and stable alternatives, which have comparable polarity to water, but more resistant to leaching under hypersaline conditions.<sup>5</sup>

Glycerol carbonate can be manufactured by transesterification from glycerol and dialkyl carbonates, such as ethylene carbonate or dimethyl carbonate. However, when ethylene carbonate is employed, glycerol carbonate is obtained along with ethylene glycol as a difficult to separate by-product.<sup>6</sup> This method is not environmentally desirable as ethylene carbonate itself is prepared by carboxylation of the carcinogenic, acutely toxic and highly flammable substance, oxirane. The alternative use of dimethyl carbonate as the transesterification source requires use of alkaline catalysts (*e.g.* K<sub>2</sub>CO<sub>3</sub>, CaO).<sup>7–9</sup> These catalysts often lose their activity after first use.<sup>9</sup> Lipases,<sup>10</sup> KF modified hydroxyapatite,<sup>11</sup> Mg/Al/Zr mixed oxides<sup>12</sup> and triethylamine<sup>13</sup> catalysts have also been employed for transesterification. The main drawbacks are the long reaction times in some cases and the use of solvents, such as THF, or complex separation procedures required for obtaining high yield and in the case of KF, its toxic nature.

Numerous methods other than transesterification have also been described for the synthesis of glycerol carbonate, including reaction of glycerol with highly toxic phosgene, reaction with carbon monoxide and oxygen, employing palladium as a catalyst with DMF as solvent.<sup>14</sup> Use of toxic reagents, such as phosgene or carbon monoxide, in making glycerol carbonate is certainly not desirable in terms of sustainable development. Direct carboxylation of glycerol carbonate from glycerol and carbon dioxide using Sn-catalysts have also been reported.<sup>15</sup> Major limitations of these methods are low yields (<35%) and high costs. Attempts to produce glycerol carbonate directly

<sup>a</sup>School of Chemistry, Monash University, Clayton, Victoria 3800, Australia.

E-mail: [terry.turney@monash.edu](mailto:terry.turney@monash.edu)

<sup>b</sup>Department of Materials Engineering, Monash University, Clayton, Victoria 3800, Australia

<sup>c</sup>Department of Civil Engineering, Monash University, Clayton, Victoria 3800, Australia

†Electronic supplementary information (ESI) available. See DOI: 10.1039/c3gc37028c

from glycerol and CO<sub>2</sub>, under supercritical conditions employing zeolites, have resulted in low product yields (8%).<sup>16</sup>

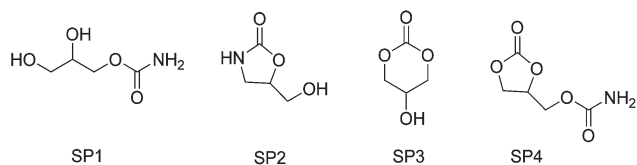
One alternative route to transesterification involves reaction of glycerol with urea, using a range of metal-containing catalysts.<sup>17,18</sup> The main advantage of this method is that urea is a readily available and cheap reactant, whilst the co-product ammonia, can be cycled back into urea manufacture, making the process quite atom economical. These catalysed reactions have variable product selectivities, quite dependent upon the nature of the catalyst, reagent ratios and reaction conditions.<sup>17,19</sup> There is a need to develop an inexpensive catalyst to produce glycerol carbonate in good yields. This paper focuses on a method for producing scalable high yields for glycerol carbonate, using zinc monoglycerolate, which is a commercially available nucleating agent for polypropylene, or its cobalt analogue as a catalyst.<sup>20,21</sup> We describe here the reaction conditions suitable for the efficient conversion of glycerol to glycerol carbonate and propose a mechanism for this catalysed reaction system.

## Results and discussion

Glycerol carbonate was successfully prepared in 83% yield by reacting glycerol with urea in a molar ratio of 1:1.5 in the presence of 5% wt ZMG at 140 °C temperature, under reduced pressure of 40 mbar. It was critical to perform the reaction under reduced pressure in order to shift the thermodynamic equilibrium by removing the by-product ammonia formed. The reaction mixture, also included minor amounts of glycerol urethane (SP1), 5-(hydroxymethyl)oxazolidin-2-one (SP2), 5-hydroxy-1,3-dioxan-2-one (SP3) and (2-oxo-1,3-dioxolan-4-yl)-methyl urethane (SP4) as shown in Scheme 1. Under these reaction conditions it was observed that at 140 °C/40 mbar, the suspended polymeric ZMG mixture bubbled and completely dissolved within 1.5 h, to afford a homogeneous system which was clear until methanol was added in the work-up to recover ZMG.

### Influence of the reaction parameters on conversion, yield and selectivity

Temperature, time, reactant ratios and the catalyst concentration influence the course of the reaction between glycerol and urea. Table 1 shows that progressively increasing the reaction temperature from 100 to 150 °C, results in a marked increase in glycerol conversion at a glycerol to urea ratio of



**Scheme 1** Minor products formed during glycerol conversion to glycerol carbonate.

**Table 1** Effect of temperature on glycerol + urea conversions

Temp (°C)	Conversion (%)	% Selectivity					Yield <sup>a</sup> (%)
		Glyc. carb.	SP1	SP2	SP3	SP4	
100	12	48	46	3	0	2	6
110	17	46	50	4	0	0	8
120	26	72	24	2	2	0	18
130	31	74	22	2	2	0	24
140	61	90	2	4	1	3	55
150	71	92	1	1	5	1	65

Reaction conditions: catalyst (ZMG) amount 5% wt with respect to glycerol, time 7 h, molar ratio of glycerol-urea = 1:1, pressure 40 mbar.<sup>a</sup>Yields of glycerol carbonate determined by gas chromatography.

1:1. Reaction selectivity also varied with temperature; with glycerol urethane (SP1) being formed at lower temperatures and consumed at temperatures above 140 °C. Increases in the yield of glycerol carbonate match the consumption of the urethane as temperatures increased, hence supporting the likelihood of the urethane being an intermediate.

Reaction of glycerol with urea does proceed slowly under these conditions, even in the absence of a catalyst. However, the yield of glycerol carbonate did not exceed 25% (Table 2 and ESI, Fig. S1†). A relatively small proportion of glycerol urethane, SP1, was present in the uncatalysed reaction as early as 0.5 h and increased over the first 1.5 h of reaction, to plateau out thereafter at about 20% selectivity. At all stages of the uncatalysed reaction, SP1 was detected alongside the glycerol carbonate. In contrast in the catalysed reaction, the urethane selectivity decreased with time as glycerol was converted to glycerol carbonate, suggesting a catalysed pathway for conversion to the cyclic species. Other minor products, SP2, SP3 and SP4 slowly appear with time as glycerol conversion increases. The data indicate that the catalyst accelerates both glycerol consumption and decreases the selectivity of the urethane SP1 with respect to glycerol carbonate.

Systematic variation of catalyst loading from 0 to 5 wt%, (glycerol-urea = 1:1 at 140 °C), showed that an optimal conversion of 79% and a yield of 69% of glycerol carbonate could be achieved with only 1% ZMG (see Table S1†). When the molar ratio of glycerol to urea was increased from 1:1 to 1:1.5 there was a significant increase in both glycerol conversion and yield of glycerol carbonate (Table 3). By increasing the proportion of urea, a maximum glycerol conversion of 98% could be obtained at 140 °C, affording an 83% yield of glycerol carbonate. Thus, although addition of an excess of urea and elevated temperatures enhance both the rate of glycerol and glycerol urethane, SP1, conversion, the overall selectivity for glycerol carbonate decreases through further reaction with urea to form the urethane, SP4.

Use of ZnO instead of ZMG as catalyst gave a conversion of 76% and yield of 71% after 7 h at 140 °C/40 mbar pressure (Table S2†). With both ZMG and ZnO, we observed that upon reaching 140 °C/40 mbar pressure and once the bubbling

**Table 2** Catalysed vs. uncatalysed reactions of glycerol with urea

Time (h)	Glycerol Conversion (%)	% Selectivity					Yield of glycerol carbonate (%)
		Glycerol carbonate	SP1	SP2	SP3	SP4	
0.5	15 (2)	87 (96)	13 (5)	0	0	0	13 (2)
1.0	24 (5)	91 (93)	9 (7)	0	0	0	22 (5)
1.5	30 (6)	91 (81)	9 (19)	0	0	0	27 (5)
2.0	41 (10)	91 (80)	9 (20)	1 (0)	1 (0)	1 (0)	37 (8)
3.0	42 (17)	92 (79)	7 (20)	1 (0)	0 (1)	1 (0)	39 (13)
4.0	48 (20)	88 (85)	4 (15)	2 (0)	1 (1)	2 (0)	42 (17)
5.0	50 (22)	90 (78)	4 (20)	2 (1)	1 (1)	2 (0)	45 (17)
6.0	58 (26)	90 (82)	4 (16)	3 (1)	1 (1)	2 (0)	52 (21)
7.0	61 (30)	90 (82)	2 (17)	4 (1)	1 (1)	3 (0)	55 (25)

Reaction conditions: Temperature 140 °C, molar ratio of glycerol-urea = 1 : 1, pressure 40 mbar. Selectivities and conversions determined by gas chromatography, with analyses performed in triplicate. Standard deviations were between 0–2 absolute % figures. Data in parentheses are for the uncatalysed reaction.

**Table 3** Comparison of change of molar ratio at 140 and 150 °C on glycerol conversion and glycerol carbonate selectivity

Temperature (°C)	Molar ratio Gly : urea	Conversion (%)	% Selectivity					Yield <sup>a</sup> (%)
			Glyc. carb.	SP1	SP2	SP3	SP4	
140	1 : 1	61	90	2	4	1	3	55
140	1 : 1.5	98	85	2	1	6	6	83
150	1 : 1	71	92	1	1	5	1	65
150	1 : 1.5	91	82	1	3	3	11	75

Reaction conditions: Catalyst (ZMG) amount 5% wt with respect to glycerol, time 7 h and pressure 40 mbar.<sup>a</sup>Yields determined by gas chromatography.

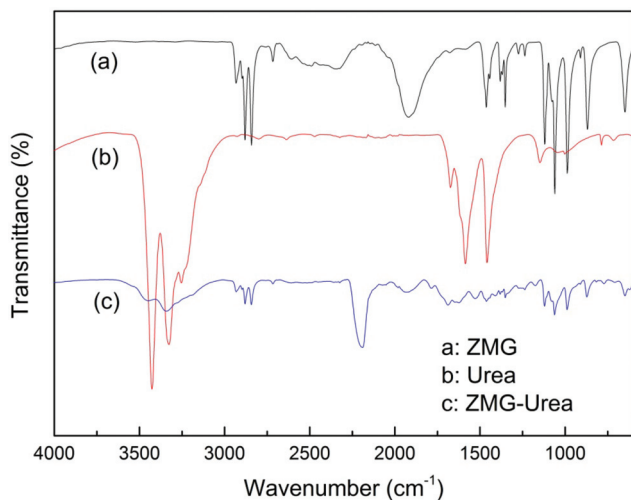


**Fig. 1** Stoichiometric reaction between ZMG and urea, (a) FTIR spectrum of ZMG; (b) FTIR spectrum of urea; (c) stoichiometric reaction mixture between ZMG and urea (1 : 2) in the absence of glycerol taken at  $t = 3$  h.

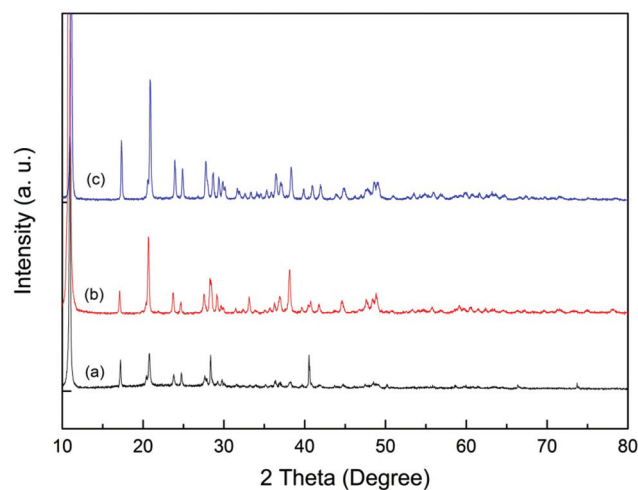
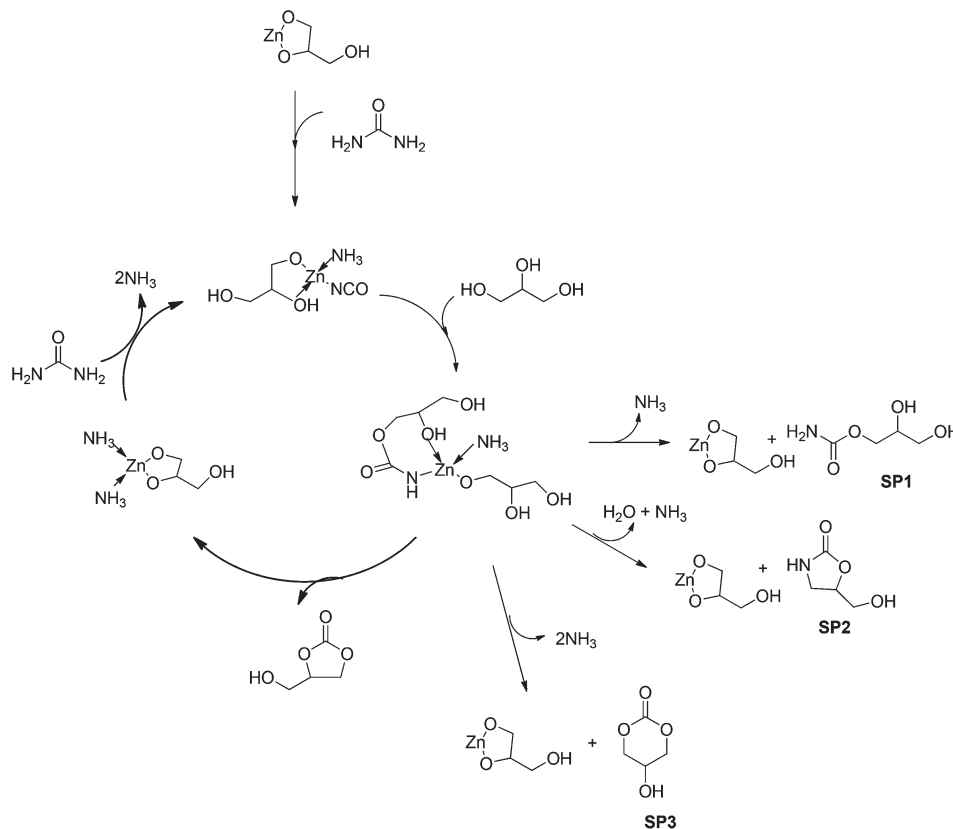


**Fig. 2** Stoichiometric reaction between ZMG and urea. (a) XRD of reaction mixture of urea and ZMG in a 2 : 1 molar ratio; (b) solid from reaction after methanol work-up; (c) commercial ZMG used in reaction.

subsided, the suspended catalyst had completely dissolved within 1.5 h, resulting in a clear solution. Upon work-up with methanol a white precipitate was produced, which was identified as ZMG, by FTIR and XRD in comparison with authentic samples (Fig. S3,† cf. Fig. 1a and 2c), irrespective of whether the starting material was ZnO or ZMG. It is known that ZnO readily converts to ZMG in the presence of glycerol and this

reaction is the basis of the industrial production of ZMG.<sup>21</sup> It is most probable that in the case of ZnO as a starting material, the actual catalyst is ZMG (Scheme 2).

When cobalt monoglycerolate was employed as a catalyst, conversions were comparable with the zinc analogue, giving a yield of 52% of glycerol carbonate after 6 h (see Table S3†). The observation that the cobalt glycerolate system also



**Scheme 2** Reaction mechanism with ZMG as a catalyst precursor.

catalyses the production of glycerol carbonate, implies that the presence of a zinc-containing catalyst is not necessary and that other metals capable of generating a metal glycerolate complex can also be effective.

### Mechanistic studies

The re-usability of the catalyst was evaluated over two cycles when 5% wt ZMG was reacted with a 1 : 1 mole equivalent of glycerol to urea (Table S4<sup>†</sup>). By weight, 90% of the added ZMG could be recovered from this reaction, after MeOH precipitation, and was identified from its characteristic XRD powder pattern. The recovered material could be re-used several times to produce glycerol carbonate with essentially the same selectivity and yields. There was no evidence for other zinc containing species in either the recovered catalyst or the isolated glycerol carbonate. In the reaction of glycerol with urea, it is evident that the metal glycerolate plays a catalytic role in forming both the glycerol urethane and glycerol carbonate itself. Reaction conversion, selectivity and yield were dependent upon temperature, reactant ratios and catalyst levels.

The proposed mechanism for the uncatalysed reaction of urea with alcohols involves two key processes. In the case of glycerol, carbamoylation affords exclusively the 1-glycerol urethane, liberating one mole of ammonia with no evidence for formation of a urethane at the 2-position of glycerol. However, at the mole ratios used here, glycerol carbonate was the predominant product, even at very low conversions, with

the urethane, SP1, only appearing as during the latter part of the reaction as glycerol was consumed (Table 2).

In order to determine possible roles of the metal glycerolate in the catalysed formation of glycerol carbonate, urea alone was reacted with ZMG, in a 2 : 1 mole ratio, at 140 °C/40 mbar for 3 h, in the absence of glycerol. Fig. 1 shows the FTIR of the reaction mixture, containing urea and ZMG, where a strong IR band at 2207  $\text{cm}^{-1}$  is clearly visible, characteristic of  $\nu_{\text{asymm}}(\text{NCO})$  of a coordinated isocyanate ligand.<sup>22</sup> This mixture remained a suspension throughout the course of the reaction. Although ammonia was liberated on heating, the FTIR spectrum of the product still exhibited  $\nu(\text{N-H})$  vibrations at 3327 to 3459  $\text{cm}^{-1}$  (Fig. 1). However, no crystalline product was formed, with the powder XRD pattern of this solid, after washing with methanol, showing only the presence of unreacted ZMG (Fig. 2). This observation is in marked contrast to the known microcrystalline product,  $\text{Zn}(\text{NH}_3)_2(\text{NCO})_2$  [ $\nu(\text{NCO}) = 2220 \text{ cm}^{-1}$ ], reported from the reaction of  $\text{ZnCl}_2$  and  $\text{KOCN}$  in aqueous ammonia or by heating a mixture of  $\text{ZnO}$ , urea and methanol.<sup>22,23</sup> It indicates a dominant role for glycerol in determining the structures of these reaction intermediates. It is likely that  $\text{Zn}(\text{NH}_3)_2(\text{NCO})_2$  is not a direct intermediate in the present catalytic cycle, but both it or ZMG itself will form an intermediate glycerolate and/or glycerol urethane complex of zinc isocyanate, presumably with labile ammine ligands (see Scheme 2). It is worth noting, that when urea alone is heated to 140 °C at 40 mbar, no species

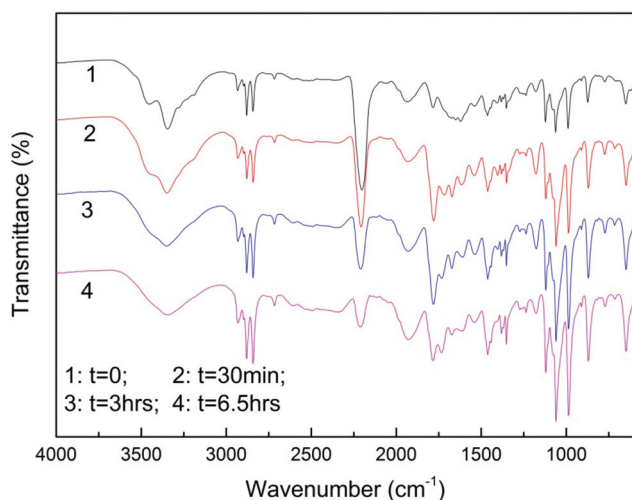


**Fig. 3** FTIR spectra of *in situ* reaction of ZMG-urea reaction mixture with glycerol (ZMG-urea-glycerol = 1 : 2 : 3 mol. equiv.).

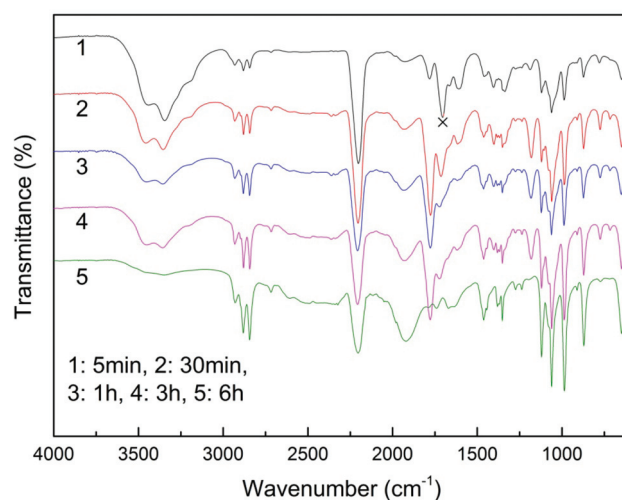


**Fig. 4** FTIR spectra of reaction of  $\text{Zn}(\text{NCO})_2(\text{NH}_3)_2$  with 1.5 molar equivalents of glycerol over time.

exhibiting significant  $\nu(\text{NCO})$  bands (by FTIR) are formed and in particular, free isocyanic acid ( $\text{HNCO}$ ) is reported not to be produced from decomposition of urea at an appreciable rate at temperatures below  $180\text{ }^\circ\text{C}$ .<sup>24–26</sup> Reaction of the ZMG-urea product with glycerol (ZMG-urea-glycerol = 1 : 2 : 3 mol. equiv.) showed a gradual decrease in intensity but no frequency shift of the  $\nu(\text{NCO})$  band from  $2207\text{ cm}^{-1}$  by FTIR over the course of 6.5 h (Fig. 3). During such reactions, both glycerol carbonate and SP1 are produced. It appears therefore, that the intermediate isocyanate is stabilised by metal coordination, to form discrete molecular species here in the case of ZMG or from ZnO and glycerol.<sup>27</sup> An intermediate N-coordinated glyceryl carbamate ligand can then directly eliminate by  $\text{H}^+$  transfer to glycerol urethane, SP1, or cyclise with the elimination of  $\text{NH}_3$  to afford glycerol carbonate as shown in Scheme 2. The conversion improves as a function of time, whilst the selectivity remains relatively constant throughout the metal catalysed reaction (Tables 2, 3 and S2†).

The isocyanate complex,  $\text{Zn}(\text{NCO})_2(\text{NH}_3)_2$ , has previously been synthesised by Edwards *et al.*, who also reported a detailed assignment of its vibrational spectrum.<sup>23</sup> We have repeated that synthesis and can confirm that the powder XRD pattern and infrared spectrum ( $\nu(\text{NCO}) = 2209\text{ cm}^{-1}$ ) of that material appears identical to the product proposed by Zhao *et al.*<sup>22</sup> (see Fig. S4 and S5†). Reaction of this isocyanate complex with a stoichiometric amount of glycerol afforded glycerol carbonate in 67% yield. Fig. S6a† shows the XRD of the reaction mixture that was a suspension (prior to MeOH work-up) and Fig. S6b,† the isolated solid (after MeOH work-up). As can be seen from that data, the solid material in each case was ZMG. Their XRD powder diffraction patterns are both very similar to ZMG itself (Fig. S6c†), each with an intense basal (001) spacing at  $10.8^\circ$  ( $d = 0.81\text{ nm}$ ), arising from the layered structure of ZMG, together with prominent 011 and 111 peaks at  $0.52\text{ nm}$  and  $0.43\text{ nm}$  respectively.<sup>21</sup> Weak intensity differences between other parts of XRD spectra in Fig. S6† are partly

due to orientational effects, often encountered in highly layered species (*e.g.*, clays). The single medium intensity peak in Fig. S6a† at  $41^\circ$  which is not present in ZMG, is an unassigned species, with insufficient data available to draw conclusions from that lone peak. Thus, the main crystalline product isolated from the reaction between  $\text{Zn}(\text{NCO})_2(\text{NH}_3)_2$  and glycerol was ZMG. However from FTIR analysis of the reaction mixture (Fig. 4), the reaction also involved a non-crystalline product with a retained isocyanate ligand. Infrared analysis during the course of this reaction showed a slow decrease in the intensity of the  $\nu(\text{NCO})$  peak at  $= 2207\text{ cm}^{-1}$  and that comparison with an authentic sample of ZMG (Fig. 1a) shows that ZMG was indeed formed from the early stages of the reaction. The importance of an OCN-metal glycerolate intermediate is also suggested by the stoichiometric reaction of cobalt monoglycerolate with urea to afford a very similar isocyanate product [ $\nu(\text{NCO}) = 2202\text{ cm}^{-1}$ ] to ZMG (see Fig. S7†).

## Conclusions

The polymeric glycerolate complexes of Zn and Co form a homogeneous catalyst, containing a coordinated isocyanate ligand, in the presence of mixtures of glycerol and urea to produce glycerol carbonate selectively, in high yields in the case of ZMG. Optimal conditions for this transformation are 5% by weight of ZMG catalyst with respect to glycerol at  $140\text{ }^\circ\text{C}$  under 40 mbar reduced pressure with a glycerol to urea molar ratio of 1 : 1.5 (Table 3). It is proposed that the polymeric glycerolate structure is broken down in the reaction with urea to afford an intermediate complex containing a coordinated isocyanate ligand. Rearrangement of this species generates a carbamate derivative of the glycerolate ligand. This in turn can reversibly be displaced by further glycerol and eventually cyclize to glycerol carbonate, regenerating the metal

monoglycerolate with the liberation of  $\text{NH}_3$  under vacuum conditions.

## Experimental

Urea, glycerol and HPLC-grade methanol were purchased from Merck. Commercial samples of zinc monoglycerolate and nanoparticulate ZnO (particle size =  $39 \pm 4$  nm) were obtained from Micronisers Pty Ltd (Dandenong, Victoria Australia) and used as received. Diammine diisocyanatozinc(II),  $\text{Zn}(\text{NCO})_2(\text{NH}_3)_2$ , and cobalt monoglycerolate were synthesised according to literature.<sup>23,28</sup>

Gas chromatography was performed on an Agilent 6850 Series II Network GC System, equipped with an FID detector and an HP-1 column (30 m  $\times$  0.32 mm ID). Helium was used as a carrier gas at a flow-rate of 2.0 mL  $\text{min}^{-1}$ , and a temperature program of 40–250 °C at 10 °C  $\text{min}^{-1}$  was employed. Detector response factors (from multiple-point calibration curves) were determined for all of the starting materials and reaction products.

FTIR-Infrared spectra were obtained on an ATR-Perkin Elmer spectrum RX1 series Fourier Transform infrared spectrometer. FTIR spectra were recorded in the mid-IR region (400–4000  $\text{cm}^{-1}$ ) at a resolution of 2  $\text{cm}^{-1}$  with 16 scans co-added. Powder XRD spectra were collected on a Philips PW1140 diffractometer from 2–80°  $2\theta$  at 4°  $\text{min}^{-1}$  with a step size of 0.02° using a Cu  $K\alpha$  source ( $\lambda = 1.54$  nm). A 1° divergence slit, 1° receiving slit and 0.2° scatter aperture were used. Samples were prepared as front-loaded packed powders in aluminium sample holders.

### Reaction procedure

Reactions were performed in a 100 mL Schlenk flask connected to a vacuum line. In a typical experiment, glycerol (10 g, 0.108 mol) was reacted with urea (6.52 g, 0.108 mol) and zinc monoglycerolate. The amount of catalyst used was 5% by weight of the initial amount of glycerol. The reaction was magnetically stirred at a constant rate of 630 rpm and heated in an oil bath at the desired temperature. Reactions were run under reduced pressure (40 mbar) and in the absence of solvent. After the reaction, methanol was added and the catalyst was removed by filtration. The catalyst was washed with acetone to remove any adsorbed products. The filtrate was concentrated under reduced pressure and products were analysed by gas chromatography and  $^1\text{H-NMR}$  (data not shown). Product quantification by gas chromatography was made using methanol as a solvent. Conversion, selectivity and yield were calculated with respect to glycerol. Minor products (SP1–4) were analysed by GC-MS (data not shown). Calculation of percent glycerol conversion and yield of glycerol carbonate were based on chromatographic intensities.

**Reaction of glycerol and urea at different temperatures (Table 1).** Separate reaction mixtures containing a mixture of glycerol, urea and ZMG were heated at 100, 110, 120, 130, 140 and 150 °C under constant magnetic stirring of 630 rpm for

7 h, while the ammonia liberated during the reaction was removed *in vacuo*. At the end of each reaction, the mixture was cooled to room temperature, methanol added to precipitate out the catalyst; followed by filtration. This was then concentrated and analysed by gas chromatography.

**Reaction of glycerol and urea with and without ZMG (Table 2).** Glycerol (10 g, 0.108 mol) and urea (6.52 g, 0.108 mol) were heated at 140 °C/40 mbar in the absence of ZMG. The reaction was sampled at  $t = 0.5, 1, 1.5, 2, 3, 4, 5, 6$  and 7 h. At the end of each time interval, an aliquot (10 mg) of the reaction mixture was centrifuged with methanol (1 mL) and analysed by gas chromatography. This was repeated in the presence of 5% wt ZMG (500 mg) and analysed at the same time intervals.

**Reaction of glycerol and urea at different molar ratios (Table 3).** The reactions of glycerol and urea in molar ratios 1:1 and 1:1.5 were carried out as in the above general procedure using 5% wt ZMG at 150 °C and 140 °C, under reduced pressure. These reactions were monitored at 3, 4, 5, 6 and 7 h. At the end of each time interval the mixture was cooled, methanol added; then filtered and analysed by gas chromatography.

**Reaction of glycerol and urea at different catalyst loadings (Table S1†).** Glycerol (5 g, 0.054 mol), urea (3.26 g, 0.054 mol) and ZMG (1% wt, 50 mg) were heated at 140 °C/40 mbar. The reaction mixture was analysed by gas chromatography at  $t = 3, 4, 5$  and 6 h. The above set-up was used with 0.1 and 0.5% wt ZMG as well.

**Reaction of glycerol and urea with cobalt monoglycerolate (Table S3†).** Glycerol (5 g, 0.054 mol), urea (3.26 g, 0.054 mol) and CMG (5% wt, 250 mg) were heated at 140 °C/40 mbar. The reaction mixture was analysed by gas chromatography, after centrifuging an aliquot with methanol, at  $t = 1, 2, 3, 4, 5$  and 6 h.

**Recycling experiments (Table S4†).** Glycerol (10 g, 0.109 mol), urea (6.52 g, 0.109 mol) and ZMG (5% wt, 0.5 g) were heated at 140 °C/40 mbar. Reaction aliquots were sampled at  $t = 3, 4, 5$  and 6 h by gas chromatography. The final mixture was taken-up in 100 mL of methanol and the solid filtered and dried in a vacuum oven (at 40 °C). The identity of this solid was confirmed by FTIR to be ZMG (0.45 g, 90% recovery). This was used as 5% wt to glycerol (9.0 g, 0.098 mol) with urea (5.87 g, 0.098 mol) at 140 °C/40 mbar and monitored at similar time intervals as above. The workup to recover ZMG (0.38 g, 84% recovery) was as above (Table S4†).

**Reaction of ZMG with urea (Fig. 1 and 2).** Urea (3.84 g, 0.064 mol) and ZMG (5 g, 0.032 mol) were combined and heated at 140 °C under reduced pressure of 40 mbar. After 3 h, the mixture was cooled and analysed by FTIR and XRD. The cooled reaction mixture was then washed with methanol, the solid filtered and re-analysed by FTIR and XRD.

**Reaction of ZMG–urea with glycerol (Fig. 3).** A sample of the above solid (0.5 g; prior to methanol wash) was reacted with glycerol (17.7 g, 0.19 mol) (ZMG–urea–glycerol = 1:2:3 mol. equiv.) at 140 °C/40 mbar. The final mixture was suspended in methanol and filtered. The solid (254 mg) was analysed by

FTIR and XRD to be ZMG. The yield of glycerol carbonate from the reaction mixture at 6.5 h by gas chromatography was 89%.

**Reaction of diamminediisocyanatozinc(II) with glycerol (Fig. 4 and S6†).** Zn(NCO)<sub>2</sub>(NH<sub>3</sub>)<sub>2</sub> (0.51 g, 0.0028 mol) and glycerol (0.39 g, 0.0042 mol) were combined and heated to 140 °C/40 mbar. The reaction was periodically monitored by gas chromatography and FTIR over 6 h. At the end, the mixture was suspended in methanol and solid filtered (250 mg of ZMG) and the filtrate concentrated to give glycerol carbonate (67% yield).

**Reaction of glycerol and urea with zinc oxide (Table S2 and Fig. S2 and S3†).** Glycerol (10 g, 0.109 mol), urea (6.52 g, 0.109 mol) and ZnO (5% wt, 500 mg) were heated at 140 °C at 40 mbar. The reaction mixture was analysed by gas chromatography, after centrifuging an aliquot with methanol at  $t = 0.5, 1.5, 2, 3, 4, 5, 6$  and 7 h. After 7 h, the catalyst was precipitated by adding methanol, filtered, then washed several times with acetone and dried before being analysed by FTIR and powder XRD.

## Acknowledgements

The authors are grateful to Micronisers Pty Ltd for supply of zinc glycerolate and ZnO nanoparticles, the Australian Research Council for financial support (Grant No: DP1095129), the Faculty of Science for providing an international PhD fees scholarship (US) and wish to thank Mingdeng Luo and Sally Duck from Monash University for instrumental support.

## References

- C.-H. Zhou, J. N. Beltramini, Y.-X. Fan and G. Q. Lu, *Chem. Soc. Rev.*, 2008, **37**, 527.
- D. J. C. Constable, P. J. Dunn, J. D. Hayler, G. R. Humphrey, J. L. Leazer, R. J. Linderman, K. Lorenz, J. Manley, B. A. Pearlman, A. Wells, A. Zaks and T. Y. Zhang, *Green Chem.*, 2007, **9**, 411.
- Y. Chernyak, *J. Chem. Eng. Data*, 2006, **51**, 416.
- M. Onikata, M. Kondo, N. Hayashi and S. Yamanaka, *Clays Clay Miner.*, 1999, **47**, 672.
- B. Schäffner, S. P. Verevkin and A. Börner, *Chem. Unserer Zeit*, 2009, **43**, 12.
- M. J. Climent, A. Corma, P. De Frutose, S. Iborra, M. Noy, A. Velyt and P. Concepcion, *J. Catal.*, 2010, **269**(1), 140.
- G. Rokicki, P. Rakoczy, P. Parzuchowski and M. Sobiecki, *Green Chem.*, 2005, **7**, 529.
- F. S. H. Simanjuntak, T. K. Kim, S. D. Lee, B. S. Ahn, H. S. Kim and H. Lee, *Appl. Catal., A*, 2011, **401**, 220.
- J. Li and T. Wang, *React. Kinet., Mech. Catal.*, 2011, **102**, 113.
- K. H. Lee, C.-H. Park and E. Y. Lee, *Bioprocess Biosyst. Eng.*, 2010, **33**, 1059.
- R. Bai, S. Wang, F. Mei, T. Li and G. Li, *J. Ind. Eng. Chem.*, 2011, **17**, 777.
- M. Malyaadri, K. Jagadeeswaraiyah, P. S. Sai Prasad and N. Lingaiah, *Appl. Catal., A*, 2011, **401**, 153.
- J. R. Ochoa-Gomez, O. Gomez-Jimenez-Aberasturi, C. Ramirez-Lopez and B. Maestro-Madurga, *Green Chem.*, 2012, **14**, 3368.
- (a) J. Hu, Y. Gu, Z. Guan, J. Li, W. Mo, T. Li and G. Li, *ChemSusChem*, 2011, **4**, 1767; (b) J. Hu, J. Li, Y. Gu, Z. Guan, W. Mo, Y. Ni, T. Li and G. Li, *Appl. Catal., A*, 2010, **386**, 188.
- J. George, Y. Patel, S. M. Pillai and P. Munshi, *J. Mol. Catal. A: Chem.*, 2009, **304**, 1.
- C. Vieville, J. W. Yoo, S. Pelet and Z. Mouloungui, *Catal. Lett.*, 1998, **56**, 245.
- C. Hammond, J. A. Lopez-Sanchez, M. Hasbi Ab Rahim, N. Dimitratos, R. L. Jenkins, A. F. Carley, Q. He, C. J. Kiely, D. W. Knight and G. J. Hutchings, *Dalton Trans.*, 2011, **40**, 3927.
- L. Wang, Y. Ma, Y. Wang, S. Liu and Y. Deng, *Catal. Commun.*, 2011, **12**, 1458.
- D.-W. Kim, M.-S. Park, M. Selvaraj, G.-A. Park, S.-D. Lee and D.-W. Park, *Res. Chem. Intermed.*, 2011, **37**, 1305.
- Anonymous, *The IP.com Journal*, 2006, **6**(3B), 5.
- E. W. Radoslovich, M. R. Raupach, P. G. Slade and R. M. Taylor, *Aust. J. Chem.*, 1970, **23**, 1963.
- W. Zhao, W. Peng, D. Wang, N. Zhao, J. Li, F. Xiao, W. Wei and Y. Sun, *Catal. Commun.*, 2009, **10**, 655.
- H. G. M. Edwards, D. W. Farwell, I. R. Lewis and N. Webb, *J. Mol. Struct.*, 1992, **271**, 27.
- H. Wang, M. Wang, W. Zhao, W. Wei and Y. Sun, *React. Kinet., Mech. Cat.*, 2010, **99**, 381.
- A. Lundstrom, T. Snelling, P. Morsing, P. Gabrielsson and E. Senar, *Appl. Catal., B*, 2011, **106**, 273.
- P. M. Schaber, J. Colson, S. Higgins, D. Thielen, B. Anspach and J. Brauer, *Thermochim. Acta*, 2004, **424**, 131.
- Q. Li, W. Zhang, N. Zhao, W. Wei and Y. Sun, *Catal. Today*, 2006, **115**, 111.
- P. G. Slade, E. W. Radoslovich and M. Raupach, *Acta Crystallogr., Sect. B: Struct. Crystallogr. Cryst. Chem.*, 1971, **27**, 2432.